Cyclic Carbonates from Sugars and Carbon Dioxide: Synthesis, Polymerisation and Biomedical Applications

Gregory, Georgina

Award date:
2017

Awarding institution:
University of Bath

Cyclic Carbonates from Sugars and Carbon Dioxide: Synthesis, Polymerisation and Biomedical Applications

Georgina L. Gregory

A thesis submitted for the Degree of Doctor of Philosophy

Department of Chemistry

University of Bath

April 2017

Table of Contents

Acknowledgements

Firstly, I would like to thank my supervisor, Dr Antoine Buchard for all his support, advice and encouragement over the years. Particularly, for introducing the Buchard group rules, which are as follows: 1. Always do a crude NMR, 2. Always be tidy and 3. Sometimes you can't get it from the crude NMR.

I would also like to thank all the MChem, NatSci, MRes and summer students who have contributed to various aspects of this work. Namely, Marion Ulmann who carried out the initial work using TsCl in combination with CO_2 to prepare cyclic carbonates (Chapter 2) and Lucy Cotton who investigated the method with glycerol and aromatic alcohol substrates. In Chapter 3, Liliana Jenisch carried out initial ROP experiments of the mannose-based cyclic carbonate and Bethan Charles, as part of her MRes project took some interesting FTM images of the mannose-derived polycarbonates as well as performed cell attachment studies. These formed the basis of the cell work with the thymidine-derived polycarbonates (Chapter 4), where Liz Hierons also investigated the Boc- protection of thymidine. Thank you also to all current members of the group for their ideas, discussion, and advice. Nominally, Dr Eva López-Vidal, who is continuing the work with the CS_2 based monomers in Chapter 5 and alongside Tanguy Tomes, investigating the derivatisation of the mannose-derived cyclic carbonate, Thom Mcguire whose PhD project involves continuing to build upon the method for the direct coupling of CO_2 with diols and has already led to some exciting developments as well as Andy Hall for his novel practical ideas and expertise with fixing the NMR machine. Outside of the group, I am also thankful to everyone, past and present in the 5W 3.11 lab and 3.12 office for their discussion of ideas, support, biscuits, and encouragement, throughout my PhD. Thank you to Mike Joyes for use of the HFIP SEC.

The expertise of my co-supervisor, Dr Ram Sharma and various members of his group namely, Jamie Courtenay and Marcus Johns have also been vital for carrying out the cell attachment studies. A particular thank you is extended to Dr Kociok-Köhn for all the single-crystal X-ray diffraction analysis as well as members of CCAF, Rémi Castaing and Shaun Reeksting for training and advice on the TGA-MS, DSC, SEC and MALDI-ToF instruments.

Finally, I would like to thank the EPSRC for funding and the Doctoral Training Centre for Sustainable Chemical Technologies particularly, Janet Scott, Tim Mays and Matthew

Davidson as well as everyone in Cohort 2012, for the many opportunities it has provided. For example, my industrial placement at Syngenta and the public engagement activities I have enjoyed being part of. My family have of course also provided me with a lot of support and encouragement over the many years, for which I will always be very grateful.

List of Publications

- Gregory, G. L.; Kociok-Kohn, G.; Buchard, A., Polymers from sugars and CO_2: ring-opening polymerisation and copolymerisation of cyclic carbonates derived from 2-deoxy-D-ribose. *Polym. Chem*. **2017**, 8 (13), 2093-2104.
- Gregory, G. L.; Hierons, E. M.; Kociok-Kohn, G.; Sharma, R. I.; Buchard, A., CO_2-Driven stereochemical inversion of sugars to create thymidine-based polycarbonates by ring-opening polymerisation. *Polym. Chem*. **2017**, 8 (10), 1714-1721.
- Gregory, G. L.; Lopez-Vidal, E. M.; Buchard, A., Polymers from sugars: cyclic monomer synthesis, ring-opening polymerisation, material properties and applications. *Chem. Commun.* **2017**, 53 (14), 2198-2217.
- Gregory, G. L.; Jenisch, L. M.; Charles, B.; Kociok-Köhn, G.; Buchard, A., Polymers from Sugars and CO_2: Synthesis and Polymerization of a D-Mannose-Based Cyclic Carbonate. *Macromolecules* **2016**, 49 (19), 7165-7169.
- Gregory, G. L.; Ulmann, M.; Buchard, A., Synthesis of 6-membered cyclic carbonates from 1,3-diols and low CO_2 pressure: a novel mild strategy to replace phosgene reagents. *RSC Adv.* **2015,** *5* (49), 39404-39408.

Abstract

The biodegradability and when functionalised biocompatibility of aliphatic polycarbonates (APCs) makes them an attractive class of materials for biomedical applications such as tissue engineering scaffolds and drug-delivery carriers. One route to accessing a wide-range of well-defined and functional APCs is the controlled ring-opening polymerisation (ROP) of cyclic carbonates. In turn, these would ideally be prepared by the direct coupling of CO_2 with diols to give water as the only by-product. In this way, the combination of CO_2 and sugar-derived diols draws upon two natural renewable building blocks for the construction of polycarbonates that are anticipated to show good biocompatibility properties.

Chapter 2 develops a simple and mild alternative to the traditional use of phosgene derivatives for the synthesis of six-membered cyclic carbonates from 1,3-diols and CO_2. DFT calculations highlighted the need to lower both the CO_2-insertion and ring-closing kinetic barriers to cyclic carbonate formation. Organic superbase, 1,8- diazabicyclo[5.4.0]undec-7-ene (DBU) enabled the formation of carbonate species at 1 atm CO_2 pressure whereas, the introduction of a leaving group strategy lowered the cyclisation barrier. Mechanistic considerations suggested a kinetic preference for ring- closing *via* a nucleophilic addition-elimination pathway rather than a S_N2-like intramolecular cyclisation.

Chapter 3 applies the procedure with CO_2 to the preparation of a novel monomer from natural sugar, D-mannose. ROP was carried out *via* an organocatalytic approach and a preference for head-tail linkages in the polycarbonate backbone indicated by NMR spectroscopy and supported by DFT calculations. Chapter 4 utilises CO_2 to invert the natural stereochemistry of sugars and create a thymidine-based monomer. The thermodynamic parameters of the ROP with 1,5,7-triazabicyclo[4.4.0]dec-5-ene (TBD) catalyst are determined and the properties of the polycarbonates investigated to include preliminary cell attachment studies. Finally, chapter 5 details the synthesis of cyclic carbonates from 2- deoxy-D-ribose and the investigation into the different ROP behaviour of the α- and β- anomers. The ability to tune the polymer properties through copolymerisation with trimethylene carbonate (TMC) is also discussed.

Abbreviations

APC	Aliphatic Polycarbonate
cpcm	Conductor-like polarisable continuum model
Đ	Polymer molecular weight distribution M_w/M_n
DBU	1,8-Diazabicyclo[5.4.0]undec-7-ene
DP	Degree of Polymerisation
DFT	Density Functional Theory
DSC	Differential Scanning Calorimetry
DMAP	4-(Dimethylamino) pyridine
DMC	Dimethyl carbonate
DMF	*N*,*N*-dimethylformamide
FTIR	Fourier Transform Infra-Red Spectroscopy
HFIP	Hexafluoroisopropanol
HR-MS(ESI)	High Resolution Mass Spectrometry (Electrospray Ionisation)
M_n	Number-Average Molecular Weight
M_W	Weight-Average Molecular Weight
MALDI-ToF MS	Matrix-Assisted Laser Desorption Time-of-Flight Mass spectrometry
Oct	2-Ethylhexanoate
PBS	Phosphate Buffered Saline
PMMA	Poly(Methyl MethAcrylate)
ROCOP	Ring-Opening Copolymerisation
ROP	Ring-Opening Polymerisation
rt	Room temperature
SEC	Size-Exclusion Chromatography
TBD	1,5,7-Triazabicyclo[4.4.0]dec-5-ene
TBDMSCl	*Tert*-butyl-di-methyl silyl chloride
TFA	Trifluoro acetic acid
TGA	Thermogravimetric analysis
T_g	Glass transition temperature
TMC	Trimethylene Carbonate
TS	Transition State

1. Introduction

1.1. Polymers from Renewable Resources

Today, polymers are widely used in countless industrial sectors including packaging, automotive parts, textiles and construction as well as finding niche applications in medicine, electronics and agriculture: in 2015, 322 Mt of plastics were produced worldwide.[1] Moreover, polymers with advanced properties such as biodegradability, biocompatibility, conductivity or self-healing characteristics are also being sought for emerging applications in areas of regenerative medicine, flexible electronics and solar cells. However, the polymers that currently dominate the market, (polyolefins such as polypropylene and polyesters like polyethylene terephthalate) rely on finite fossil-based resources* and are environmentally persistent or costly to degrade, leading to concerns over growing ocean and landfill waste.[2,3] These environmental considerations have driven the investigation into polymers derived from renewable raw materials. This includes both the preparation of existing petrochemically derived-polymers from biomass as well as the design of new synthetic polymers from renewable building blocks that may show novel or enhanced properties such as degradability.[4-6]

For polymers to be considered sustainable, they should be cost-effective to produce, performance competitive with currently available polymers and to address end-of-life concerns, readily recyclable by degradation into environmentally benign products (over a reasonable timescale) or safe to incinerate allowing for some energy recovery.[7, 8] Examples of polymers derived from renewable feedstocks[4, 5, 9-12] include, those from lignin,[13, 14] vegetable oils,[15, 16] terpenes and terpenoids,[17, 18] amino-acids,[19, 20] carbohydrates[21] and carbon dioxide.[22, 23] Currently, bioderived polymers represent less than 1% of the total annual global production.[24] The utilisation of both CO_2 and sugars, in the preparation of aliphatic polycarbonates (APCs) for biomedical applications, forms the focus of this work.

Natural monosaccharides present a pool of readily available building blocks that are cheap, non-toxic, stereochemically rich and structurally diverse (linear and ring forms). They also provide huge scope for functionalisation and thus tailoring of polymer properties *via* the

* ~6% of oil produced worldwide is used in the manufacture of polymers.[1]

often high hydroxyl group content (Section 1.5).[21, 25] As such, sugars have been investigated as convenient raw materials for the development of synthetic polymers with characteristics, competitive to those of classical industrial polymers such as PET,[26-28] that mimic the structure and function of biomacromolecules[29, 30] and that target advanced properties such as biocompatibility.[31-33] Compared with natural polysaccharides such as cellulose, synthetic sugar-based polymers are attractive for overcoming some of the limitations of natural polymers in terms of source variability, contamination with biological toxins and need for extensive purification.[34]

Emitted from a myriad of industrial processes, carbon dioxide is an abundant, renewable, and safe (non-toxic and non-flammable) raw material. Hence, CO_2 is an attractive alternative C1 synthon to the use of hazardous phosgene or phosgene derivatives in conventional synthetic routes to polycarbonates or cyclic carbonate monomers (see Sections 1.3 and 1.4).[35-38] Although CO_2 is a contributor to global warming and reducing rising levels in the atmosphere is a current and urgent issue, its capture and utilisation by transformation into polycarbonates makes a marginal contribution to CO_2 mitigation. Moreover, the degradation of polycarbonates releases CO_2 and offers the potential for an overall carbon neutral process.[39-41] In 2016, 32.1 Gt of CO_2 was emitted globally,[42] industrial utilisation is around 200 Mt yr^{-1} and thus accounts for just 0.6% of anthropogenic emissions.[38] Uses of CO_2 as a feedstock include the synthesis of urea as a fertiliser (~160 Mt yr^{-1}), inorganic carbonates (~60 Mt yr^{-1}), polyurethanes (~18 Mt yr^{-1}), acrylic acids and acrylates (~10 Mt yr^{-1}), polycarbonates (~4 Mt yr^{-1}), organic carbonates (~100 kt yr^{-1}) and salicylic acid (~60 kt yr^{-1}).[43, 44]

1.2. Aliphatic Polycarbonates (APCs) for Biomedical Applications

Polycarbonates can be broadly classified into two groups based on the presence or absence of aromatic groups between the repeating [-O-C(O)-O-] carbonate linkages. To date, aromatic polycarbonates have received the most attention commercially. In particular, bisphenol-A polycarbonate, prepared in the 1950s, led to the widespread industrial development of aromatic polycarbonates and their now common use as engineering plastics in aircrafts, electronics, construction and biomedical materials owing to their high thermal stability, impact resistance, mechanical strength and optical transparency.[45] Aliphatic polycarbonates (APCs) on the other hand, have characteristically low melting points, poor

thermal stability and are more susceptible to hydrolysis. However, their degradability as well as low toxicity and mechanical properties (e.g. elasticity), similar to those of living tissues, have led to a renewed interest in their potential as versatile, soft degradable materials for biomedical applications.[46]

In particular, current research focus is on the construction of functionalised APCs showing enhanced biocompatibility and biodegradability properties as promising materials for tissue engineering scaffolds and drug-delivery carriers.[47-50] Traditional polycarbonates, lacking functionality and showing high hydrophobicity such as poly(trimethylene carbonate) resulted in insufficient cell compatibility (poor wetting and thus poor cell spreading, interaction and attachment). Hydrophilicity/functionality can be introduced *via* the choice and derivatisation of the monomer, by post-polymerisation modification of pendent reactive groups or through copolymerisation.[47, 51] For example, diblock copolymers comprised of monomethoxy-polyethylene glycol and hydrophilic APC segments derived from dihydroxyacetone have been used to prepare injectable hydrogels that showed good *in vivo* biocompatibility and biodegradability to inert products.[52] Hydrogels, chemically or physically cross-linked polymer networks capable of holding large amounts of water, have applications in wound dressings, personal care products and tissue engineering scaffolds.[53,54] Nanohydrogels constructed from hyperbranched and cationic APCs bearing multiple amine and hydroxyl functional groups were reported by Jia *et al.*[55] and showed pH response behaviour that was potentially promising for local drug release in acidic microenvironments. Guanidinium-rich amphiphilic oligocarbonates have also been designed and synthesised as biodegradable vectors for the delivery and release of small interfering RNA.[56]

The natural origin and high hydroxyl group content of many sugars makes them attractive versatile building blocks for the preparation of hydrophilic functional APCs that are likely to impart biocompatibility properties and lead to benign degradation products. Many of the targeted applications of sugar-based polymers, in general fall within the biomedical field (See Section 1.5).[21] Moreover, polymers bearing pendent carbohydrate groups can display specific interactions with proteins such as the protein receptors on cell surfaces, aiding both cell attachment in tissue engineering applications and for targeting specific cells such as cancer cells.[47] The cyclic structure often adopted by monosaccharides, when retained upon incorporated into a polymer backbone, can also impart stiffness to the main chain leading to higher glass transition temperatures (T_g).[57] A high T_g is one consideration in materials for

tissue engineering scaffolds as it corresponds to a low free volume in the polymer network, which limits the access of water and results in enhanced stability to hydrolytic degradation in the aqueous medium for cell growth.[58]

In contrast to aliphatic polyesters such as poly(lactic acid) or poly(lactic-*co*-glycolic acid), which have being widely investigated as degradable biomaterials, the hydrolytic degradation of APCs leads to less acidic breakdown products, the accumulation of which *in vivo*, can be detrimental to loaded drugs or surrounding tissues. APCs are generally also considered to be more resistant to hydrolysis than aliphatic polyesters, which can be advantageous for tissue-engineering scaffolds as well as be exploited through copolymerisation to yield desired degradation profiles for specific applications. Copolymers of trimethylene carbonate and lactide have already found application as sutures and in controlled drug delivery.[51]

1.3. Synthetic Routes to APCs

There are three main routes to polycarbonates: polycondensation of diols with phosgene, phosgene derivatives or dialkyl carbonates [Figure 1.01(a)], ring-opening copolymerisation (ROCOP) of epoxides with CO_2 [Figure 1.01(b)] and ring-opening polymerisation (ROP) of cyclic carbonates [Figure 1.01(c)].

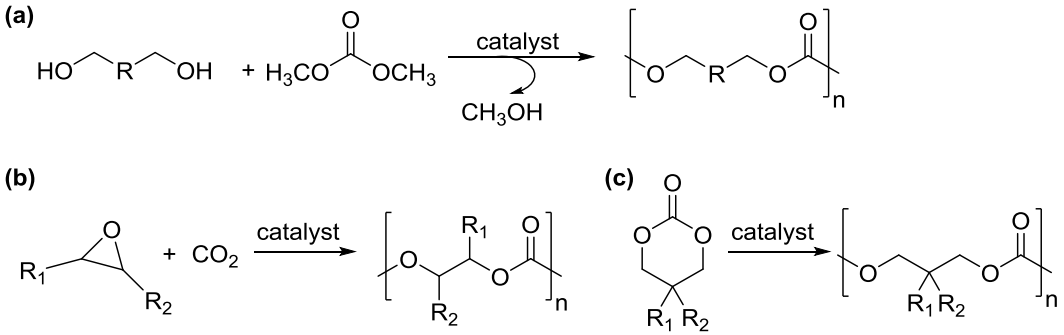

Figure 1.01. Preparation of APCs by **(a)** polycondensation of aliphatic diols with dialkyl carbonates, **(b)** ring-opening copolymerisation (ROCOP) of epoxides with CO_2 and **(c)** the ring-opening polymerisation (ROP) of cyclic carbonates.

CO_2 can be utilised by direct incorporation into the polycarbonate backbone or in the synthesis of cyclic carbonate monomers for ROP. Nevertheless, the direct transformation of CO_2 presents significant thermodynamic and kinetic challenges. As an entropic by-product of combustion, giving carbon in its already most oxidised state, CO_2 is a relatively stable and inert building block (ΔG_f° = -394 kJ mol^{-1}).[36, 38] Reactions of CO_2 are often endothermic,

requiring a large energy input or the use of a highly reactive partner. In nature, photosynthesis transforms around 200 billion tonnes of CO_2 per year into carbohydrates but there are relatively few synthetic reactions capable of achieving this large scale conversion.[37] Non-reductive CO_2 transformation, as for the synthesis of carbonates and polycarbonates (where the +IV oxidation state of the carbon is maintained) is promising because of the lower energy input required compared with reductive transformations such as the hydrogenation of CO_2 to methanol or formic acid. Reactions may then be moderately thermodynamically favourable but still require the development of catalysts and processes to the lower the kinetic energy barrier (Figure 1.02).[35, 39, 40, 59, 60]

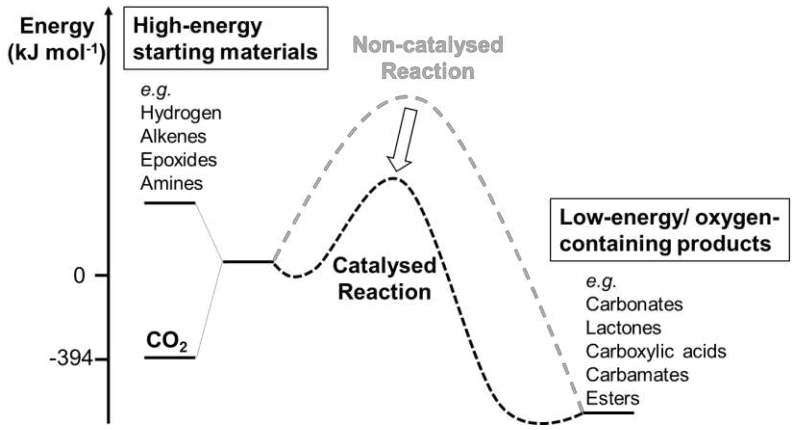

Figure 1.02. Schematic illustration of the energy balance for chemical fixation of CO_2. Reproduced from Peters *et al*.[39]

1.3.1. Polycondensation

APCs have been widely prepared by traditional polycondensation routes with phosgene or phosgene derivatives. However, the highly toxic and hazardous nature of phosgene gas and its preparation *via* an energy intensive process that generates a large amount of chlorinated waste, has led to its replacement with dialkyl carbonates.[61] In particular, dimethyl carbonate (DMC) is considered to be a more environmental benign reagent, which can be prepared from CO_2.[62] Nevertheless, and although industrially used, the step-growth polymerisation is often associated with poor control over polymer molecular weights (number-average molecular weight, M_n and weight-average molecular weight, M_w) as well as broad molecular weight distributions (Đ= M_w/M_n). These parameters are known to significantly impact both polymer degradation and mechanical properties.[46] Further drawbacks include high reaction temperatures and long reaction times.

Poly(butylene carbonate), poly(pentamethylene carbonate) and poly(hexamethylene carbonate) were however, prepared by Zhu *et al.*[63] with M_w over 166 000 g mol^{-1} and narrow Đ (≤ 1.86) using a TiO_2/SiO_2 based-catalyst (TSP-44) in the melt with DMC (Figure 1.03). The two-step process, involving transesterification and polycondensation gave polymer yields of over 85% but required reactions temperatures up to 230 °C and polymerisation times over 24 hours.

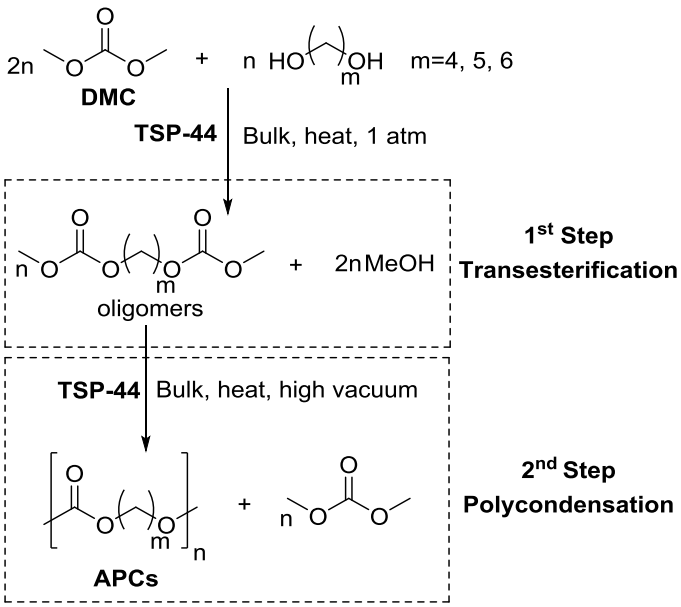

Figure 1.03. High M_w APCs by a two-step polycondensation of DMC with aliphatic diols. Reported by Zhu *et al.*[63]

Despite the inertness of CO_2 and the severe equilibrium limitation of the reaction, Tomishige and coworkers[64] reported the direct copolymerisation of CO_2 with diols using CeO_2 catalyst and 2-cyanopyridine promotor (See also Section 1.4.1: cyclic carbonates from CO_2 and diols with CeO_2/2-cyanopyridine). Although only co-oligomers (M_n ≤ 1650 g mol^{-1}) were prepared, at CO_2 pressures of 0.5 to 5 MPa and 130 °C, high diol conversions (up to 99%) and selectivities (>99%) for alternating copolymerisation were reported and for various C4- C10 α,ω-diols (Scheme 1.01).

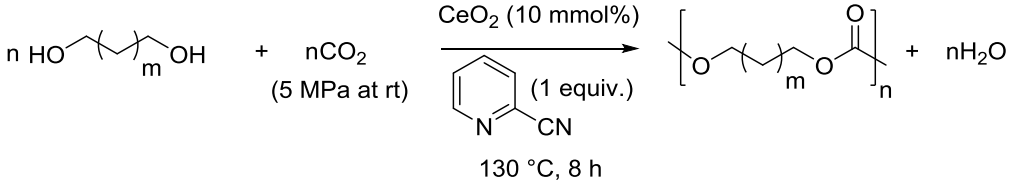

Scheme 1.01. Direct copolymerisation of CO_2 with diols reported by Tomishige and coworkers.[64] Polymerisation conditions refer to a typical procedure with 1,4-butanediol.

Sugar-based polycarbonates have also been prepared by polycondensation. For example, homo-polycarbonates of isosorbide, derived from starch (Scheme 1.02), were synthesised by a two-step melt polycondensation with DMC using lithium acetylacetonate catalyst.[65] Isosorbide conversions of 95% were achieved giving M_n of up 28 800 g mol^{-1} (Đ 1.61) and owing to the rigid bicyclic sugar structure, the polycarbonates exhibited high T_g values of up to 167 °C by differential scanning calorimetry (DSC). Amorphous co-polycarbonates were also prepared from isosorbide, DMC and equimolar amounts of aliphatic diols to give M_n up to 34 400 g mol^{-1} (Đ 1.64) with T_g values ranging from 46 to 88 °C.

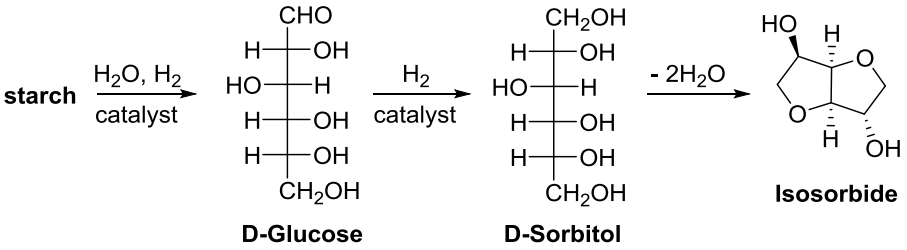

Scheme 1.02. General scheme for the synthesis of isosorbide from starch. Reproduced from the 2010 review article by Fenouillot *et al.*[57] on the use of 1,4:3,6-dianhydrohexitols; isosorbide, isomannide and isoidide in polymers (mainly polyesters by polycondensation).

Wooley and coworkers[66] employed multiple protection-deprotection sequences to prepare four regioisomeric diols from D-glucose. Polycondensation with phosgene comonomer yielded linear poly(glucose carbonates) with different backbone regio-connectivites (Figure 1.04). M_n above 10 000 g mol^{-1} (Đ ≤ 1.67) where prepared from the 2,6- and 3,6- diols compared with less than 8 000 g mol^{-1} (Đ ≤ 1.20) for the carbohydrate monomers with an unprotected hydroxyl group at the anomeric centre (1,4- and 1,6- diols). The different regio- connectivity in the polycarbonate backbones impacted on the polymer thermal properties. Those with 2,6- and 3,6- regio-connectivity displayed significantly higher glass transition temperatures of 83 and 85 °C, respectively compared with those with 1,4- and 1,6- backbone linkages (T_g ~ 33 °C). Higher thermal stability was also observed, by thermogravimetric analysis (TGA), for the polycarbonates where the linkages were not from the anomeric carbon (2,6- and 3,6-APCs).

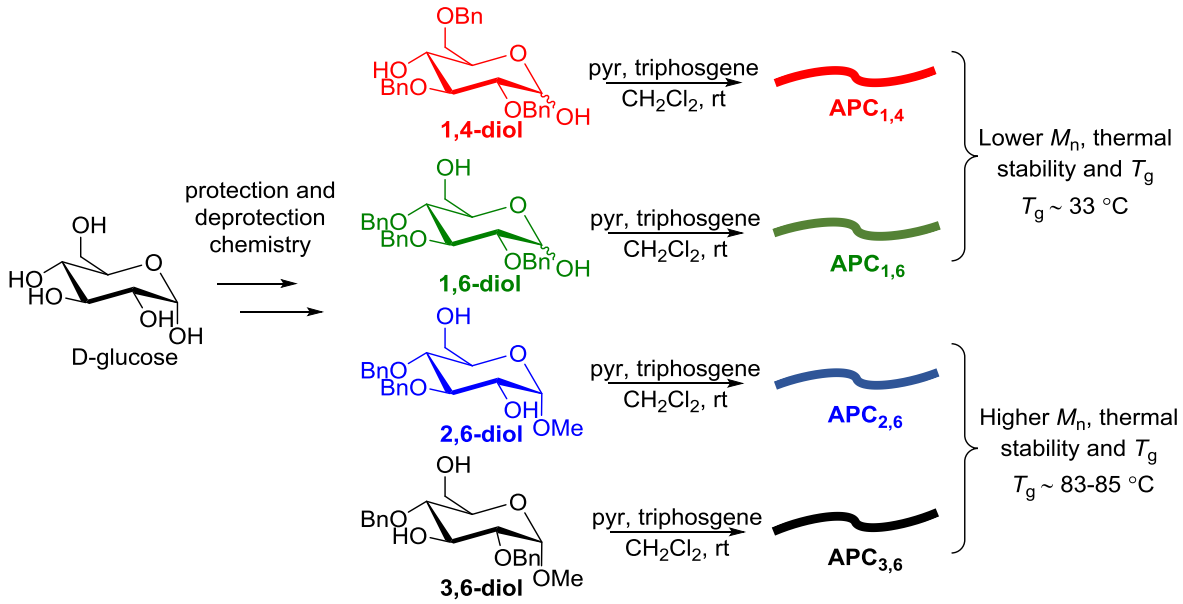

Figure 1.04. Synthesis of four regioisomeric diol monomers from D-glucose and polycondensation with phosgene (formed *in situ* from triphosgene) to prepare glucose-based APCs with different backbone connectivities. Modified from Wooley and coworkers.[66]

1.3.2. Ring-opening copolymerisation (ROCOP) of epoxides and CO_2

The alternating copolymerisation of CO_2 with epoxides has been extensively studied as a promising, more sustainable route to polycarbonate production. Lying in a potential energy well, the coupling of CO_2 with high-energy strained heterocycles can make the thermodynamics of CO_2 transformation more favourable. Importantly, the development of a range of catalysts has also enabled the limiting kinetic energy barrier to be lowered.[22] Since the initial discovery of a heterogeneous zinc-based catalyst by Inoue and coworkers[67] in 1969, numerous homogeneous and heterogeneous catalysts have been reported for the ring- opening copolymerisation (ROCOP) of epoxides with CO_2. Many of these, alongside mechanistic insights are summarised in several comprehensive review articles.[23, 68-71] Examples of active homogenous metal-based catalysts include those bearing porphyrin, β- diiminate, phenoxy-amine and Schiff base (salen and salan) ligand classes (Figure 1.05). Reported heterogeneous catalysts include metal oxides, zeolite and smectite catalysts as well as supported organic bases, organometallic catalysts and ionic liquids.[72, 73]

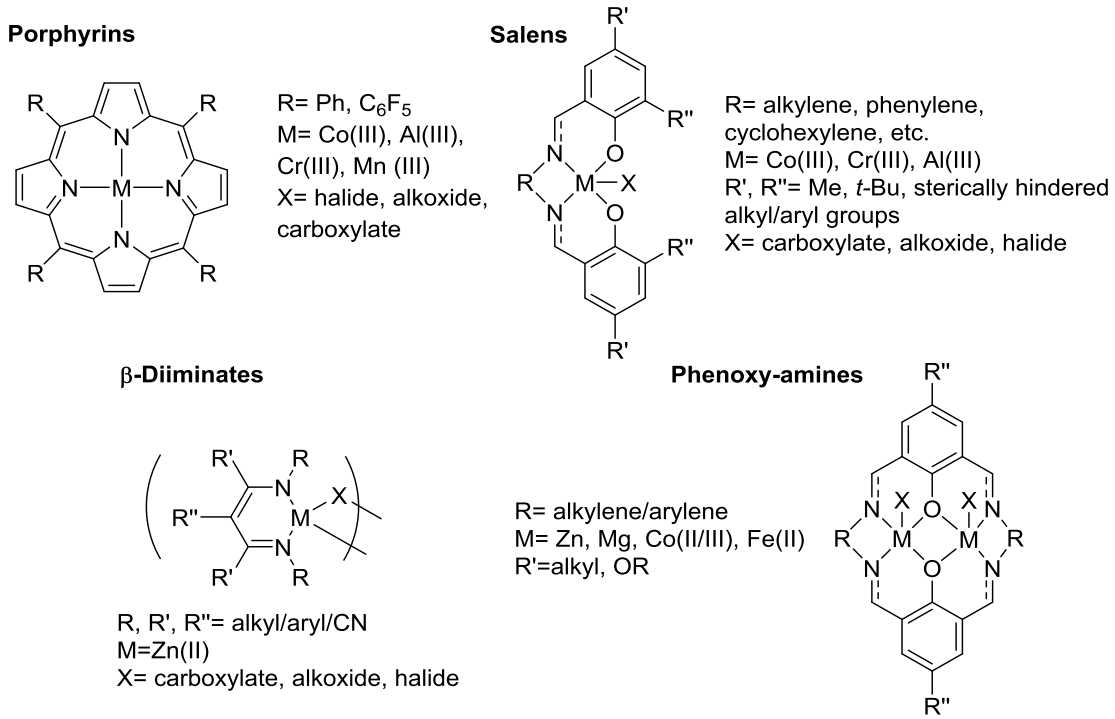

Figure 1.05. Examples of active homogenous metal catalysts for ROCOP of CO_2 and epoxides. Reproduced from Romain *et al.*[69]

The coordination-insertion mechanism for CO_2 and epoxide copolymerisation catalysed by for example, metal halide or carboxylate complexes is shown in Figure 1.06. Initiation occurs by coordination of the epoxide to the metal centre and nucleophilic ring opening with the halide or carboxylate anion to form a metal-bound alkoxide. This undergoes CO_2 insertion to a metal-bound carbonate for chain propagation by nucleophilic attack on another coordinated epoxide. Alternating copolymerisation of the epoxide and CO_2 comonomers leads to polycarbonate formation but consecutive epoxide ring-opening or decarboxylation reactions can introduce ether linkages into the main chain, affecting the polymer properties. Chain transfer by intramolecular back-biting of the polymer end, reforming the metal alkoxide species, can also lead to five-membered cyclic carbonate by-products. These are thermodynamically stable with respect to the polymer and do not readily undergo ROP like the six-membered analogues (see Section 1.3.3).[69, 71] Catalyst design has led to the suppression of these competing side-reactions, yielding good selectivity for polycarbonate *versus* cyclic carbonate formation with minimal polyester linkages. For example, bifunctional cobalt salen complexes bearing pendent ammonium cations on the ligand framework showed high selectivity ($\geq$ 90%) for formation of poly(propylene carbonate) with over 99% carbonate linkages at 20 bar CO_2 pressure and 80 °C.[74] Moreover, the tolerance of

dinuclear Zn and Mg catalysts to impurities in CO_2 captured from a power plant was demonstrated by Chapman *et al.*[75]

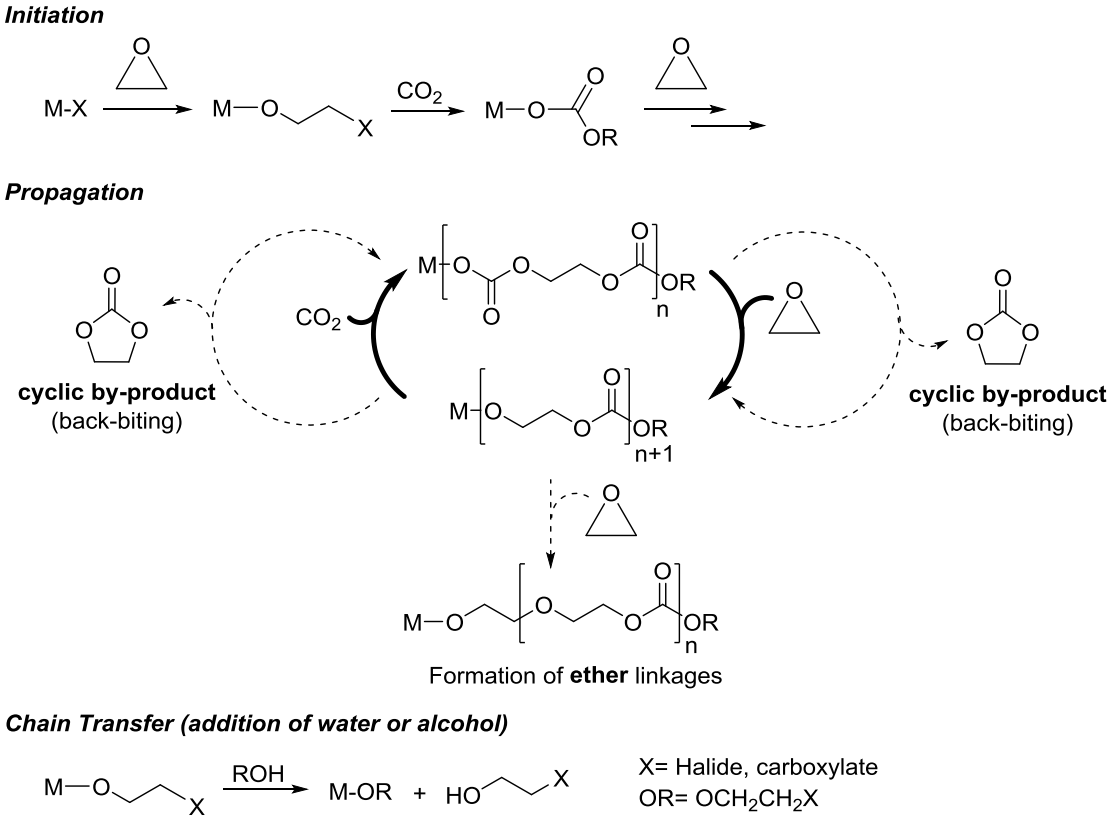

Figure 1.06. Proposed catalytic cycle for the copolymerisation of epoxides with CO_2. Consecutive epoxide ring-opening can lead to polyether linkages and backbiting of the polymer chain, to five-membered cyclic carbonate by-products. Modified from Romain *et al.*[69] and Kember *et al.*[71]

Hence, the main limiting factor in this approach to polycarbonates is the substrate scope. Regardless of the catalyst, some epoxides such as cyclohexene oxide tend to readily give rise to polycarbonates whereas ethylene oxide or propylene oxide often lead to cyclic carbonate formation. Catalysts can also be selective for certain epoxides such as terminal epoxides, limiting their scope. Epoxides are typically prepared by the oxidation of alkenes or dehydration of alcohols and commonly reported examples for ROCOP with CO_2 are propylene, cyclohexene and styrene oxide. Further to petroleum-derived epoxides, there are also those prepared from natural renewable resources such as limonene oxide[76] and 1,4- cyclohexadiene oxide from plant oil derivatives.[77] Nevertheless, the ease of synthesis particularly, with regards to carbohydrate feedstocks and the difficultly in handling highly reactive epoxides can be limiting.

Although the synthesis and handling of four-membered cyclic ethers, oxetanes can still pose a challenge, their alternating ROCOP with CO_2 can also be carried out to yield polycarbonates with minimal ether linkages.[78] In this case, the cyclic carbonate by-product is a six-membered ring (Scheme 1.03), which readily undergoes ROP. At 50 °C and 10 bar CO_2 pressure, trimethylene carbonate (TMC) was isolated exclusively using a (salen)Cr(III)Cl complex with *n*-Bu_4NX co-catalyst,[79] whereas at 110 °C this was an effective catalyst for the formation of poly(trimethylene carbonate). Halide ions in solution were thought to bring about the anionic ROP of the cyclic carbonate at higher temperatures.[80]

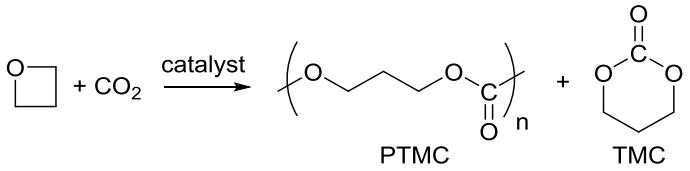

Scheme 1.03. Copolymerisation of oxetanes with CO_2 to form APCs and six-membered cyclic carbonate by-products.[79]

1.3.3. Ring-opening polymerisation (ROP) of cyclic carbonates

Since the publication of the thermally induced ring-opening polymerisation (ROP) of TMC (with K_2CO_3 initiator) by Carothers in 1930,[81] many ROP processes have been developed and classified by their mechanism of action namely, anionic, cationic, zwitterionic, radical, metathesis, and coordination–insertion.[82] Represented generally in Figure 1.07 for heterocyclic monomers possessing polarised functional groups, is the heterolytic bond dissociation on ring-opening with a nucleophile (anionic ROP) or electrophile (cationic ROP). The ability of cyclic monomers to undergo ROP is governed by both the kinetics, which is influence by the choice of catalyst and the thermodynamic equilibrium behaviour. The conversion of monomers into a macromolecule must be allowed thermodynamically ($\Delta G_p < 0$) and as the entropy term is generally unfavourable ($\Delta S_p^\circ < 0$), the relief of ring strain must be large enough to yield a negative free enthalpy ($\Delta H_p^\circ < 0$). Therefore, ring size and substitution pattern can have a significant impact on the polymerisation behaviour. For example, the presence of multiple substituents does not generally favour polymerisation.[83] In the most typical case, when $\Delta S_p^\circ < 0$ and $\Delta H_p^\circ < 0$, low temperatures and high monomer concentration favour polymerisation equilibrium thermodynamics.[84, 85]

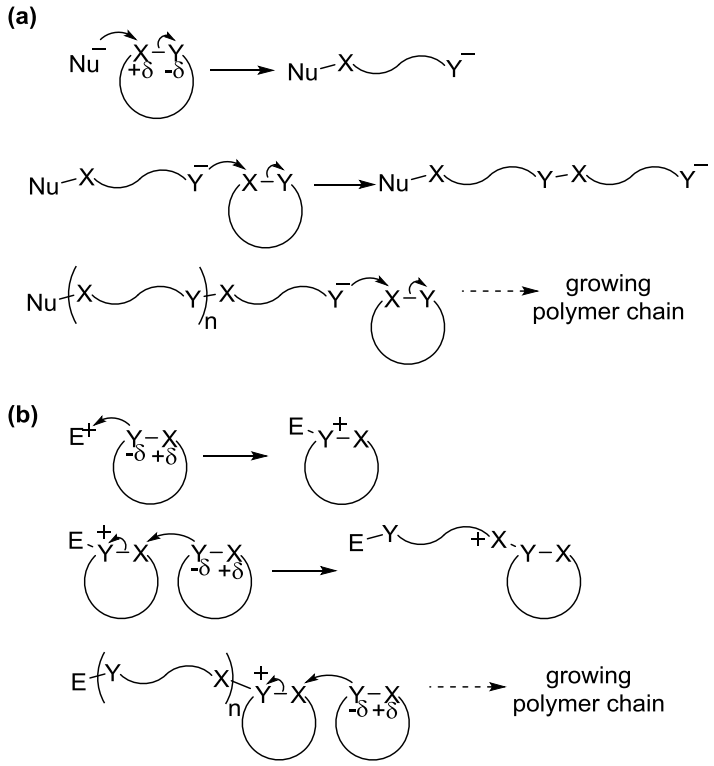

Figure 1.07. General mechanism for **(a)** anionic and **(b)** cationic ROP (S_N2 shown, S_N1 also possible), adapted from Endo.[86]

Significant developments in ROP catalysis[9] has enabled the controlled polymerisation of numerous cyclic monomers[10] and under mild reaction conditions, leading to high and predictable molecular weight polymers with low Đ.[46] Due to the structural similarity, the majority of ROP catalysts developed for cyclic esters are also active for cyclic carbonate monomers though, differences in the electrophilicity of the carbonyl carbon can lead to changes in the polymerisation kinetics.[87] In addition to many metal-based ROP catalysts,[88,89] there are also a variety of organocatalytic systems[90] including 4-(dimethylamino)pyridine, 1,8-diazabicyclo[5.4.0]undec-7-ene (DBU), 1,5,7-triazabicyclo[4.4.0]dec-5-ene (TBD),[91] 4- pyrrolidinopyridine, *N*-heterocyclic carbenes, ureas,[92] thioureas,[93, 94] as well as various phosphines, phosphazenes and organic phosphoric acids.[95] The functional diversity of cyclic carbonate monomers compared with lactones like lactide and ε-caprolactone combined with the controllable nature of ROP techniques offers the potential to access a wide-range of well- defined and functional degradable polymers.[51]

Many of the cyclic carbonates reported to undergo ROP are six-membered rings though, there are examples of seven-,[96] eight-[97] and highly strained five-[98-100] membered monomers. Typically, the latter do not undergo polymerisation or require forcing conditions (such as high temperatures) that result in elimination of CO_2 and formation of polyether linkages.[82]

Those that undergo ROP, under mild reaction conditions and without decarboxylation, contain the five- membered cyclic carbonate *trans*-fused to a cyclohexane,[98] cyclohexene,[99] or pyranose sugar ring (see Chapter 5).[100] In contrast to the unreactive *meso*- carbonate, the polymerisation of *trans*-cyclohexene carbonate proceeded with both metal- and organo-based catalysts and alcohol initiator at 60 to 130 °C to afford polycarbonates with M_n up to 17 000 g mol^{-1}.[98] ROP of *trans*-1,4-cyclohexadiene carbonate, under similar conditions, was less reactive indicating subtle effects of the *trans*-fused six-membered ring on the monomer ring stain.[99]

Traditionally, cyclic carbonate synthesis involves the use of phosgene or phosgene derivatives. Thus, both for sustainable polycarbonate synthesis by ROP and the various other applications of cyclic carbonates (as solvents and battery electrotypes),[40] a growing research effort has focused on the avoidance of these reagents. In particular, the utilisation of CO_2 as a carbonylating agent has become an active field of research. Ideally, from an atom-economy perspective, the most efficient method would be to directly couple CO_2 with diols to yield the cyclic carbonate with water as the only by-product.

1.4. Cyclic Carbonates from CO_2 and Diols

Compared to the well-established synthesis of five-membered cyclic carbonates by the cycloaddition of CO_2 with epoxides (industrialised in the 1950s),[40] the direct coupling of CO_2 with diols is more challenging due to the lower reactivity of hydroxy groups. Many of these reactions are only slightly thermodynamically favourable or even unfavourable. Thus, dehydrating agents are often used to remove the water by-product and pull the equilibrium over towards the cyclic carbonate product and can be categorised into two types: reactive and non-reactive. Non-reactive dehydration systems include inorganic absorbents, gas phase systems and membrane separation techniques and have the advantage of not significantly impacting on the kinetics of the reaction or activity of the catalyst employed. Drawbacks however include a limitation of the CO_2 pressure to below 5 bar with membrane systems and reaction temperatures below 100 °C for inorganic absorbents such as molecular sieves. Reactive dehydration systems use inorganic or organic reagents that react with the water present in the reaction media and thus can work at temperatures above the boiling point of water. The exothermic nature of the hydration of nitriles, for example can also provide a further driving force in carbonate synthesis. Such systems should however be safe, easy to

handle and produce minimum side-products. Non-catalytic dehydration systems that have been employed include CH_3I, trimethylphosphate, *N,N'*-dicyclohexylcarbodiimide, acetals, butylene oxide and ionic liquids. The hydration of acetonitrile is a commonly reported dehydration method but often results in the formation of by-products.[101]

Further to the thermodynamic limitation, the high kinetic energy barrier for CO_2 transformations, requires the development of catalysts. Currently, there are few efficient catalysts reported for the direct coupling of diols with CO_2 to form cyclic carbonates. Most achieve low yields or selectivities and focus on the preparation, from 1,2-diols, of the more stable and thus easier to prepared five-membered cyclic carbonates such as ethylene and propylene carbonate. The catalysts can be broadly categorised into heterogeneous metal oxides and homogeneous, organotin-compounds, metal acetates and metal carbonates as well as metal-free routes. Many were included in the review by Tamura *et al.*[102]

1.4.1. Heterogeneous metal oxide catalysts

To date, arguably the most efficient system for the direct coupling of CO_2 and diols to form both five- and six-membered cyclic carbonates is the use of CeO_2 catalyst with 2- cyanopyridine dehydrating agent, reported in 2014 by Tomishige and coworkers [Figure 1.08(a)].[103] This carboxylation/hydration cascade system gave both high yields and selectivities for a range cyclic carbonates. For example, an almost quantitative yield was reported for the preparation of propylene carbonate from 1,2-propanediol and several six- membered rings were also prepared in high yields (62-97%). However, the process requires harsh reaction conditions, temperatures of up to 150 °C and 50 bar CO_2 pressure as well as 10 equivalents of the expensive 2-cyanopyridine dehydrating reagent, which (though potentially recyclable) can also be problematic to separate from the cyclic product. Moreover, the activity of the catalyst is highly sensitive to the size of the ceria particles. The proposed mechanism [Figure 1.08(b)] involves adsorption of one of the hydroxyl groups onto a Lewis acidic site of the CeO_2 catalyst to form a cerium alkoxide species. CO_2 insertion into the Ce-O bond and ring-closing by a nucleophilic addition-elimination mechanism yields the cyclic carbonate product and regenerates the catalyst. The molecule of water also eliminated is successively removed by hydration of 2-cyanopyridine, catalysed by the CeO_2 leading to high yields of the carbonate product.

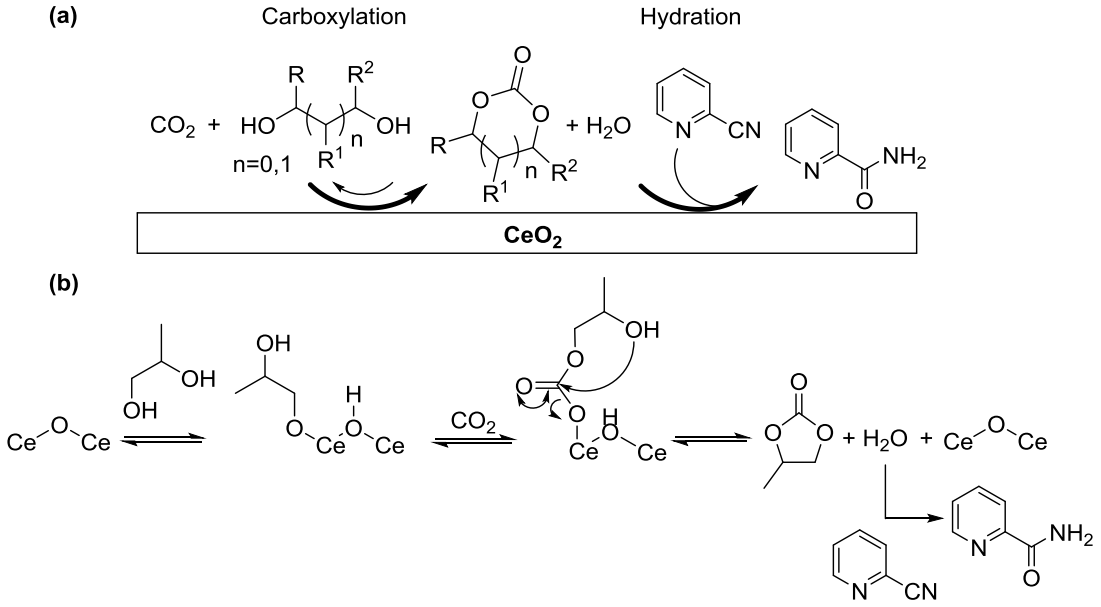

Figure 1.08. (a) Carboxylation/hydration cascade for the synthesis of cyclic carbonates from CO_2 and diols with CeO_2 catalyst and 2-cyanopyridne dehydrating agent. (**b)** Proposed mechanism with 1,2-propanediol and CO_2 to form propylene carbonate. Reproduced from Honda *et al.*[103]

The system built upon earlier work,[104, 105] using heterogeneous CeO_2-ZrO_2 systems, at similar reaction temperatures but lower 35 bar CO_2 pressure, which showed high selectivity (>99%) for the synthesis of five-membered ethylene and propylene carbonates but corresponding yields of only 1 to 2%. The use of KI/ZnO at 160 °C and 100 bar CO_2 pressure (supercritical conditions), gave higher 26% yields for propylene carbonate but with a reduced selectivity of 61%.[106] Acetonitrile was used as the solvent because of its role as a reactive dehydrating agent, undergoing hydrolysis to the acetamide. Removal of the water by-product led to improvements in the cyclic carbonate yield though, subsequent reaction of the acetamide with unreacted diol in the reaction mixture, to form diol acetates and ammonia, resulted in lower selectivities (Figure 1.09).

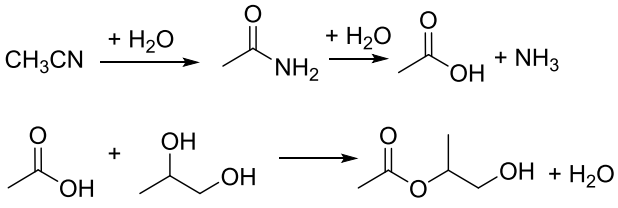

Figure 1.09. Role of acetonitrile as a dehydrating agent and subsequent reactions leading to unwanted side-products.

Magnesium and its oxide were also investigated as cheap and low toxic catalysts for the carbonylation of a variety of 1,2-diols with CO_2.[107] However, only low yields were reported (≤ 3% for the synthesis of propylene carbonate) at 180 °C and 150 bar CO_2 pressure

(supercritical conditions). *N*,*N*-Dimethylformamide (DMF) improved the catalytic performance alongside the use of a ketal dehydrating agent. The proposed mechanism (Figure 1.10) involves CO_2 insertion into the Mg-O bond of cyclic species **I**, formed on reaction of the diol with Mg. Ring-closing by intramolecular attack of the alkoxide at the carbonyl in the seven-membered ring intermediate **II**, eliminates the cyclic carbonate product and regenerates the catalyst.

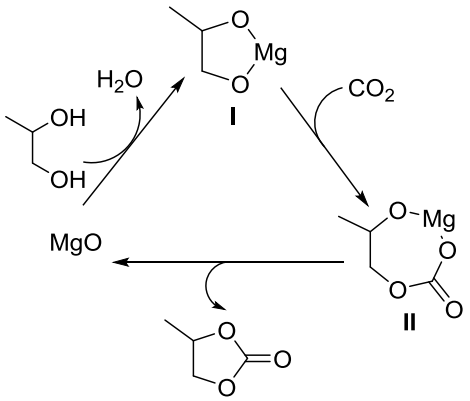

Figure 1.10. Mechanism postulated by Du *et al.*[107] for the Mg-catalysed synthesis of propylene carbonate from 1,2- propanediol and CO_2.

1.4.2. Homogeneous organotin compounds

Du *et al.*[108] first reported the use of dibutyltin oxide, *n*-Bu_2SnO and dibutyltin dimethoxide, *n*-$Bu_2Sn(OMe)_2$ as selective catalysts for the synthesis of propylene carbonate from 1,2- propanediol and CO_2 under supercritical conditions (180 °C and 200 bar CO_2 pressure). No cyclic carbonate was detected below 100 °C. Again, the use of DMF co-solvent led to enhanced catalytic activity and ketals were shown to be useful dehydrating agents in improving the cyclic carbonate yield, of which the maximum achieved was 42%.

These organotin compounds, alongside $Sn(OMe)_2$ were also investigated by Aresta *et al.*[109] for the catalytic conversion of CO_2 at lower 50 bar CO_2 pressure with glycerol, a waste product produced in large amounts during biodiesel production. After 15 hours at 180 °C, just 7% conversion was observed with *n*-$Bu_2Sn(OMe)_2$, for the reaction carried out neat with molecular sieves to remove the water by-product. At molar ratios, greater than 1.14:1 of carbonate to *n*-$Bu_2Sn(OMe)_2$, the rate of carbonate formation was found to decrease due to the formation of oligomers of the catalyst exhibiting lower catalytic activity.

Also using molecular sieves as a dehydrating agent, George *et al.*[110] reported a 35% yield for the formation of five-membered glycerol carbonate using 1 mol% *n*-Bu_2SnO at 120 °C and 138 bar CO_2 pressure. Under the same reaction conditions, cyclic carbonate yields of 42% and 61% were reported with 1,2-propanediol and 1,2-ethanediol, respectively. A methanol solvent was required for the reaction to proceed and this in combination with spectroscopic data, led to the proposed reaction pathway *via* *n*-$Bu_2Sn(OMe)_2$, shown in Figure 1.11.

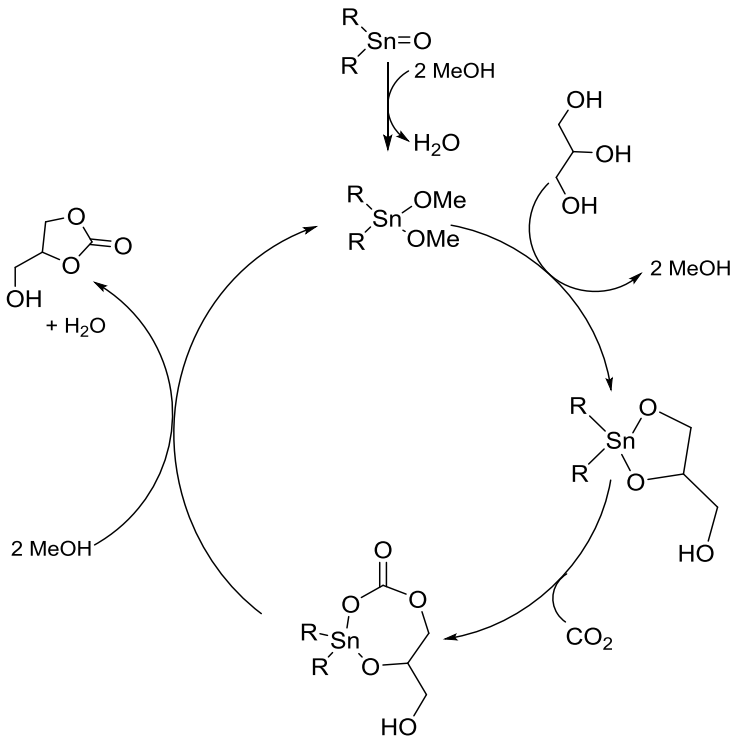

Figure 1.11. Reaction pathway proposed by George *et al.*[110] for glycerol carbonate formation with *n*-Bu_2SnO catalyst.

1.4.3. Metal acetates

Of several metal acetates screened, Huang *et al.*[111] reported anhydrous zinc acetate to exhibit the highest catalytic activity for the synthesis of propylene carbonate from CO_2 and 1,2-propanediol. After 12 hours at 2.5 mol% catalyst loading, 170 °C and 100 bar CO_2 pressure using acetonitrile as a dehydrating agent, a 24% yield (39% conversion) was achieved. No product was detected in the absence of acetonitrile and diol acetates such as 2-hydroxypropyl acetate (from reaction of the diol with the acetonitrile hydrolysis product) were detected in the reaction mixture in 13% yield. For less stable six-membered cyclic carbonates: 1,3- butylene carbonate and 1,3-propylene carbonate, lower yields (12-14%) and conversions (20-23%) were reported.

Zhao and coworkers[112] used *in situ* FTIR spectroscopy to monitor the zinc acetate catalysed reaction with 1,2-propanediol and CO_2 at a lower 160 °C reaction temperature and 30 bar CO_2 pressure. A shift in the hydroxyl stretch of the diol on interaction with the zinc acetate (from 3323 to 3184 cm^{-1}) implied a weakening of the bond consistent with species **I** in the proposed reaction mechanism shown in Figure 1.12. An increase in the ratio of the intensity of the Zn-O bond relative to that of the carboxylic acid anion also suggested formation of species **III**.

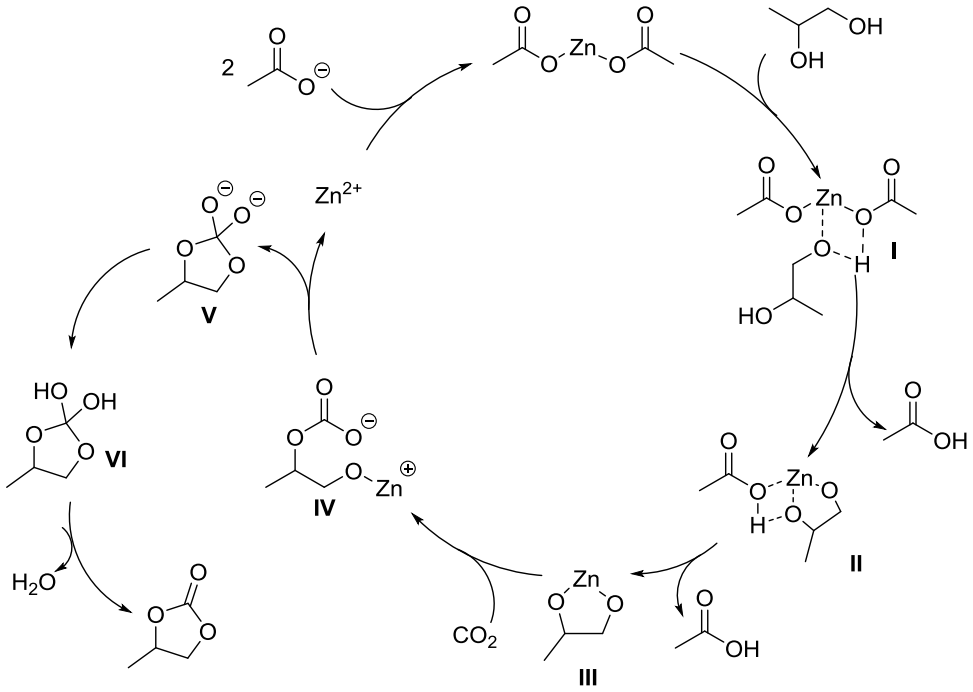

Figure 1.12. Mechanistic cycle proposed by Zhao *et al.*[112] for the direct coupling of diols with CO_2 using zinc acetate catalyst.

1.4.4. Alkali metal carbonates

The cyclic carbonate yield was found to depend upon the basicity of the alkali metal carbonate catalyst employed. Stronger bases gave higher yields because they promoted the hydration of the acetonitrile solvent with the water by-product from cyclocarbonation.[113] Under the same reaction conditions (15 hours, 100 bar CO_2, 175 °C and 5 mmol% catalyst loading), decreasing propylene carbonate yields of 16, 12 and 6% where obtained with Cs_2CO_3, Na_2CO_3. with K_2CO_3, respectively. Addition of ammonium carbonate resulted in enhanced selectivities for the cyclic carbonate, including 100% in combination with Cs_2CO_3 catalyst (compared to 59% without NH_4CO_3) but lowered the yield to 11%. Thermal decomposition of the ammonium carbonate to generate ammonia was suggested to inhibit

the dehydrating role of the solvent. Under the same conditions of temperature and CO_2 pressure, propylene carbonate was also reported in 20% yield using benzonitrile dehydrating solvent.[114]

Cs_2CO_3 has also been used in non-catalytic amounts with haloalcohols for the synthesis of several five and six-membered cyclic carbonates under mild reaction conditions (1 atm CO_2 pressure and 40 °C).[115] From 3-chloro-1-propanol, a 95% yield of TMC was reported after 15 hours in DMF solvent. The alkali metal carbonate was proposed to be acting as base, deprotonating the hydroxyl group to form the alkoxide as a better nucleophile for reaction with CO_2 (Figure 1.13). Intramolecular ring-closure then occurs by elimination of the chloride and formation of CsCl. Nevertheless, conversion of the diol to the haloalcohol entails extra synthetic steps.

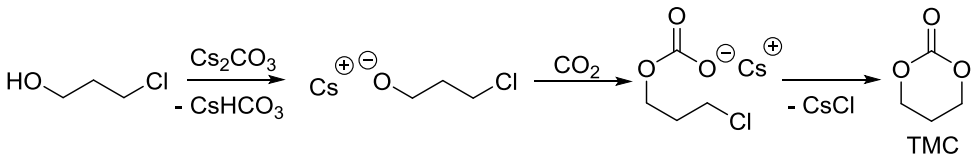

Figure 1.13. Reaction mechanism proposed by Reithofer *et al.*[115] for the formation trimethylene carbonate (TMC) with Cs_2CO_3 acting as a base.

1.4.5. N-Heterocyclic carbenes and metal-free routes

In line with the growing interest in *N*-heterocyclic carbenes for CO_2 activation *via* formation of imidazolium carboxylates, Dyson and coworkers[116] recently described the synthesis of cyclic carbonates from diols and CO_2 using heterocyclic carbene catalysts. The reaction also required Cs_2CO_3 base to proceed and an alkyl halide to act as a leaving group. The optimised reaction conditions are detailed in Scheme 1.04 for the synthesis of a six-membered cyclic carbonate in reasonable 53% yield. The proposed reaction mechanism is shown in Figure 1.14. ^{13}C labelled CO_2 was used to confirm this was main source of the carbonyl group incorporated into the carbonate.

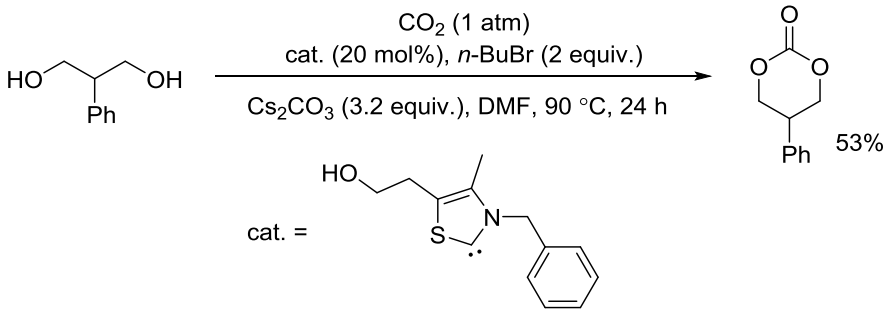

Scheme 1.04. Cyclic carbonate synthesis from diols and CO_2 using heterocyclic carbene catalysts with Cs_2CO_3 base and alklyl halide leaving group in DMF at 90 °C.[116]

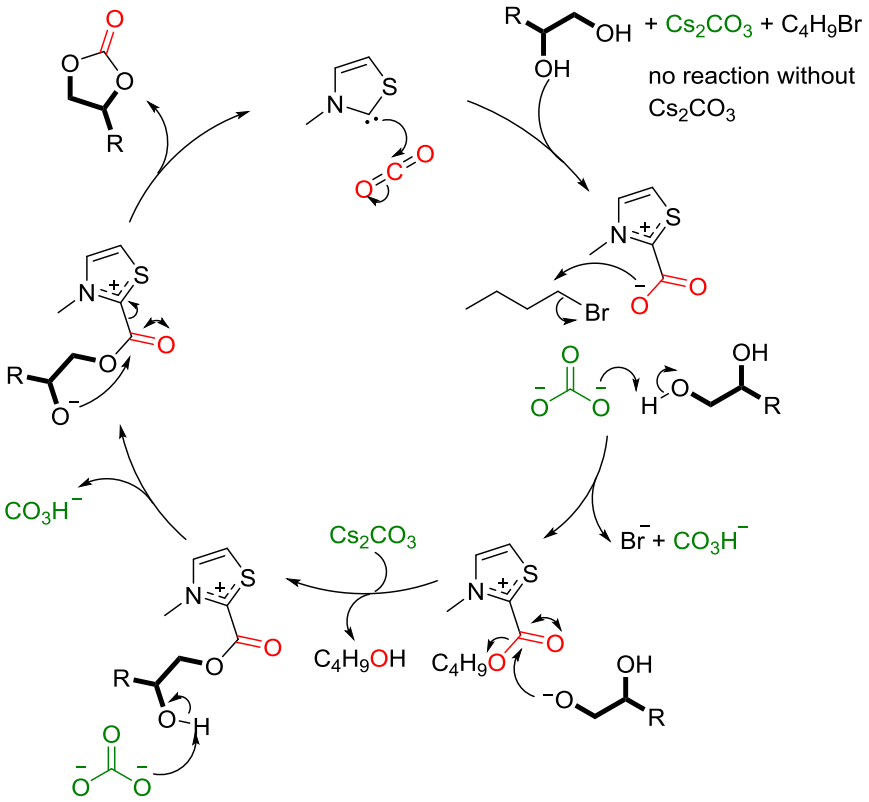

Figure 1.14. Tentative mechanism proposed by Dyson and coworkers[116] for the carbene catalysed formation of cyclic carbonates from diols and CO_2 with Cs_2CO_3 and *n*-BuBr. Substituents on the carbene are omitted for clarity.

Lu and co-workers[117] also used *N*-heterocyclic carbenes in combination with methyl iodide and K_2CO_3 for the synthesis of five-membered cyclic carbonates under mild reaction conditions of 40 °C and 1 atm CO_2 pressure. The carbene was generated electrochemically from ionic liquid imidazolium cations by single electron cathodic reduction (Scheme 1.05). A maximum yield of 60% was reported after 2.5 hours, for the synthesis of styrene carbonate from the corresponding diol and CO_2.

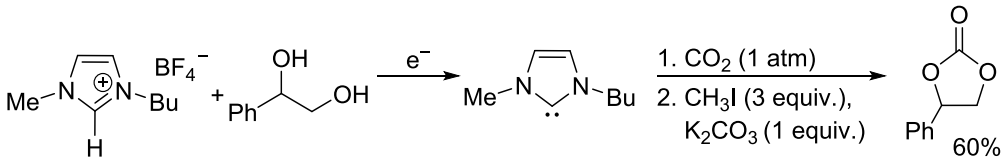

Scheme 1.05. Electrosynthesis of styrene carbonate from CO_2 and glycol *via* an electrogenerated *N*-heterocyclic carbene.[117]

Discussed in detail in Chapter 2, organic superbases such as TBD and DBU have also been reported for both the catalytic and non-catalytic coupling of diols with CO_2. Huang *et al.*[118] used 2.5 mmol% catalyst loading for the direct coupling of 1,2-propanediol with CO_2 to form propylene carbonate in yields of up 23% in acetonitrile solvent after 15 hours at 175 °C and 100 bar CO_2 pressure (supercritical conditions). Jang and coworkers[119] also reported the use of amidine and guanidine bases for both five- and six-membered cyclic carbonate formation but in non-catalytic amounts.

1.4.6. Other non-phosgene based methods to cyclic carbonates

Further to the direct coupling of CO_2 with diols, other non-phosgene based methods have also been developed for the synthesis of cyclic carbonates. These include strategies that either start from diols or utilise CO_2 as a C1 resource. For example, the direct oxidative carboxylation of olefins builds upon the fixation of CO_2 with epoxides by combining the processes of epoxidation and carbonation. However, in addition to being limited to five- membered cyclic carbonates, both homogeneous Rh-catalysts and heterogeneous metal oxides (especially Nb_2O_2), investigated for the preparation of styrene carbonate from styrene, oxygen and CO_2, gave yields of only 1 to 2%.[120]

Aresta and co-workers[121] reported a high yielding route to ethylene carbonate by reaction of the ketal formed from 1,2-ethanediol and cyclohexanone with supercritical CO_2 (sc-CO_2) in the presence of a metal catalyst. Several catalysts were tested, the most active being the copper and iron complexes of the perfluoro diketone ligand shown in Figure 1.15. This approach is however limited by slow kinetics and the need to separate the products to recycle the cyclohexanone.

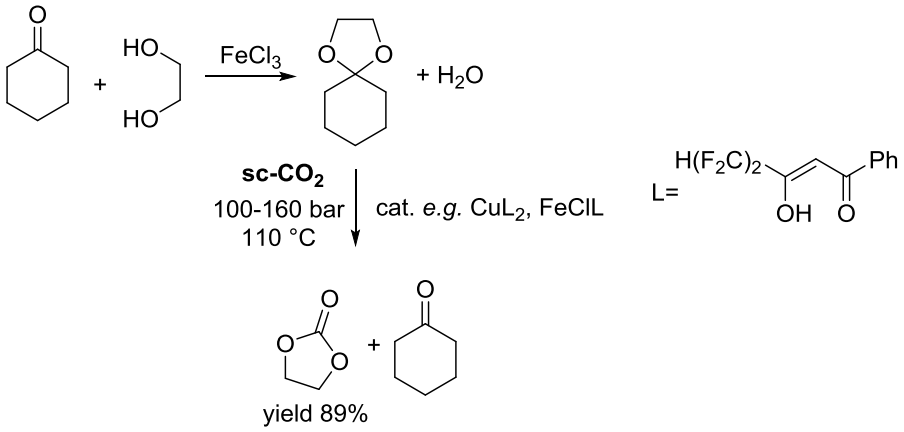

Figure 1.15. Synthesis of ethylene carbonate by reaction of the ketal with sc-CO_2 in presence of a metal catalyst bearing perfluoro alkyl groups.[121]

Finally, Gabriele *et al.*[122] synthesised several five and six-membered cyclic carbonates by direct carbonylation of the corresponding 1,2- and 1,3-diols using carbon monoxide under oxidative conditions with PdI_2 catalyst and KI (Figure 1.16). Reactions were carried out at 100 °C in *N*,*N*-dimethylacetamide using trimethyl orthoacetate dehydrating agent (up to 3 equivalents) and a CO/air mixture (4:1 *v/v*, 20 bar) with molecular oxygen acting as the sole oxidising agent.

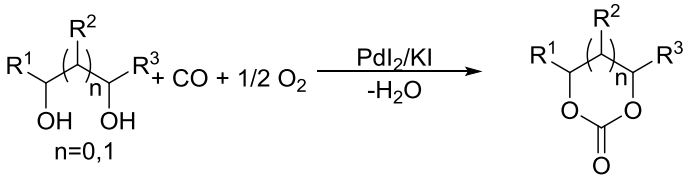

Figure 1.16. Carbonylation of 1,2 and 1,3-diols with CO, oxygen and a Pd catalyst. Reported by Gabriele *et al*.[122]

Cyclic carbonates were isolated in reasonable to good yield. For example, after 24 hours with 1 mol% PdI_2 and a PdI_2/KI ratio of 10, an isolated yield of 66% was reported for the synthesis of the six-membered cyclic carbonate of 1,3-butanediol. D-Glucose was also used as a substrate and underwent di-carbonylation to yield glucose in its furanose ring form with five-membered cyclic carbonates at the 1,2 and 5,6 positions (Scheme 1.06).

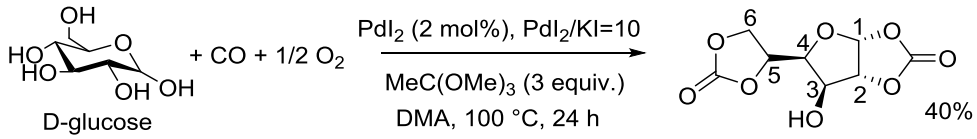

Scheme 1.06. PdI_2/KI-catalysed oxidative carbonylation of D-glucose to yield the di-carbonate product in 40% yield. Reported by Gabriele *et al*.[122]

The proposed mechanism (Figure 1.17) involves reaction of CO, PdI_2 and the diol with subsequent loss of hydrogen iodide to form an alkoxycarbonylpalladium species. This can then undergo intramolecular nucleophilic displacement by the second hydroxyl group with loss of Pd(0) and hydrogen iodide. The Pd (+II) iodide species is regenerated by oxidation with iodine formed from the eliminated hydrogen iodide.

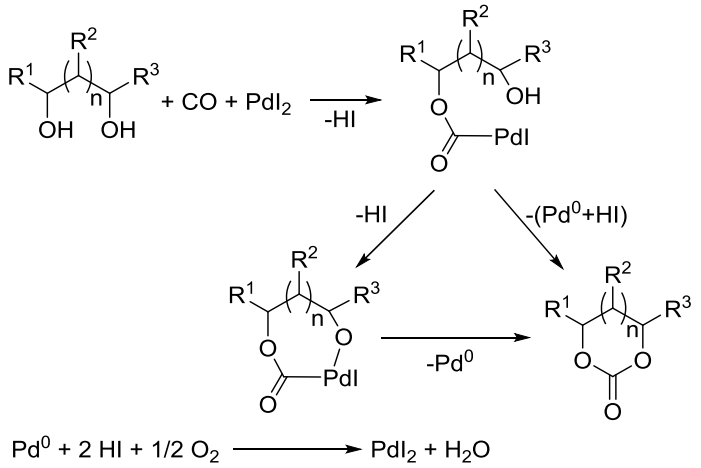

Figure 1.17. Mechanism proposed by Gabriele *et al.*[122] for PdI_2/KI-catalysed oxidative carbonylation of diols to cyclic carbonates. The high activity of palladium was suggested to be due to the efficient re-oxidation mechanism of the Pd(0) species.

1.5. Sugar-Based Cyclic Monomers for ROP

Challenges in the direct coupling of diols with CO_2 inevitably extends to the use of sugar derived diols and the formation of sugar-based cyclic carbonate monomers. However, even with traditional routes involving phosgene or phosgene derivatives there are relatively few examples of sugar-based cyclic carbonates and prior to this work, there were no examples of sugar-based cyclic carbonates prepared using CO_2 carbonylating agent. Moreover, a distinction can be made between cyclic monomers derived indirectly from sugar crops by chemical or biological fermentation processes yielding monomer precursors that do not maintain the original sugar structure and those that are synthesised directly from monosaccharides and bear resemblance to the structure and functionality of the starting molecule. A classic example of the former, is the fermentation of corn starch to produce lactic acid (Figure 1.18), which is typically converted into a low M_w pre-polymer before being depolymerised to the cyclic di-ester, lactide.[123] ROP of this lactic acid dimer has been extensively investigated with focus on the development of catalysts that offer control over the tacticity of the resulting polyester from a mixture of lactide stereoisomers.[124-126]

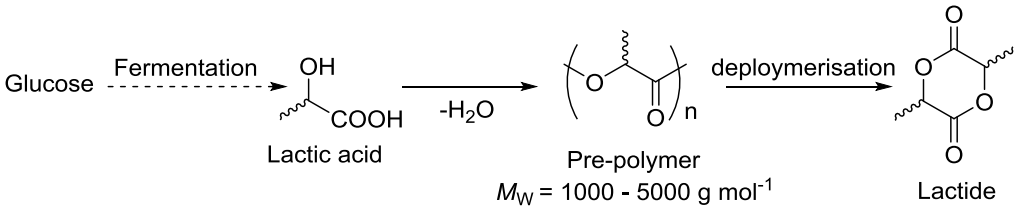

Figure 1.18. Lactide from lactic acid derived from sugar.

Other examples of cyclic monomers that can be prepared from sugar derived oxygenated synthons are depicted in Figure 1.19 and include lactic acid *O*-carboxyanhydride,[127, 128] glycolide from cellulosic biomass,[129] ε-caprolactone and thus ε-caprolactam from glucose,[130] fructose and mannose sugars *via* 5-(hydroxylmethyl)furfural,[131] β-methyl-δ-valerolactone from mevalonate fermentation product,[132] angelica lactone from sugar-derived levulinic acid, γ-butyrolactone and 2-pyrrolidone from succinic acid produced by microbial fermentation of glucose,[133-136] β-propiolactone from 3-hydroxylpropionic acid produced by biosynthetic pathways,[137] malolactonate and L-malic *O*-carboxyanhydride from L-malic acid glucose metabolite[138] and finally cyclic carbonates prepared using phosgene from dihydroxyacetone ketose[139, 140] and diols from the reduction of succinic, levulinic and itaconic acid sugar derivatives.[96]

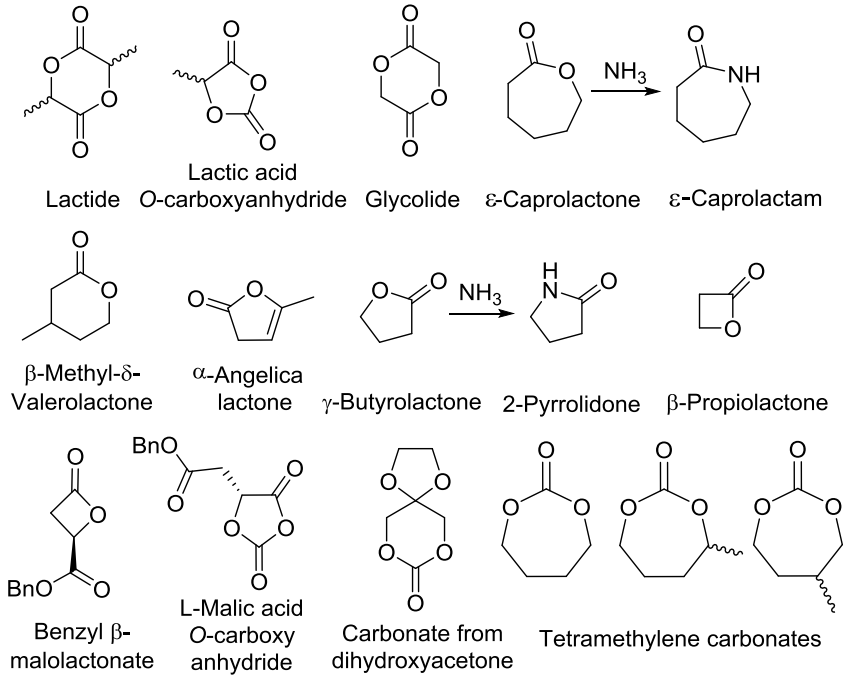

Figure 1.19. Lactone, lactam, and cyclic carbonate monomers derived indirectly from sugars *via* chemical or biological fermentation processes. They bear little resemblance to the original sugar structure.

Monomers made directly from sugars where the core carbohydrate structure is maintained is a largely undeveloped area and forms the focus of this work. There are relatively few examples of cyclic carbonate monomers that fall within this area. These are summarised in Figure 1.20 and their synthesis and ROP are considered in detail in the relevant chapters.

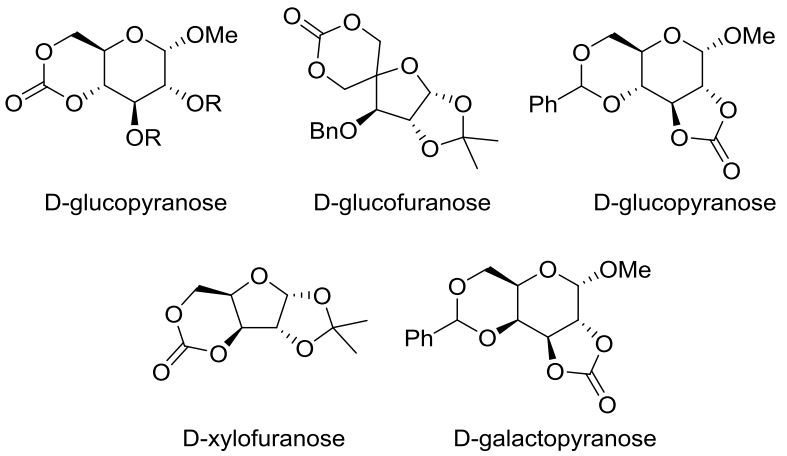

Figure 1.20. Overview of sugar-based cyclic carbonate monomers reported within the literature where the core carbohydrate structure is maintained. The synthesis and ROP of each is considered in the relevant chapters.

This section considers then, the synthesis, ROP and applications of other cyclic monomers namely, lactones and lactams derived from sugars where the original sugar structure is maintained. Also, briefly discussed are examples where the sugar-derived component does not form part of the polymer backbone but is pendent to the main chain.

1.5.1. Sugar-based 1,5-lactones

Lactones derived from carbohydrates contain a cyclic sugar structure, which is lost on polymerisation. However, the large number of defined stereocentres in natural sugars can be used to impart stereochemistry into the polymer backbone. Carbohydrate derived 1,5- lactones (Figure 1.21) are attractive as they can be readily prepared in good yield by oxidation of the corresponding glycoside. However, homopolymerisation to aliphatic polyesters has proved challenging.

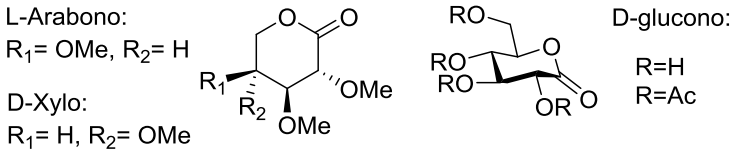

Figure 1.21. Carbohydrate 1,5-lactones with L-arabono-,[141] D-xylo-[142] and D-glucono-[143-145] stereochemistry.

Early work by Haworth and Drew[141] suggested evidence for the ROP of 2,3,4-*O*-trimethyl-L-arabono-1,5-lactone. Over several weeks, exposure to trace amounts of acetyl chloride or HCl led to an estimated molecular weight of 1900 g mol^{-1}. Later work by Galbis and coworkers[142] reported the synthesis of the analogous monomer with D-xylose stereochemistry and a 2002 patent claimed the ROP of D-glucono-1,5-lactone though, characterisation of the products were limited.[143] Following the procedure outlined by Joseph *et al.*,[144] the tetra-*O*-acetyl derivative was prepared by Williams and Haider[145] in 90% yield by treatment of commercially available D-glucono-1,5-lactone with acetic anhydride and trifluoroacetic acid. However, ROP of the neat monomer at 80 °C with tin (II) 2- ethylhexanoate ($Sn(Oct)_2$) and 1,4-butanediol initiator yielded only dimers and trimers (Scheme 1.07).

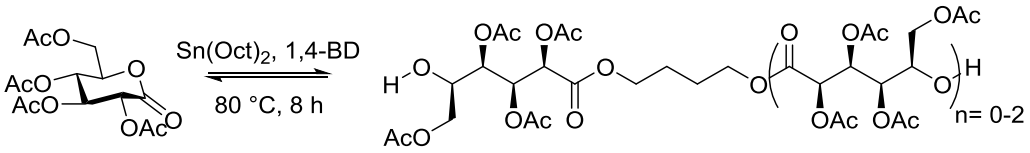

Scheme 1.07. ROP of tetra-*O*-acetyl-D-glucono-1,5-lactone with $Sn(Oct)_2$ and 1,4-butanediol (1,4-BD) carried out by Williams and Haider[145] yielded only low molecular weight oligomers (M_n 1470 g mol^{-1}).

MALDI-ToF mass spectrometry of the mono-, di- and tri- aldaric esters, isolated in 30% yield, showed two hydroxyl end groups and no cyclic or carboxylic acid terminated species. Consequently, the oligoesters were used as macroinitiators in the ROP of *R*- and *S*-lactide to form triblock ABA copolymers.

In contrast, less substituted carbohydrate-1,5-lactone, prepared by Williams and coworkers[146] in two high yielding steps (95%), underwent ROP with $Sn(OBu)_2$ to form cyclic atactic polyesters with M_n ranging from 1800 to 7300 g mol^{-1} (Schemes 1.08 and 1.09). The cyclic topology was reasoned to be due to the relatively low ring strain of the monomer resulting in a rate of chain propagation comparable to the rate of transesterification leading to backbiting reactions. The polymer (M_n = 2900 g mol^{-1}, Đ 1.26) showed high thermal stability with the onset of degradation not occurring until 250 °C but loss of the rigid sugar ring upon polymerisation resulted in a low T_g of 18 °C. The oxygen-rich materials also showed enhanced hydrophilic character compared with poly(lactic acid); swelling on addition of water and a static water contract angle of ~33° (cf. ~ 80° for polylactide).

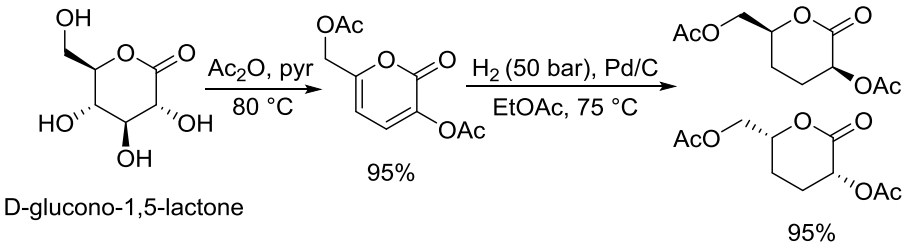

Scheme 1.08. Two-step, high yielding synthesis of less-substituted racemic carbohydrate 1,5-lactone from D-glucono-1,5-lactone.[146]

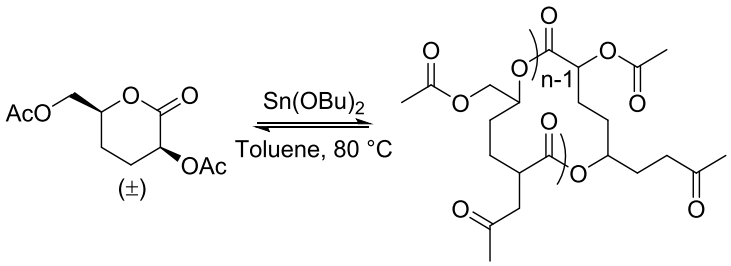

Scheme 1.09. ROP of carbohydrate-1,5-lactone with $Sn(OBu)_2$ to form cyclic amorphous polyesters.[146]

Targeting tissue engineering applications, where degradation of the polymer scaffold should correspond to the rate of tissue regeneration, copolymers of the lactone with *S*,*S*-lactide were also prepared to address the slow degradation of poly(lactic acid) (Scheme 1.10).[147] Random copolymers composed of 1-25 wt% of the carbohydrate lactone with M_n ranging from 8800 to 44 000 g mol^{-1} (Đ 1.36-1.51) were prepared at room temperature using a zinc ethoxide catalyst (LZnOEt). Higher loadings of the sugar-1,5-lactone resulted in enhanced degradation properties for example, a decrease in the degradation temperature from 290 (at 1 wt%) to 255 °C (at 25 wt%). This may be attributed to the loss of crystallinity observed upon copolymerisation. The T_g also decreased, from 55 to 46 °C, with greater 1,5-lactone content. Cell viability and attachment studies carried out on electrospun fibres of the copolymers indicated that at all compositions, 90% of human osteogenic sarcoma Saos-2 cells were viable. SEM images revealed a greater spread of the cells on the copolymer with the highest ratio of the 1,5-lactone, which was attributed to the accompanying increase in hydrophilicity of the scaffold.

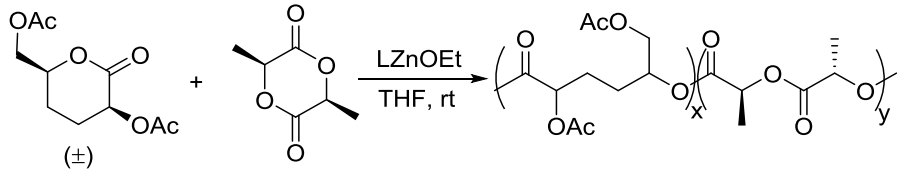

Scheme 1.10 Random copolymers of the *rac*-carbohydrate-1,5-lactone with *S*,*S*-lactide targeting tissue engineering applications.[147]

1.5.2. Sugar-based 1,6-lactones

In contrast to the synthesis of the carbohydrate-1,5-lactones, reported 1,6-lactones require more elaborate synthetic sequences and protecting group chemistry. The *O*-methyl protected derivative of D-glucono-1,6-lactone was prepared by Galbis and coworkers[148] *via* lactonisation of the ω-hydroxyacid intermediate (Scheme 1.11), synthesised in reasonable yield by two different multi-step routes. Only that involving fewer synthetic steps and resulting in a higher yield is shown in Scheme 1.11. Treatment of fully protected D-glucose diethylmercaptal with $Hg(ClO_4)_2$, to form the aldehyde for oxidisation to the carboxylic acid and subsequent acid removal of the primary protecting group, yielded the pre-cyclisation intermediate in 90% yield.

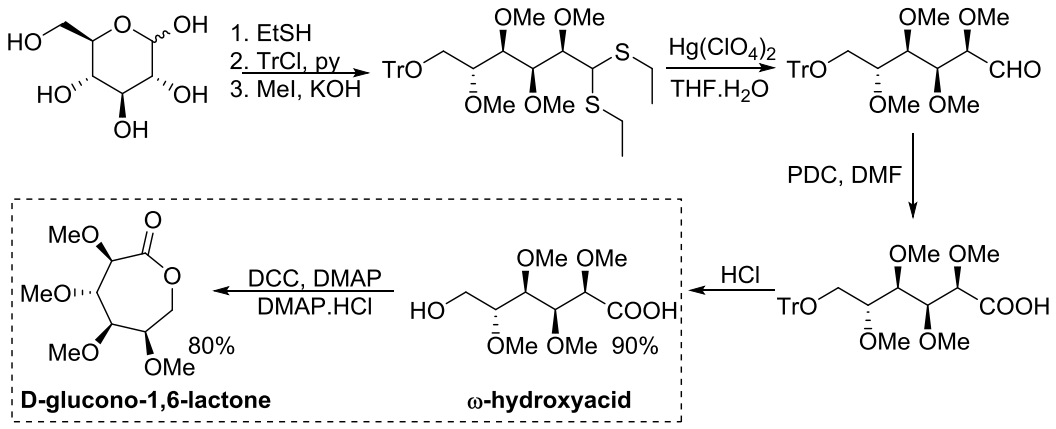

Scheme 1.11. Synthesis 2,3,4,5-tetra-*O*-methyl-D-glucono-1,6-lactone from D-glucose *via* the diethylmercaptal intermediate (route 2).[148] PDC= pyridinium dichromate; DCC= *N,N'*-dicyclohexylcarbodiimide and DMAP= 4-(dimethylamino)pyridine.

Valera and coworkers[149] prepared the analogous monomer with D-galactose stereochemistry in a shorter, 3-step synthetic route from D-galactono-1,4-lactone (Scheme 1.12). The pre- cyclisation product, D-galactonic acid was prepared in an overall 47% yield, the final lactonisation being achieved as above. Guan and Urakami[150] also prepared this 1,6-lactone as a *racemic* mixture from reduced sugar D-dulcitol in 60% yield (Scheme 1.12). Dehydrogenation of either of the free primary hydroxyl groups in the otherwise *O*-methyl protected sugar was carried out with Na_2CO_3 and Shvo's catalyst to give both possible enantiomers.

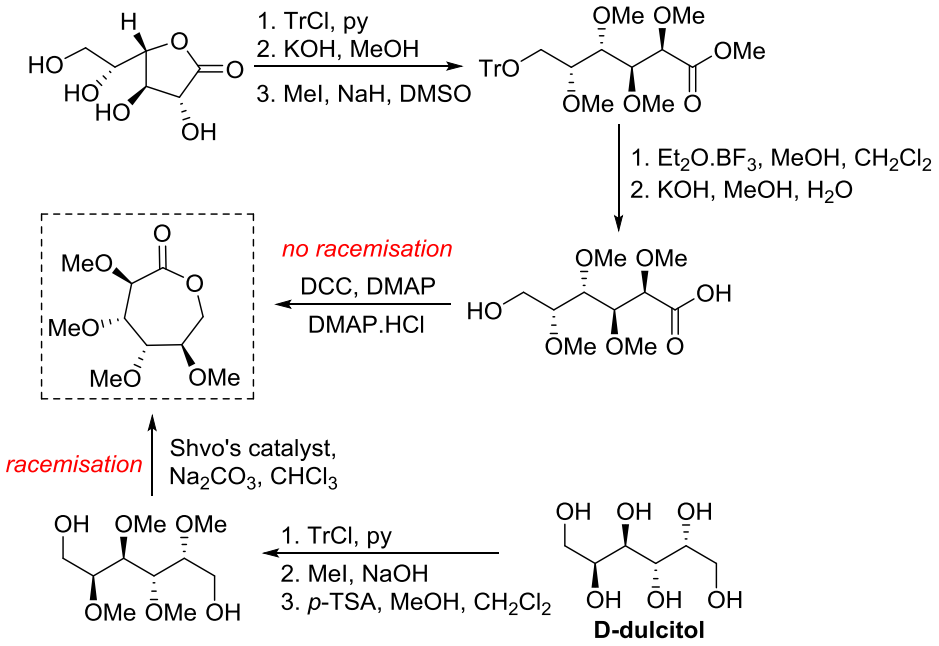

Scheme 1.12. Synthesis of enantiopure tetra-*O*-methyl-D-galactono-1,6-lactone from D-galactono-1,4-lactone[149] or as a *racemic* mixture from D-dulcitol.[150] PDC= pyridinium dichromate; DCC= *N,N'*-dicyclohexylcarbodiimide and DMAP= 4-(dimethylamino)pyridine; Shvo's catalyst= 1-hydroxytetraphenylcyclopentadienyl(tetraphenyl-2,4-cyclopentadien-1-one)-μ-hydrotetracarbonyldiruthenium(II).

Compared to the enantiopure 1,6-lactones, only the *racemic* galactono-1,6-lactone was reported to undergo homopolymerisation. Using Y(O*i*Pr)$_3$ in toluene at room temperature (Scheme 1.13), homo-polyesters were isolated in yields of 85-95% with M_n ranging from 5300- 40 100 g mol^{-1} (Đ 1.12-1.17). The lack of stereoregularity resulted in an amorphous polymer, exhibiting a T_g of 52 °C.

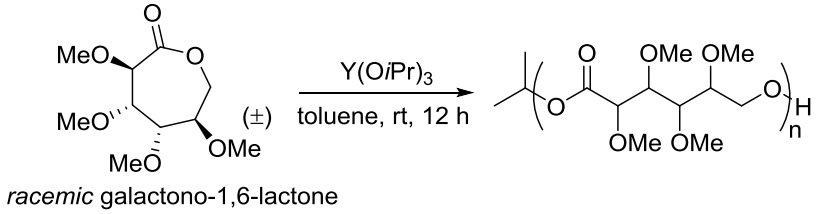

Scheme 1.13. Rare-earth metal initiated homo-ROP of *racemic* tetra-*O*-methyl-galactono-1,6-lactone, prepared from D-dulcitol by Guan and Urakami.[150]

Enantiopure D-glucono-1,6-lactone could however, be copolymerised with L-lactide in the bulk at 110 °C using Sn(Oct)$_2$ to afford a maximum sugar monomer incorporation of 2.2%[148] and 10% of D-galactono-1,6-lactone was incorporated into the polyester chain of poly(ε- caprolactone).[149] The coupling of the hydrophilic methoxy side groups with the hydrophobic surface of unsubstituted ε-caprolactone in diblock copolymers prepared with the *racemic* galactono-1,6-lactone imparted self-assembly and protein-resistant properties

(Scheme 1.14).[150] A 27:73 diblock of the *racemic* monomer: caprolactone (M_n 8230 g mol^{-1}) was reported to result in a fully protein resistant material. Thermal analysis of the copolymers showed they were fully miscible, exhibiting a single T_g from 10 to -17 °C, depending upon the composition.

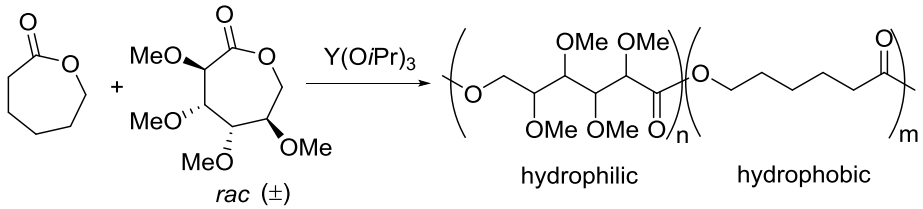

Scheme 1.14. Diblock copolymers prepared from *rac*-2,3,4,5-tetra-*O*-methyl-D/L-galactono-1,6-lactone and ε-caprolactone showed self-assembly and protein resistant properties.[150]

1.5.3. Sugar-based β-lactams

In contrast to the reported carbohydrate lactones, sugar derived β-lactam monomers have been found to readily undergo ROP. In 2012, Grinstaff and coworkers[151] reported the improved one-step synthesis from benzyl protected D-glucal and chlorosulfonyl isocyanate of known[152] glucose-derived β-lactam (Scheme 1.15). Following a stereoselective [2+2]-cycloaddition between the glucal and isocyanate, *in situ* reductive removal of the sulfonyl group gave the monomer in 42% yield. Later, they also prepared, using the same synthetic methodology the corresponding galactose monomer, differing in the axial rather than equatorial configuration of the C-4 substituent.[153]

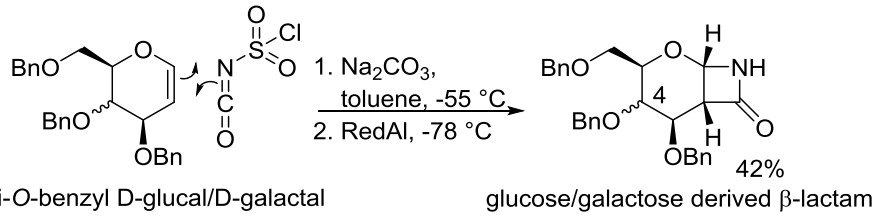

Scheme 1.15. Synthesis of D-glucose[151] and D-galactose[153] derived β-lactam monomers.

Anionic ROP was carried out with LiHMDS catalyst at 0 °C with the initiator generated *in situ* from the monomer on addition of 4-*tert*-butylbenzoyl or 4-nitrobenzoyl chloride (Scheme 1.16). Complete conversion to enantiopure poly-amido-saccharides was observed and in high yield (89 ± 5%) giving M_n up to 56 200 g mol^{-1} with narrow dispersities (Đ = 1.1). A Birch reduction was used to affect complete debenzylation and resulted in minimal

broadening or decrease in chain length (by SEC) for the smaller polymers ($M_n \leq 16.700$ g mol^{-1}). Poor solubility made analysis of longer chain lengths difficult.

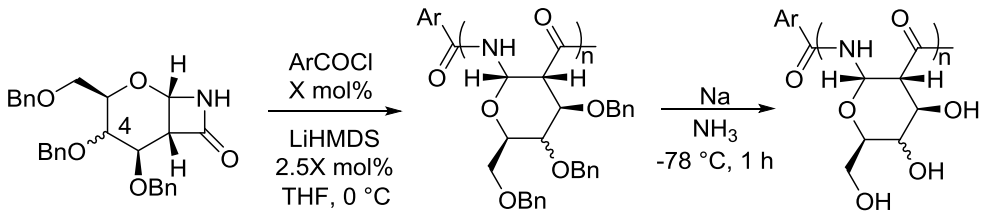

Scheme 1.16. Anionic ROP of β-lactam sugar monomers and subsequent benzyl deprotection with sodium metal in ammonia.[151, 153] LiHMDS = $LiN(SiMe_3)_2$.

The minor change in stereochemistry of the galactose-based repeat unit resulted in highly water soluble polymers compared to the glucose derived analogue. Investigation into the structure of both sugar-derived polyamides by NMR spectroscopy, circular dichroism and molecular dynamic simulations suggested that the relatively rigid chair conformation adopted by the pyranose repeat unit contributed towards the formation of a defined helical secondary structure.[154]

The galactose-derived polyamides were also found to be non-cytotoxic to HeLa, HepG2 and CHO cell lines after incubation for 48 hours and cellular uptake into human hepatocyte cells expressing a galactose specific receptor was observed, by confocal microscopy, with fluorescently labelled derivatives.[153] The biological activity of the deprotected glucose-derived poly-amido-saccharides was also demonstrated with a natural carbohydrate binding protein. Recognition and binding, at the same pocket as natural glucose derivatives, was shown by a measured increase in the turbidity of the solution upon aggregate formation and inhibition of glucose binding. High molecular weight polymers were required to form multiply binding interactions and elicit a response.[151]

Subsequent work, also by Grinstaff and coworkers[155] subjected the debenzylated glucose poly-amido-saccharides to TEMPO-mediated oxidation to introduce an ionisable carboxylic acid group at the primary C-6 position of the repeat unit [Figure 1.22 (a)]. This was carried out to mimic natural polysaccharides such as hyaluronic acid, aliginic acid and oxidised forms of cellulose, which have been investigated and used for a variety of applications, including as protein stabilising agents. Using lysozyme as a model protein, the oxidised poly-amido-saccharides were found to be significantly more effective at lessening the loss of

activity during a repeated freeze-drying process compared to trehalose, a commonly used protein stabilising agent. Gel electrophoresis suggested formation of a complex between the protein and polyamide, accounting for the stabilising effect.

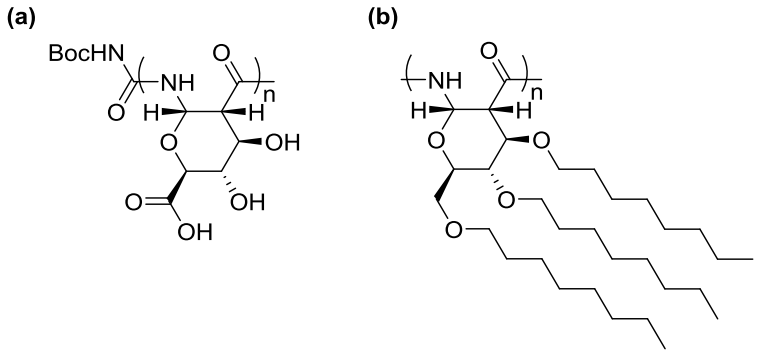

Figure 1.22. (a) Oxidised poly-amido-saccharides showed promise as protein stabilising agents[155] and **(b)** octyl ether functionalised poly-amido-saccharides as liquid crystalline materials.[156]

The glucose derived β-lactam monomer was also prepared with octyl ether chains [Figure 1.22 (b)] in place of benzyl protecting groups.[156] Derivatisation with hydrophobic long chain alkyl groups imparted self-assembly properties and served as a molten phase against the rod-like carbohydrate backbone, promoting the formation of liquid crystalline phases. Depending upon the temperature and polymer chain length, lamellar and hexagonal columnar mesophases were formed. The hydrophobic materials showed thermal stability up to 200 °C and the larger polymers (M_n 26 300 -47 400 g mol^{-1}) revealed T_g values of 15 to 25 °C.

Galbis and co-workers[157] also synthesised a carbohydrate derived β-Lactam [Figure 1.23(a)] *via* cyclisation of a protected amino-D-altronic acid derivative. ROP with potassium *tert*-butoxide catalyst at room temperature gave an optically active and water soluble amorphous polyamide (M_w 10 500 g mol^{-1}, Đ 1.59). Finally, carbohydrate derived *N*-carboxyanhydride [Figure 1.23(b)] was also prepared in a multi-step synthesis from 2-acetamido-2-deoxy-D-glucose[158] involving cyclisation with trichloromethyl chloroformate. Treatment of the monomer with triethylamine in DMF gave polyglucoamides with M_w of 10 000 g mol^{-1} after 2 days stirring at room temperature.

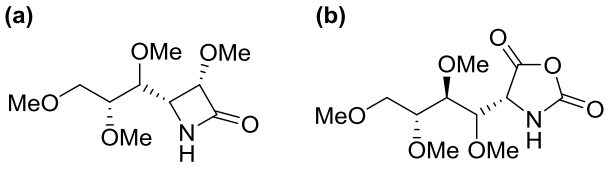

Figure 1.23. (a) Carbohydrate derived β-lactam[157] and **(b)** *N*-carboxyanhydride from D-glucose derivative.[158]

1.5.4. Sugars pendent from the main chain

The above sugar-based monomers lead to carbohydrate units in the main polymer chain. There are however examples of polycarbonates bearing pendent saccharide groups. Hedrick and coworkers[159] prepared a family of amphiphilic block copolycarbontes bearing pendent D-glucose, D-galactose and D-mannose carbohydrates for targeted drug delivery (Figure 1.24). Following ROP, the diacetonide protected sugars were selectively deprotected with aqueous formic acid and the glycopolymers self-assembled into micelles showing a high density of sugar molecules on the surface. Galactose-containing micelles were loaded with a drug used for liver cancer treatment and showed strong targeting for a protein receptor on the surface of liver cells.

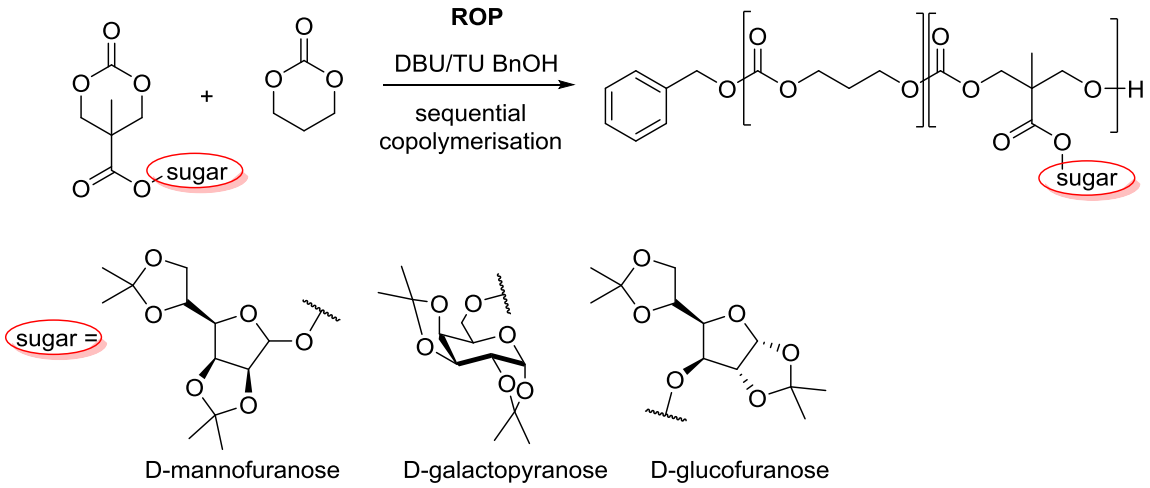

Figure 1.24. Diblock copolymers with pendent mannose, glucose and galactose sugar groups prepared by ROP with DBU/thiourea (TU) of sugar-functionalised cyclic carbonates. Deprotection of the acetonide groups was carried out post-polymerisation with $HCOOH/H_2O$ to yield amphiphilic block glycopolymers.[159]

1.6. Aims and Objectives

The first aim of this project was to develop methods for the direct coupling of 1,3-diols and CO_2 to form six-membered cyclic carbonate monomers using common lab reagents and under mild reaction conditions (room temperature and low CO_2 pressure). The design and development of strategies to achieve this was guided by DFT calculations of the kinetic and thermodynamic barriers for the direct coupling of CO_2 with 1,3-butanediol as a model compound for sugars. Building upon reported methods for the efficient capture and activation of CO_2 under mild reaction conditions, the objective was to take both metal and non-metal based approaches to promoting cyclisation and ultimately a homogeneous catalytic system was targeted (Figure 1.25).

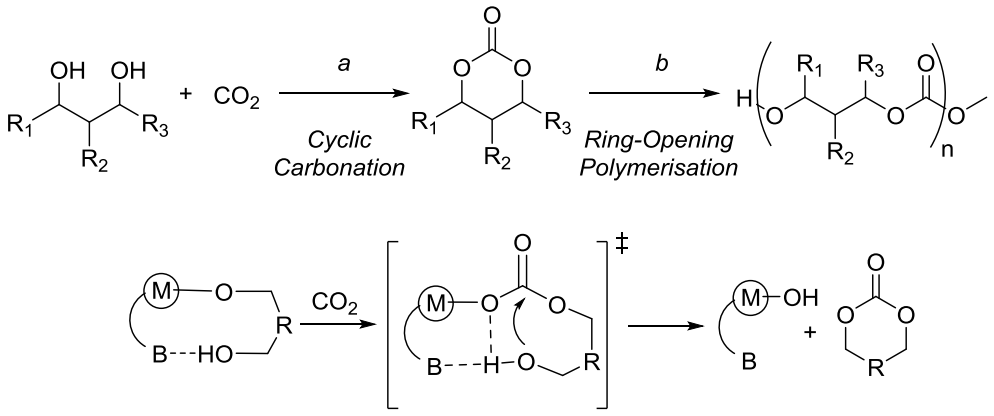

Figure 1.25. Development of methods for the direct coupling of 1,3-diols with CO_2 to form six-membered cyclic carbonates as precursors to polycarbonates by ROP. One target was a metal-based catalyst featuring a labile basic moiety to aid cyclisation.

The second aim was to prepare novel cyclic carbonate monomers from sugar-based diols and investigate their ROP to carbohydrate-derived polycarbonates. One target was the synthesis of previously unreported cyclic carbonates of 2-deoxy-D-ribofuranose sugars (Figure 1.26). These sugars form the backbone of DNA and would provide access to DNA-derived APCs with potentially attractive biocompatibility and self-assembly properties. The objective was to carry out polymerisations using known ROP catalysts with a focus on readily available organocatalytic systems owing to their simplicity, anticipated tolerance to diol impurities and assumed low toxicity for biomedical applications.

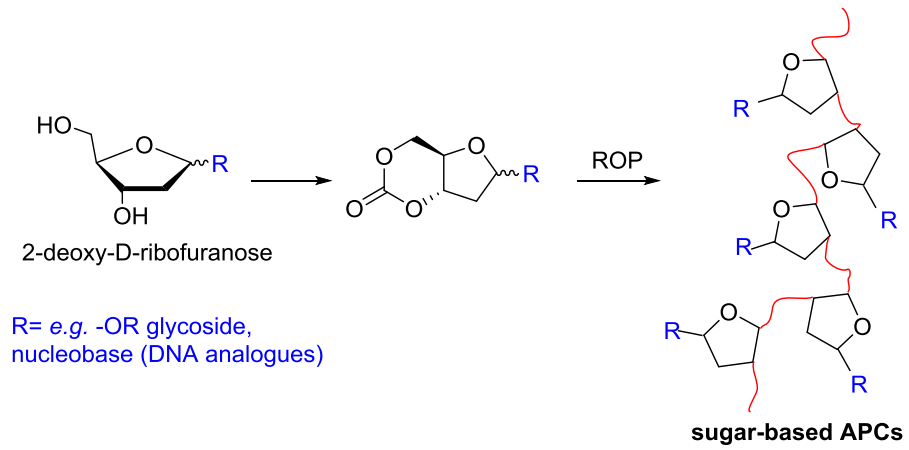

Figure 1.26. Example of targeted sugar-based cyclic carbonate based on 2-deoxy-D-ribose, which forms the core of DNA.

The final aim was to fully characterise and investigate the materials properties of the prepared sugar-based APCs as well as assess their potential biomedical application. This included measuring polymer glass transition temperatures by differential scanning calorimetry and examining the thermal degradation behaviour by thermogravimetric analysis. Biocompatibility testing of the materials and cell-attachment studies with MG-63 cancer cell line were targeted to assess their potential for tissue-engineering scaffolds.

1.7. References

1. http://www.plasticseurope.org/information-centre/publications.aspx, *Plastics-the Facts 2016*, (accessed 19/03/2017).
2. K. L. Law and R. C. Thompson, *Science*, 2014, **345**, 144-145.
3. O. Talon, in *Environmental Impact of Polymers*, eds. T. Hamaide, R. Deterre and J.-F. Feller, John Wiley, 2014, ch. 6, pp. 91-107.
4. Y. Zhu, C. Romain and C. K. Williams, *Nature*, 2016, **540**, 354-362.
5. C. K. Williams and M. A. Hillmyer, *Polym. Rev.*, 2008, **48**, 1-10.
6. S. A. Miller, *ACS Macro Lett.*, 2013, **2**, 550-554.
7. A. Llevot, P.-K. Dannecker, M. von Czapiewski, L. C. Over, Z. Söyler and M. A. R. Meier, *Chem. Eur. J.*, 2016, **22**, 11510-11521.
8. T. Iwata, *Angew. Chem. Int. Ed.*, 2015, **54**, 2-8.
9. A. Gandini, T. M. Lacerda, A. J. F. Carvalho and E. Trovatti, *Chem. Rev.*, 2015, **116**, 1637-1669.
10. P. F. H. Harmsen, M. M. Hackmann and H. L. Bos, *Biofuels, Bioprod. Bioref.*, 2014, **8**, 306-324.
11. M. J. L. Tschan, E. Brule, P. Haquette and C. M. Thomas, *Polym. Chem.*, 2012, **3**, 836-851.
12. S. L. Kristufek, K. T. Wacker, Y.-Y. T. Tsao, L. Su and K. L. Wooley, *Nat. Prod. Rep.*, 2017, **34**, 433-459.
13. A. L. Holmberg, N. A. Nguyen, M. G. Karavolias, K. H. Reno, R. P. Wool and T. H. Epps, *Macromolecules*, 2016, **49**, 1286-1295.
14. A. L. Holmberg, K. H. Reno, N. A. Nguyen, R. P. Wool and T. H. Epps, *ACS Macro Lett.*, 2016, **5**, 574-578.
15. L. Montero de Espinosa and M. A. R. Meier, *Eur. Polym. J.*, 2011, **47**, 837-852.
16. M. A. R. Meier, J. O. Metzger and U. S. Schubert, *Chem. Soc. Rev.*, 2007, **36**, 1788.
17. H. C. Quilter, M. Hutchby, M. G. Davidson and M. D. Jones, *Polym. Chem.*, 2017, **8**, 833-837.
18. P. A. Wilbon, F. Chu and C. Tang, *Macromol. Rapid Comm.*, 2013, **34**, 8-37.
19. N. G. Ricapito, C. Ghobril, H. Zhang, M. W. Grinstaff and D. Putnam, *Chem. Rev.*, 2016, **116**, 2664-2704.
20. H. Lu, J. Wang, Z. Song, L. Yin, Y. Zhang, H. Tang, C. Tu, Y. Lin and J. Cheng, *Chem. Commun.*, 2014, **50**, 139-155.
21. J. A. Galbis, M. d. G. García-Martín, M. V. de Paz and E. Galbis, *Chem. Rev.*, 2015, **116**, 1600-1636.
22. Y. Qin, X. Sheng, S. Liu, G. Ren, X. Wang and F. Wang, *J. CO2 Util.*, 2015, **11**, 3-9.
23. G. Trott, P. K. Saini and C. K. Williams, *Phil. Trans. R. Soc. A.*, 2016, **374**, 20150085.
24. http://www.european-bioplastics.org/market, (accessed 19/03/2017).
25. J. A. Galbis and M. G. García-Martín, *Top. Curr. Chem.*, 2010, **295**, 147-176.
26. C. Japu, A. Martinez de Ilarduya, A. Alla, M. G. Garcia-Martin, J. A. Galbis and S. Munoz-Guerra, *Poly. Chem.*, 2013, **4**, 3524-3536.
27. C. Lavilla, A. Martinez de Ilarduya, A. Alla and S. Munoz-Guerra, *Polym. Chem.*, 2013, **4**, 282-289.
28. S. Munoz-Guerra, C. Lavilla, C. Japu and A. Martinez de Ilarduya, *Green Chem.*, 2014, **16**, 1716-1739.
29. R. McHale and R. K. O'Reilly, *Macromolecules*, 2012, **45**, 7665-7675.
30. D. Cunliffe, S. Pennadam and C. Alexander, *Eur. Polym. J.*, 2004, **40**, 5-25.
31. O. Goerz and H. Ritter, *Polym. Int.*, 2013, **62**, 709-712.
32. L. Gu, A. Faig, D. Abdelhamid and K. Uhrich, *Acc. Chem. Res.*, 2014, **47**, 2867-2877.
33. N. D. Stebbins, W. Yu and K. E. Uhrich, *Biomacromolecules*, 2015, **16**, 3632-3639.
34. S. Bhatia, in *Natural Polymer Drug Delivery Systems: Nanoparticles, Plants, and Algae*, Springer Int., Cham, 2016, pp. 95-118.
35. T. Sakakura, J.-C. Choi and H. Yasuda, *Chem. Rev.*, 2007, **107**, 2365-2387.
36. M. Aresta and A. Dibenedetto, *Dalton Trans.*, 2007, 2975-2992.

37. A. Dibenedetto, A. Angelini and P. Stufano, *J. Chem. Technol. Biotechnol.*, 2014, **89**, 334-353.
38. M. Aresta, A. Dibenedetto and A. Angelini, *Chem. Rev.*, 2014, **114**, 1709-1742.
39. M. Peters, B. Köhler, W. Kuckshinrichs, W. Leitner, P. Markewitz and T. E. Müller, *ChemSusChem*, 2011, **4**, 1216-1240.
40. M. Mikkelsen, M. Jorgensen and F. C. Krebs, *Energy Environ. Sci.*, 2010, **3**, 43-81.
41. W. Chen, L.-x. Zhong, X.-w. Peng, R.-c. Sun and F.-c. Lu, *ACS Sustainable Chem. Eng.*, 2015, **3**, 147-152.
42. https://www.iea.org, *International Energy Agency*, (accessed 23/03/2017).
43. A. Al-Mamoori, A. Krishnamurthy, A. A. Rownaghi and F. Rezaei, *Energy Technol.*, 2017, DOI: 10.1002/ente.201600747.
44. N. MacDowell, N. Florin, A. Buchard, J. Hallett, A. Galindo, G. Jackson, C. S. Adjiman, C. K. Williams, N. Shah and P. Fennell, *Energy Environ. Sci.*, 2010, **3**, 1645-1669.
45. *Advances in Polycarbonates*, eds. D.J Brunelle and M. R. Korn, American Chemical Society: Washington DC, 2005, 898, 1.
46. J. Xu, E. Feng and J. Song, *J. Appl. Polym. Sci.*, 2014, **131**, 39822.
47. J. Feng, R.-X. Zhuo and X.-Z. Zhang, *Prog. Polym. Sci.*, 2012, **37**, 211-236.
48. W. Chin, C. Yang, V. W. L. Ng, Y. Huang, J. Cheng, Y. W. Tong, D. J. Coady, W. Fan, J. L. Hedrick and Y. Y. Yang, *Macromolecules*, 2013, **46**, 8797-8807.
49. S. M. Guillaume and L. Mespouille, *J. Appl. Polym. Sci.*, 2014, **131**, 40081.
50. W. Chen, F. Meng, R. Cheng, C. Deng, J. Feijen and Z. Zhong, *J. Control. Release*, 2014, **190**, 398-414.
51. S. Tempelaar, L. Mespouille, O. Coulembier, P. Dubois and A. P. Dove, *Chem. Soc. Rev.*, 2013, **42**, 1312-1336.
52. P. N. Zawaneh, S. P. Singh, R. F. Padera, P. W. Henderson, J. A. Spector and D. Putnam, *Proc. Natl. Acad. Sci. U. S. A.* , 2010, **107**, 11014-11019.
53. S. Van Vlierberghe, P. Dubruel and E. Schacht, *Biomacromolecules*, 2011, **12**, 1387-1408.
54. I. M. El-Sherbiny and M. H. Yacoub, *Glob. Cardiol. Sci. Pract.*, 2013, **38**, 316-342.
55. H.-z. Jia, H.-f. Wang, C.-w. Liu, C. Li, J. Yang, X.-d. Xu, J. Feng, X.-z. Zhang and R.-x. Zhuo, *Soft Matter*, 2012, **8**, 6906-6912.
56. E. I. Geihe, C. B. Cooley, J. R. Simon, M. K. Kiesewetter, J. A. Edward, R. P. Hickerson, R. L. Kaspar, J. L. Hedrick, R. M. Waymouth and P. A. Wender, *Proc. Natl. Acad. Sci. U. S. A.*, 2012, **109**, 13171-13176.
57. F. Fenouillot, A. Rousseau, G. Colomines, R. Saint-Loup and J. P. Pascault, *Prog. Polym. Sci.*, 2010, **35**, 578-622.
58. E. S. Place, J. H. George, C. K. Williams and M. M. Stevens, *Chem. Soc. Rev.*, 2009, **38**, 1139-1151.
59. K. Müller, L. Mokrushina and W. Arlt, *Chem. Ing. Tech.*, 2014, **86**, 1-8.
60. I. Omae, *Catal. Today*, 2006, **115**, 33-52.
61. S. Fukuoka, M. Kawamura, K. Komiya, M. Tojo, H. Hachiya, K. Hasegawa, M. Aminaka, H. Okamoto, I. Fukawa and S. Konno, *Green Chem.*, 2003, **5**, 497.
62. F. Arico and P. Tundo, *Russ. Chem. Rev.*, 2010, **79**, 479-489.
63. W. Zhu, X. Huang, C. Li, Y. Xiao, D. Zhang and G. Guan, *Polym. Int.*, 2011, **60**, 1060-1067.
64. M. Tamura, K. Ito, M. Honda, Y. Nakagawa, H. Sugimoto and K. Tomishige, *Sci. Rep.*, 2016, **6**, 24038.
65. Q. Li, W. Zhu, C. Li, G. Guan, D. Zhang, Y. Xiao and L. Zheng, *J. Polym. Sci. Part A: Polym. Chem.*, 2013, **51**, 1387-1397.
66. A. T. Lonnecker, Y. H. Lim, S. E. Felder, C. J. Besset and K. L. Wooley, *Macromolecules*, 2016, **49**, 7857-7867.
67. D. J. Darensbourg and M. W. Holtcamp, *Coord. Chem. Rev.*, 1996, **153**, 155-174.
68. D. J. Darensbourg, *Inorg. Chem.*, 2010, **49**, 10765-10780.
69. C. Romain, A. Thevenon, P. K. Saini and C. K. Williams, in *Carbon Dioxide and Organometallics*, ed. X.-B. Lu, Springer International Publishing, Cham, 2016, vol. 53, pp. 101-142.
70. D. J. Darensbourg, *Chem. Rev.*, 2007, **107**, 2388-2410.

71. M. R. Kember, A. Buchard and C. K. Williams, *Chem. Commun.*, 2011, **47**, 141-163.
72. G. A. Luinstra, *Polym. Rev.*, 2008, **48**, 192-219.
73. W.-L. Dai, S.-L. Luo, S.-F. Yin and C.-T. Au, *Appl. Catal. A*, 2009, **366**, 2-12.
74. E. K. Noh, S. J. Na, S. S, S.-W. Kim and B. Y. Lee, *J. Am. Chem. Soc.*, 2007, **129**, 8082-8083.
75. A. M. Chapman, C. Keyworth, M. R. Kember, A. J. J. Lennox and C. K. Williams, *ACS Catal.*, 2015, **5**, 1581-1588.
76. C. Li, R. J. Sablong and C. E. Koning, *Eur. Poly. J.*, 2015, **67**, 449-458.
77. M. Winkler, C. Romain, M. A. R. Meier and C. K. Williams, *Green Chem.*, 2015, **17**, 300-306.
78. D. J. Darensbourg, P. Ganguly and W. Choi, *Inorg. Chem.*, 2006, **45**, 3831-3833.
79. D. J. Darensbourg and A. I. Moncada, *Macromolecules*, 2010, **43**, 5996-6003.
80. D. J. Darensbourg, A. I. Moncada and S.-H. Wei, *Macromolecules*, 2011, **44**, 2568-2576.
81. W. H. Carothers and F. J. V. Natta, *J. Am. Chem. Soc.*, 1930, **52**, 314-326.
82. G. Rokicki and P. G. Parzuchowski, in *Polymer Science: A Comprehensive Reference*, eds. K. Matyjaszewski and M. Möller, Elsevier, Amsterdam, 2012, pp. 247-308.
83. P. Olsén, K. Odelius and A.-C. Albertsson, *Biomacromolecules*, 2016, **17**, 699-709.
84. A. Duda and A. Kowalski, in *Handbook of Ring-Opening Polymerisation*, eds. P. Dubois, O. Coulembier and J.-M. Raqeuz, Wiley-VCH Verlag GmbH & Co/ KGaA, 2009, ch. 1, pp. 1-51.
85. J. Matsuo, K. Aoki, F. Sanda and T. Endo, *Macromolecules*, 1998, **31**, 4432-4438.
86. T. Endo, in *Handbook of Ring-Opening Polymerisation*, eds. P. Dubois, O. Coulembier and J.-M. Raqeuz, Wiley-VCH Verlag GmbH & Co/ KGaA, 2009, ch. 2, pp. 53-63.
87. S. M. Guillaume and J.-F. Carpentier, *Catal. Sci. Technol.*, 2012, **2**, 898-906.
88. M. Helou, O. Miserque, J.-M. Brusson, J.-F. Carpentier and S. M. Guillaume, *ChemCatChem*, 2010, **2**, 306-313.
89. N. Ajellal, J.-F. Carpentier, C. Guillaume, S. M. Guillaume, M. Helou, V. Poirier, Y. Sarazin and A. Trifonov, *Dalton Trans.*, 2010, **39**, 8363-8376.
90. N. E. Kamber, W. Jeong, R. M. Waymouth, R. C. Pratt, B. G. G. Lohmeijer and J. L. Hedrick, *Chem. Rev.*, 2007, **107**, 5813-5840.
91. B. G. G. Lohmeijer, R. C. Pratt, F. Leibfarth, J. W. Logan, D. A. Long, A. P. Dove, F. Nederberg, J. Choi, C. Wade, R. M. Waymouth and J. L. Hedrick, *Macromolecules*, 2006, **39**, 8574-8583.
92. B. Lin and R. M. Waymouth, *J. Am. Chem. Soc.*, 2017, **139**, 1645-1652.
93. A. P. Dove, R. C. Pratt, B. G. G. Lohmeijer, R. M. Waymouth and J. L. Hedrick, *J. Am. Chem. Soc.*, 2005, **127**, 13798-13799.
94. X. Zhang, G. O. Jones, J. L. Hedrick and R. M. Waymouth, *Nat. Chem.*, 2016, **8**, 1047-1053.
95. J. Liu, S. Cui, Z. Li, S. Xu, J. Xu, X. Pan, Y. Liu, H. Dong, H. Sun and K. Guo, *Polym. Chem.*, 2016, **7**, 5526-5535.
96. P. Brignou, M. Priebe Gil, O. Casagrande, J.-F. Carpentier and S. M. Guillaume, *Macromolecules*, 2010, **43**, 8007-8017.
97. S. Venkataraman, V. W. L. Ng, D. J. Coady, H. W. Horn, G. O. Jones, T. S. Fung, H. Sardon, R. M. Waymouth, J. L. Hedrick and Y. Y. Yang, *J. Am. Chem. Soc.*, 2015, **137**, 13851-13860.
98. W. Guerin, A. K. Diallo, E. Kirilov, M. Helou, M. Slawinski, J.-M. Brusson, J.-F. Carpentier and S. M. Guillaume, *Macromolecules*, 2014, **47**, 4230-4235.
99. A. K. Diallo, E. Kirillov, M. Slawinski, J.-M. Brusson, S. M. Guillaume and J.-F. Carpentier, *Polym. Chem.*, 2015, **6**, 1961-1971.
100. K. Tezuka, K. Koda, H. Katagiri and O. Haba, *Polym. Bull.*, 2015, **72**, 615-626.
101. M. Honda, M. Tamura, Y. Nakagawa and K. Tomishige, *Catal. Sci. Technol.*, 2014, **4**, 2830-2845.
102. M. Tamura, M. Honda, Y. Nakagawa and K. Tomishige, *J. Chem. Technol. Biotechnol.*, 2013, **89**, 19-33.
103. M. Honda, M. Tamura, K. Nakao, K. Suzuki, Y. Nakagawa and K. Tomishige, *ACS Catal.*, 2014, **4**, 1893-1896.

104. K. Tomishige, H. Yasuda, Y. Yoshida, M. Nurunnabi, B. Li and K. Kunimori, *Catal. Lett.*, 2004, **95**, 45-49.
105. K. Tomishige, H. Yasuda, Y. Yoshida, M. Nurunnabi, B. Li and K. Kunimori, *Green Chem.*, 2004, **6**, 206-214.
106. S. Huang, S. Liu, J. Li, N. Zhao, W. Wei and Y. Sun, *Catal. Lett.*, 2007, **118**, 290-294.
107. Y. Du, L. He and D. Kong, *Catal. Commun.*, 2008, **9**, 1754-1758.
108. Y. Du, D.-L. Kong, H.-Y. Wang, F. Cai, J.-S. Tian, J.-Q. Wang and L.-N. He, *J. Mol. Chem. Catal. A*, 2005, **241**, 233-237.
109. M. Aresta, A. Dibenedetto, F. Nocito and C. Pastore, *J. Mol. Catal. A*, 2006, **257**, 149-153.
110. J. George, Y. Patel, S. M. Pillai and P. Munshi, *J. Mol. Catal. A*, 2009, **304**, 1-7.
111. S.-Y. Huang, S.-G. Liu, J.-P. Li, N. Zhao, W. Wei and Y.-H. Sun, *J. Fuel Chem. Technol.*, 2007, **35**, 701-705.
112. X. Zhao, N. Sun, S. Wang, F. Li and Y. Wang, *Ind. Eng. Chem. Res.*, 2008, **47**, 1365-1369.
113. S. Huang, S. Liu, J. Li, N. Zhao, W. Wei and Y. Sun, *Catal. Lett.*, 2006, **112**, 187-191.
114. E. Da Silva, W. Dayoub, G. Mignani, Y. Raoul and M. Lemaire, *Catal. Commun.*, 2012, **29**, 58-62.
115. M. R. Reithofer, Y. N. Sum and Y. Zhang, *Green Chem.*, 2013, **15**, 2086.
116. F. D. Bobbink, W. Gruszka, M. Hulla, S. Das and P. J. Dyson, *Chem. Commun.*, 2016, **52**, 10787-10790.
117. L.-X. Wu, H. Wang, Z.-Y. Tu, B.-B. Ding, Y. Xiao and J.-X. Lu, *Int. J. Electrochem. Sci.* , 2012, **7**, 11540-11549.
118. S. Huang, J. Ma, J. Li, N. Zhao, W. Wei and Y. Sun, *Catal. Commun.*, 2008, **9**, 276-280.
119. Y. N. Lim, C. Lee and H.-Y. Jang, *Eur. J. Org. Chem.*, 2014, **9**, 1823-1826.
120. M. Aresta, A. Dibenedetto and I. Tommasi, *Appl. Organomet. Chem.*, 2000, **14**, 799-802.
121. M. Aresta, A. Dibenedetto, C. Dileo, I. Tommasi and E. Amodio, *J. Supercritical Fluids 25*, 2003, **25**, 177-182.
122. B. Gabriele, R. Mancuso, G. Salerno, L. Veltri, M. Costa and A. Dibenedetto, *ChemSusChem*, 2011, **4**, 1778-1786.
123. M. Dusselier, P. Van Wouwe, A. Dewaele, E. Makshina and B. F. Sels, *Energy & Environ. Sci.*, 2013, **6**, 1415-1442.
124. R. H. Platel, L. M. Hodgson and C. K. Williams, *Polym. Rev.*, 2008, **48**, 11-63.
125. B. J. O'Keefe, M. A. Hillmyer and W. B. Tolman, *J. Chem. Soc., Dalton Trans.*, 2001, 2215-2224.
126. O. Dechy-Cabaret, B. Martin-Vaca and D. Bourissou, *Chem. Rev.*, 2004, **104**, 6147-6176.
127. H. R. Kricheldorf and J. M. Jonté, *Polym. Bull.*, 1983, **9**, 276-283.
128. K. C. Prousis, J. Markopoulos, V. Mckee and O. Igglessi-Markopoulou, *Tetrahedron*, 2015, **71**, 8637-8648.
129. J. Zhang, X. Liu, M. Sun, X. Ma and Y. Han, *ACS Catal.*, 2012, **2**, 1698-1702.
130. S. Hu, Z. Zhang, J. Song, Y. Zhou and B. Han, *Green Chem.*, 2009, **11**, 1746-1749.
131. A. A. Rosatella, S. P. Simeonov, R. F. Frade and C. A. Afonso, *Green Chem.*, 2011, **13**, 754-793.
132. M. Xiong, D. K. Schneiderman, F. S. Bates, M. A. Hillmyer and K. Zhang, *Proc. Natl. Acad. Sci. U. S. A.*, 2014, **111**, 8357-8362.
133. C. Yu, Y. Cao, H. Zou and M. Xian, *Appl. Microbiol. Biotechnol.*, 2011, **89**, 573-583.
134. C. Wang, A. Thygesen, Y. Liu, Q. Li, M. Yang, D. Dang, Z. Wang, Y. Wan, W. Lin and J. Xing, *Biotechnol. Biofuels*, 2013, **6**, 74.
135. M. L. Jansen and W. M. van Gulik, *Curr. Opin. Biotechnol.*, 2014, **30**, 190-197.
136. C. Delhomme, D. Weuster-Botz and F. E. Kühn, *Green Chem.*, 2009, **11**, 13-26.
137. X. Jiang, X. Meng and M. Xian, *Appl. Microbiol. Biotechnol.*, 2009, **82**, 995-1003.
138. X. Zou, Y. Zhou and S.-T. Yang, *Biotechnol. Bioeng.*, 2013, **110**, 2105-2113.
139. J. Simon, J. V. Olsson, H. Kim, I. F. Tenney and R. M. Waymouth, *Macromolecules*, 2012, **45**, 9275-9281.
140. A. N. Zelikin and D. Putnam, *Macromolecules*, 2005, **38**, 5532-5537.
141. H. D. K. Drew and W. N. Haworth, *J. Chem. Soc.*, 1927, 775-779.

142. F. Zamora, M. Bueno, I. Molina, H. A. Orgueira, O. Varela and J. A. Galbis, *Tetrahedron: Asymmetr.*, 1996, **7**, 1811-1818.
143. Y. T. A. Oishi, K. Fujita,, A. Oishi, Y. Taguchi, K. Fujita, Jpn. Pat. JP2003252968, 2003.
144. C. C. Joseph, H. Regeling, B. Zwanenburg and G. J. F. Chittenden, *Tetrahedron*, 2002, **58**, 6907-6911.
145. A. F. Haider and C. K. Williams, *J. Polym. Sci. Part A: Polym. Chem.*, 2008, **46**, 2891-2896.
146. M. Tang, A. J. P. White, M. M. Stevens and C. K. Williams, *Chem. Commun.*, 2009, 941-943.
147. M. Tang, Y. Dong, M. M. Stevens and C. K. Williams, *Macromolecules*, 2010, **43**, 7556-7564.
148. I. M. Pinilla, M. B. Martínez and J. A. Galbis, *Carbohydr. Res.*, 2003, **338**, 549-555.
149. C. L. Romero Zaliz and O. Varela, *Carbohydr. Res.*, 2006, **341**, 2973-2977.
150. H. Urakami and Z. Guan, *Biomacromolecules*, 2008, **9**, 592-597.
151. E. L. Dane and M. W. Grinstaff, *J. Am. Chem. Soc.*, 2012, **134**, 16255-16264.
152. M. Chmielewski and Z. Kałuza, *Carbohydr. Res.*, 1987, **167**, 143-152.
153. E. L. Dane, S. L. Chin and M. W. Grinstaff, *ACS Macro Lett.*, 2013, **2**, 887-890.
154. S. L. Chin, Q. Lu, E. L. Dane, L. Dominguez, C. J. McKnight, J. E. Straub and M. W. Grinstaff, *J. Am. Chem. Soc.*, 2016, **138**, 6532-6540.
155. S. E. Stidham, S. L. Chin, E. L. Dane and M. W. Grinstaff, *J. Am. Chem. Soc.*, 2014, **136**, 9544-9547.
156. C. Ghobril, B. Heinrich, E. L. Dane and M. W. Grinstaff, *ACS Macro Lett.*, 2014, **3**, 359-363.
157. M. de Gracia, G. Martin, M. V. de Paz Báñez and J. A. Galbis Pérez, *Carbohydr. Res.*, 1993, **240**, 301-305.
158. M. Bueno, J. A. Galbis, M. G. García-Martín, M. V. De Paz, F. Zamora and S. Muñoz-Guerra, *J. Polym. Sci. Part A: Polym. Chem.*, 1995, **33**, 299-305.
159. F. Suriano, R. Pratt, J. P. K. Tan, N. Wiradharma, A. Nelson, Y.-Y. Yang, P. Dubois and J. L. Hedrick, *Biomaterials*, 2010, **31**, 2637-2645.

Chapter 2

Cyclic Carbonate Monomers from CO_2 and Diols

2. Cyclic Carbonate Monomers from CO_2 and Diols

2.1. Introduction

2.1.1. CO_2 capture with organic superbases

The capture of CO_2 by insertion into an alcohol group with bicyclic amidine base 1,8- diazabicyclo[5.4.0]undec-7-ene (DBU) was first reported by Jessop *et al.*[1] in 2005. On bubbling, gaseous CO_2 at one atmosphere pressure and room temperature through a 1:1 mixture of the amine base and a primary alcohol, a marked increase in both the polarity and viscosity of the liquid mixture was noted. This was attributed to the formation of an amidinium alkyl carbonate salt (Scheme 2.01) based on changes in the chemical shifts of key protons in the ^{1}H NMR spectrum as well as solvatochromic measurements before and after exposure to CO_2. The ionic liquid was readily converted back to its non-ionic components upon exposure to an atmosphere of nitrogen or argon at room temperature or heating above 40 °C.

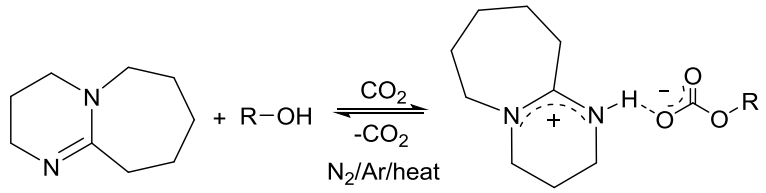

Scheme 2.01. Reversible formation of an amidinium alkyl carbonate salt on reaction of DBU, CO_2 and an alcohol.

Alcohol solutions of strong amidine and guanidine bases such as 1,5,7- triazabicyclo[4.4.0]dec-5-ene (TBD; pK_a= 26.0),* DBU (pK_a= 24.3) and 1,5- diazabicyclo[4.3.0]non-5-ene (DBN; pK_a= 23.8) have been found to be particularly effective in this reversible binding of CO_2. Compared to weaker bases triethylamine (pK_a= 18.8), 1,4-diazabicyclo[2.2.2]octane (DABCO, pK_a= 18.3) and pyridine (pK_a= 12.5), they rapidly form stabilised amidinium or guanidinium alkylcarbonates.[2-7]

Within the literature, much of the work with these reversible liquid systems has been in the development of CO_2 switchable solvents. For example, dissolving the reagents for a chemical reaction in the neutral apolar mixture and then precipitating the product in the polar zwitterionic liquid formed on exposure to CO_2.[8-11] Song *et al.*[12] used three equivalents of

* All pK_a values refer to the conjugate acid of the base in acetonitrile.

DBU to both dissolve crystalline cellulose in DMSO as the CO_2 derivative and then as an *in situ* organocatalyst for graft copolymerisation with L-lactide by ring-opening polymerisation (ROP). Introducing DBU and gaseous CO_2 has also been used to switch "off" the ROP of trimethylene carbonate (TMC). Conversion of the propagating alcohol end-group to the amidinium alkyl carbonate salt gave a means of stopping the polymerisation, which could be readily turned back "on" by bubbling N_2 through the solution (Figure 2.01).[13]

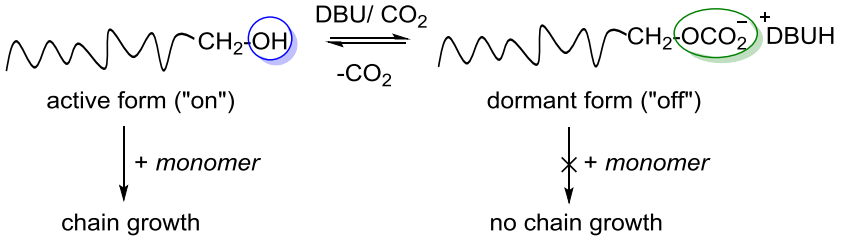

Figure 2.01. Switching ROP "on" and "off" by reversible formation of an amidinium alkyl carbonate salt. Reported by Coulembier *et al.*[14]

CO_2 switchable ligands have also been reported. In the hydroformylation of 1-octene with $[Rh(acac)(CO)_2]$ (acac= 2,4-pentanedione), phosphine ligands tagged with amidate groups enabled the reversible transfer of the catalyst between organic and aqueous phases on reaction with CO_2.[14, 15]

These systems also present a potentially efficient means for CO_2 fixation showing high volumetric and gravimetric capacity as well as being recyclable for industrial applications.[16] Abundant saccharides; D-glucose, D-mannose, β-cyclodextrin, alginic acid and mannitol in combination with DBU and tetramethylguanidine (TMG) superbases have been studied for CO_2 capture. With D-mannose, a 0.625 ratio of DBU equivalents to saccharide alcohol groups resulted in a CO_2 uptake of 13.9% corresponding to conversion of roughly 3 of the 5 alcohol groups to carbonates.[17]

The underlying mechanism of DBU-facilitated CO_2 insertion was suggested by Pérez *et al.*[18,19] to involve CO_2 activation by the amidine base through the formation of an isolable DBU-CO_2 zwitterion (Figure 2.02). Resonances were assigned at 160.7 and 166.4 ppm in the ^{13}C NMR data to the carbamic and amidinium carbon, respectively. However, thought to be a result of the crystallisation process, single-crystal X-ray diffraction data revealed a molecular structure corresponding to the bicarbonate salt $[DBUH]^+HCO_3^-$. Heldebrant *et al.*[20] disagreed with the formation of an isolable adduct suggesting instead that it is the

bicarbonate salt that forms in solution, due to the presence of water in the reaction medium. Based on NMR data no reaction was suggested to occur between DBU and CO_2 when thoroughly dried solvents were used. However with TBD, a CO_2 adduct has been isolated and its X-ray crystal structure determined.[21]

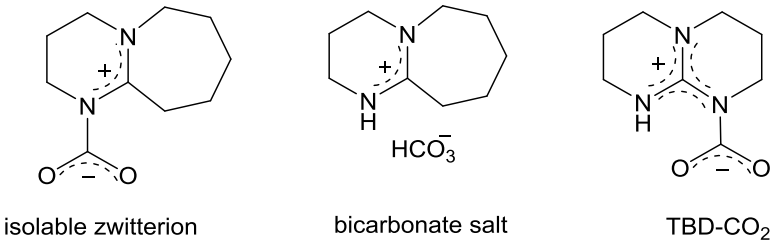

Figure 2.02. Formation of an isolable DBU-CO_2 zwitterion *versus* a bicarbonate salt in the presence of water.

Later, Wang *et al.*[22] carried out computational mechanistic studies of the propyl carbonate salt formed from CO_2, DBU and propanol. At the B3LYP/6-31G(d) level of theory in acetonitrile, four proposed mechanisms were investigated based on the various possible combinations of the three non-ionic reactants (Figure 2.03). **Mechanism-1**, nucleophilic addition of the propanol hydroxyl group at the carbonyl carbon of the CO_2 molecule was concluded to pose too high a kinetic barrier ($\Delta\Delta G^{\ddagger}$= +43.0 kcal mol^{-1}) to be achievable at reasonable reaction temperatures. The alkyl carbonic acid intermediate is also known experimentally to be unstable at room temperature, readily undergoing decarboxylation. Proton transfer from the alcohol to DBU in **mechanism-2** to form an alkoxide anion for subsequent reaction with CO_2, was also concluded to be unlikely based on pK_a considerations in acetonitrile solvent. Both the two-step bimolecular reaction (**mechanism- 3**), involving formation of a DBU-CO_2 adduct prior to alcoholysis ($\Delta\Delta G$= - 8.2 kcal mol^{-1}), and the single step trimolecular reaction (**mechanism-4**), were calculated to be the most plausible. In fact, a consideration of the kinetic parameters led to the suggestion that the trimolecular mechanism ($\Delta\Delta G^{\ddagger}$= +7.3 kcal mol^{-1}) was preferred, whereby proton transfer from the alcohol to the DBU occurs at the same time as CO_2 insertion.

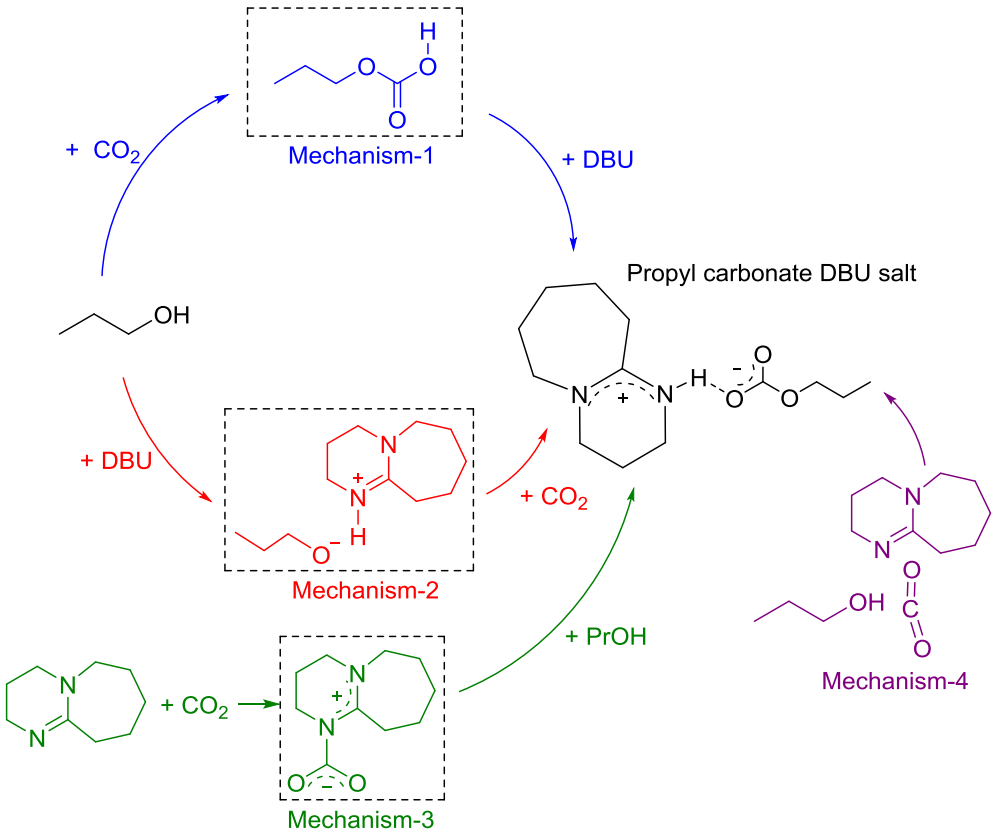

Figure 2.03. Four proposed mechanisms investigated computationally at the B3LYP/6-31G(d)/MeCN/298 K level of theory for the formation of propyl carbonate DBU salt. Intermediates are highlighted in boxes. Adapted from Wang *et al.*[22]

2.1.2. Cyclic carbonate formation

The role of organic bases such as DBU, DBN and TBD in facilitating the insertion of CO_2 into alcohols has been extended to their use in the direct coupling of diols with CO_2 in the synthesis of cyclic carbonates. Jang and co-workers[23] reported the preparation in reasonable yield of several cyclic carbonates using two equivalents of organic superbase at a temperature of 70 °C and 5 to 10 bar CO_2 pressure. The highest isolated yield reported was 86% for the coupling of glycerol and CO_2 with DBU to form five-membered glycerol carbonate after a reaction time of 18 hours. The use of dibromomethane as a solvent was found, through controlled experiments, to play a key role in cyclic carbonate formation with no product being isolated in its absence or with iodomethane solvent. A lower yield was achieved with dichloromethane (37% compared to 56% with CH_2Br_2 for the synthesis of phenyl- substituted ethylene carbonate). Ionic liquid, 1-butyl-3-methylimidazolium ($bmimPF_6$) was also used to enhance CO_2 solubility and more than doubled the yield of ethylene carbonate isolated. Under these reaction conditions, harder to synthesise six-

membered cyclic carbonate, 5,5-dimethyl-1,3-dioxan-2-one was also obtained in a moderate yield of 50% (Scheme 2.02).

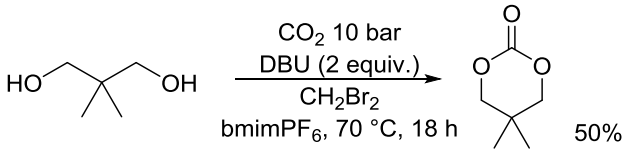

Scheme 2.02. Preparation of six-membered cyclic carbonate from 2,2-dimethyl-1,3-propanediol and CO_2.[23]

^{18}O-labelling of one of the hydroxyl oxygen atoms of an optically pure diol revealed no exchange of the ^{18}O isotope alongside retention of stereochemistry in the cyclic carbonate product. This led to the proposed mechanism shown in Figure 2.04 whereby, intramolecular cyclisation was aided by the formation of an -OCH_2Br leaving group. Ring closure by an intramolecular S_N2-type reaction with the carbonate nucleophile (resulting in inversion of stereochemistry) was suggested to be unlikely due to geometry constraints and therefore not observed.

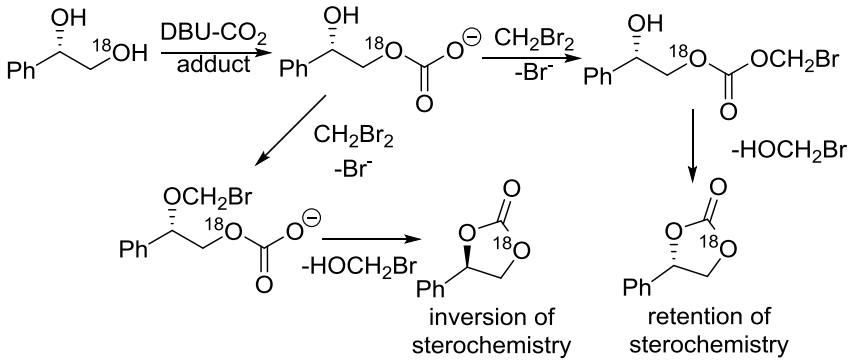

Figure 2.04. Mechanism proposed by Jang and co-workers[23] for cyclic carbonate formation in CH_2Br_2 solvent where retention of stereochemistry and no exchange of the ^{18}O label were observed.

Organic bases TBD, DBU and triethylamine were also reported by Huang *et al.*[24] as effective catalysts (2.5 mmol%) for the direct carbonation of 1,2-propanediol with CO_2, giving propylene carbonate in yields of 22.5, 12.6 and 6.2%, respectively. This was achieved after 15 hours at 175 °C and 100 bar CO_2 pressure (supercritical conditions) in acetonitrile solvent. The decreasing yields reflected the lower basicity of the non-ionic nitrogen bases used. Stronger bases are thought to favour the reaction by increasing the ability of the water by-product to hydrolyse the acetonitrile solvent, aiding its role as a dehydrating agent. Corresponding selectivities were however only around 60% in all cases with

1- hydroxylpropan-2-yl acetate being detected from the full hydrolysis of the solvent to acetic acid and subsequent reaction with the diol. Addition of ammonium carbonate was found to enhance the catalytic selectivity (>99%) though even lower yields of cyclic carbonate were then reported (see Section 1.4.4). No control experiments were carried out to investigate the effect of just using the ammonium carbonate.

2.2. Direct Coupling of 1,3-Butanediol and CO_2 in the Absence of a Catalyst

As a benchmark, the thermodynamics and kinetics for the direct coupling of 1,3-butanediol with CO_2 to give the corresponding cyclic carbonate and water by-product were considered computationally in the absence of any additional reagents or catalyst. 1,3-Butanediol serves as a simple model compound for sugars containing both a primary and secondary hydroxyl group. Density Functional Theory (DFT) calculations were carried out with the 6-31++G(d,p) basis set at a temperature of 298 K using the rωb97xd long-range corrected hybrid functional developed by Chai and Head-Gordon.[25, 26] This functional includes an empirical dispersion correction and has been shown to give good agreement with experimental data for both thermodynamic and kinetic properties.[27] Solvent effects were taken into account by means of a conductor-like polarisable continuum model (cpcm)[28] and methanol initially assigned the solvent of choice, as ideally reactions would be carried out experimentally in neat diol.

The resulting reaction profile shown in Figure 2.05 considers only the *(R)*-stereoisomer of 1,3-butanediol and highlights two key transition states: CO_2 insertion (**TS_{AB}**) and intramolecular ring-closing (**TS_{DE}**). Overall the reaction from diol and CO_2 to cyclic carbonate and water was calculated to be thermodynamically unfavourable by $\Delta\Delta G$ = +3.1 kcal mol^{-1}. This is small, the average thermal energy per mole of molecules is ~1 kcal mol^{-1} at 298 K and emphasises the need to drive off the water by-product to pull the equilibrium over in favour of the cyclic carbonate. For further comparison, the energy difference between the lowest and highest energy conformers of 1,3-butanediol located (corresponding to rotation about the butane backbone) was +3.5 kcal mol^{-1}. (For context, $\Delta\Delta G$ calculated at the same level of theory for the coupling of 1,2-propanediol with CO_2 to form five-membered propylene carbonate was 0.0 kcal mol^{-1}).

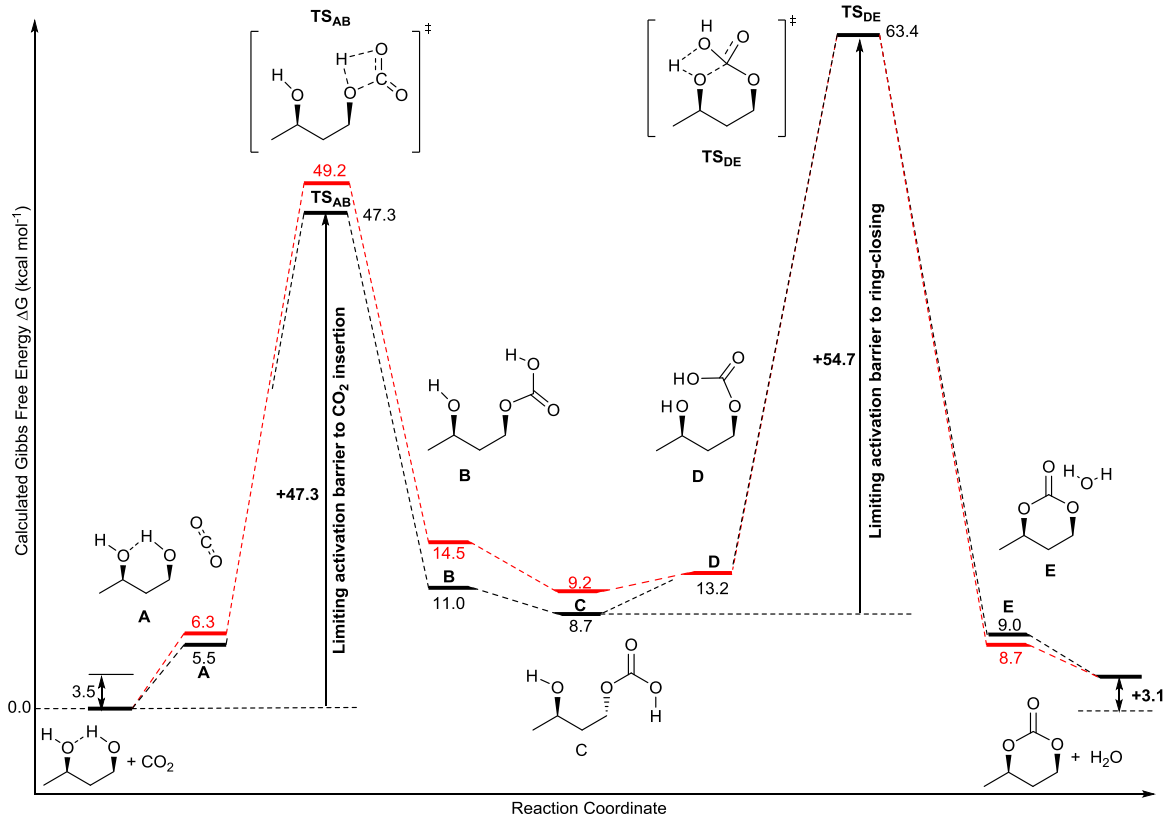

Figure 2.05. Schematic showing the relative DFT calculated Gibbs free energies (kcal mol^{-1}) at the 6-31++G(d,p)/rωb97xd/cpcm=MeOH/298 K level of theory for the reaction between *(R)*-1,3-butanediol and CO_2 in the absence of a catalyst. The combined free energies for CO_2 and the lowest energy conformer found for 1,3-butanediol (where the butane backbone is staggered and orientated to allow for a hydrogen-bonding interaction) were taken as the reference point (0.0 kcal mol^{-1}), to which all other values are quoted relative to. The scheme in black refers to reaction at the primary hydroxyl group to which all chemical structures relate and in red, reaction at the secondary alcohol.

The minimum kinetic barrier to CO_2 insertion (**TS_{AB}**) was calculated as $\Delta\Delta G^{\ddagger}$= +47.3 kcal mol^{-1} and corresponds to nucleophilic attack of the primary hydroxyl group at the carbonyl carbon alongside a proton transfer to one of the CO_2 oxygen atoms. Less steric hindrance on approach of the CO_2 molecule to the primary rather than secondary alcohol group is likely the reason for the slightly lower barrier to insertion at this centre. The optimised transition state shown in Figure 2.06(b) was verified by intrinsic reaction coordinate calculations to connect the two minima either side, Figure 2.06(a) and Figure 2.06(c). It shows the loss of linearity of the CO_2 molecule, lengthening of the C=O bond from 1.17 Å (in the preceding intermediate **A**) to 1.27 Å as well as the breaking of the O-H bond and migration of the proton to the carbonyl oxygen.

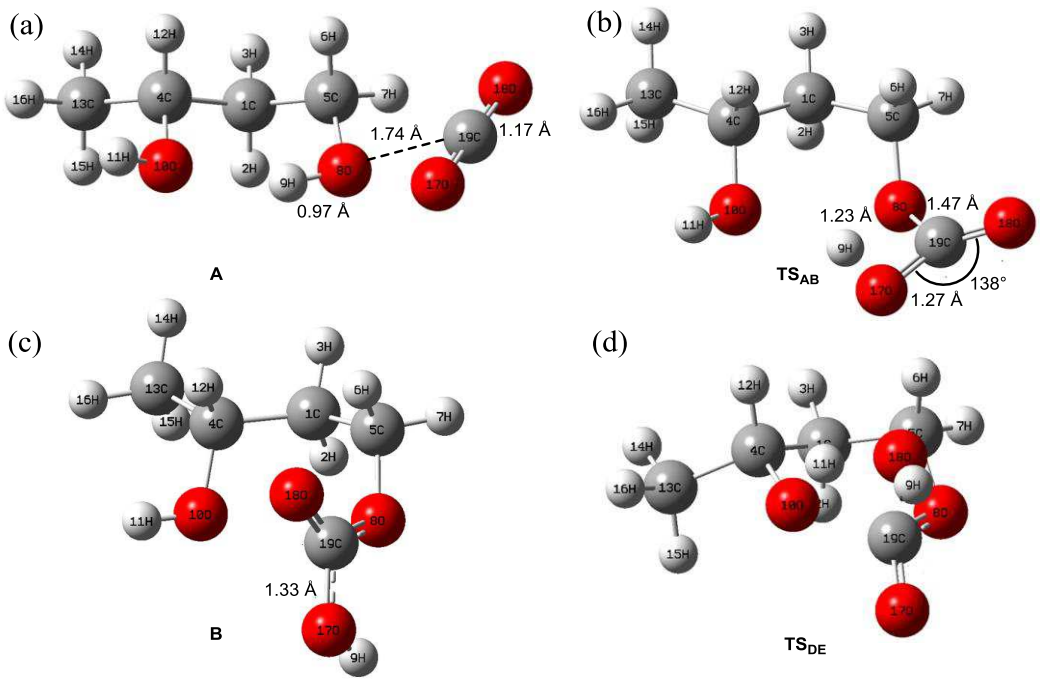

Figure 2.06. GaussView 5.0.8 images of the computed outputs at the 6-31++G(d,p)/rωb97xd/cpcm=MeOH/298 K level of theory for **(a)** CO_2 approaching the primary hydroxyl group, **(b)** the CO_2 insertion transition state $\mathbf{TS_{AB}}$, **(c)** the resulting carbonate intermediate and **(d)** the ring-closing transition state $\mathbf{TS_{DE}}$. Hydrogen atoms are in white, carbon in grey and oxygen in red.

Ring-closing to form the cyclic carbonate by an intramolecular nucleophilic addition-elimination pathway requires conformational re-organisation of the carbonic acid intermediate to the pre-cyclisation geometry **D** at 13.2 kcal mol^{-1} in the reaction profile (Figure 2.05). The ring-closing transition state $\mathbf{TS_{DE}}$ [Figure 2.06(d)], eliminating a molecule of water, presents at even higher barrier to cyclic carbonate formation (relative to CO_2 insertion) of $\Delta\Delta G^{\ddagger}$= +54.7 kcal mol^{-1} from the lowest energy carbonic intermediate located (**C**, Figure 2.05). Based on these calculations, both the barrier to CO_2 insertion and ring-closing are not expected to be achievable experimentally at ambient reaction conditions without additional reagents or the aid of a catalyst. For context, assuming first order reaction kinetics for conversion of the diol to the cyclic carbonate, reaching 99% conversion in 24 hours requires a rate constant of ~5.33×10^{-5} s^{-1}. To achieve this at a temperature of 298 K, the Gibbs free energy of the transition state would need to be less than ~23 kcal mol^{-1} (Eyring Equation).

2.3. CO_2-Insertion with DBU

2.3.1. Mono- and di- inserted products

CO_2 insertion into 1,3-butanediol was investigated with DBU. Reaction of one equivalent of the base with anhydrous (±)-1,3-butanediol in the presence of CO_2 at 1 atmosphere pressure and room temperature resulted in similar observations to those noted by Jessop *et al.*[1] Namely, an increase in viscosity was observed when the reaction was carried out neat or as a concentrated solution ($[diol]_0 \geq 1$ mol L^{-1}) alongside an associated broadening of the ^1H NMR signals. Changes in both the chemical shifts and number of ^1H and ^{13}C NMR environments was consistent with the formation of multiple amidinium alkyl carbonate species of the diol. The ^1H NMR spectra of the reaction carried out directly in $CDCl_3$ before and after CO_2 was bubbled though the reaction mixture at room temperature and atmospheric pressure for 12 hours is shown in Figure 2.07.

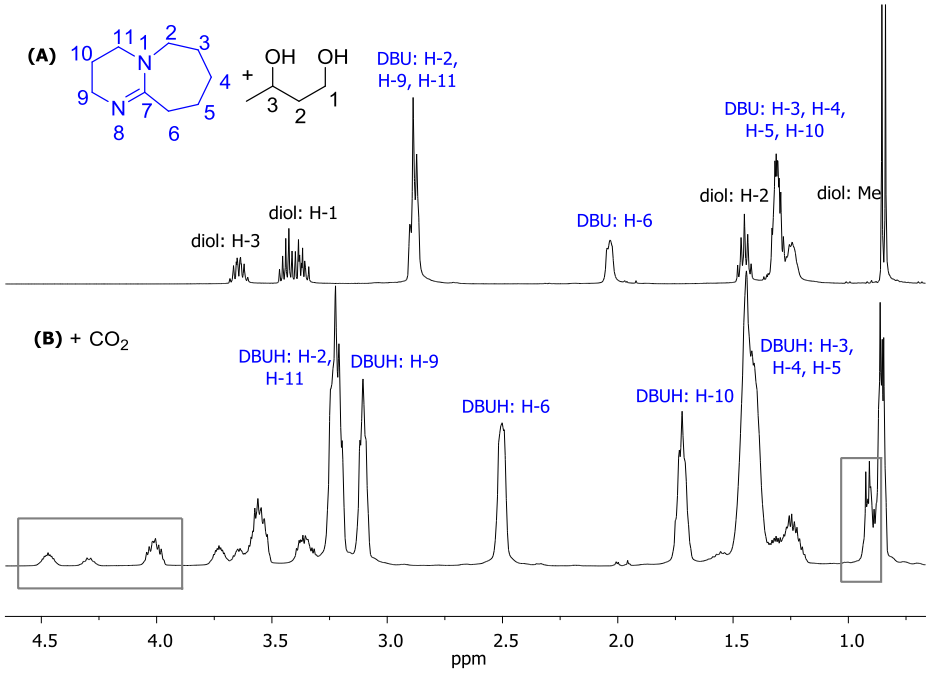

Figure 2.07. ^1H NMR spectra ($CDCl_3$, 400 MHz) of **(A)** 1,3-butanediol with 1 equiv. DBU in the absence of CO_2 and **(B)** after bubbling CO_2 through the reaction mixture at 1 atm and rt for 12 hours. New 1,3-butanediol resonances are highlighted between 4.0 and 4.6 ppm as well as methyl environments in the region below 1 ppm.

On introducing CO_2, a downfield shift in the DBU methylene proton environments and in particular, those assigned to carbon positions 2, 6, 9, 10 and 11 was observed, consistent with protonation at the N8 nitrogen atom. New proton environments associated with the 1,3-butanediol were clearly visible in the 4.0 to 4.6 ppm region alongside the presence of

additional methyl resonances below 1 ppm. Particular care was taken to carry out all manipulations under a dry CO_2 atmosphere using anhydrous reagents and solvents to avoid introducing water into the reaction medium and formation of $[DBUH]^+HCO_3^-$ salt.

CO_2-insertion into 1,3-butanediol (**1a**) can occur into either the primary (**1'a$_I$**) or secondary (**1'a$_{II}$**) hydroxyl groups as well as into both to yield di-inserted product, **1'a$_{bis}$** (Scheme 2.03). Formation of the latter inevitably results in less than 100% conversion with one equivalent of DBU.

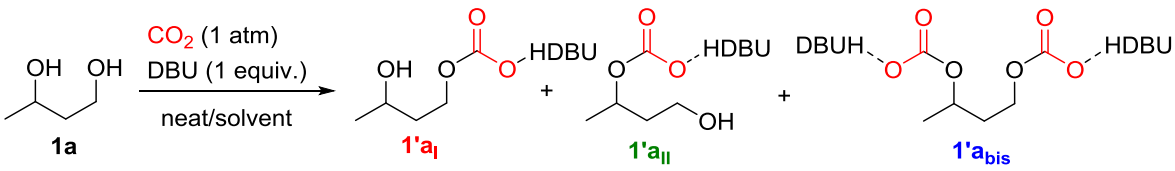

Scheme 2.03. CO_2 insertion with DBU reagent into the hydroxyl groups of 1,3-butanediol (**1a**) to form the primary (**1'a$_I$**), secondary (**1'a$_{II}$**) or di- (**1'a$_{bis}$**) carbonate species.

Full NMR assignment of the alkyl carbonate species was aided by 2D NMR experiments as well as an increase in the intensity of the signals assigned to **1'a$_{bis}$** with more concentrated reaction conditions and numbers of DBU equivalents (Figure 2.08).

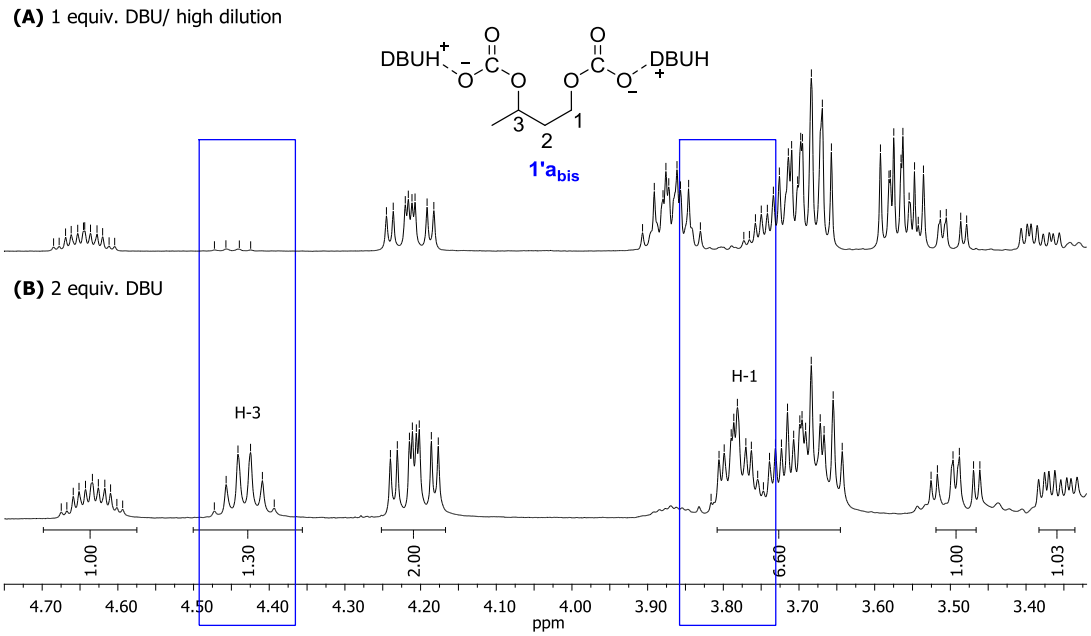

Figure 2.08. ^1H NMR spectra (400 MHz, $CDCl_3$) in the region from 4.75 to 3.32 ppm of **(A)** the CO_2 insertion reaction mixture at low diol concentration (0.1 mol L^{-1}) and with 1 DBU equivalent where the assigned H-1 and H-3 environments of the di-CO_2 inserted product **1'a$_{bis}$** are almost absent compared to in **(B)** at more concentration reactions conditions or with 2 DBU equivalents.

The signal centred at 4.43 ppm in Figure 2.08B correlated to a methine CH signal (HSQC and DEPT135 experiments). It also showed COSY cross peaks to both a methyl environment at 1.03 ppm ($^3J_{3\text{-Me}}$ = 6.2 Hz) and a CH_2 signal (H-2) in the 1.3 to 1.7 ppm region (not shown). The environment around 3.80 ppm was assigned to the H-1 methylene protons in **1'a$_{bis}$**, neighbouring the other carbonate group and thus slightly deshielded relative to the corresponding CH_2 of the unreacted diol.

Assignment of the corresponding proton environments in mono-inserted products, **1'a$_I$** and **1'a$_{II}$** is shown in Figure 2.09. The most downfield environment (δ_H ~ 4.64 ppm) was assigned to the methine H-3 in **1'a$_{II}$**, next to the electron-withdrawing carbonate group. Signals at both 4.20 and ~3.7 ppm correlated to the same methylene group and were assigned to H-1 and H-1' in **1'a$_I$**. A large coupling constant of 11.6 Hz was consistent with a germinal ^2J coupling. The reason for the chemical inequivalence of these two methylene protons may be conformational restriction brought about by the bulky amidinium carbonate salt; it is assumed that the DBUH cation remains associated with the carbonate anion acting to stabilise it. The analogous protons (H-1 and H-1'), adjacent to the primary hydroxyl group in **1'a$_{II}$** were also inequivalent, centred at 3.50 and 3.30 ppm and exhibited a similar ^2J coupling constant of 11.7 Hz.

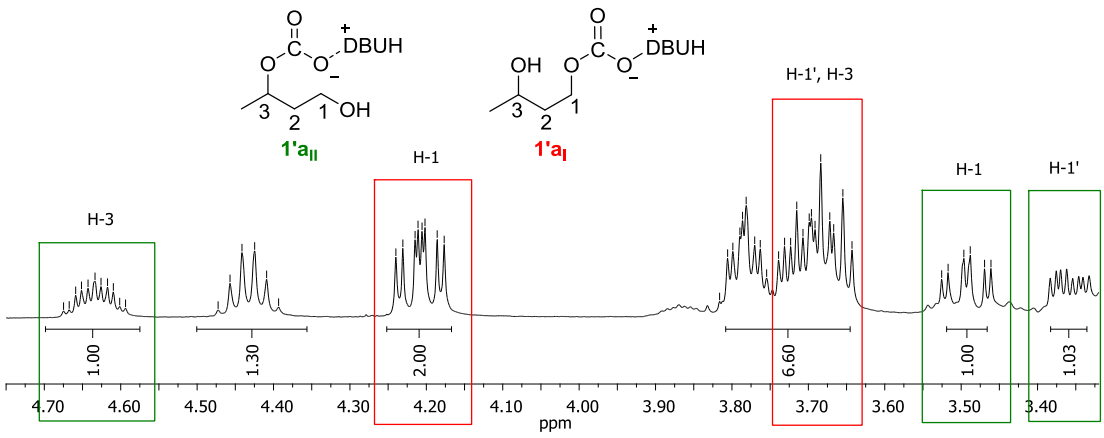

Figure 2.09. ^{1}H NMR (400 MHz, $CDCl_3$) in the region 4.75 to 3.32 ppm showing assignment of H-1 and H-3 environments in mono-inserted products **1'a$_I$** and **1'a$_{II}$**. Chemical inequivalence of H-1 and H-1'was attributed to conformational restrictions due to the bulky carbonate salt.

In the $^{13}C\{^1H\}$ NMR spectrum, the appearance of resonances in the region of 156 to 158 ppm was characteristic of carbonate salt formation (Figure 2.10). With two DBU equivalents, environments at 158.6 and 158.2 ppm were assigned to the C=O resonances of the di-inserted product. Assignment of the carbon environments in mono-inserted products

1'a$_I$ and **1'a$_{II}$** was based on proximity to the electron-withdrawing carbonate group. For example, in **1'a$_{II}$** the C-3 environment residing next to the carbonate appears at higher chemical shift compared to in **1'a$_I$** where the same carbon is adjacent to the alcohol group. In addition, the relative peak intensity (although only qualitative) is consistent with more of the mono-insertion product into the less sterically hindered primary hydroxyl group as observed in the corresponding ^{1}H NMR data. Subsequently, carbonate environments at 159.0 and 159.1 ppm were assigned to mono-inserted products **1'a$_I$** and **1'a$_{II}$**, respectively.

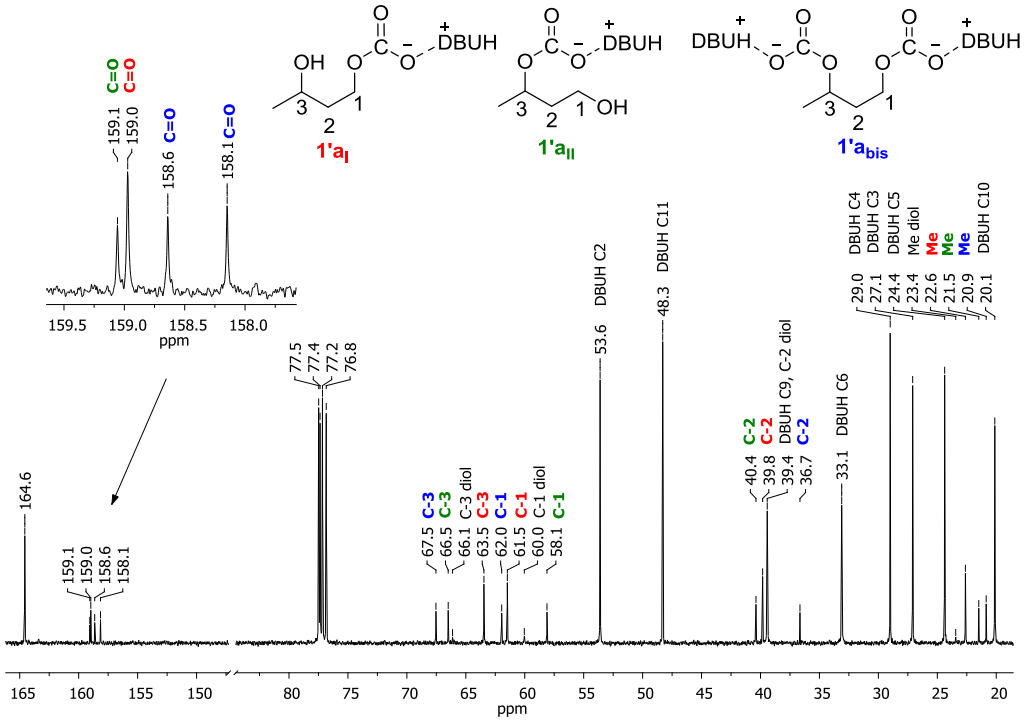

Figure 2.10. $^{13}C\{^1H\}$ NMR spectrum (101 MHz, $CDCl_3$) for the reaction of 1,3-butanediol with CO_2 in the presence of 2 equivalents of DBU after 12 hours at room temperature and atmospheric pressure. The carbon environments for mono-inserted products, **1'a$_I$** and **1'a$_{II}$** are in red and green, respectively with those for the di-inserted product **1'a$_{bis}$** in blue.

2.3.2. Variation of the reaction conditions

Following NMR assignment of the carbonate species of 1,3-butanediol (**1a**), the conversion to CO_2-inserted products and selectivity for mono-insertion (**1'a$_I$** and **1'a$_{II}$**) was investigated under various reaction conditions of temperature, solvent and equivalents of DBU. The key findings are summarised in Table 2.01. In neat diol (Entry 1), conversion was limited by the increase in viscosity upon CO_2 insertion and ionic liquid formation, hindering stirring. The addition of solvent also played a role in providing a medium for CO_2 dissolution. Regardless of the choice of solvent, CO_2 insertion following dropwise addition of DBU proceeded

quickly at room temperature and 1 atm CO_2 pressure, with generally good selectivity towards mono-inserted products (*ca.* 60% of products). A preference for carbonation into the less sterically hindered primary hydroxyl group was consistently observed with roughly twice the percentage conversion to **1'a$_I$** over **1'a$_{II}$**. CO_2 insertion occurred readily into methanol, when used as the solvent, significantly reducing the percentage conversion to carbonate products of **1a** (Entry 2).

Table 2.01. Reaction of 1,3-butanediol (**1a**) with DBU and 1 atm CO_2.[a]

					Conversion to carbonated products [b] (%)				
Entry	**DBU (eq.)**	**Solvent**	**T (°C)**	**[1a] (mol L^{-1})**	**Total**	**1'a$_{I+II}$**	**1'a$_I$**	**1'a$_{II}$**	**1'a$_{bis}$**
1	1	Neat	25	-	47	44	31	14	3
2	1	MeOH	25	1.7	18	18	18	0	0
3	1	C_7D_8	25	1.7	60	56	37	19	4
4	1	DMSO-d_6	25	1.7	57	46	31	15	11
5	1	CD_3CN	25	1.7	73	58	40	18	15
6	1	$CDCl_3$	25	1.7	78	69	46	23	9
7[c]	1	$CDCl_3$	25	1.7	69	52	35	17	17
8	2	$CDCl_3$	25	1.7	92	66	45	21	26
9	3	$CDCl_3$	25	1.7	>99	57	40	17	43
10[d]	1	$CDCl_3$	25	1.7	62	56	37	19	6
11	1	$CDCl_3$	25	1	77	69	46	23	8
12	1	$CDCl_3$	25	0.5	75	68	47	21	7
13	1	$CDCl_3$	25	0.1	78	73	49	24	5
14	1	$CDCl_3$	0	1.7	77	62	43	19	15
15[e]	1	$CDCl_3$	0	1.7	84	69	47	22	15
16	1	$CDCl_3$	-78	1.7	77	68	45	23	9
17	1	$CDCl_3$	60	1.7	64	58	39	19	6
18	1	CD_3CN	70	1.7	63	52	38	14	11
19	1	CD_3CN	90	1.7	50	47	35	12	3
20[f]	1	CD_3CN	90	1.7	55	48	35	13	7

[a] Reaction conditions: diol (5.6 mmol, 1.7 mol L^{-1}), DBU (5.6 mmol), rt, CO_2 (1 atm), 2 h (saturation). [b] Determined by relative integration of methine signals in ^{1}H NMR spectrum. [c] Addition of 1-butyl-3-methylimidazolium hexafluorophosphate (bmimPF$_6$, 5.6 mmol). [d] 1 equiv. TBD used. [e] 4 h (saturation). [f] 8 bar CO_2 pressure.

Reactions in apolar toluene-d_8 resulted in lower conversions compared to more polar solvents, $CDCl_3$ and MeCN-d_3 due to a lower solubility of both the starting diol and carbonated products, resulting in formation of a toluene-ionic liquid biphasic mixture (Entry 3). More polar solvents were anticipated to stabilise the carbonate salt, though DMSO-d_6

gave similar total percentage conversions to toluene but with more di-inserted product being observed (Entry 4). Overall, greater total percentage conversions to CO_2-inserted products, **1'a$_{I}$**, **1'a$_{II}$** and **1'a$_{bis}$** (over 70%) were observed when solvents such as chloroform or acetonitrile were used. Nevertheless, even in solution and with ionic liquid bmimPF_6, reported by Lim *et al.*[23] to increase CO_2 solubility (Entry 7), full conversion was not observed with one DBU equivalent.

Doubling the number of equivalents of DBU added to the reaction mixture resulted in a 92% total conversion compared to 78% under the same conditions with one equivalent (Entries 6 and 8). Addition of three equivalents resulted in near full conversion to carbonate species (Entry 9) with roughly equal percentages of **1'a$_{bis}$** and **1'a$_{I}$**. Experiments with more basic TBD gave a similar distribution of CO_2 inserted products to DBU (under the same reaction conditions) but was more sensitive to the presence of moisture in the reaction mixture (Entry 10). Weaker bases, triethylamine and pyridine resulted in no observable carbonation of the diol.

Dilution of the reaction conditions in $CDCl_3$ from 1.7 to 0.1 mol L^{-1} resulted in similar total percentage conversions but showed a greater selectivity to mono-inserted products due to the occurrence of less di-carbonation (Entry 13). Cooling the reaction mixture to 0 °C to enhance CO_2 solubility and drive the postulated trimolecular reaction resulted in similar total percentage conversions to those at room temperature after the same reaction time (Entry 14). However, after a further 2 hours, (accounting for the slower rate of reaction) the total conversion plateaued at 84% (Entry 15), with a product distribution consisting of more di-inserted product. As already reported, heating above 40 °C leads to decarboxylation of the amidinium alkyl carbonate salts (Entries 17-19).

Under none of these reaction conditions was the cyclic carbonate observed by NMR spectroscopy, GC-MS, high resolution- electrospray ionisation mass spectrometry [HR-MS (ESI)] or FTIR analysis. The most extreme conditions trialled were heating to 90 °C under an 8 bar CO_2 pressure to prevent decarboxylation (Entry 20). In this case, acetonitrile was used as the solvent due to its potential to act as a dehydrating agent, one mole being required per mole of diol that undergoes cyclisation to produce a stoichiometric water by-product. Thus, as further corroboration of the lack of cyclic carbonate formation, no acetamide or acetic acid hydrolysis products of the acetonitrile solvent were detected either.

2.3.3. DFT modelling of DBU facilitated CO_2 insertion

In agreement with the work carried out by Wang *et al.*,[18] calculations at the rωb97xd/6-31+G(d) level of theory in methanol suggested that a trimolecular mechanism was plausible for the capture of CO_2 with *(R)*-1,3-butanediol using DBU. Significantly lower kinetic barriers were calculated for CO_2 insertion into the primary (**TS_{AB}**, $\Delta\Delta G^{\ddagger}$= +13.6 kcal mol^{-1}) and secondary (**$TS_{AB'}$**, $\Delta\Delta G^{\ddagger}$= +18.9 kcal mol^{-1}) hydroxyl groups with DBU compared to in its absence ($\Delta\Delta G^{\ddagger}$= +47.3 kcal mol^{-1}). Represented in Figure 2.11, **TS_{AB}** shows transfer of the primary hydroxyl proton to the DBU nitrogen atom together with the bending of the CO_2 molecule on approach to the alcohol oxygen.

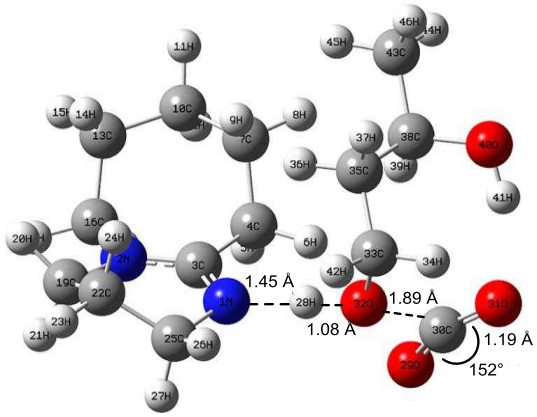

Figure 2.11. GaussView 5.0.8 image of the optimised transition state (rωb97xd/6-31+G(d)/cpcm=MeOH/298 K) for CO_2 insertion into the primary hydroxyl group (**TS_{AB}**). Hydrogen atoms are in white, carbon in grey, oxygen in red and nitrogen in blue.

The resulting DBUH cation readily migrates (**TS_{BC}** in Figure 2.12) from residing at the alcohol oxygen atom (intermediate **B**) to the CO_2 oxygen atom of the newly formed alkyl carbonate anion (intermediate **C**). Formation of this alkyl amidinium carbonate salt provides a thermodynamic driving force for CO_2 insertion: $\Delta\Delta G$= -8.5 kcal mol^{-1} for formation of the DBUH carbonate salt compared to +8.7 kcal mol^{-1} for the carbonic acid without DBU.

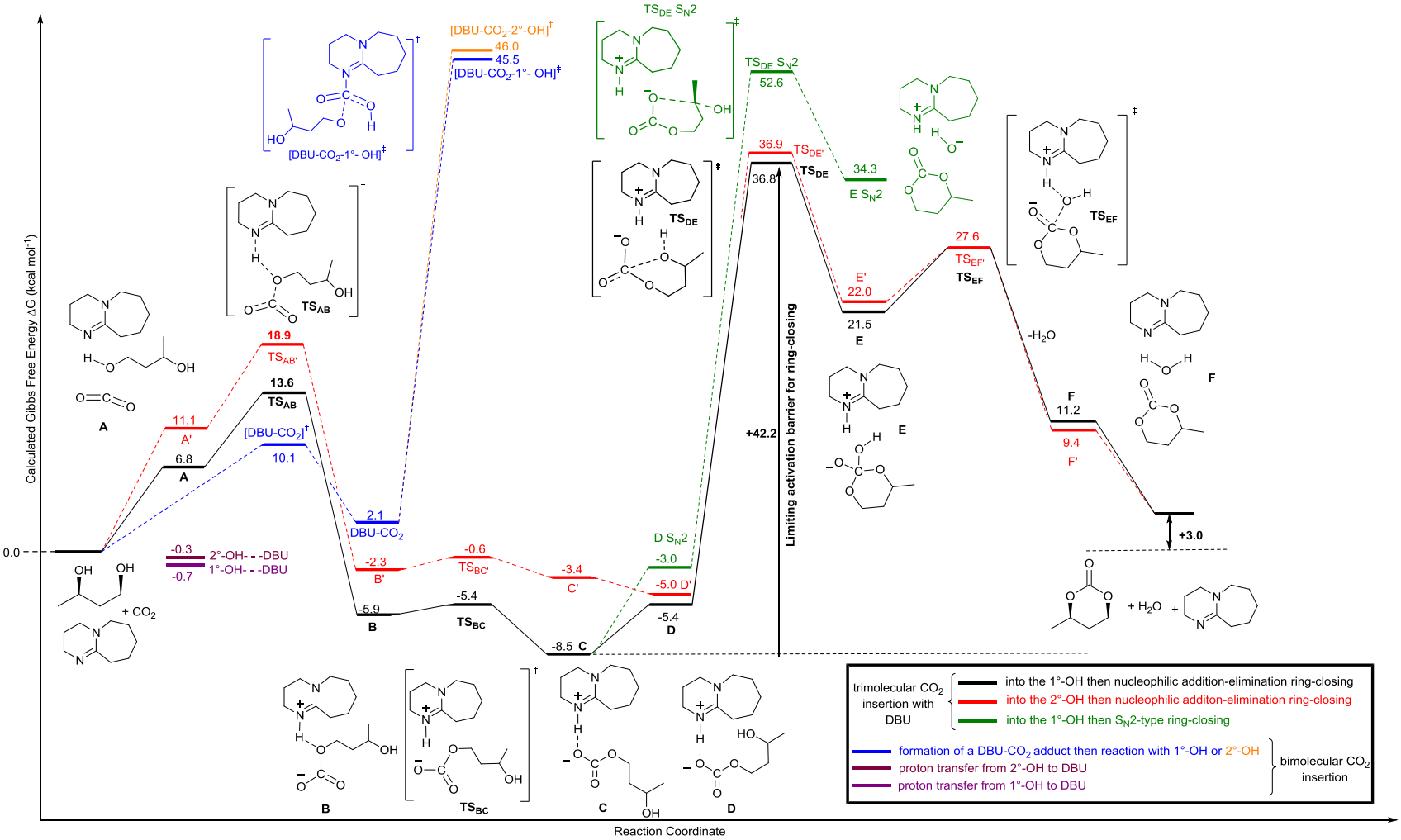

Figure 2.12. DFT modelling at the rωb97xd/6-31+G(d)/cpcm=MeOH/298 K level of theory for the reaction between DBU, CO_2 and *(R)*-1,3-butanediol (0.0 kcal mol^{-1}). The most favourable pathway calculated (in black) refers to CO_2 insertion with DBU *via* a trimolecular mechanism into the primary hydroxyl group (1°-OH) to form **1'a$_I$** (intermediate **C**). Ring-closing to form the cyclic carbonate by either a nucleophilic addition-elimination or S_N2-type mechanism (green) pose activation barriers to high to be able achievable at reasonable conditions. Reaction at the secondary hydroxyl group (2°-OH) is shown in red, formation of a DBU-CO_2 adduct in blue and interaction of the DBU with the -OH groups in purple.

Comparatively, activation of CO_2 by formation of a DBU-CO_2 adduct and subsequent reaction with either alcohol group only lowers the CO_2-insertion barrier by 3-4 kcal mol^{-1} (blue profile in Figure 2.12) relative to no DBU being present. Interaction of the hydroxyl proton with the DBU amidinium nitrogen was calculated to be slightly thermodynamically favourable (purple profile in Figure 2.12) though, complete proton transfer to form an alkoxide is unlikely in the methanol solvent.

Ring-closing (**TS_{DE}**) was calculated to pose a minimum activation energy barrier $\Delta\Delta G^{\ddagger}$ of +42.2 kcal mol^{-1} and corresponds to nucleophilic attack of the secondary alcohol at the primary carbonate carbonyl to form a DBU-stabilised intermediate **E**. Subsequent loss of water leads to formation of the cyclic carbonate product. Although this is 12.5 kcal mol^{-1} lower than the barrier to ring-closing in the absence of DBU, it was still too high to be achievable at reasonable reaction conditions. Comparatively, ring closure by an S_N2-type mechanism involving backside attack of the carbonate anion and loss of a hydroxide anion, as a poor leaving group, was calculated to be even less kinetically feasible ($\Delta\Delta G^{\ddagger}$= +61.1 kcal mol^{-1}, green profile in Figure 2.12).

2.4. Cyclisation *via* a Leaving Group Strategy

DBU significantly lowered the barrier to CO_2 insertion but had insufficient impact on the subsequent cyclisation step. To lower this limiting kinetic barrier to cyclic carbonate formation, a leaving group strategy was applied. Following the selective mono-insertion of CO_2 into 1,3-butanediol at 0.1 mol L^{-1} in chloroform, one equivalent of tosyl chloride and triethylamine were added and the reaction mixture stirred at room temperature. Rapid formation of the corresponding cyclic carbonate, 4-methyl-[1,3]-dioxane-2-one (**2a**) was observed by NMR spectroscopy and confirmed by mass spectrometry. The carbonyl environments due to the carbonate salt at 158-159 ppm in the $^{13}C\{^{1}H\}$ NMR spectrum disappeared and a new resonance at 147 ppm was observed, characteristic of the cyclic species.

The cyclic carbonate was isolated in a 44% yield, 60% conversion based on the percentage of mono-CO_2 inserted products, **1'a_I** and **1'a_{II}** (Table 2.02, Entry 1). Column chromatography from the crude reaction mixture gave the best isolated yields of **2a** and in the highest purity compared to standard organic work-ups involving aqueous and acidic

washes, which resulted in significant ring-opening. By-products of the reaction determined by mass spectrometry included tosylated derivatives of the diol as well as dimeric and trimeric carbonate species. A higher isolated yield of 68% (99% conversion based on mono-inserted products) was achieved in the same reaction time but under more concentrated conditions of 1.7 mol L^{-1} (Table 2.02, Entry 2). This was reasoned to be due to the slower rate of reaction and decreased stability of the ionic salt pair at lower concentrations leading to more decarboxylation during the cyclisation conditions. Thus, there was a trade-off between low diol concentrations favouring both mono-CO_2 insertion and desired unimolecular cyclisation compared to the lower volume of solvent required at higher concentrations and greater $RCO_3^-DBUH^+$ ion pair stability. Importantly, the yields were comparable to traditional phosgene based (50%)[29] and oxidative carbonylation methods (45%)[30] for the synthesis of **2a.**

Methanesulphonyl chloride was also investigated as a leaving group strategy, owing to the slightly better overall atom economy of the process (22 *versus* 19% with TsCl), but resulted in lower conversions to the cyclic carbonate. Significantly lower conversions (28% relative to a styrene internal standard) were also observed in the absence of pyridine or triethylamine bases and cyclisation did not occur in the presence of triethylamine alone. The reaction was found to be robust; although, most effective with dried reagent grade CO_2 (introduced using Schlenk line techniques), a balloon filled with CO_2 from sublimed dry ice could also be used, albeit resulting in a lower isolated yield (48%). This was attributed to moisture deactivating the DBU as the DBUH carbonate salt (Table 2.02, Entry 3). The reaction also proceeded without solvent giving a 30% yield.

The substrate scope of the procedure was investigated with a range of 1,3-diols, **1a-1j** (Table 2.02) containing both primary and secondary alcohol groups as well as additional functionalities to yield known cyclic carbonates **2a-2j**. Conversions were based on the percentage of mono-CO_2 inserted product determined by NMR analysis for each diol and is considered an indicator of decarboxylation on addition of the tosyl chloride.

Table 2.02. Synthesis of known 6-membered cyclic carbonates, **2a-2j** by DBU-facilitated CO_2 insertion (1 atm pressure) followed by *in situ* cyclisation at room temperature (rt) with tosyl chloride and triethylamine. Unless otherwise stated, $[diol]_0 = 1.7$ mol L^{-1}.

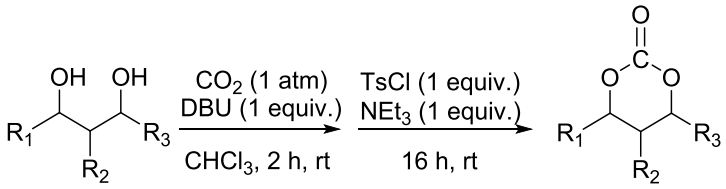

1 **2**

Entry	Diol		Yield (%) [conv.] [a], [b]	Product	
1[c]	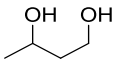	**1a**	44 [60]	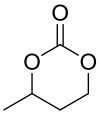	**2a**
2	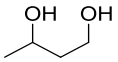	**1a**	68 [99]	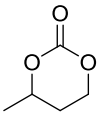	**2a**
3[d]	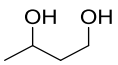	**1a**	48 [60]	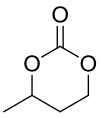	**2a**
4	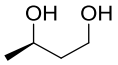	**(*R*)-1a**	68	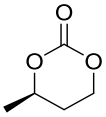	**(*R*)-2a**
5	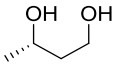	**(*S*)-1a**	70	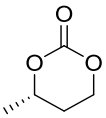	**(*S*)-2a**
6	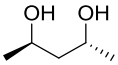	**1b**	53 [71]	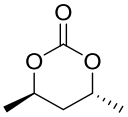	**2b**
7	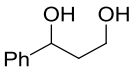	**1c**	55 [96]	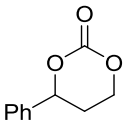	**2c**
8		**1d**	53 [82]	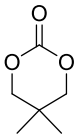	**2d**
9	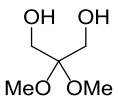	**1e**	49 [78]	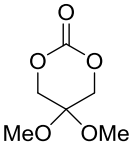	**2e**

10	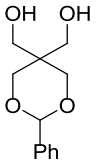	**1f**	46 [71]	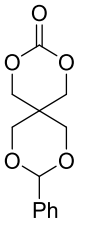	**2f**
11	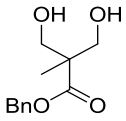	**1g**	41 [70]	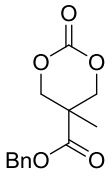	**2g**
12		**1h**	68 [80]	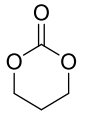	**2h**
13	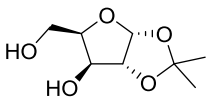	**1i**	11	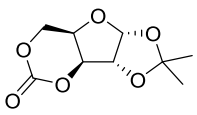	**2i**
14[e]	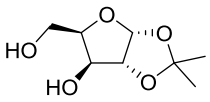	**1i**	67	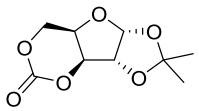	**2i**
15[e]	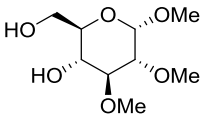	**1j**	62	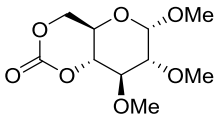	**2j**

[a] Isolated yield. [b] Based on % conversion to mono-CO_2 inserted product determined by ^{1}H NMR spectroscopy. [c] 0.1 mol L^{-1} $[diol]_0$. [d] CO_2 from sublimed dry ice. [e] 0.1 mol L^{-1} $[diol]_0$ in MeCN with CO_2 saturation and addition of TsCl solution at 0 °C.

In general, high conversions (60 -99%) from the mono-CO_2 insertion products to the cyclic carbonate product indicated that the cyclisation proceeded efficiently under the reaction conditions. Moderate yields were obtained for most diols, comparable with phosgene-based and alternative methods. For example, the cyclic carbonate of 2,2-dimethyl-1,3-propanediol (**2d**, Entry 8) isolated in a 53% yield has previously been reported using phosgene derivatives (60%),[31] oxidative carbonylation (50%)[32] and the metal-free dibromomethane cyclisation route detailed in Section 2.1.2 (50%).[23] For some diols, poor solubility in organic solvents was overcome on reaction with CO_2 to form a soluble ionic salt. Attempts with 1,4-butanediol, under these reaction conditions, to yield a seven-membered cyclic carbonate monomer were unsuccessful. Mass spectrometry provided evidence for the formation of dimeric and trimeric carbonate species only.

For sugar based 1,3-diols (**1i** and **1j**, Entries 13-15), high dilution and cold temperatures were found to be key in favouring the desired unimolecular cyclisation over the competing dimerisation reaction. The orientation of the 1,3-diol component imposed by the sugar ring may mean that such conformationally restrained systems are more prone to bimolecular dimerisation reactions. An isolated yield of just 11% was achieved for the cyclisation of *O*-isopropylidene-protected D-xylose monomer (**1i**, Entry 13) under the reaction conditions used for the preceding cyclic carbonates **2a** to **2j**. Dilution of the reaction conditions to 0.1 mol L^{-1} and cooling to 0 °C, both to increase the concentration of dissolved CO_2 and favour unimolecular cyclisation resulted in a substantially improved yield of 67% (Entry 14). The requirement for more solvent with sugar-based diols also prompted the replacement of chlorinated solvents with acetonitrile. In the literature, **1i** was isolated in 41% yield using ethyl chloroformate and triethylamine (see Chapter 3, Section 3.1).[33] Similarly, under these improved reaction conditions, bicyclic protected D-glucose based monomer **2j** (Entry 15) was prepared in a 62% yield, a significant improvement on existing methods namely, 36% using bis(pentafluorophenyl)carbonate at 60 °C[34] or 25% with ethyl chloroformate (see Chapter 3, Section 3.1).[35]

2.5. Mechanistic Considerations

The mechanism for cyclisation of **1'a$_I$** (or **1'a$_{II}$**) with tosyl leaving group was envisaged to proceed by two routes (Figure 2.13). Firstly, tosylation of the CO_2 introduced carbonate could occur leading to cyclisation *via* a nucleophilic addition-elimination pathway and retention of any stereochemistry present. Secondly, tosylation could occur at the free hydroxyl group leaving the carbonate to act as the nucleophile in a concerted intramolecular substitution reaction. Displacement of the tosyl group in this "S_N2-like" mechanism would result in inversion of any stereochemistry present. Strictly speaking, as this is a unimolecular cyclisation and not a bimolecular reaction this is not an S_N2 process (it would show S_N1 kinetics). Nevertheless, "S_N2-type" is used here to describe a concerted process involving nucleophilic backside attack (180°) of the carbonate anion and concomitant elimination of the tosylate.

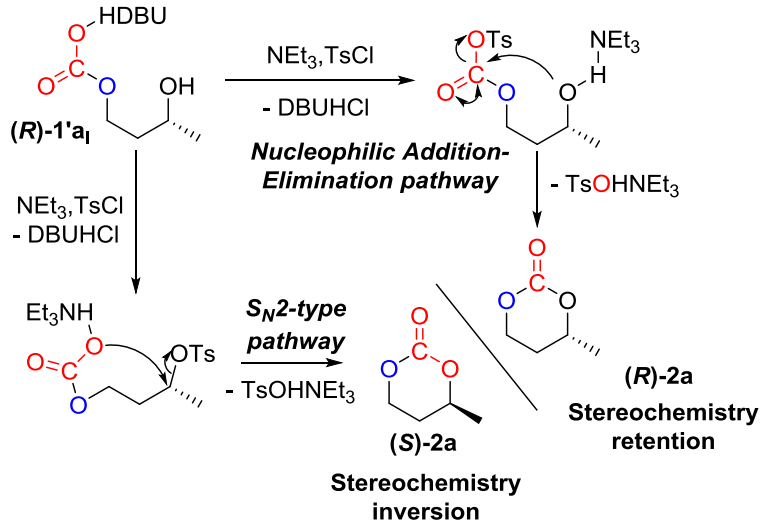

Figure 2.13. Two plausible mechanisms for cyclic carbonate formation from **1'aI** with NEt_3 and TsCl: tosylation of the carbonate leading to cyclisation *via* a nucleophilic addition-elimination pathway or tosylation of the alcohol group leading to inversion of stereochemistry by an S_N2-type displacement of the tosyl group.

Cyclisation of enantiopure *(R)*- and *(S)*-1,3-butanediols (Table 2.02, Entries 4 and 5) and polarimetry measurements of both the diol and cyclic carbonate product indicated retention of the stereochemistry and thus a nucleophilic addition-elimination mechanism. Further confirmation by chiral HPLC proved challenging due to the polarity of the cyclic carbonate. Moreover, the (*R,R)*-cyclic carbonate (**2b**) was detected and isolated exclusively from cyclisation of *(2R,4R)*-pentane-2,4-diol, **1b** (Table 2.02, Entry 6 and Figure 2.14). Inversion of the stereochemistry at either chiral carbon centre in an intramolecular S_N2-type cyclisation would result in formation of the *meso*-compound. The unstable nature of the tosylated carbonate and its rapid cyclisation, meant it could not be isolated to further confirm the presence of the reaction intermediate.

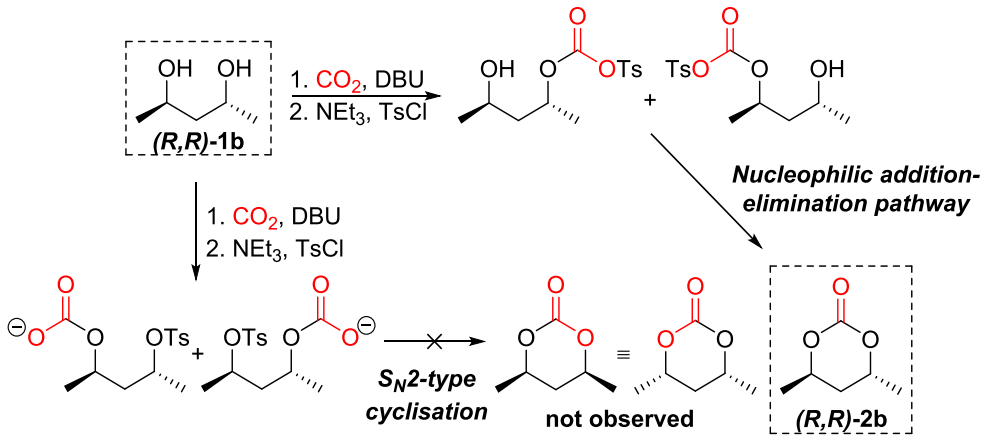

Figure 2.14. Cyclocarbonation of (2*R*,4*R*)-pentane-2,4-diol (**1b**) with retention of stereochemistry to yield (*R,R*)-**2b**. Inversion of the stereochemistry at either stereocentre to yield the *meso*-compound was not observed supporting cyclisation *via* a nucleophilic addition-elimination mechanism.

Glycerol, a high-volume waste material from industry, resulted in exclusive formation of the more thermodynamically favoured five-membered glycerol carbonate product (Figure 2.15). Based on geometry constraints, it is unlikely that cyclisation to the five- membered ring could occur *via* an S_N2-type backside attack, this further supported the nucleophilic addition-elimination pathway.

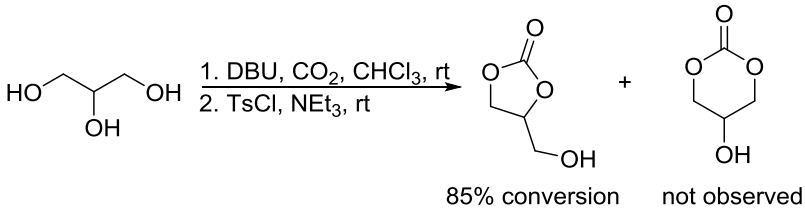

Figure 2.15. Formation of glycerol 1,2-carbonate, $[diol]_0 = 0.1$ mol L^{-1}. Conversion determined by ^1H NMR spectroscopy.

Finally, the *cis*- and *trans*- configurations (indicated by the *J*-coupling constants in the ^1H NMR spectra) of the xylose (**2i**) and glucose (**2j**)-derived cyclic carbonates, respectively were consistent with the stereochemistry of the analogous monomers synthesised using phosgene derivatives[34] (also a nucleophilic addition-elimination mechanism). These configurations were verified by single crystal X-ray diffraction.

2.5.1. DFT modelling of the cyclisation step

DFT calculations were performed at the rωb97xd/6-31+G(d)/298 K level of theory and initially in methanol for comparison with the above calculations. Nucleophilic addition of the secondary alcohol group at the primary tosylated carbonate had a calculated $\Delta\Delta G^{\ddagger}$ of +30.1 kcal mol^{-1}. Increasing the nucleophilicity of the ring-closing hydroxyl group by introducing triethylamine base (Figure 2.16), lowered this barrier further to +16.9 kcal mol^{-1}. That is, the barrier was more than halved in the presence of triethylamine and the tosyl leaving group compared to when only DBU was present (+42 kcal mol^{-1}) and is comparable to the calculated barriers for DBU-aided CO_2 insertion. Formation of NEt_3Cl and DBUHOTs salts also provided a strong thermodynamic driving force ($\Delta\Delta G$= -41.7 kcal mol^{-1}) for cyclisation from the alkyl amidinium carbonate. This overcomes the equilibrium limitation of the direct coupling of 1,3-butanediol with CO_2 by eliminating altogether the water by- product. Similarly, nucleophilic backside attack of the primary carbonate anion eliminating the secondary tosylate (Figure 2.17) had a calculated energy barrier ($\Delta\Delta G^{\ddagger}$) of only +20.7 kcal mol^{-1}.

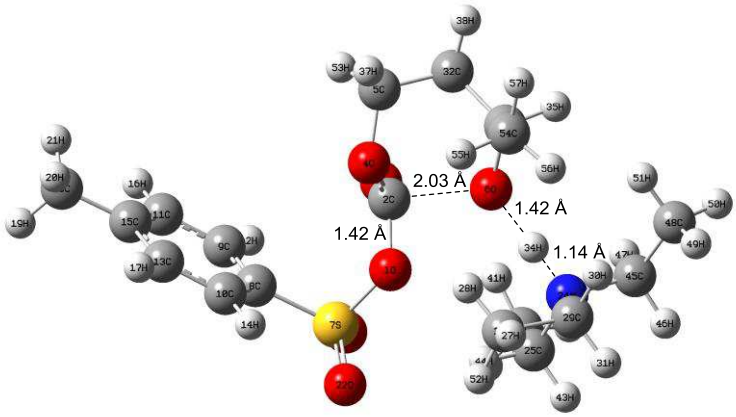

Figure 2.16. GaussView 5.0.8 image of the optimised nucleophilic addition-elimination ring-closing transition state (rωb97xd/6-31+G(d)/cpcm=MeOH/298 K) showing nucleophilic attack of the secondary hydroxyl group, aided by triethylamine, at the tosylated primary carbonate. Hydrogen atoms are in white, carbon in grey, oxygen in red, nitrogen in blue and sulfur in yellow.

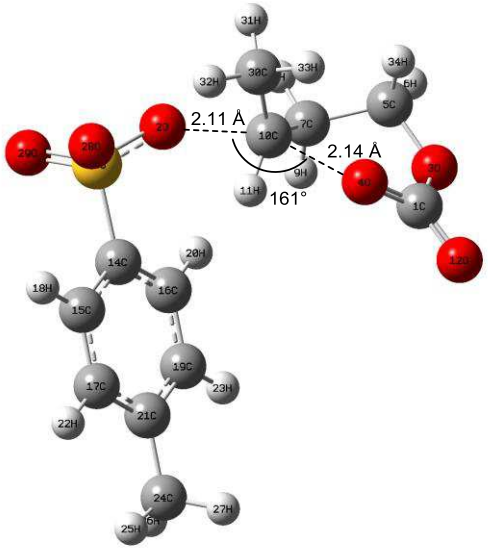

Figure 2.17. GaussView 5.0.8 image of the optimised S_N2-type cyclisation transition state (rωb97xd/6-31+G(d)/cpcm=MeOH/298 K) showing attack of the primary carbonate anion to eliminate the secondary tosylate (the DBUH cation has been omitted for clarity). Hydrogen atoms are in white, carbon in grey, oxygen in red and sulfur in yellow.

The Gibbs free energy profile, calculated in chloroform to better represent experimental conditions is summarised in Figure 2.18 starting from the primary DBUH-carbonate salt (***R*-1'a$_I$**).

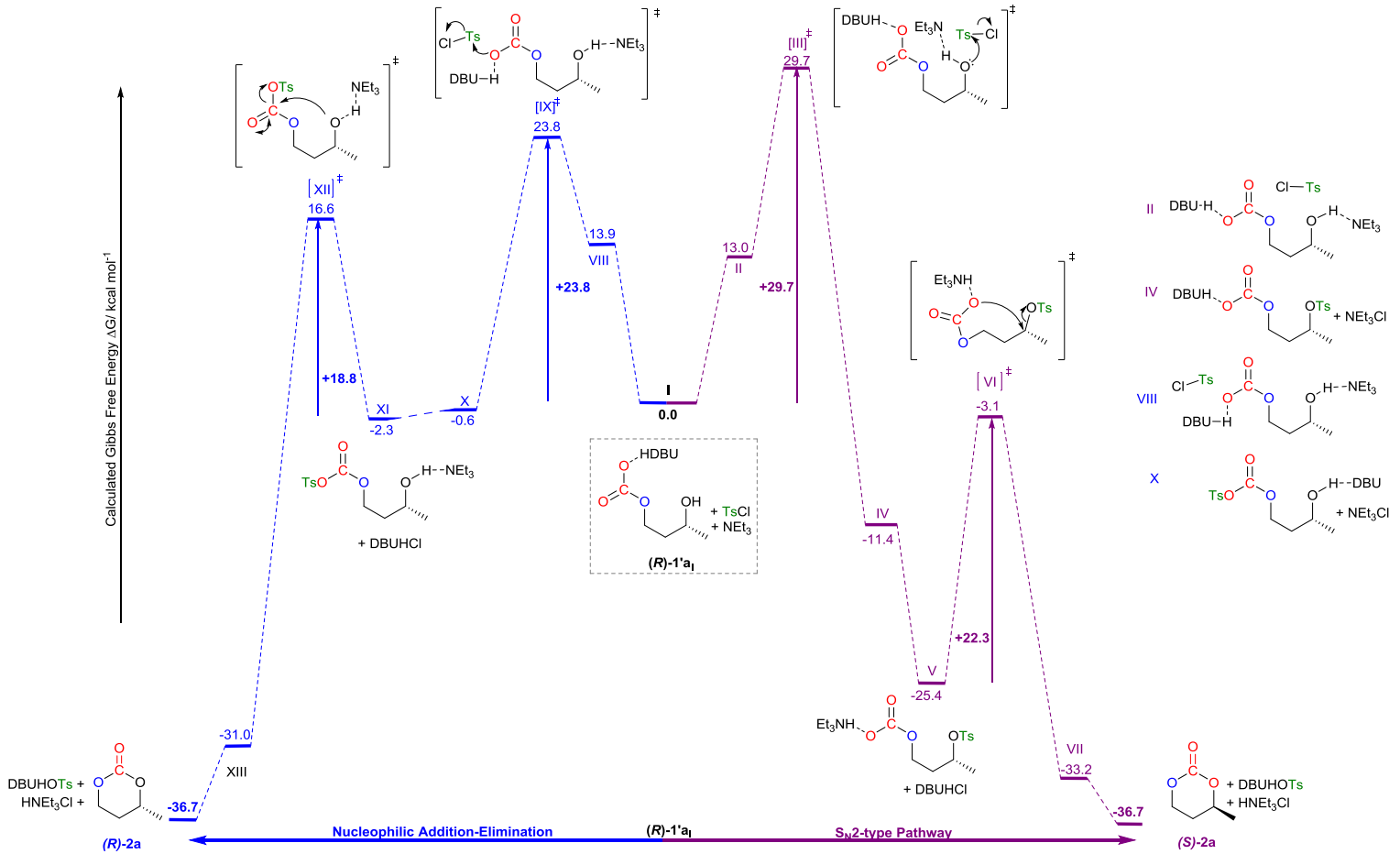

Figure 2.18. DFT computed pathways at the rωb97xd/6-31+G(d)/cpcm=$CHCl_3$/298 K level of theory for cyclisation of ***(R)*-1'a$_I$** with TsCl and NEt_3 (0.0 kcal mol^{-1}) to either ***(S)*-2a** by an S_N2-type mechanism (purple) or ***(R)*-2a** by a nucleophilic addition-elimination mechanism (blue). Both ring-closing kinetic barriers are low enough to be achievable at ambient conditions, though intramolecular cyclisation by a nucleophilic addition-elimination mechanism is 5.9 kcal mol^{-1} more favourable compared to ring-closing by an S_N2-type pathway.

Based on these calculations, the preference for one ring-closing mechanism over the other resides in the tosylation step. Tosylation of the carbonate anion occurs more readily ($\Delta\Delta G^{\ddagger}$= +23.8 kcal mol^{-1}, [IX]‡) compared to tosylation with triethylamine of the neutral and thus less nucleophilic alcohol group ($\Delta\Delta G^{\ddagger}$= +29.7 kcal mol^{-1}, [III]‡). This gives a kinetic preference for the nucleophilic addition-elimination pathway over the intramolecular S_N2-type mechanism of +5.9 kcal mol^{-1}. The tosylated alcohol intermediate where the carbonate salt is retained is however the more thermodynamically favoured product compared to the tosylated carbonate (intermediates **IV** and **V** compared to **X** or **XI**). Rapid cyclisation of the kinetic tosylation product **XI** (in line with the low calculated activation barrier) would give rise to the overall preference observed experimentally for a nucleophilic addition-elimination pathway.

Experimental evidence for the feasibility of the S_N2-type route for cyclic carbonate formation was demonstrated through the mono-tosylated derivative of 1,3-butanediol. DBU-facilitated CO_2 insertion (at room temperature and 1 atm pressure) into the free secondary hydroxyl group of the primary tosylated intermediate followed by *in situ* cyclisation gave the cyclic carbonate in good conversion (76% relative to a styrene internal standard). This mechanism was later found to be important in the synthesis of otherwise challenging sugar-based cyclic carbonates (Chapters 4 and 5).

DFT calculations (rωb97xd/6-31+G(d)/cpcm=$CHCl_3$/298 K protocol) also suggested that cyclic carbonate formation may be feasible through the di-insertion product (**1'a$_{bis}$**) by an S_N2-type process. Intramolecular displacement of the primary tosylation carbonate with the secondary carbonate anion (Figure 2.19) gave a calculated energy barrier ($\Delta\Delta G^{\ddagger}$) of +24.5 kcal mol^{-1}. Moreover, the entropic release of CO_2 gas could provide an additional thermodynamic driving force ($\Delta\Delta G$ = -35.0 kcal mol^{-1}). Thus, di-insertion of CO_2 into diols may not be detrimental to cyclic carbonate synthesis *via* this method (it was previously assumed that only the mono-CO_2 insertion products would lead to the desired product). Nevertheless, the number of equivalents of reagent already used in the procedure and accompanying salt by-products (moreover chlorinated species), makes the use of further DBU equivalents to from **1'a$_{bis}$** undesirable.

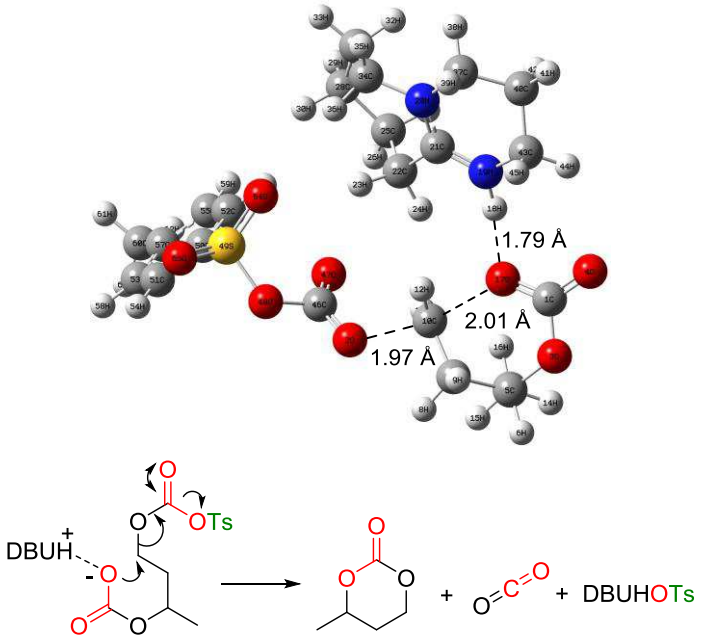

Figure 2.19. GaussView 5.0.8 of the optimised transition state (rωb97xd/6-31+G(d)/cpcm=$CHCl_3$/298 K) and proposed mechanism for cyclic carbonate formation from mono-tosylated **1'a$_{bis}$**. Hydrogen atoms are in white, carbon in grey, oxygen in red, nitrogen in blue and sulfur in yellow.

Although there is scope for recovery and regeneration of the salt by-products, the development of a catalytic system is desirable to reduce the number of equivalents of reagent required. The overall atom economy of the process is just 19%, compared to 87% for the reaction of 1,3-butanediol with CO_2 to form the cyclic carbonate and water as the only by-product. Nevertheless, the overall thermodynamics of the direct coupling of diols with CO_2 means that the use of a dehydrating agent will always be necessary to drive the reaction equilibrium over towards the cyclic product.

2.6. Looking Forward: Metal-Based Catalysts

2.6.1. Activation of CO_2 by metal complexes

CO_2 activation by insertion into metal-X bonds (where X= H, O, C, N, Si, P and other metals) to afford M-OC(O)X fragments is well known, where preferential formation of a new M-O rather than M-C bond means that insertion to give products of the general type M-C(O)OX are often not observed.[36, 37] For the catalytic coupling of CO_2 with diols to form cyclic carbonates, CO_2 insertion into metal-alkoxide bonds to form metallo-alkylcarbonate complexes is thought to be driven by the nucleophilicity of the alkoxide ligand and not the strong coordination of CO_2 to the metal centre.[38, 39] No open coordination site on the metal

centre is required as it is postulated to proceed *via* a concerted four-membered transition state (Figure 2.20), in which breaking of the metal-alkoxide bond occurs alongside both nucleophilic attack at the CO_2 carbon and formation of a new M-O bond.[40, 41]

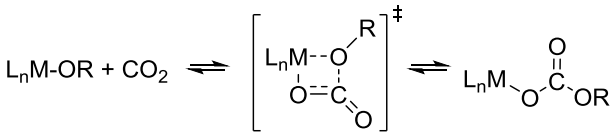

Figure 2.20. Reversible CO_2 insertion into metal alkoxide bonds *via* a four-membered transition state.

The reaction is also generally considered to be reversible due to the similar M-O bond strengths between the metal-alkoxide and metallo-alkylcarbonate species.[42] Examples of metal-alkoxide complexes shown to undergo CO_2 insertion typically bear nucleophilic ligands and include those based on zinc,[40] cobalt,[43] lead,[44] magnesium,[45] aluminium[46] and tin metal centres.[47, 48] Among those, organo- zinc, aluminium and magnesium based catalysts are attractive due to their low toxicity and low cost.

2.6.2. Ligand synthesis and diethyl zinc complexation

Preliminary catalyst design was based on the use of anionic ligands (for +II zinc metal centres) bearing a labile Lewis basic pendent arm, to aid the cyclisation step by increasing the nucleophilicity of the ring-closing hydroxyl group (Figure 2.21).

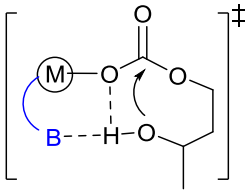

Figure 2.21. Initial catalyst design based on a Lewis basic side arm to increase the nucleophilicity of the ring-closing hydroxyl group.

As an initial investigation, three ligands **HL(1-3)** (Figure 2.22) bearing pendent pyridyl groups were synthesised according to the literature procedures. *N,N'*-β-diketiminate ligand (**HL1**) was synthesised in reasonable yield from 2,6-diisopropylaniline, acetylacetone and 2-picolylamine in two Mannich condensation steps.[49] Phenol based ligand, **HL2**[50] and the corresponding Schiff base, **HL3**[51] were prepared following condensation of 3,5-di-*tert*-butyl-2-hydroxybenzaldehyde with 2-picolylamine.

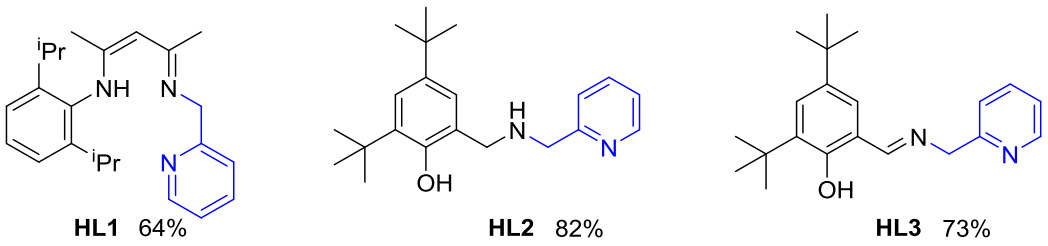

Figure 2.22. β-diketiminate ligand, **HL1** and phenoxide ligands, **HL2** and **HL3** synthesised according to the literature procedures.[50-52] The pyridine arm (in blue) was derived from 2-picolylamine.

Heteroleptic zinc ethyl complexes were then prepared by alkane elimination (Scheme 2.04) as per the literature procedure for diethyl zinc complexation to **HL1**.[52] The complexes were very air and moisture sensitive; the intense colour changes observed upon complexation being lost within minutes upon exposure to air.

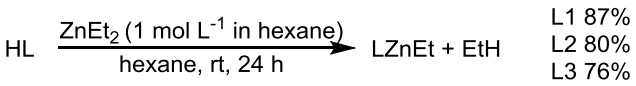

Scheme 2.04. Diethyl zinc complexation of **HL(1-3)**.

2.6.3. Characterisation by X-ray crystallography and NMR spectroscopy

L1ZnEt was previously determined[52] to exist as a dimmer in the solid state (Figure 2.23). Formation of monomeric or dimeric species was reported to depend upon the steric bulk of the substituent bound to the imine.

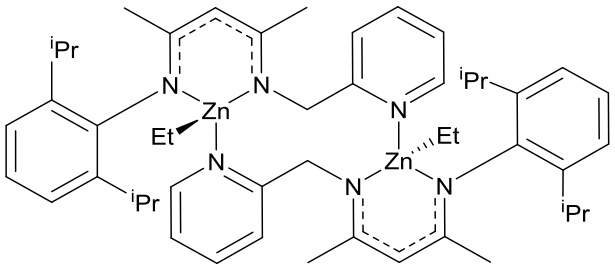

Figure 2.23. Dimmer formed on complexation of **HL1** to $ZnEt_2$.

Under an argon atmosphere, layering of hexanes over a C_6D_6 solution of the complexes formed with **HL2** and **HL3** resulted in crystals suitable for single crystal X-ray diffraction. L2ZnEt was found to exist in monomeric form with a distorted tetrahedral geometry around the Zn metal centre (Figure 2.24). Both Zn-N bonds are similar in length, with that to the pyridine side-arm being slightly longer.

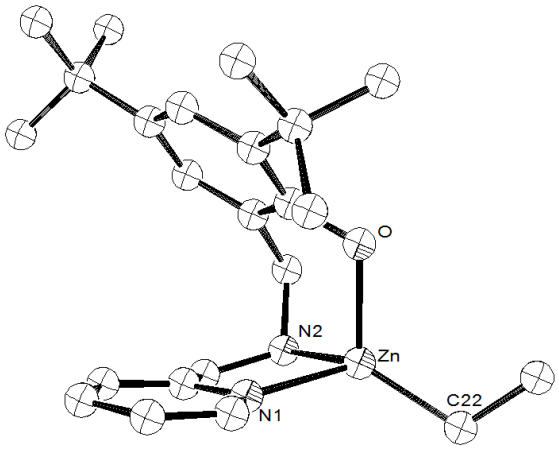

Figure 2.24. ORTEP[53] drawing of L2ZnEt with thermal ellipsoids at the 50% probability level with selected atoms labelled. Hydrogen atoms have been omitted for clarity. Selected bond lengths (Å) and angles (°): Zn-C(22) 1.975(2), Zn-O 1.9961(15), Zn-N(2) 2.1083(19), Zn-N(1) 2.125(2), C(22)-Zn-O 119.16(8), C(22)-Zn-N(2) 133.37(9), O-Zn-N(2) 93.68(7), C(22)-Zn-N(1) 121.17(9), O-Zn-N(1) 98.72(7), N(2)-Zn-N(1) 80.83(8).

In contrast, L3ZnEt existed as a dimer in the solid state (Figure 2.25). The geometry around each zinc centre was a distorted tetrahedron and the bond to the imine nitrogen longer than that to the pyridine donor arm by 0.12 Å (compared to a difference of 0.02 Å for L2ZnEt).

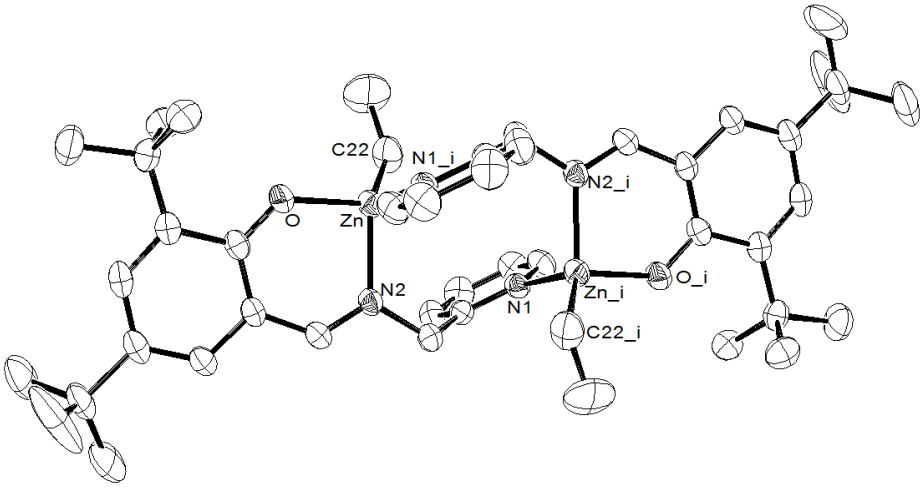

Figure 2.25. ORTEP[53] drawing with thermal ellipsoids at the 50% probability level of L3ZnEt with selected atoms labelled. Hydrogen atoms and co-crystallised solvents are omitted for clarity. Selected bond lengths (Å) and angles (°): Zn-O 1.9550(12), Zn-C(22) 1.978(2), Zn-N(2) 2.0533(16), Zn-N(1) 2.1695(16), O-Zn-C(22)116.54(8), O-Zn-N(2)91.22(6), C(22)-Zn-N(2)128.11(9), O-Zn-N(1) 97.95(6), C(22)-Zn-N(1) 120.76(9), N(2)-Zn-N(1) 94.99(6).

NMR spectroscopy of the zinc-ethyl complexes of ligands 2 and 3 were consistent with the single crystal X-ray data and that for L1ZnEt with the literature data.[52] It was also verified that the solid-state structures were representative of the bulk solution by re-dissolving the crystals in deuterated solvent. Although it varies with ligand architecture, ^{1}H and $^{13}C\{^{1}H\}$ NMR environments consistent with literature data[52] for a zinc-bound ethyl group were observed for both ligand 2 and 3 ZnEt complexes. For example, in the ^{1}H NMR spectrum

(C_6D_6) of the Schiff base complex, a triplet at 1.45 ppm and a quartet at 0.05 ppm (^3J = 8.0 Hz) were observed for the ethyl -CH_3 and -CH_2 environments, respectively. The corresponding carbon environments appeared at 14.1 and -2.1 ppm in the $^{13}C\{^1H\}$ NMR spectrum (C_6D_6) of the L2ZnEt complex. The very upfield shift of the latter was consistent with direct coordination to the electropositive Zn(II) centre.

Consistent with conformational restriction upon complexation, comparison of the ^1H NMR spectra for **HL2** and L2ZnEt in the region from 2.5 to 8.5 ppm (Figure 2.26) showed splitting of the two methylene singlets in the ligand into four separate environments. In the aromatic region, the most noticeable change was an upfield shift of the pyridine proton environments especially at the assigned two-pyridine position and separation of the 3- and 5- pyridine environments.

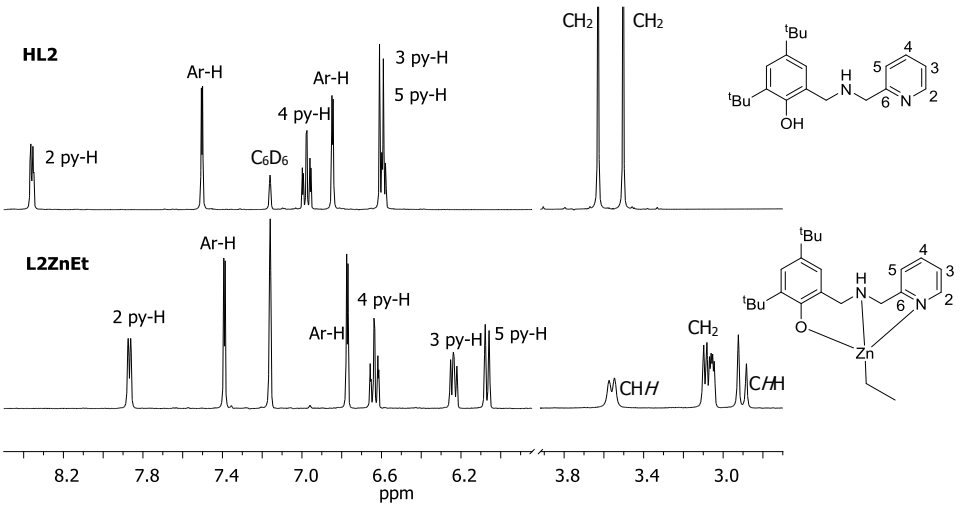

Figure 2.26. Comparison of the ^1H NMR spectra (400 MHz, C_6D_6) of **HL2** (top) and its zinc ethyl complex (bottom). The chemical shift scale is cut from 3.8 to 5.8 ppm to show clearly both the aromatic and CH_2 regions.

Similarly, changes in the aromatic region upon complexation of **HL3** were also observed (Figure 2.27). The imine proton shifted from 7.9 to 7.5 ppm upon coordination and one of the phenyl doublets appeared more downfield at 7.8 ppm. The pyridine proton environments were also distinguishable in the ^1H NMR spectrum of L3ZnEt and in particular, that assigned to the 5-pyridine position shifted further into the shielding region by about 0.5 ppm. For both ligand 2 and ligand 3 zinc ethyl complexes, the resonance at ~14 ppm (not shown), assigned to the phenol OH was lost upon coordination.

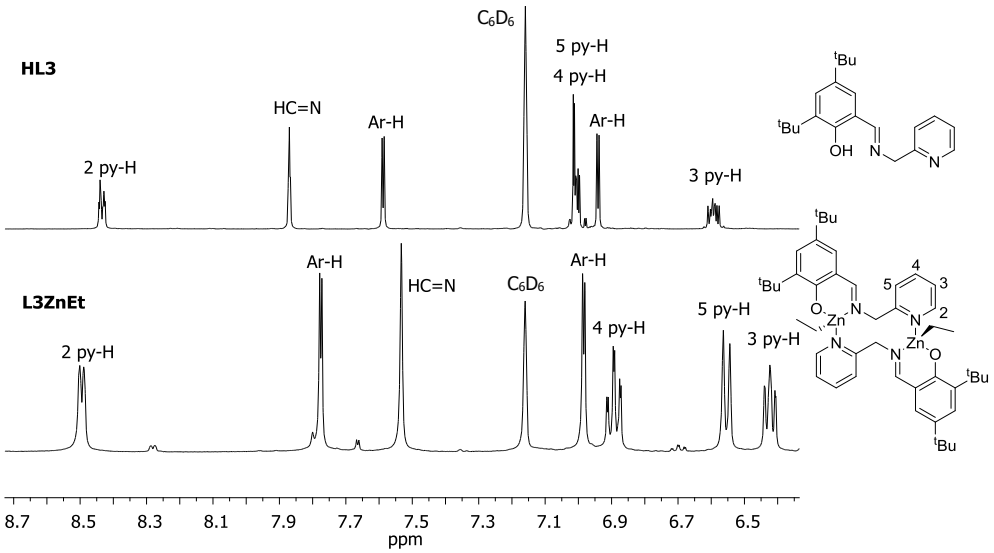

Figure 2.27. Comparison of the aromatic region of ^{1}H NMR spectra (400 MHz, C_6D_6) of **HL3** (top) and its zinc ethyl complex (bottom).

2.6.4. Catalytic activity with 1,3-butanediol and CO_2

The targeted catalytic cycle (Figure 2.28) involved formation of a zinc-alkoxide species with the diol, CO_2 insertion into the Zn-O bond and intramolecular ring-closing to eliminate the cyclic carbonate and generate a zinc-hydroxide species. Loss of water on coordination of another diol molecule, requiring the use of a dehydrating agent, regenerates the zinc-alkoxide species.

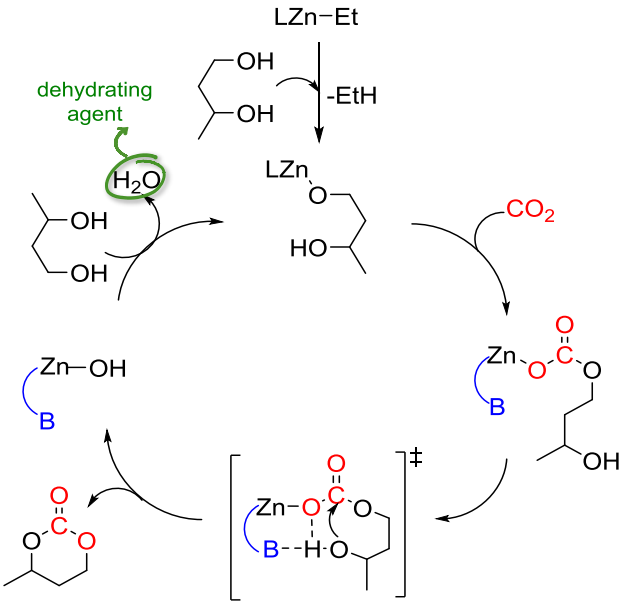

Figure 2.28. Targeted catalytic cycle for metal-catalysed cyclic carbonate formation from CO_2 and 1,3-diols.

Computationally, at the rωb97xd/6-31+G(d) level of theory at 298 K in methanol, reaction of the zinc ethyl complexes with 1,3-butanediol to form the zinc-alkoxide species was calculated to be thermodynamically favourable for all three ligands ($\Delta\Delta G$ = -19.9 to -26.3 kcal mol^{-1}). Preference for coordination of the primary over the secondary hydroxyl group to the metal centre was only significant for L1ZnEt by +6.4 kcal mol^{-1}. CO_2 insertion into the zinc-alkoxide bonds to form metallo-alkylcarbonate complexes was also calculated to be thermodynamically favourable for all complexes ($\Delta\Delta G$ = -2.6 to -4.2 kcal mol^{-1}). Encouragingly, the kinetic energy barriers for CO_2 insertion (calculated only for phenoxides ligands 2 and 3) were comparable to those for DBU-aided CO_2 insertion at the same level of theory ($\Delta\Delta G^{\ddagger}$= +10.2 to +12.3 kcal mol^{-1}). However, the optimised ring-closing transition states showed that a longer side-arm was required for the pyridine motif to facilitate ring-closing; the calculated kinetic barriers ($\Delta\Delta G^{\ddagger}$) were nearly +50 kcal mol^{-1} for both ligand 2 and ligand 3 complexes, comparable to those without a catalyst. Nonetheless, DFT modelling of complexes bearing longer side arms that were able to reach the reaction site had lower calculated barriers to ring-closing and may form the basis of future ligand design (Figure 2.29).

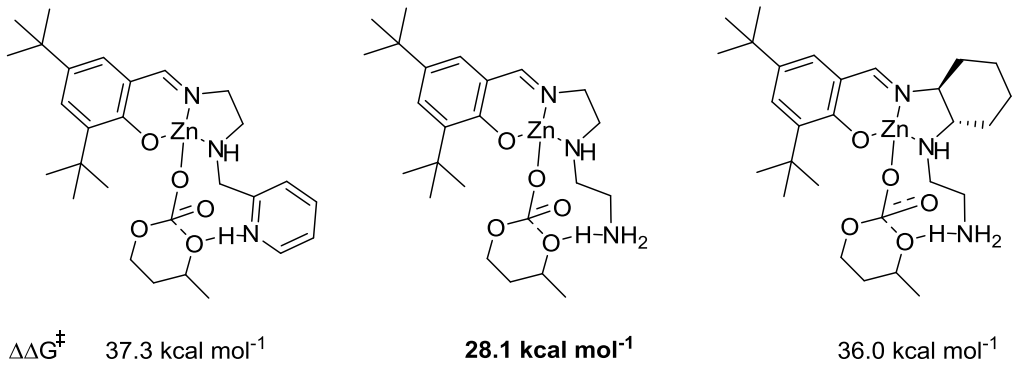

Figure 2.29. DFT modelling at the rωb97xd/6-31+G(d)/cpcm=MeOH/298 K level of theory of ligand architectures bearing longer labile side arms able to aid ring-closing to the cyclic carbonate.

Experimentally, catalytic tests with 10 mol% L(1-3)ZnEt in toluene, acetonitrile or THF solvents with 10 wt% molecular sieves at room temperature and 80 °C showed no catalytic activity with only unreacted diol being isolated. Moreover, reaction of equimolar amounts of 1,3-butanediol and zinc ethyl complex to form the zinc- alkoxide for investigation into the CO_2 insertion potential suggested the occurrence of equilibriums **1** to **3** in solution (Figure 2.30).

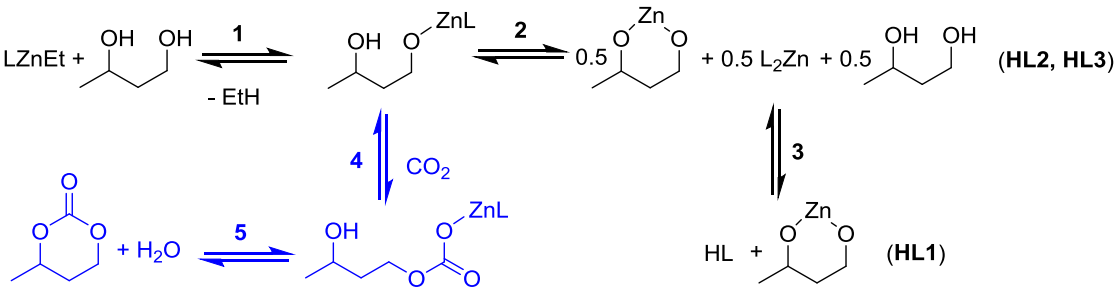

Figure 2.30. Schlenk equilibrium proposed to be occurring in solution on addition of 1,3-butanediol to L(1-3)ZnEt complexes. For L(2-3)ZnEt complexes, equilibriums 1 and 2 led to formation of monomeric bis-ligand species L_2Zn. For L1ZnEt, re-protonated ligand (**HL1**) was isolated suggesting equilibriums 1 to 3 occurred.

For L1ZnEt with one equivalent of 1,3-butanediol, re-protonation of the ligand was observed. For example, ^{1}H NMR spectroscopy showed a loss of the coordinated ethyl group environments and appearance of a broad resonance at 11.3 ppm due to the NH environment. In addition, the absence of any diol signals suggested that the reaction precipitate was composed of a zinc-diol species. Upon coordination of the first alcohol group to form the zinc-alkoxide species, chelation of the second hydroxyl is driven by the chelate effect.

For complexes L(2-3)ZnEt, equilibriums **1** and **2** were thought to be occurring. The lower pK_a of the phenoxide ligands compared to the β-diketiminate, resulted in the bis-ligand species, $L(2\text{-}3)_2Zn$ being stable in the presence of the diol suppressing equilibrium **3**. NMR analysis of the reaction mixtures with L2ZnEt or L3ZnEt and one equivalent of 1,3-butanediol, revealed environments inconsistent with both the isolated zinc-ethyl complexes and uncomplexed ligands. Assignment of the environments to those of the monomeric bis-ligand complexes was verified by targeted synthesis of the L_2Zn species and comparison of the NMR data (shown for L3ZnEt in Figure 2.31).

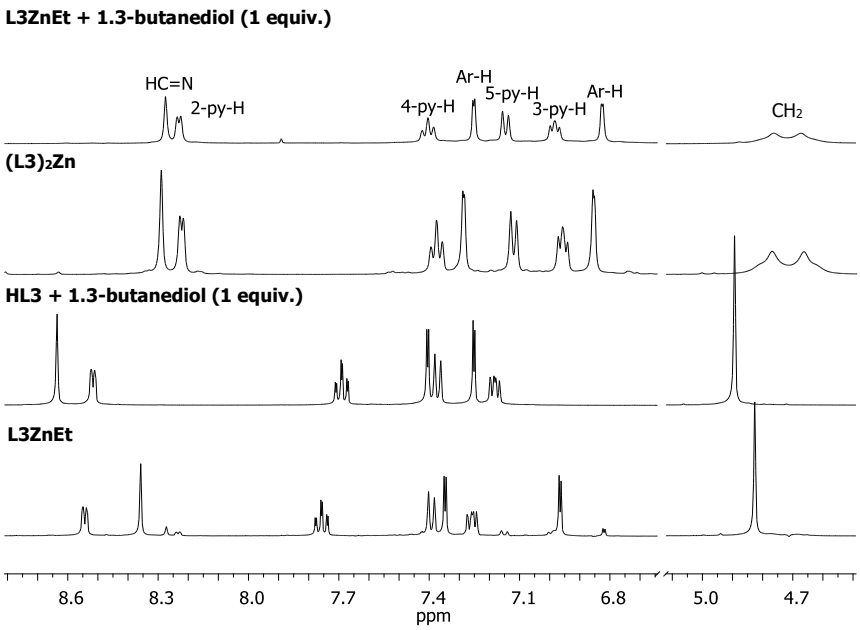

Figure 2.31. Comparison of the ^{1}H NMR spectra (400 MHz, THF-d_8) in the region from 4.6 to 8.8 ppm for the reaction between L3ZnEt and 1,3-butanediol (1 equiv.) after 3 hours stirring at room temperature (top), the isolated $(L3)_2Zn$ complex prepared by reaction of $ZnEt_2$ with **HL3** (2 equiv.), a 1:1 molar ratio of **HL3** and 1,3-butanediol and the L3ZnEt complex (bottom). In the latter, formation of $(L3)_2Zn$ can be seen as a minor impurity (11%).

This was further confirmed for ligand 3 by single-crystal X-ray diffraction analysis of crystals grown by layering hexanes over a C_6D_6 solution of the reaction mixture. Crystals in the triclinic space group of $P\bar{1}$ revealed coordination of two ligands around one zinc centre in a distorted square pyramidal geometry (see Appendix). Moreover, in accordance with equilibrium **2** (Figure 2.30), the unchanged proton environments of 1,3-butanediol were observed in the ^{1}H NMR spectra of the reaction mixtures at half the expected integration. The same gel-like precipitate was also formed as for the reaction with L1ZnEt complex, accounting for the other half equivalent of diol and was assumed to be a molecular or polymeric species of the diol with zinc. (Experiments with only half an equivalent of diol resulted in no diol resonances in the NMR spectra). In the absence of the diol, all ligand zinc ethyl complexes showed no change in the NMR spectra when left in THF-d_8 solution for one week under argon. No uptake of CO_2 or environments consistent with CO_2 insertion in the $^{13}C\{^{1}H\}$ NMR spectra were observed during these reactions carried out at room temperature and 1 atm CO_2 pressure. Thus, in addition to the need for a dehydrating agent to remove the water by-product and better ligand architectures that lower the barrier to ring-closing, trapping of the zinc- alkoxide species for CO_2 insertion (equilibrium **4**, Figure 2.30), perhaps at low temperatures, is required for cyclic carbonate formation.

2.7. Conclusions and Further Work

To conclude, DFT calculations of the direct coupling of CO_2 with 1,3-butanediol (a model compound for sugars) suggested that both the CO_2 insertion and ring-closing kinetic barriers needed to be lowered for cyclic carbonate formation. In addition, a dehydrating agent is required to remove the water by-product and overcome the thermodynamic limitation. Bicyclic amidine base, DBU sufficiently lowered the barrier to CO_2 insertion, enabling the formation of a mixture of alkyl carbonate salts at room temperature and 1 atm CO_2 pressure. Addition of a tosyl leaving group and triethylamine lowered the ring-closing kinetic barrier and the formation of salt by-products negated the need for a dehydrating agent leading to cyclic carbonate formation under mild reaction conditions. The method was applied to the synthesis of a range of known six-membered cyclic carbonates including those derived from D-glucose and D-xylose sugar diols and gave yields competitive with other non-phosgene alternatives. For sugar-based diols conditions of high dilution and cold temperatures were required to achieve reasonable yields of the cyclic monomer.

Although, the developed method highlights that the barriers to cyclic carbonate synthesis from CO_2 and diols can be readily overcome with the use of simple reagents under mild reaction conditions, further work is required to reduce the number of equivalents of reagent used and ultimately to develop a catalytic system. Though, a dehydrating agent will still be required to drive the equilibrium over to the cyclic carbonate product. Preliminary investigations into the development of zinc-based homogeneous catalysts were carried out with a β-diketiminate and two phenoxide ligands bearing pyridine side-arms to aid in the cyclisation step by increasing the nucleophilicity of the ring-closing hydroxyl group. Insight was gained into the length of the side-arm required for it to reach the reaction site and guided by DFT calculations, the ligand bearing a longer pendent amine group (Figure 2.32) may be a good starting point for further ligand design. Moreover, disproportionation of the zinc ethyl complexes was observed in solution with 1,3-butanediol and requires further investigation to determine whether the zinc-alkoxide species can be trapped for CO_2 insertion.

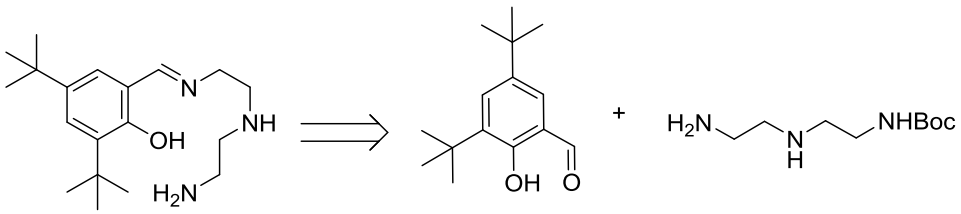

Figure 2.32. Retrosynthesis of a ligand bearing a longer side arm.

Experiments with enantiopure diols and supported by DFT calculations, suggested that cyclisation with TsCl and triethylamine occurred *via* a nucleophilic addition-elimination pathway following tosylation of the carbonate rather than an S_N2-type mechanism following tosylation of the free hydroxyl group. Nevertheless, the feasibility of the latter, which would result in stereochemical inversion was demonstrated both computationally and experimentally. Further work may look to explore alternative leaving group strategies such as acetic anhydride and bases that may favour interaction at the free hydroxyl group. The carbonate would then be acting as a protecting group for the primary hydroxyl position and depending upon the choice of leaving group or base, the stereochemical outcome of the cyclisation could be tailored *via* control over the mechanistic pathway.

Finally, the method may be applied to the synthesis of isocyanates (Figure 2.33), used in the production of polyurethanes and traditionally prepared by reaction of an amine with phosgene. The reaction of CO_2 with primary and secondary amines is known to generate carbamate ions but their reactivity is generally dominated by the nitrogen centre of the carbamate not the oxygen. In the presence of alkyl halides, this leads to the formation of secondary and tertiary amines. The use of sterically hindered guanidine bases however, has been found to promote reaction of the carbamate ions at the oxygen, leading to selective *O*- alkylation. This is postulated to be due to the sufficient charge separation between the carbamate anion and bulky counterion.[54]

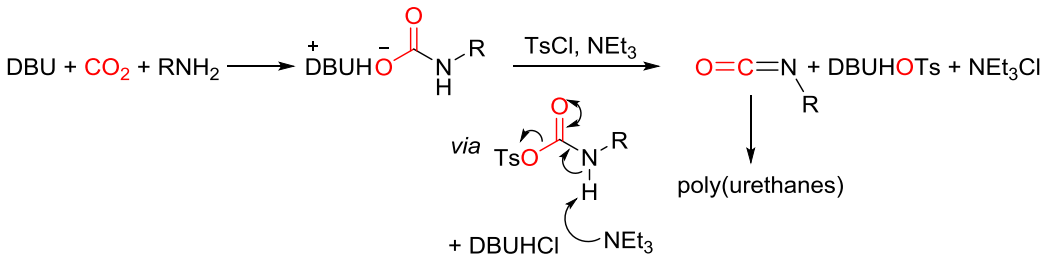

Figure 2.33. Proposed reaction scheme for synthesis of isocyanates using CO_2 in place of phosgene as a carbonating agent.

2.8. References

1. P. G. Jessop, D. J. Heldebrant, X. Li, C. A. Eckert and C. L. Liotta, *Nature*, 2005, **436**, 1102-1102.
2. R. Nicholls, S. Kaufhold and B. N. Nguyen, *Catal. Sci. Technol.*, 2014, **4**, 3458-3462.
3. F. S. Pereira, E. R. deAzevedo, E. F. da Silva, T. J. Bonagamba, D. L. da Silva Agostíni, A. Magalhães, A. E. Job and E. R. Pérez González, *Tetrahedron*, 2008, **64**, 10097-10106.
4. R. Lo and B. Ganguly, *New J. Chem.*, 2012, **36**, 2549.
5. D. J. Heldebrant, P. K. Koech, M. T. C. Ang, C. Liang, J. E. Rainbolt, C. R. Yonker and P. G. Jessop, *Green Chem.*, 2010, **12**, 713-721.
6. I. Kaljurand, A. Kütt, L. Sooväli, T. Rodima, V. Mäemets, I. Leito and I. A. Koppel, *J. Org. Chem.*, 2005, **70**, 1019-1028.
7. K. Kaupmees, A. Trummal and I. Leito, *Croat. Chem. Acta*, 2014, **87**, 385-395.
8. P. G. Jessop, S. M. Mercer and D. J. Heldebrant, *Energy Environ. Sci.*, 2012, **5**, 7240-7253.
9. L. Phan, D. Chiu, D. J. Heldebrant, H. Huttenhower, E. John, X. Li, P. Pollet, R. Wang, C. A. Eckert, C. L. Liotta and P. G. Jessop, *Ind. Eng. Chem. Res.*, 2008, **47**, 539-545.
10. L. Phan, J. R. Andreatta, L. K. Horvey, C. F. Edie, A.-L. Luco, A. Mirchandani, D. J. Darensbourg and P. G. Jessop, *J. Org. Chem.*, 2008, **73**, 127-132.
11. Y. Liu, P. G. Jessop, M. Cunningham, C. A. Eckert and C. L. Liotta, *Science*, 2006, **313**, 958-960.
12. L. Song, Y. Yang, H. Xie and E. Liu, *ChemSusChem*, 2015, **8**, 3217-3221.
13. O. Coulembier, S. Moins, R. Todd and P. Dubois, *Macromolecules*, 2014, **47**, 486-491.
14. M. Mokhadinyana, S. L. Desset, D. B. G. Williams and D. J. Cole-Hamilton, *Angew. Chem. Int. Ed.*, 2012, **51**, 1648-1652.
15. S. L. Desset and D. J. Cole-Hamilton, *Angew. Chem. Int. Ed.*, 2009, **48**, 1472-1474.
16. D. J. Heldebrant, C. R. Yonker, P. G. Jessop and L. Phan, *Energy Environ. Sci.*, 2008, **1**, 487-493.
17. G. V. S. M. Carrera, N. Jordao, L. C. Branco and M. Nunes da Ponte, *Faraday Discuss.*, 2015, **183**, 429-444.
18. E. R. Pérez, R. H. A. Santos, M. T. P. Gambardella, L. G. M. de Macedo, U. P. Rodrigues-Filho, J.-C. Launay and D. W. Franco, *J. Org. Chem.* , 2004, **69**, 8005-8011.
19. E. R. Pérez, M. O. da Silva, V. C. Costa, U. P. Rodrigues-Filho and D. W. Franco, *Tetrahedron Lett.*, 2002, **43**, 4091-4093.
20. D. J. Heldebrant, P. G. Jessop, C. A. Thomas, C. A. Eckert and C. L. Liotta, *J. Org. Chem.*, 2005, **70**, 5335-5338.
21. C. Villiers, J.-P. Dognon, R. Pollet, P. Thuéry and M. Ephritikhine, *Angew. Chem. Int. Ed.*, 2010, **49**, 3465-3468.
22. Y. Wang, Q. Han and H. Wen, *Mol. Simul.*, 2013, **39**, 822-827.
23. Y. N. Lim, C. Lee and H.-Y. Jang, *Eur. J. Org. Chem.*, 2014, **9**, 1823-1826.
24. S. Huang, J. Ma, J. Li, N. Zhao, W. Wei and Y. Sun, *Catal. Commun.*, 2008, **9**, 276-280.
25. J.-D. Chai and M. Head-Gordon, *Phys. Chem. Chem. Phys.* , 2008, **10**, 6615-6620.
26. J.-D. Chai and M. Head-Gordon, *J. Chem. Phys.*, 2008, **128**, 084106.
27. A. Buchard, F. Jutz, M. R. Kember, A. J. P. White, H. S. Rzepa and C. K. Williams, *Macromolecules*, 2012, **45**, 6781-6795.
28. M. Cossi, N. Rega, G. Scalmani and V. Barone, *J. Comput. Chem.*, 2003, **24**, 669-681.
29. H. Yasuda, M.-S. Aludin, N. Kitamura, M. Tanabe and H. Sirahama, *Macromolecules*, 1999, **32**, 6047-6057.
30. B. Gabriele, R. Mancuso, G. Salerno, L. Veltri, M. Costa and A. Dibenedetto, *ChemSusChem*, 2011, **4**, 1778-1786.
31. B. J. Ludwig and E. C. Piech, *J. Am. Chem. Soc.*, 1951, **73**, 5779-5781.
32. D. M. Pearson, N. R. Conley and R. M. Waymouth, *Adv. Synth. Catal.*, 2011, **353**, 3007-3013.
33. Y. Shen, X. Chen and R. A. Gross, *Macromolecules*, 1999, **32**, 2799-2802.

34. K. Mikami, A. T. Lonnecker, T. P. Gustafson, N. F. Zinnel, P. J. Pai, D. H. Russell and K. L. Wooley, *J. Am. Chem. Soc.*, 2013, **135**, 6826-6829.
35. T. P. Gustafson, A. T. Lonnecker, G. S. Heo, S. Zhang, A. P. Dove and K. L. Wooley, *Biomacromolecules*, 2013, **14**, 3346-3353.
36. D. H. Gibson, *Coord. Chem. Rev.*, 1999, **185–186**, 335-355.
37. R. D. Simpson and R. G. Bergman, *Organometallics*, 1992, **11**, 4306-4315.
38. D. J. Darensbourg, K. M. Sanchez, J. H. Reibenspies and A. L. Rheingold, *J. Am. Chem. Soc.*, 1989, **111**, 7094-7103.
39. M. Kunert, M. Bräuer, O. Klobes, H. Görls, E. Dinjus and E. Anders, *Eur. J. Inorg. Chem.*, 2000, **2000**, 1803-1809.
40. H. Brombacher and H. Vahrenkamp, *Inorg. Chem.*, 2004, **43**, 6042-6049.
41. X. Yin and J. R. Moss, *Coord. Chem. Rev.*, 1999, **181**, 27-59.
42. D. J. Darensbourg, W.-Z. Lee, A. L. Phelps and E. Guidry, *Organometallics*, 2003, **22**, 5585-5588.
43. S. Elmas, M. A. Subhani, H. Vogt, W. Leitner and T. E. Muller, *Green Chem.*, 2013, **15**, 1356-1360.
44. E. C. Y. Tam, N. C. Johnstone, L. Ferro, P. B. Hitchcock and J. R. Fulton, *Inorg. Chem.*, 2009, **48**, 8971-8976.
45. M. R. Kember and C. K. Williams, *J. Am. Chem. Soc.*, 2012, **134**, 15676-15679.
46. C. J. Whiteoak, N. Kielland, V. Laserna, F. Castro-Gómez, E. Martin, E. C. Escudero-Adán, C. Bo and A. W. Kleij, *Chem. Eur. J.*, 2014, **20**, 2264-2275.
47. D. Ballivet-Tkatchenko, H. Chermette, L. Plasseraud and O. Walter, *Dalton Trans.*, 2006, 5167-5175.
48. L. Ferro, P. B. Hitchcock, M. P. Coles, H. Cox and J. R. Fulton, *Inorg. Chem.*, 2011, **50**, 1879-1888.
49. X. Xu, Y. Chen, G. Zou and J. Sun, *Dalton Trans.*, 2010, **39**, 3952-3958.
50. Y.-L. Wong, Y. Yan, E. S. H. Chan, Q. Yang, T. C. W. Mak and D. K. P. Ng, *J. Chem. Soc., Dalton Trans.*, 1998, 3057-3064.
51. P. A. Cameron, V. C. Gibson, C. Redshaw, J. A. Segal, A. J. P. White and D. J. Williams, *J. Chem. Soc., Dalton Trans.*, 2002, 415-422.
52. Z. Dai, J. Zhang, Y. Gao, N. Tang, Y. Huang and J. Wu, *Cat. Sci. Technol.*, 2013, **3**, 3268-3277.
53. L. J. Farrugia, *J. Appl. Cryst.*, 2012, **45**, 849-854.
54. D. Riley, W. D. McGhee and T. Waldman, in *Benign by Design*, American Chemical Society, 1994, vol. 577, ch. 10, pp. 122-132.

Chapter 3

Synthesis and Polymerisation of a Cyclic Carbonate from D-Mannose and CO_2

3. Synthesis and Polymerisation of a Cyclic Carbonate from D-Mannose and CO_2

3.1. Introduction

There are very few reported examples of six-membered cyclic carbonate monomers fused to carbohydrate rings due to challenges in the cyclocarbonation of sugar-based diols or in the ring-opening polymerisation (ROP) itself. In 1999, Gross and coworkers[1] reported the synthesis of a D-xylose derived six-membered cyclic carbonate using phosgene derivative, ethyl chloroformate. Following ketal protection of the 1,2-diol motif, 1,2-*O*-isopropylidene-D-xylofuranose-3,5-cyclic carbonate (IPXTC, Scheme 3.01) was isolated in 41% yield. Protection of the vicinal diol was required to avoid undesired side reactions during ROP.

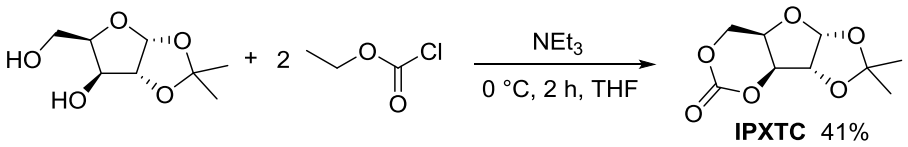

Scheme 3.01. Synthesis of D-xylose derived cyclic carbonate, IPXTC by Gross and coworkers.[1]

A range of coordinative and anionic polymerisation catalysts to include tin (II) 2- ethylhexanoate ($Sn(Oct)_2$), methylaluminoxane (MAO), isobutylaluminoxane (IBAO), *t*- BuOK, $AlEt_3$-H_2O, $ZnEt_2$-H_2O and Et_2AlOEt were investigated for the homopolymerisation of IPXTC. The highest molecular weights and yields were obtained using rare earth, yttrium isopropoxide catalyst in 1,4-dioxane solvent at 70 °C (Scheme 3.02).

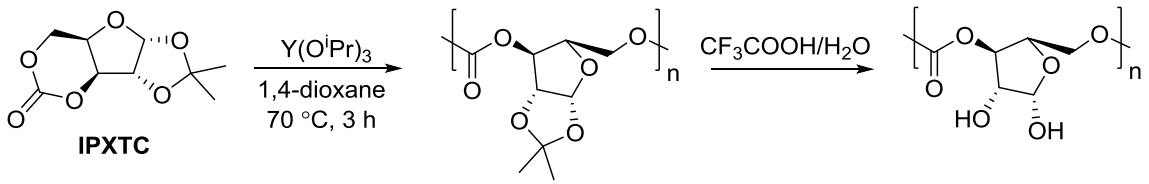

Scheme 3.02. Homopolymerisation of IPXTC using Yttrium isopropoxide.[1]

Under these reaction conditions, and for an initial monomer-to-catalyst ratio of 100:1, poly(IPXTC) was isolated in 58% yield after 3 hours with a number average molecular weight (M_n) of 13 200 g mol^{-1} and dispersity (Đ= M_w/M_n) of 1.69. Longer reaction times of up to 48 hours saw a gradual increase in yield (up to 75%) but lowering of the molecular

weights (M_n = 4300 g mol^{-1}) and further broadening of the molecular weight distribution (Đ =1.76-1.92). This was attributed to backbiting of the polymer hydroxyl end-group on the main chain. Polymerisations at room temperature or in THF, CH_2Cl_2 and toluene solvents gave substantially lower yields and molecular weights. For example, at room temperature in dioxane a yield of 34% and M_n of 4600 g mol^{-1} was reported after 8 hours though with narrower dispersity (Đ= 1.2). Post-polymerisation deprotection of the pendent ketal groups, was achieved with a mixture of trifluoroacetic acid and H_2O. The revealed vicinal hydroxyl groups rendered the polymer insoluble in $CHCl_3$, CH_2Cl_2 and THF in which poly(IPXTC) had previously been soluble. The ability to introduce free hydroxyl groups along the polycarbonate backbone is attractive for modifying polymer properties and serves as a handle for further functionalisation.

In 2013, Wooley and coworkers[2] reported the three-step synthesis of tri-methoxy-protected D-glucose derived cyclic carbonate (Scheme 3.03) from commercially available methyl 4,6-*O*-benzylidene-α-D-glucopyranoside. Compared to the *cis*- configured 1,3-diol in the IPXTC precursor, cyclic carbonylation of the *trans*-diol proved more challenging. Following methylation with MeI in DMF of the free 2,3-hydroxyl groups and hydrogenolysis to remove the benzylidene protecting group, cyclisation of the then exposed 4,6-diol was carried out using bis(pentafluorophenyl)carbonate carbonylating agent and catalytic amounts of CsF. After 25 hours at 60 °C, the bicyclic monomer was isolated in 36% yield following column chromatography and recrystallisation. Based on the original report of 1970,[3] Wooley and co-workers also prepared the cyclic carbonate using ethyl chloroformate, but in only 25% yield.[4]

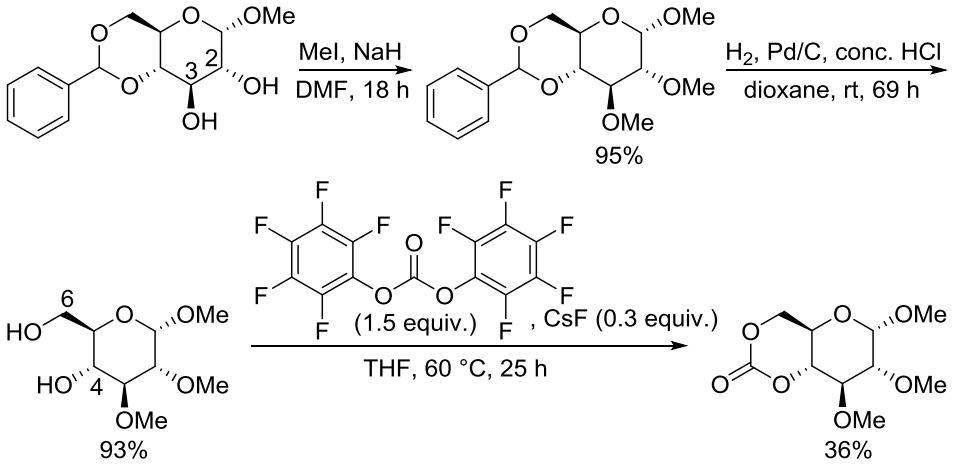

Scheme 3.03. Three step synthesis reported by Wooley and co-workers[2] of a D-glucose based cyclic carbonate monomer from commercially available glucose derivative.

The highly strained *trans*-configuration meant that the cyclic carbonate readily underwent ROP at room temperature with bifunctional organocatalyst, 1,5,7-triazabicyclo[4.4.0]dec-5-ene (TBD) and 4-methylbenzyl alcohol initiator. High monomer conversions (>99%) were achieved for example, after 7 hours in CH_2Cl_2 with 1 mol% catalyst loading and a monomer-to-initiator feed ratio of 51. Glucose-based polycarbonates with M_n up to 14 700 g mol^{-1} were reported and with narrow polydispersity ($Đ \leq 1.16$). Differential scanning calorimetry (DSC) of both glucose and xylose-derived APCs revealed high glass transition temperatures (T_g's) of 128 and 106 °C, respectively.

3.2. Synthesis of a D-Mannose Based Cyclic Carbonate

The natural stereochemistry of the hydroxyl groups in D-mannose presented the opportunity to combine the attractive components of both the glucose and xylose-derived cyclic monomers. Namely, the readily polymerisable *trans*-configured six-membered cyclic carbonate of the glucose monomer with the protected 1,2-diol motif of IPXTC, to serve as a handle for post-polymerisation modification. Following the literature precedence for isopropylidene protection of the *cis*-2,3-diol in commercially available 1-*O*-methyl-α-D-mannopyranoside,[5, 6] novel tricyclic monomer **3** (Scheme 3.04) was prepared using the method, developed in Chapter 2, of DBU facilitated CO_2 insertion coupled to a leaving group strategy.

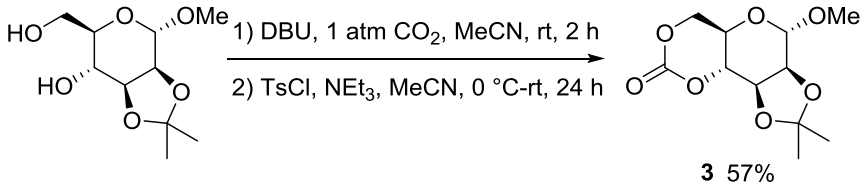

3 57%

Scheme 3.04. Synthesis of D-mannose based cyclic carbonate using CO_2 at 1 atm pressure and room temperature (rt).

CO_2 insertion with DBU reagent led predominantly to carbonate salt formation at the sterically less hindered primary hydroxyl group (6-position) as determined by $^{13}C\{^1H\}$ NMR spectroscopy (Figure 3.01). Carbonate environments at 159.2 and 158.4 ppm were attributed to CO_2 insertion at the 6- and 4- positions, respectively.

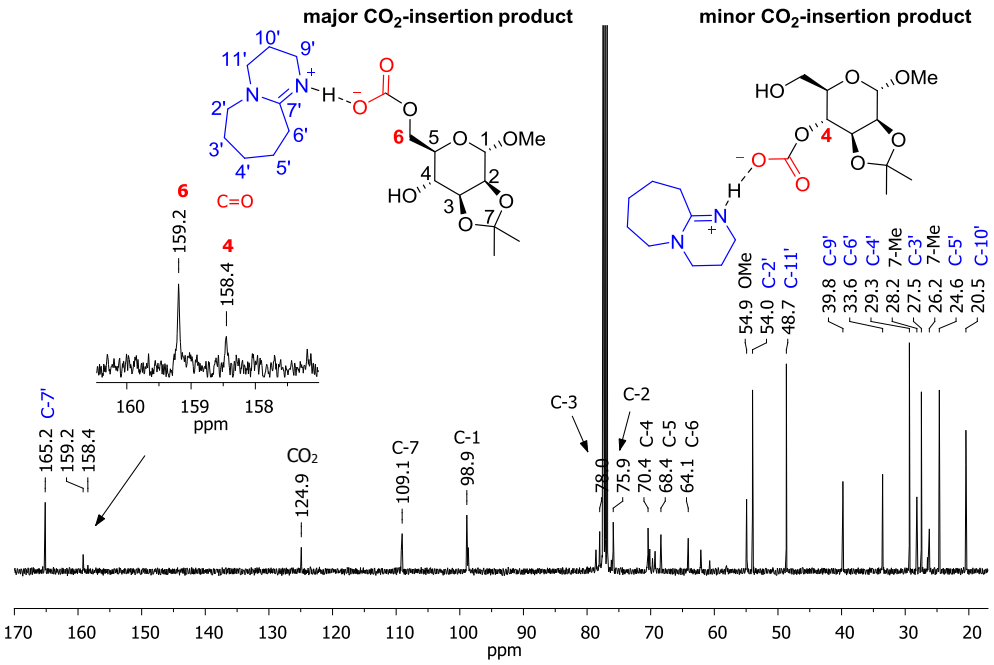

Figure 3.01. $^{13}C\{^{1}H\}$ NMR spectrum (101 MHz, $CDCl_3$) of the crude DBU facilitated CO_2 insertion reaction mixture showing one major CO_2 insertion product. This was assigned to carbonate formation at the sterically less hindered 6-position with the aid of HSQC, DEPT135 and COSY data (as for the 1,3-butanediol CO_2 insertion products in Chapter 2).

Addition of triethylamine and the tosyl leaving group resulted in 65% conversion to the cyclic product, determined by ^{1}H NMR analysis of the crude reaction mixture. Conditions of high dilution (0.1 mol L^{-1}) and low temperatures were key in favouring the intramolecular cyclisation over competing dimerisation reactions. Isolation by column chromatography and purification by recrystallisation from dry diethyl ether afforded cyclic 1-*O*-methyl-2,3-*O*-isopropylidene -4,6-*O*-carbonate-α-D-mannopyranoside **3** in 57% yield.

Structural confirmation of **3** was obtained by elemental analysis, NMR and FTIR spectroscopies, electrospray ionisation mass spectrometry (ESI-MS) and single-crystal X-ray diffraction. Characteristically of a C=O environment in a six-membered cyclic carbonate, $^{13}C\{^{1}H\}$ NMR analysis showed a resonance at 147 ppm, which was corroborated by FTIR spectroscopy, showing the presence of a strong absorption at 1763 cm^{-1} attributed to the C=O stretch. A large ^{3}J-coupling constant of 10.3 Hz in the ^{1}H NMR data was indicative of a *trans*-configured cyclic carbonate with a di-axial configuration of H-4 and H-5. This was confirmed by single-crystal X-ray diffraction analysis of colourless crystals of **3** grown by layering hexanes over $CDCl_3$ (Figure 3.02). The $^{4}C_1$ chair conformation of the pyranose ring placing C11-O3 and C3-C2 di-equatorial allows for the strained *trans*- configuration of the 4,6-cyclic carbonate.

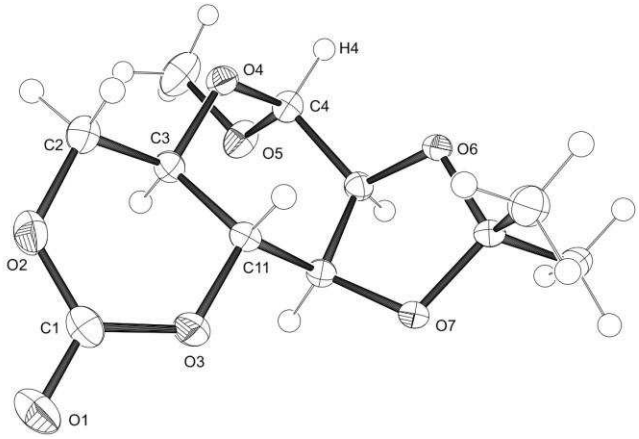

Figure 3.02. ORTEP[7] view of the crystal structure of D-mannose derived cyclic carbonate **3** with key atoms labelled and displacement ellipsoids at the 50% probability level. Selected bond lengths (Å) and angles (°): C(1)-O(1) 1.198(2), C(1)-O(2) 1.333(2), C(1)-O(3) 1.341(2), O(1)-C(1)-O(2) 120.38(14), O(1)-C(1)-O(3) 119.57(15), O(2)-C(1)-O(3)120.05(14), C(2)-C(3)-C(11)-O(3) 56.10(15).

3.3. Organocatalytic Ring-Opening Polymerisation

The ROP of the protected D-mannose based cyclic carbonate **3** was carried out *via* an organocatalytic approach with TBD catalyst and 4-methylbenzyl alcohol (4-MeBnOH) initiator (Scheme 3.05). This approach was chosen owing to its simplicity and crystalline 4-methylbenzyl alcohol used in preference to benzyl alcohol as it was more readily purified and provided both aromatic and methyl signals for end-group analysis by ^{1}H NMR spectroscopy. For polymer applications targeting the biomedical field, any potential toxicity of the catalyst should also be taken into consideration, including that of organocatalysts.

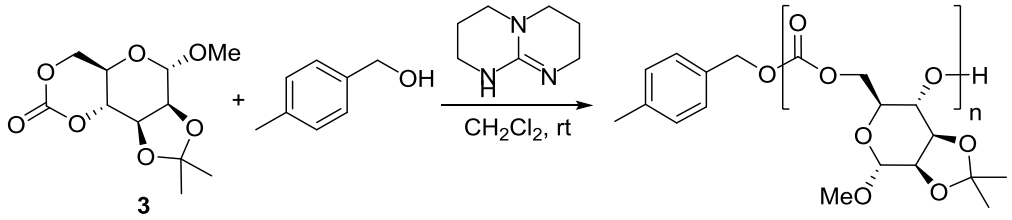

Scheme 3.05. ROP of mannose-based monomer with TBD catalyst and 4-methylbenzyl alcohol initiator.

3.3.1. Kinetics

Monomer conversion was monitored as a function of time by ^{1}H NMR spectroscopy of aliquots taken at set time intervals and quenched with benzoic acid. The polymerisation proceeded rapidly at room temperature (rt), reaching >99% conversion in 80 minutes for an

initial monomer concentration ($[M]_0$) of 1 mol L^{-1} in CH_2Cl_2, 1 mol% catalyst loading and a monomer-to-initiator feed ratio of 100 (Figure 3.03).

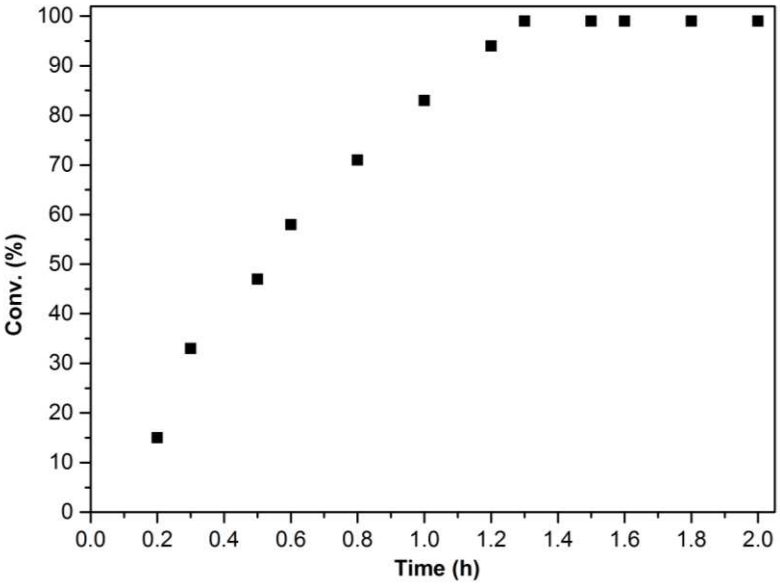

Figure 3.03. Monomer conversion as a function time for a ROP of **3** carried out with 100:1:1 $[M]_0$: $[TBD]_0$: $[4\text{-MeBnOH}]_0$ in CH_2Cl_2 at rt, where $[M]_0$ = 1 mol L^{-1}. Determined by relative integration of the anomeric (H-1) proton environments of the monomer (4.99 ppm) to the polymer (4.90 ppm) in the ^1H NMR spectra (400 MHz, $CDCl_3$) of aliquots taken at known time intervals and quenched with benzoic acid.

Linear plots of $\ln([M]_0/[M])$ against time at $[M]_0$: $[TBD]_0$: $[4\text{-MeBnOH}]_0$ of 100:1:1 and 50:1:1 showed pseudo first-order kinetics, typical of ROP (Figure 3.04). From these, values of k_{app} of 1.7 ± 0.1 and 9.9 ± 0.8 h^{-1} were determined for 1 and 2 mol% TBD loading, respectively.

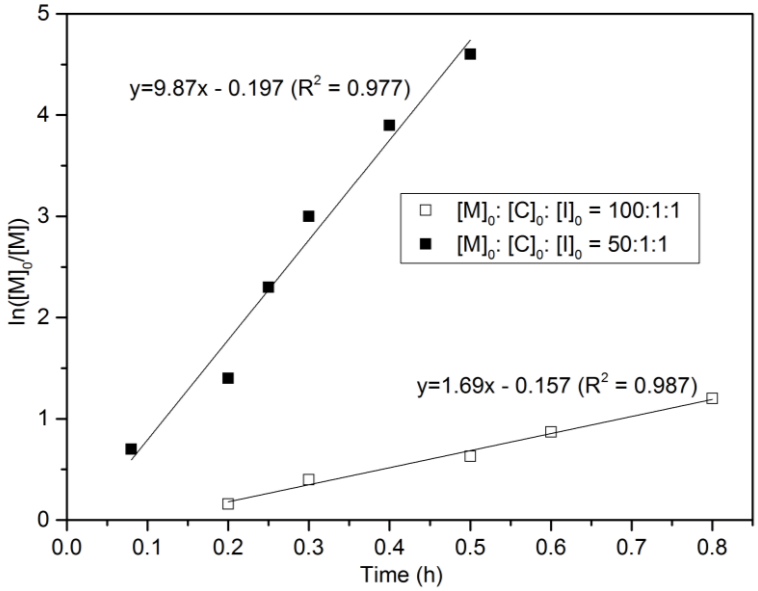

Figure 3.04. Kinetic plot showing pseudo-first order kinetics in monomer (M) concentration for polymerisations carried out in CH_2Cl_2 at rt with ratios of 100:1:1 (□) and 50:1:1 (■) $[M]_0$: $[TBD]_0$: $[4\text{-MeBnOH}]_0$ where $[M]_0$ = 1 mol L^{-1}.

3.3.2. Controlled "living" polymerisation

Polymer molecular weights and molecular weight distributions, were estimated by size elusion chromatography (SEC) *versus* polystyrene standards in THF eluent. As a function of monomer conversion, for a polymerisation with $[M]_0$: $[TBD]_0$: $[I]_0$ of 100:1:1, a roughly linear increase in M_n with conversion whilst maintaining narrow Đ (1.12-1.17) was indicative of a well-controlled polymerisation (Figure 3.05).

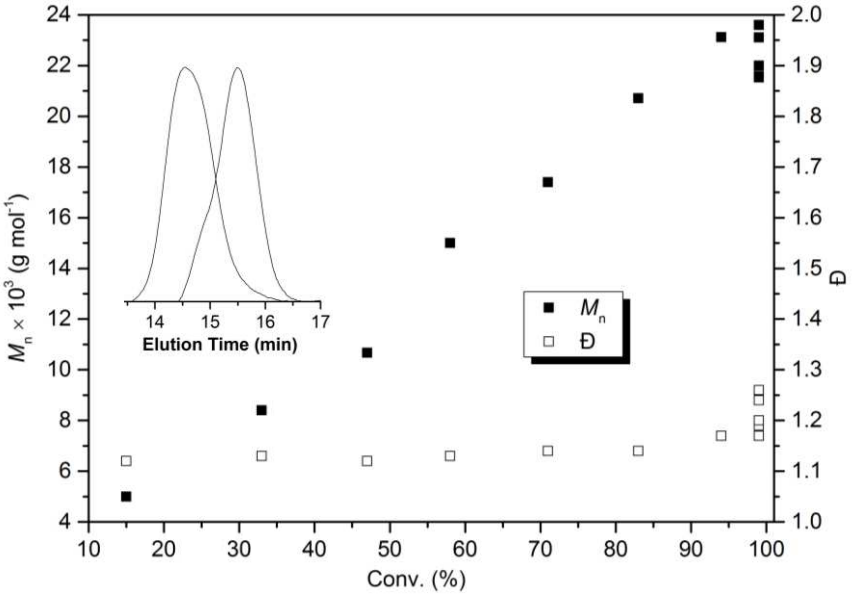

Figure 3.05. Plot of M_n (■, left axis) and Đ (□, right axis) estimated by SEC (RI detector) relative to polystyrene standards with THF eluent *vs*. conversion of **3** (determined by relative integration of the anomeric protons at 4.99 *vs*. 4.90 ppm in the ^{1}H NMR spectra). Aliquots were taken and quenched every 10 minutes for a polymerisation in CH_2Cl_2 at rt, with an $[\mathbf{3}]_0$: $[TBD]_0$: $[4\text{-MeBnOH}]_0$ ratio of 100:1:1 and $[\mathbf{3}]_0$ = 1 mol L^{-1}; **(inset)** Typical SEC trace showing increase in M_n from 5360 to 10 500 g mol^{-1} (maintaining Đ = 1.15) upon addition of 0.5 equiv. of **3** to a polymerisation with $[\mathbf{3}]_0/[4\text{-MeBnOH}]_0$ = 25 at >99% conversion.

Prolonged reaction times of 2 to 4 hours led to a decrease in M_n and a broadening of Đ to 1.3. This is likely due to chain backbiting reactions. After the polymerisation reached full conversion, addition of more monomer resulted in further chain growth (inset SEC trace to Figure 3.05) demonstrating the "living" nature of the polymerisation.

ROP experiments carried out over a range of catalyst loadings and monomer-to-initiator ratios showed good correlation between the predicted (based on the conversion and monomer-to-initiator ratio) and SEC estimated M_n (Table 3.01).

Table 3.01. Organocatalytic ROP of mannose-based monomer by TBD with 4-methylbenzyl alcohol initiator.[a]

Entry[a]	$[M]_0$: $[C]_0$: $[I]_0$	Conv. (%)[b]	Time (h)	M_n (g mol^{-1}) [c]	Calc. M_n (g mol^{-1}) [d]	Đ[e]
1	25:1:1	>99	0.5	6630	6560	1.15
2	50:1:2	>99	0.5	6260	6560	1.15
3	50:1:1	>99	1	13 600	13 000	1.17
4	100:1:2	>99	1.5	10 800	13 000	1.10
5	100:1:1	47	0.5	10 700	12 300	1.12
6	100:1:1	>99	1.3	23 600	25 900	1.17
7	150:1:1	98	3	33 400	38 300	1.19
8[f]	100:1:1	98	0.5	26 200	25 600	2.15
9[g]	100:0.5:1	60	0.5	10 900	15 700	1.22

[a] $[M]_0$= 1 mol L^{-1}, I= 4-MeBnOH. [b] Determined by relative integration of the anomeric proton (δ_H= 4.90 ppm for the monomer and 4.99 ppm for the polymer) in the ^{1}H NMR spectrum (400 MHz, $CDCl_3$). [c] Estimated by SEC (RI detector) relative to polystyrene standards with THF eluent. [d] Calculated as $M_r(I)+ (M_r(M) \times [M]_0/[I]_0 \times$ conv./100%). [e] M_w/M_n, estimated by SEC relative to polystyrene standards with THF eluent. [f] Melt conditions: 140 °C. [g] $Sn(Oct)_2$ catalyst, melt conditions: 140 °C.

Moreover, a polymer with M_n 7360 g mol^{-1} determined by SEC showed good correlation with M_n values estimated by ^{1}H NMR spectroscopy (6950 g mol^{-1}) and MALDI-ToF mass spectrometry (7550 g mol^{-1}). The polymerisation could also be carried out under industrially relevant conditions in the melt at 140 °C with TBD and $Sn(Oct)_2$ catalysts (Table 3.01, Entries 8 and 9) although with less control over the M_n and Đ.

3.3.3. End-group determination by MALDI-ToF mass spectrometry

MALDI-ToF mass spectrometry of a polycarbonate with M_n by SEC of 5000 g mol^{-1} revealed a polymeric series with the correct sugar carbonate repeat unit ($\Delta m/z$ ~260), indicating no decarboxylation had occurred during the ROP (Figure 3.06). The major series had *m/z* values consistent with the sodium adduct of the linear polymer with expected 4-methylbenzyl alcohol and -OH end-groups ($P_L + Na^+$). Also observed was a minor cyclic polymeric series with *m/z* values consistent with an integer number of mannose carbonate repeat units and no end-groups. This is evidence of chain backbiting during the polymerisation resulting in the formation of macrocycles (M_n ~ 3790 g mol^{-1}).

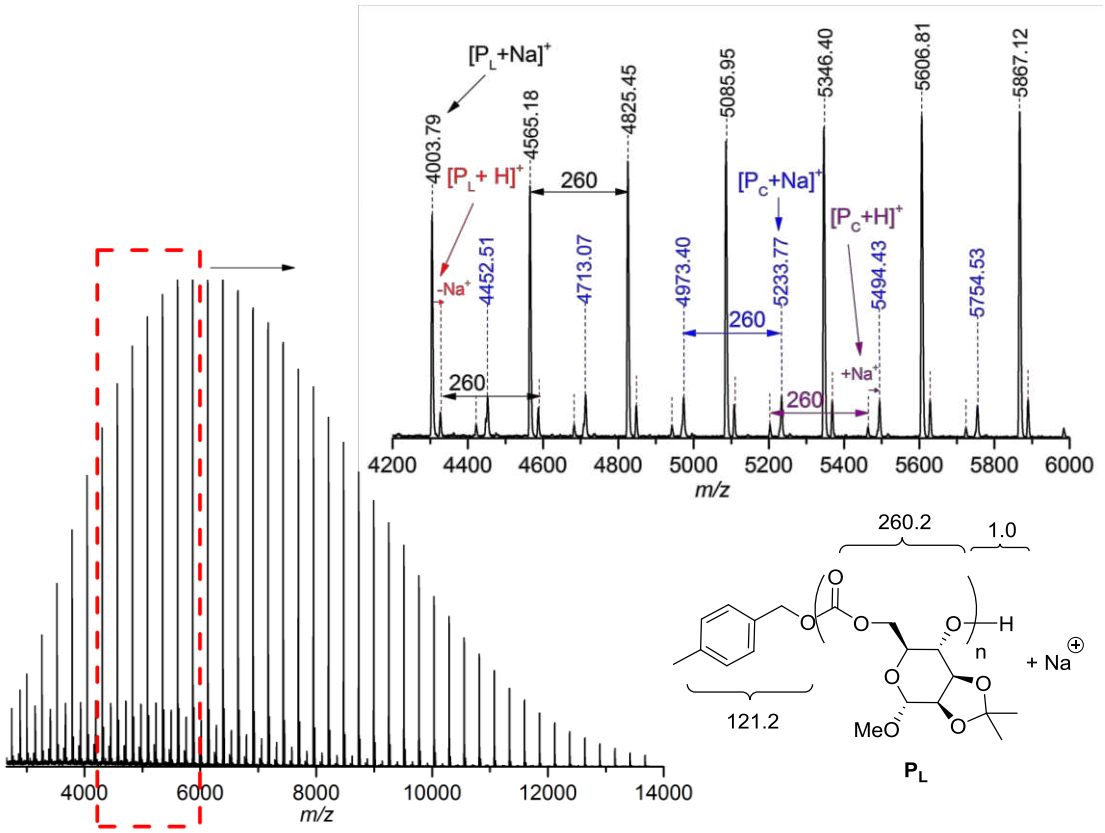

Figure 3.06. MALDI-ToF MS of polymer ($M_{n,SEC}$ = 5000 g mol^{-1}, Đ 1.12; $M_{n,\ MALDI}$ = 5500 g mol^{-1}, Đ 1.10). The major series is assigned to the sodium adduct of the linear polymer (drawn) with 4-MeBnOH and OH end-groups (e.g. n= 22 gives an *m/z* of 5869.6). Less intense series are the linear polymer without the sodium ion, $[P_L+H]^+$ ($M_{n,MALDI}$ = 4150 g mol^{-1}, Đ 1.01) and the polymeric cyclic species with the sodium ion $[P_c+Na]^+$ ($M_{n,MALDI}$ = 3790 g mol^{-1}, Đ 1.10) and without, $[P_c+H]^+$ ($M_{n,MALDI}$ = 5550 g mol^{-1}, Đ 1.06).

MALDI-ToF MS of higher M_n polymers showed a greater presence of cyclic species. For a polymer of M_n by SEC of 10 400 g mol^{-1}, a major cyclic polymeric series was detected with M_n 5280 g mol^{-1} alongside a linear polymeric series of M_n 7670 g mol^{-1} (Figure 3.07). Longer polymer chains may result in more backbiting during the polymerisation or this may be an artefact of the MALDI process, whereby smaller cyclic species are volatilised more readily than higher molecular weight linear polymers. For polymerisations carried out at higher $[M]_0/[I]_0$ ratios, estimation of the M_n by ^{1}H NMR spectroscopy, by relative integration of the aromatic signals of the 4-methylbenzyl alcohol end-group to the anomeric proton environment of the sugar repeat unit, gave values much higher than predicted based on the monomer conversion. This is consistent with the greater presence of cyclic polymeric species bearing no end-group. No distinction could be made between the proton environments of the cyclic and linear polymers and was attributed to the large size of the polymeric macrocycles.

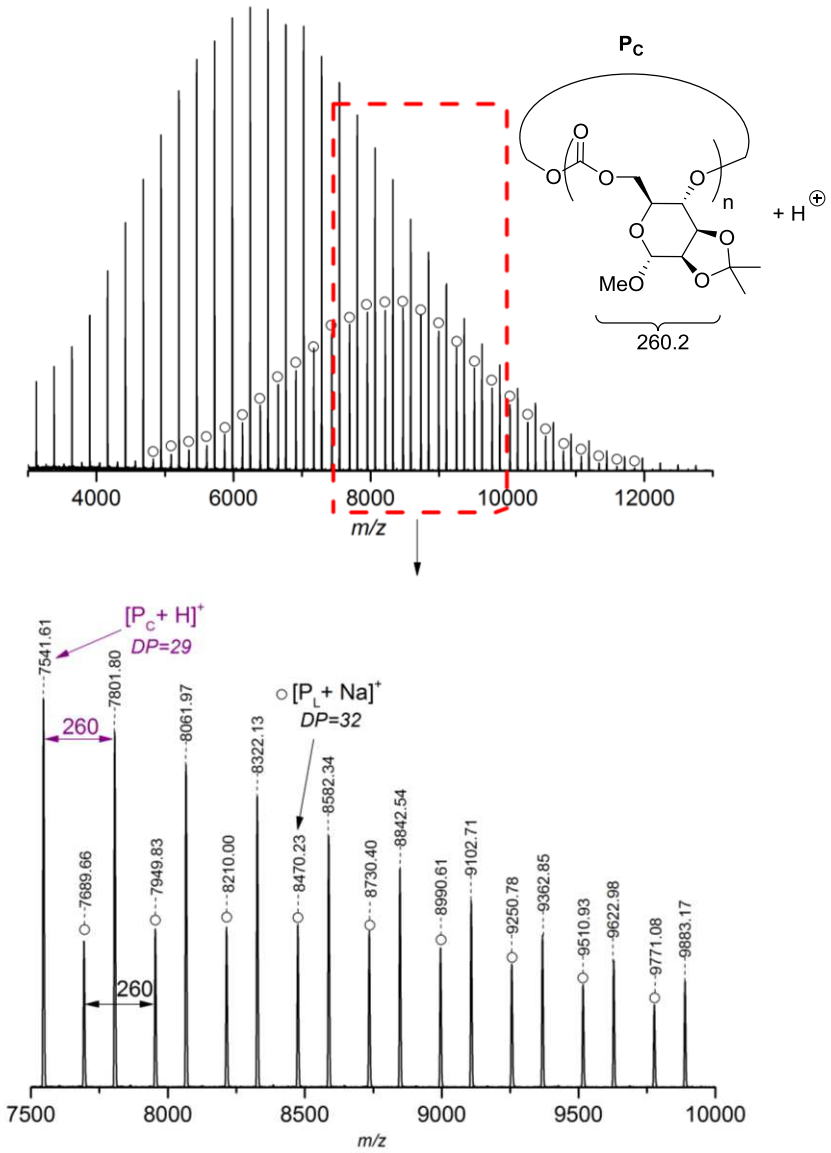

Figure 3.07. MALDI-ToF MS of polymer ($M_{n,SEC}$ = 10 400 g mol^{-1}, Đ 1.13) showing two series with sugar carbonate repeat unit $\Delta m/z$ ~ 260. The cyclic series ($[P_C+H]^+$, $M_{n,MALDI}$ = 5280 g mol^{-1}, Đ 1.11) is due to backbiting of the polymer chain and for example, a degree of polymerisation (DP) of 29 gives a predicted *m/z* of 7546.8. The second series is assigned to the sodium adduct of the linear polymer ($[P_L+Na]^+$, $M_{n,\ MALDI}$ = 7670 g mol^{-1}, Đ 1.02) with 4-methylbenzyl alcohol and OH end-groups.

In addition, at M_n greater than 15 000 g mol^{-1}, SEC traces exhibited shoulders or slight bi-modality, which may be attributed to the greater presence of the cyclic species (Figure 3.08). Such backbiting reactions likely limit the length of the polymer chain achievable. Although, M_n values of up to 33 400 g mol^{-1} where achieved at $[M]_0$: $[TBD]_0$: $[4\text{-MeBnOH}]_0$ of 150:1:1 (Table 3.01, Entry 7), larger M_n could not be reached at greater $[M]_0/[I]_0$ ratios, under these ROP conditions. The presence of trace impurities specifically, alcohols, diols, or water in **3** will also act as chain transfer agents, limiting the M_n.

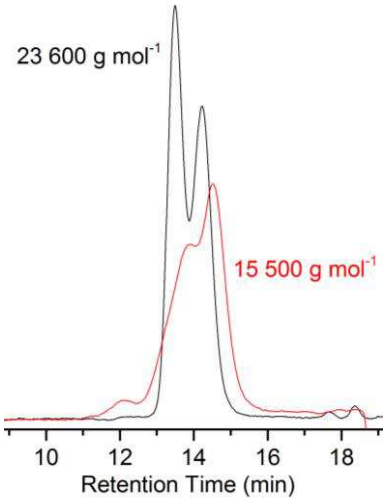

Figure 3.08. SEC traces for polycarbonates of M_n 15 500 and 23 600 g mol^{-1} showing bimodality.

3.4. Polycarbonate Structure

FTIR analysis of the mannose-derived polymers showed a characteristic strong absorption at ~1757 cm^{-1} due to the C=O stretch of the carbonate linkages. In the ^{1}H NMR spectra of the polymer, a general broadening of the environments was observed on ROP of the cyclic monomer to the macromolecule as well as changes in the chemical environments upon relief of ring strain and subsequent conformational reorganisation (Figure 3.09). Most notably, a coalescing of the signals assigned to the cyclic carbonate methylene protons (H-6 and H-6') was observed upon ring-opening as well as a downfield shift of the doublet of doublets assigned to H-4 from 4.14 ppm in the monomer to 4.73 ppm in the polymer NMR spectrum.

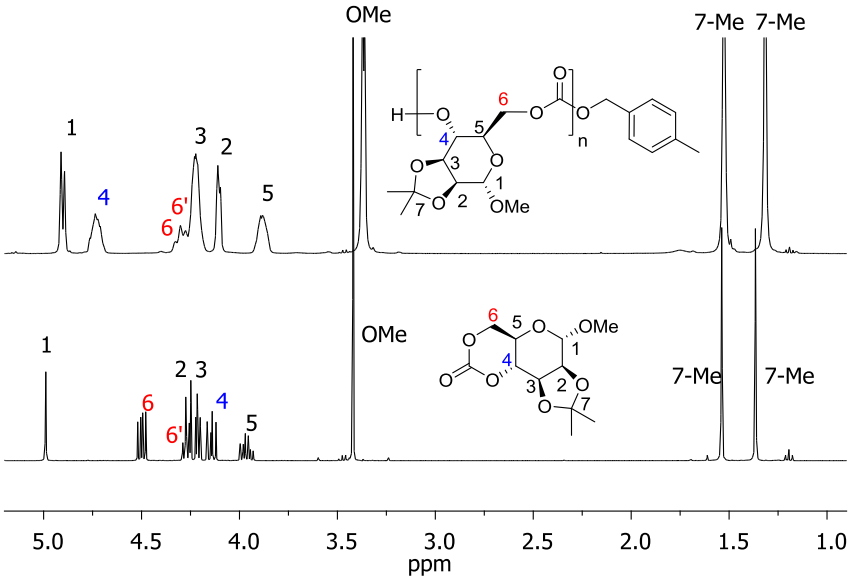

Figure 3.09. ^{1}H NMR spectra (400 MHz, $CDCl_3$) of **3** (bottom) and poly(**3**) (top, M_n 7360 g mol^{-1}, Đ 1.12).

3.4.1. Backbone regiochemistry

In the $^{13}C\{^{1}H\}$ NMR spectrum of the polymer, one distinct carbonyl resonance was observed at 154.5 ppm compared to 147.4 ppm for the monomer C=O. The presence of an easily discernible carbonate environment contrasts with that reported for the protected D-glucose and D-xylose based polycarbonates. In these cases, three distinct carbonate environments were observed, differing by as much as 0.3 to 0.5 ppm. Figure 3.10 compares the carbonyl region for the mannose, xylose and glucose derived polycarbonates prepared under the same ROP conditions with TBD catalyst. Cleavage of the acyl-oxygen bond can occur at either side of the carbonate carbonyl leading to two possible ring-opened forms in unsymmetrical cyclic monomers (Figure 3.11). Successive ring-opening of additional monomer with either the exposed primary or secondary hydroxyl group results in three possible linkage types in the polymer backbone: head-head (H-H), head-tail (H-T) and tail-tail (T-T).

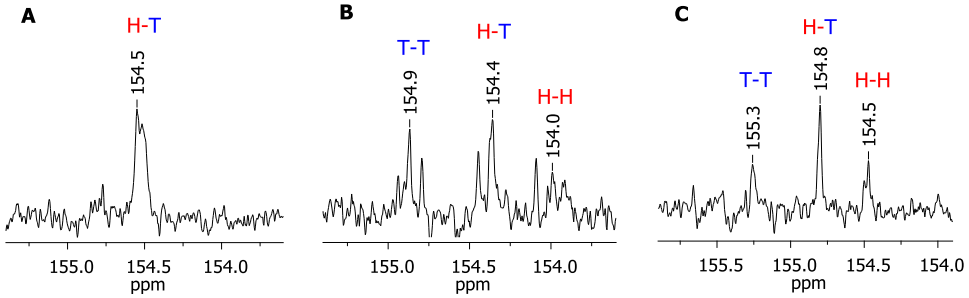

Figure 3.10. Comparison of the carbonate region of the $^{13}C\{^{1}H\}$ NMR spectra (101 MHz, $CDCl_3$) of **A:** the D-mannose derived APC ($M_{n,SEC}$ = 7360 g mol^{-1}, Đ 1.12), **B:** the regiorandom D-glucose based polymer and **C:** the D-xylose derived polycarbonate. All three sugar-based monomers were prepared using the method with CO_2 and the ROP carried out under the same polymerisation conditions: $[M]_0$: $[TBD]_0$: $[I]_0$ = 50:1:1, $[M]_0$= 1 mol L^{-1} in CH_2Cl_2, rt. The carbonyl regions for the protected glucose and xylose-based polycarbonates are entirely consistent with the literature data (where the monomer synthesis and/or polymerisation were carried out under different conditions).

For the D-xylose based polycarbonates, Gross and coworkers[1] suggested that there was no preference for cleavage to either one side based on the roughly 1:2:1 ratio of the H-H, H-T and T-T carbonyl signals by quantitative ^{13}C NMR spectroscopy, in accordance with that expected on the basis of probability. Similarly, for the glucose-based polycarbonates, detection of diagnostic fragment ions for both H-T and T-H orientations by electron transfer dissociation tandem mass spectrometry, indicated to Wooley and coworkers[2] the presence of all three linkage types. In contrast to these regiorandom sugar-based polymers, the carbonate region for the mannose derived polycarbonates suggested a preference for one regiochemistry. Specifically, a preference for H-T linkages as any H-H (or T-T) linkage

would necessarily entail a subsequent T-T (or H-H) linkage and thus give rise to two distinct environments. This was supported by DFT modelling of the initiation and first propagation step in the ROP of **3** with TBD and 4-MeBnOH (Section 3.5).

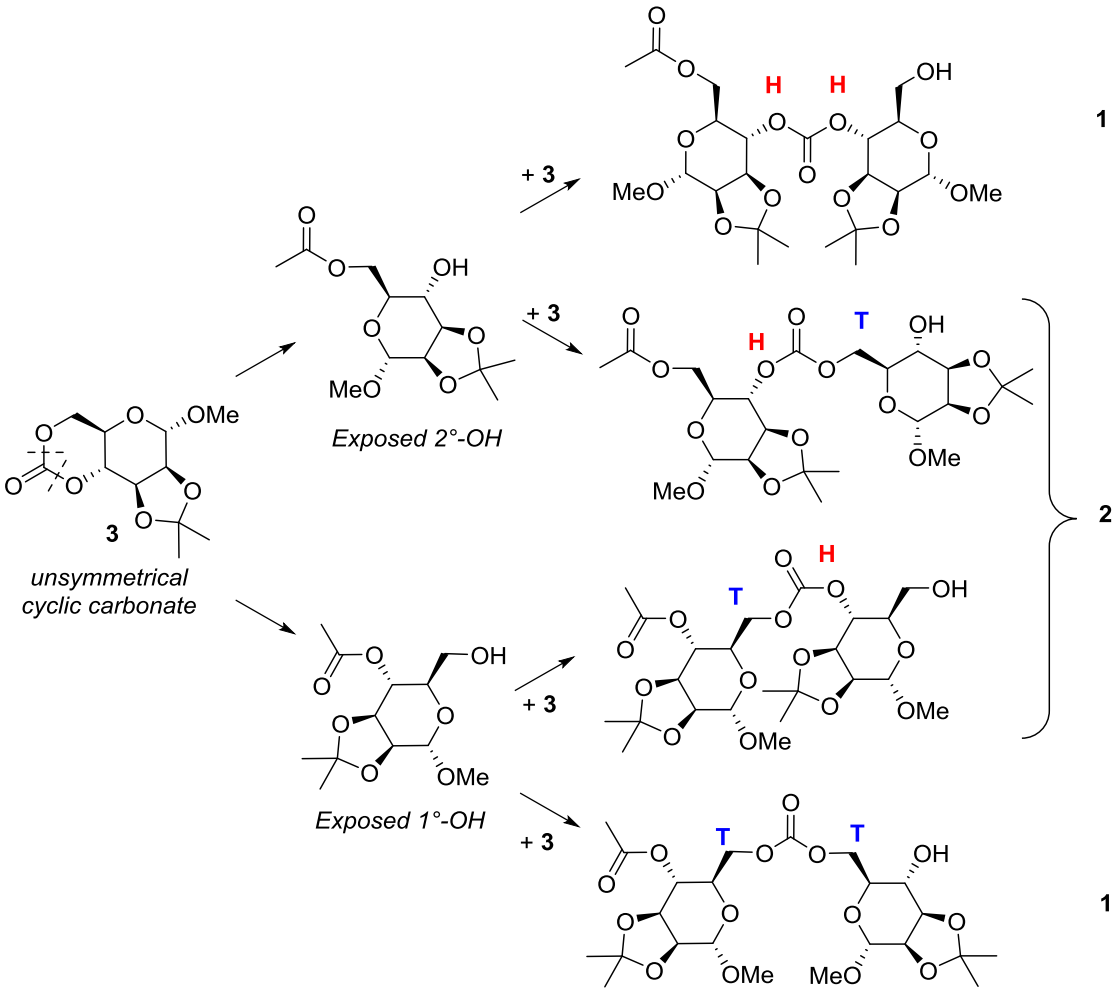

Figure 3.11. Asymmetric ring-opening leading to two possible ring-opened forms, exposing either a primary (1°-OH) or secondary (2°-OH) alcohol group. Successive ring-opening of monomer (**3**) leads to three possible regiochemistries in the polycarbonate backbone: Tail-Tail (T-T), Head-Tail (H-T) and Head-Head (H-H).

Equimolar ring-opening experiments of **3** with 4-MeBnOH in the presence of catalytic amounts of TBD showed an 88% preference for ring-opening to place the benzyl carbonate at the primary position, leaving the secondary group free for chain propagation. Comparison of the ^{1}H NMR spectrum of the ring-opened monomer with the un-cyclised protected diol (Figure 3.12) showed a similar H-4 proton environment but large downfield shift in the H-6 methylene environment from 3.58 ppm in the diol to 4.41 ppm in the ring-opened monomer, consistent with the presence of the carbonate at this position. The preference for ring-opening to the 6- rather than the 4-position was estimated by quantitative ^{13}C{^{1}H} NMR spectroscopy by integration of the C=O signal at 155.7 ppm and 155.3 ppm, respectively. A

similar regioselectivity for the organocatalytic ring-opening of substituted cyclic carbonates with TBD to form carbamates was reported by Sopeña *et al.*[8]

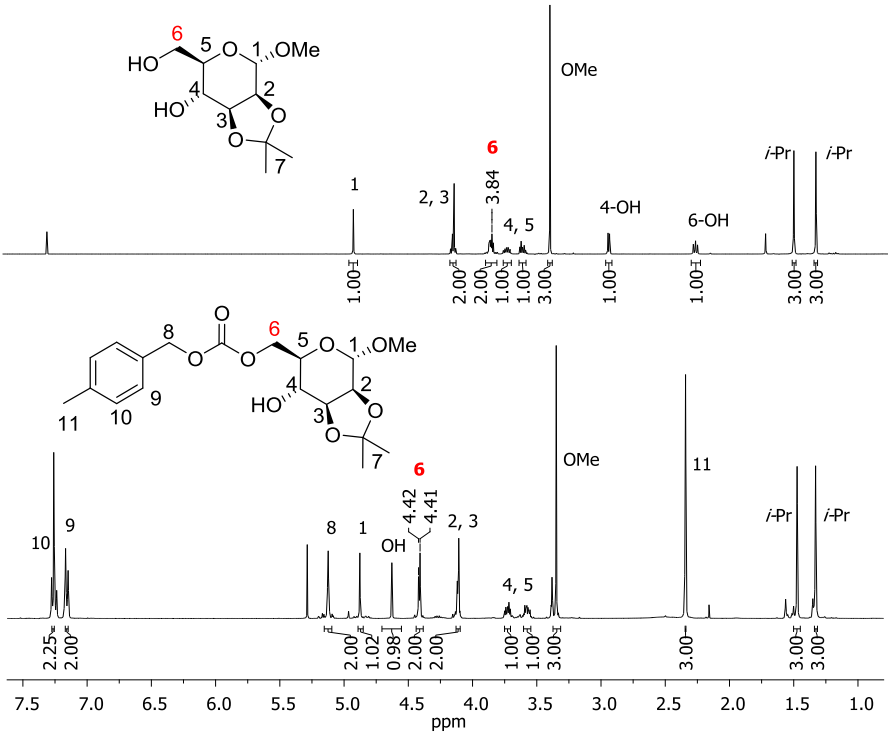

Figure 3.12. Comparison of ^{1}H NMR spectra (400 MHz, $CDCl_3$) of the protected D-mannose diol (top) and the equimolar ring-opening of cyclic carbonate **3** with 4-methylbenzyl alcohol (bottom). The presence of one major product showing a significant difference in the chemical shift of the methylene H-6 protons indicates a preference for ring-opening to place the carbonate at the less sterically hindered primary position.

3.5. DFT Modelling of the Initiation and First Propagation Steps

DFT calculations were used to further investigate the regioselectivity observed in the ROP of **3** with TBD and 4-methylbenzyl alcohol. Both the initiation and first propagation step were modelled with the rωb97xd functional at 298 K in CH_2Cl_2. A mixture of basis sets was used to allow for potential anions and nonbonding (hydrogen bonding) interactions to be considered at the key atoms whilst minimising the overall computational cost. That is, the higher split-valence triple ζ basis set with polarisation and diffuse functions, 6-311++G(d,p) was used for the carbonate, guanidine and alcohol moieties of **3**, TBD and 4-MeBnOH, respectively and the lower split-valence double ζ basis set, 6-31+G(d) for all other atoms.

In accordance with previous calculations,[9] TBD acts as a bifunctional catalyst; activating both the carbonate monomer (by increasing the electrophilicity of the carbonyl carbon) and deprotonating the attacking 4-methylbenzyl alcohol initiator or growing alcohol chain. The

ring-opening is a discrete, rather than concerted process, with TBD mediating proton transfer stepwise through tetrahedral intermediates. Outlined in Figure 3.13, following formation of a ternary complex (intermediate **I**), whereby TBD is interacting with both the carbonyl oxygen of the monomer and the hydrogen of the alcohol, nucleophilic addition of the alcohol to the carbonyl carbon (**TS$_{I-II}$**) results in the formation of tetrahedral intermediate **II**. Migration of the TBD (intermediate **III**) so that the proton from the attacking alcohol is then interacting with the oxygen of the sugar sets up the ring-opening transition state (**TS$_{III-IV}$**). This involves a proton transfer to yield either a free primary or secondary hydroxyl group (intermediate **IV**). Ring-opening of a second molecule of monomer by either the primary or secondary alcohol, can then occur *via* the same reaction pathway and constitutes the first propagation step. Finally, attack of the alcohol group (the initiator or growing chain) can occur from both above or below the carbonyl carbon, either on the same face (designated *syn*-) as the isopropylidene protecting group or the opposite face (designated *anti*-). Consequently, in Figures 3.14 to 3.16 there are four reaction profiles: subscripts **a** and **b** refer to attack *syn*- to the protecting group to expose a primary or secondary hydroxyl group, respectively and subscripts **c** and **d**, to attack *anti*- to the protecting group to expose a primary or secondary hydroxyl group, respectively.

In accordance with the experimental findings, the initiation step was found to favour, both kinetically ($\Delta\Delta G^{\ddagger}$= +9.1 kcal mol^{-1}) and thermodynamically ($\Delta\Delta G$= -11.4 kcal mol^{-1}), ring-opening to expose a secondary alcohol (**IV$_a$**, Figure 3.14). Regardless of the regioselectivity of the initiation step, subsequent propagation from either a primary (Figure 3.15) or secondary (Figure 3.16) growing polymer chain showed the same bias to secondary alcohol formation, leading to an overall preference for head-tail linkages. The lowest limiting energy barriers found, $\Delta\Delta G$ of +9.2 and +13.7 kcal mol^{-1} for the initiation and propagation steps respectively, are low enough for the reaction to proceed readily at room temperature. The overall ΔG was calculated to be –11.4 kcal mol^{-1} for initiation, and –1.8 kcal mol^{-1} for the propagation step.

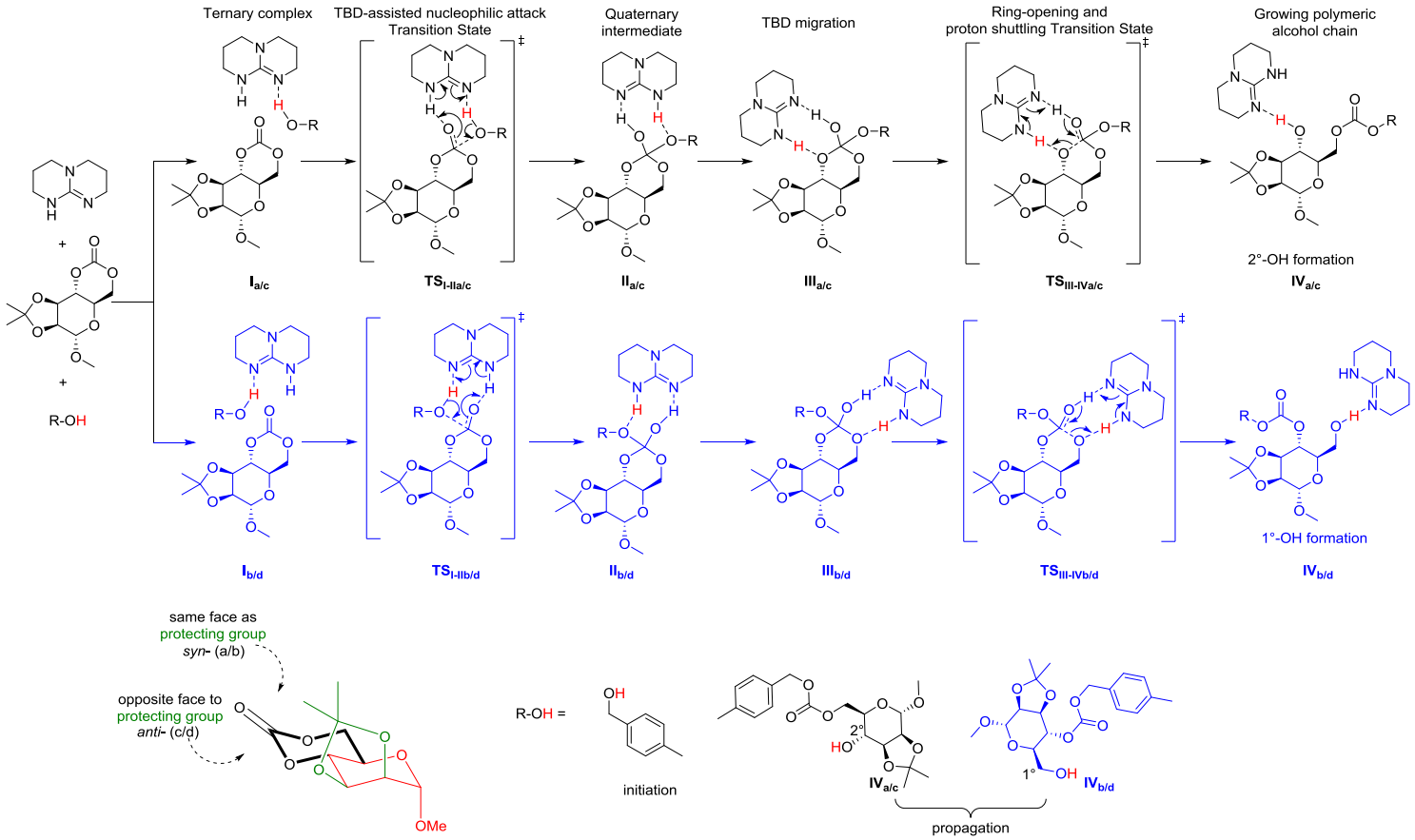

Figure 3.13. General scheme showing the DFT calculated intermediates (**I**) and transition states (**TS**) for the initiation step (R-OH= 4-methylbenzyl alcohol) and the first propagation step (R-OH= $\mathbf{IV_{a/c}}$ or $\mathbf{IV_{b/d}}$) in the ROP of **3** with TBD catalyst. Attack of the alcohol can occur at either face of the cyclic carbonate and ring-opening can expose either a primary (1°-OH) or secondary (2°-OH) alcohol for chain propagation. This gives rise to the four calculated reaction profiles in Figures 3.14 to 3.16: attack of the ring-opening alcohol on the same face as the protecting group (*syn*-) to expose a primary or secondary alcohol (profiles **a** and **b**, respectively) and attack on the face opposite to the protecting group (*anti*-) to expose a primary or secondary alcohol (profiles **c** and **d**).

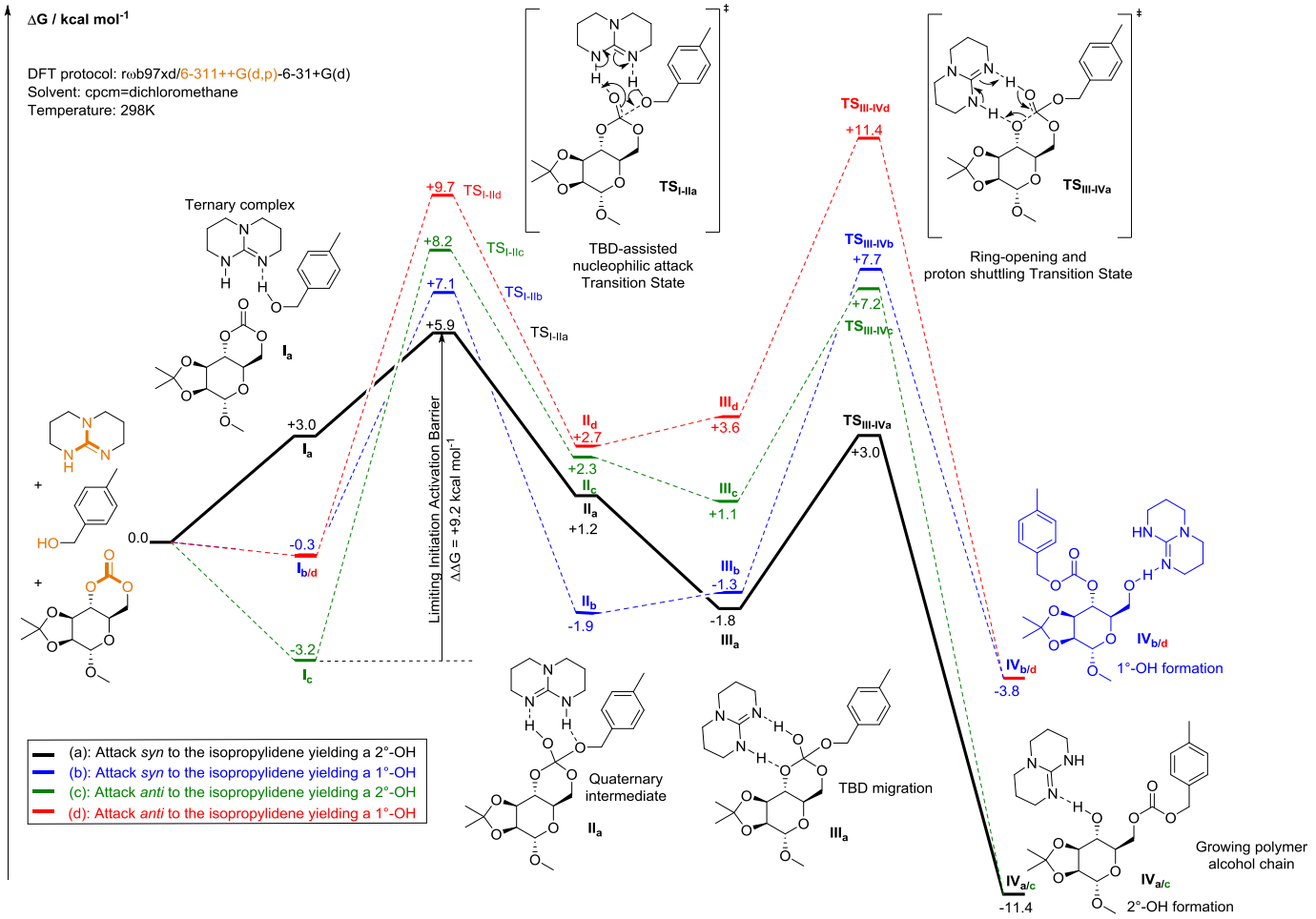

Figure 3.14. Calculated Gibbs free energy profile (**I** to **IV** *via* TS_{I-II} and TS_{III-IV}) for the initiation step in the ROP of **3** catalysed by TBD and initiated by 4-MeBnOH. Attack of the alcohol at the carbonyl carbon on the same face (*syn*-, profiles **a** and **b**) and the opposite face (*anti*-, profiles **c** and **d**) to the isopropylidene protecting group are shown and to expose either a primary (1°-OH, profiles **b** and **d**) or secondary (2°-OH, profiles **a** and **c**) alcohol group for chain propagation. The higher basis set of 6-311++G(d,p) was applied to the carbonate of the monomer, OH of 4-MeBnOH and guanidine of TBD and are highlight in orange in the starting materials. The most favourable calculated energy profile (bold, black) correlates to attack *syn* to the protecting group to expose a 2°-OH ($\Delta\Delta G$ = -11.4 kcal mol^{-1}, $\Delta\Delta G^{\ddagger}$= +9.2 kcal mol^{-1}).

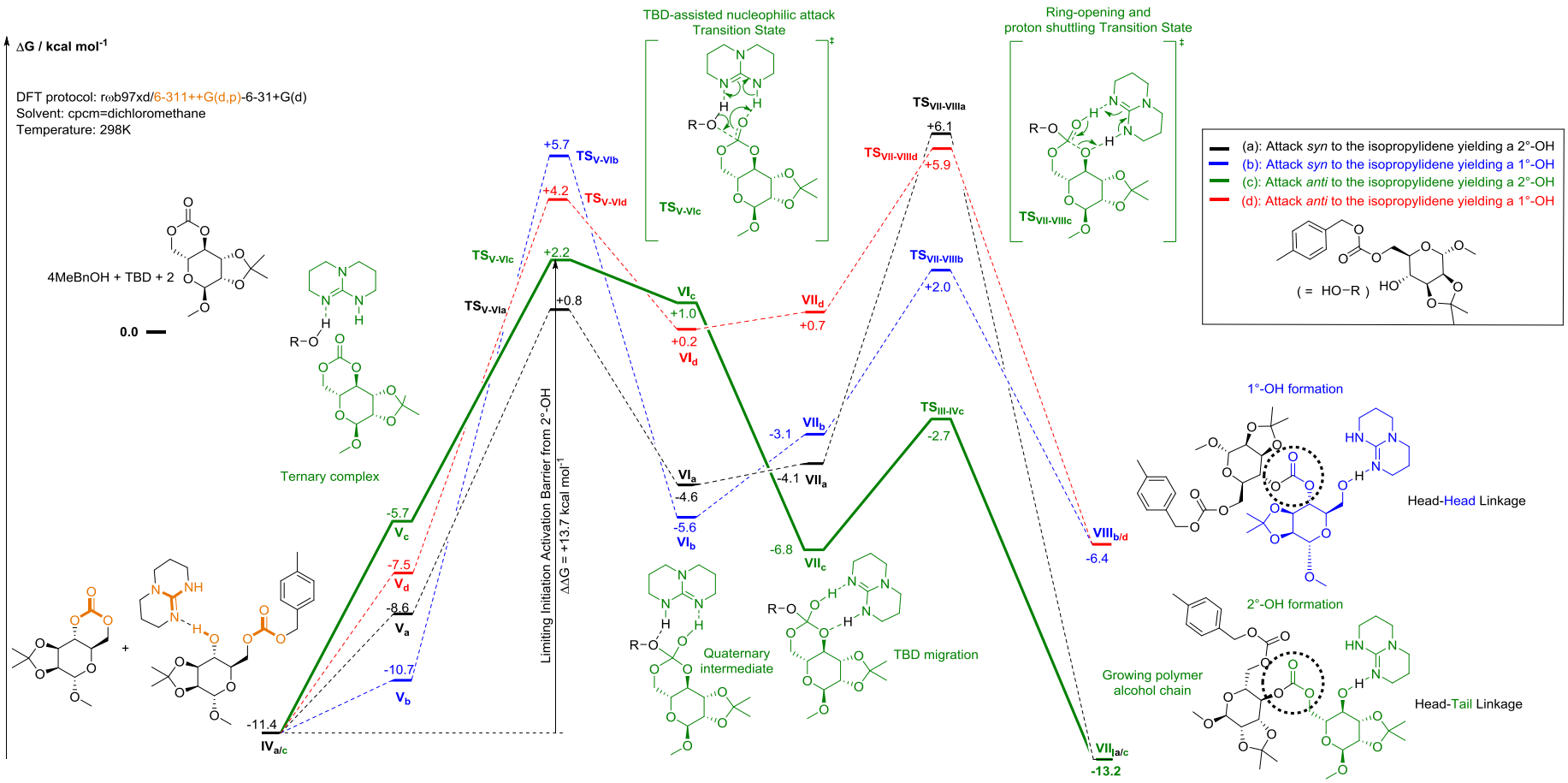

Figure 3.15. Calculated Gibbs free energy profile for the propagation step in the ROP of **3** catalysed by TBD and initiated by the secondary alcohol of the 4-MeBnOH ring-opened monomer (**IV$_{a/c}$**). Attack of the alcohol at the carbonyl carbon on the same face (*syn*-, profiles **a** and **b**) and the opposite face (*anti*-, profiles **c** and **d**) to the isopropylidene protecting group are shown and to yield either a head-head (1°-OH formation, profiles **b** and **d**) or head-tail (2°-OH formation, profiles **a** and **c**) linkage. 4-MeBnOH, TBD and 2 molecules of monomer were taken as the reference point (0.0 kcal mol^{-1}). The most favourable calculated profile (bold, green) corresponds to attack of the secondary alcohol *anti*- to the protecting group to form a head-tail linkage.

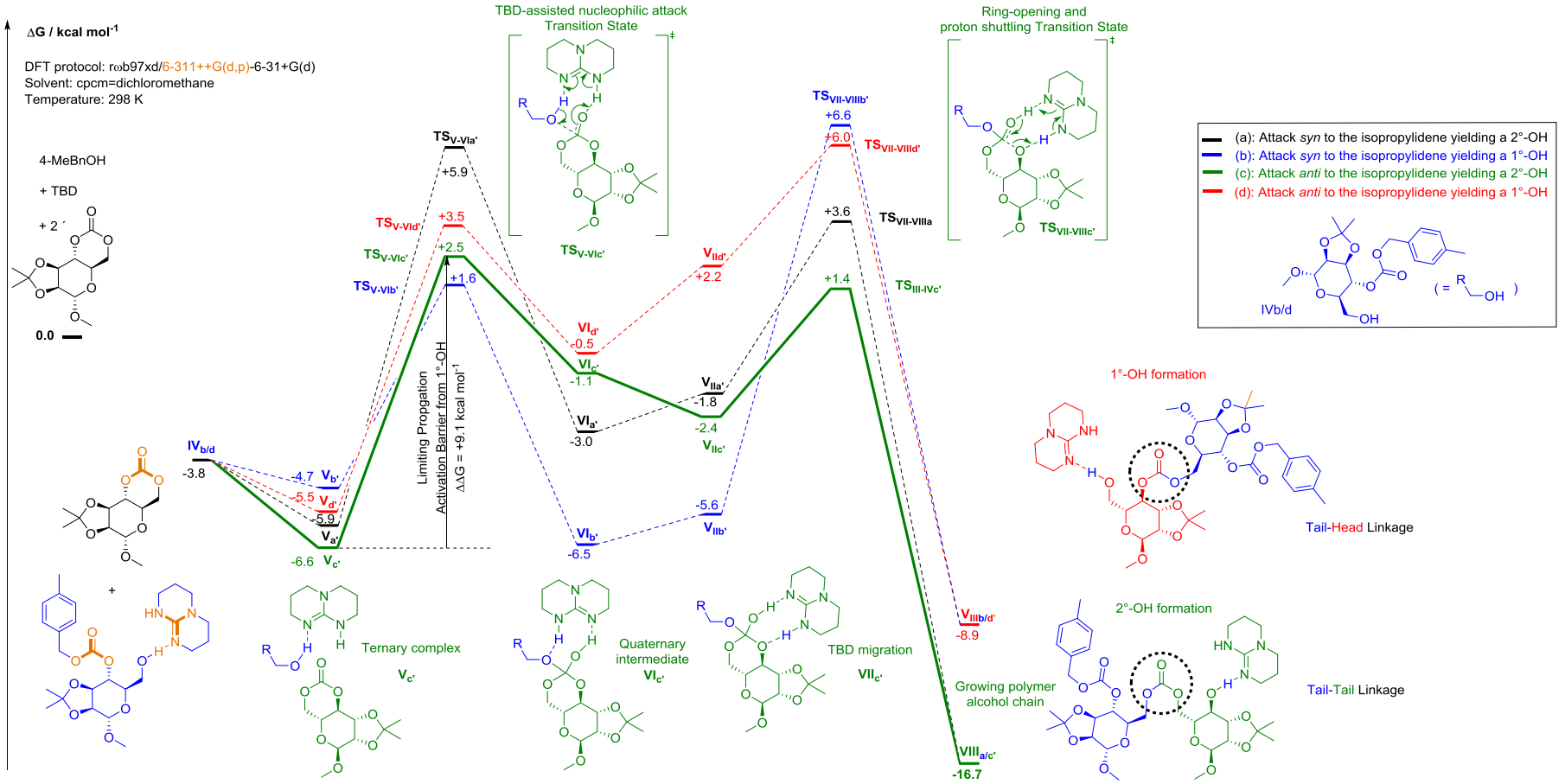

Figure 3.16. Calculated Gibbs free energy profile for the propagation step in the ROP of **3**, catalysed by TBD and initiated by the primary alcohol of the ring-opened monomer. Attack of the alcohol at the carbonyl carbon on the same face (*syn*-, profiles **a** and **b**) and the opposite face (*anti*-, profiles **c** and **d**) to the isopropylidene protecting group are shown and to yield a tail-head (1°-OH formation, profiles **b** and **d**) or tail-tail (2°-OH formation, profiles **a** and **c**). The higher basis set of 6-311++G(d,p) was applied to the carbonate of the monomer and ring-opened form as well as the guanidine of TBD and are highlighted in orange in the starting materials. 4-MeBnOH, TBD and 2 molecules of monomer were taken as the reference point (0.0 kcal mol^{-1}). The most favourable calculated energy profile (bold, green) correlates to attack *anti* to the protecting group to expose a secondary alcohol group.

3.6. Polycarbonate Properties

Differential scanning calorimetry (DSC) of the mannose-based polycarbonates revealed high glass-transition temperatures; for a polymer of M_n 13 600 g mol^{-1} (Đ 1.17), a T_g of ~152 °C was measured from the second heating and cooling cycle (Figure 3.17). For consistency, the T_g was always measured from the cooling curve and most likely represents a slight underestimate owing to the early onset of thermal degradation (Figure 3.18). Other unassigned features observed in the DSC trace were attributed to the slow rate of heating (1 K min^{-1}) and high sensitivity of the micro-DSC instrument.

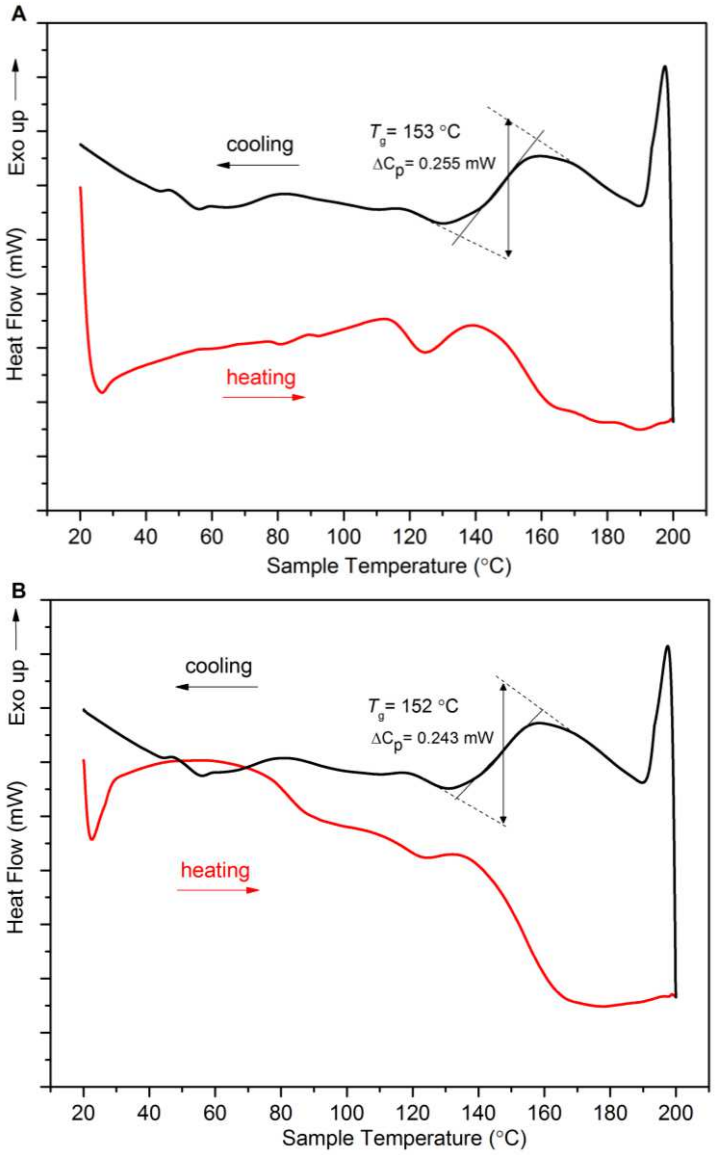

Figure 3.17. MicroDSC traces of mannose-based polycarbonate (M_n = 13 600 g mol^{-1}, Đ 1.17) showing (**A**) the first and (**B**) the second heating and cooling cycles. The sample (under argon) was heated and cooled between 20 and 200 °C at a rate of 1 K min^{-1}. The second heating cycle was carried out immediately following the first and the T_g measured at half height from the cooling curve of the second cycle.

For comparison, the tri-methoxy protected D-glucose and 2,3-*O*-isopropylidene protected D-xylose based polycarbonates (of similar M_n) had reported T_g values of 122 °C (M_n= 14 700 g mol^{-1}, Đ 1.15)[2] and 128 °C (M_n= 13 200 g mol^{-1}, Đ 1.69),[1] respectively. The elevated T_g in poly(**3**) was attributed to restricted rotation about the polymer chain imposed by the combined isopropylidene protecting group and mannopyranose sugar ring. Unlike the xylose-based polycarbonates, which showed semi-crystalline behaviour the mannose-based polycarbonates were amorphous in character, showing no signs of crystallinity by powder X-ray diffraction (Appendix, Figure A1). DSC measurements carried out in the absence of an argon atmosphere resulted in a brown residue after the first heating to 200 °C and showed a markedly different cooling curve.

Thermogravimetric analysis (TGA) of the polymer revealed a low onset of thermal degradation at around 170 °C, reaching a maximum degradation rate at ~259 °C. Almost complete mass loss (98%) was observed by 350 °C (Figure 3.18). This is attractive for applications requiring thermally degradable polymers but the closeness between the T_g and onset of degradation may limit the window for polymer processing.

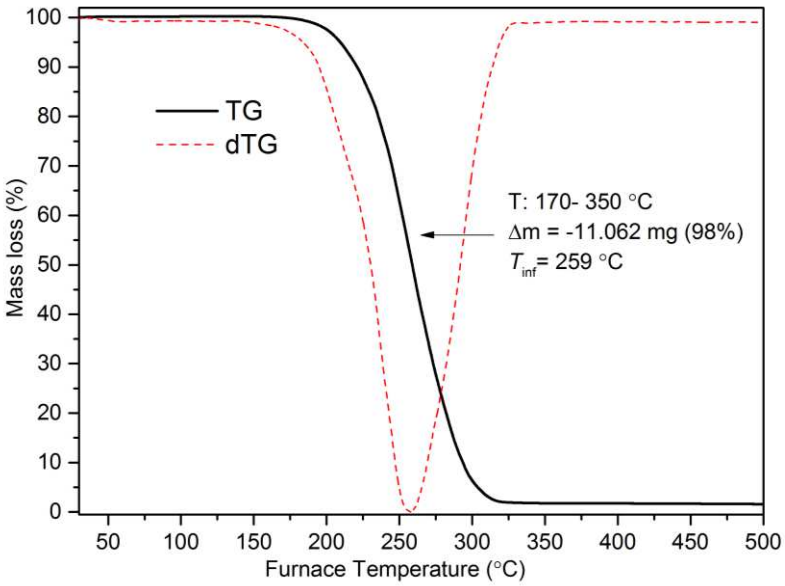

Figure 3.18. TG curve and first derivative of TG (dTG) measured for a polymer ($M_{n,SEC}$ 13 600 g mol^{-1}, Đ 1.17, Table 3.01, Entry 3) heated from 30 to 500 °C under argon at 2 K min^{-1}. The onset of thermal degradation (T_{on}) occurred at ~170 °C, reaching a maximum rate of mass loss (T_{inf}) at 259 °C (measured at half height) and resulted in an overall mass loss of 98% by 350 °C.

Analysis of the gases evolved during thermal degradation by tandem mass spectrometry detected major ions at *m/z* 44 and 58 attributed to the loss of CO_2^+ and $(CH_3)_2CO^+$, respectively (Figure 3.19). The latter arises from loss of the protecting group.

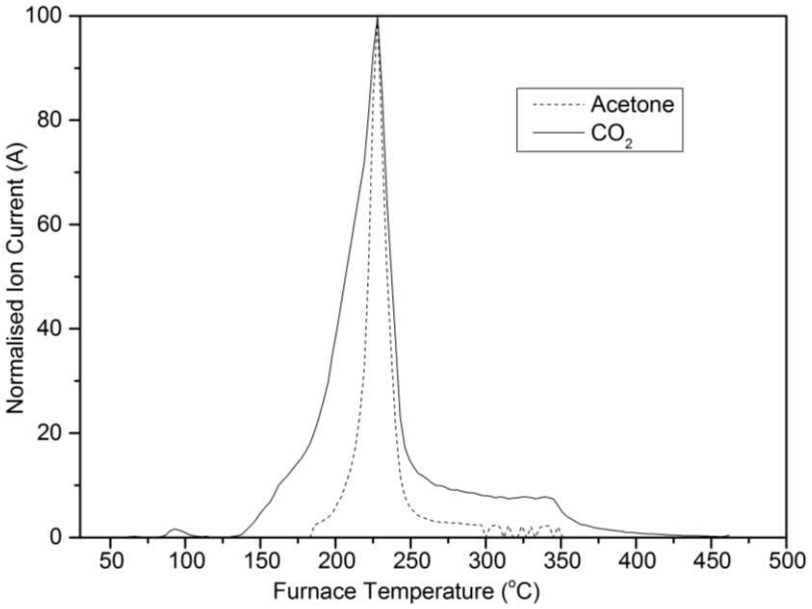

Figure 3.19. Tandem mass spectrometry of the gases evolved during TGA of the polymer (M_n 13 600 g mol^{-1}). The major ions detected at *m/z* 58 and 44 were assigned to loss of acetone and CO_2, respectively. Plotted as a function of furnace temperature, the peak in both ions occurs around 240 °C and coincides with the TGA profile.

3.7. Post-Polymerisation Deprotection of the Pendent Ketal Group

Deprotection of the pendent ketal groups to expose the vicinal diol was investigated by treatment of the polymer with an 80:20 *v/v* trifluoroacetic acid (TFA): H_2O mixture (Scheme 3.06).[10]

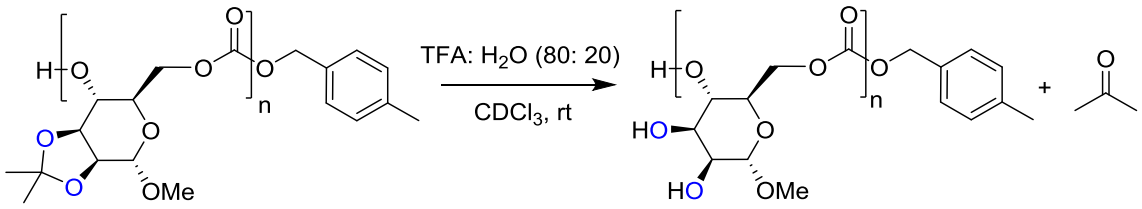

Scheme 3.06. Deprotection of the ketal group along the polycarbonate backbone with CF_3COOH: H_2O to eliminate acetone and expose free hydroxyl groups for functionalisation and modification of the polymer properties.

For a solution of the polymer (M_n 9330 g mol^{-1}, Đ 1.15) in $CDCl_3$, loss of the *i*-Pr proton environments and evolution of acetone was monitored by ^{1}H NMR spectroscopy, relative to the -OMe signals (Figure 3.20). After 12 hours at room temperature, 8% of the mannose repeat units were estimated to have been deprotected and analysis by SEC after 17% removal was observed indicated minimal hydrolysis of the carbonate linkages (M_n 9290 g mol^{-1}, Đ 1.15).

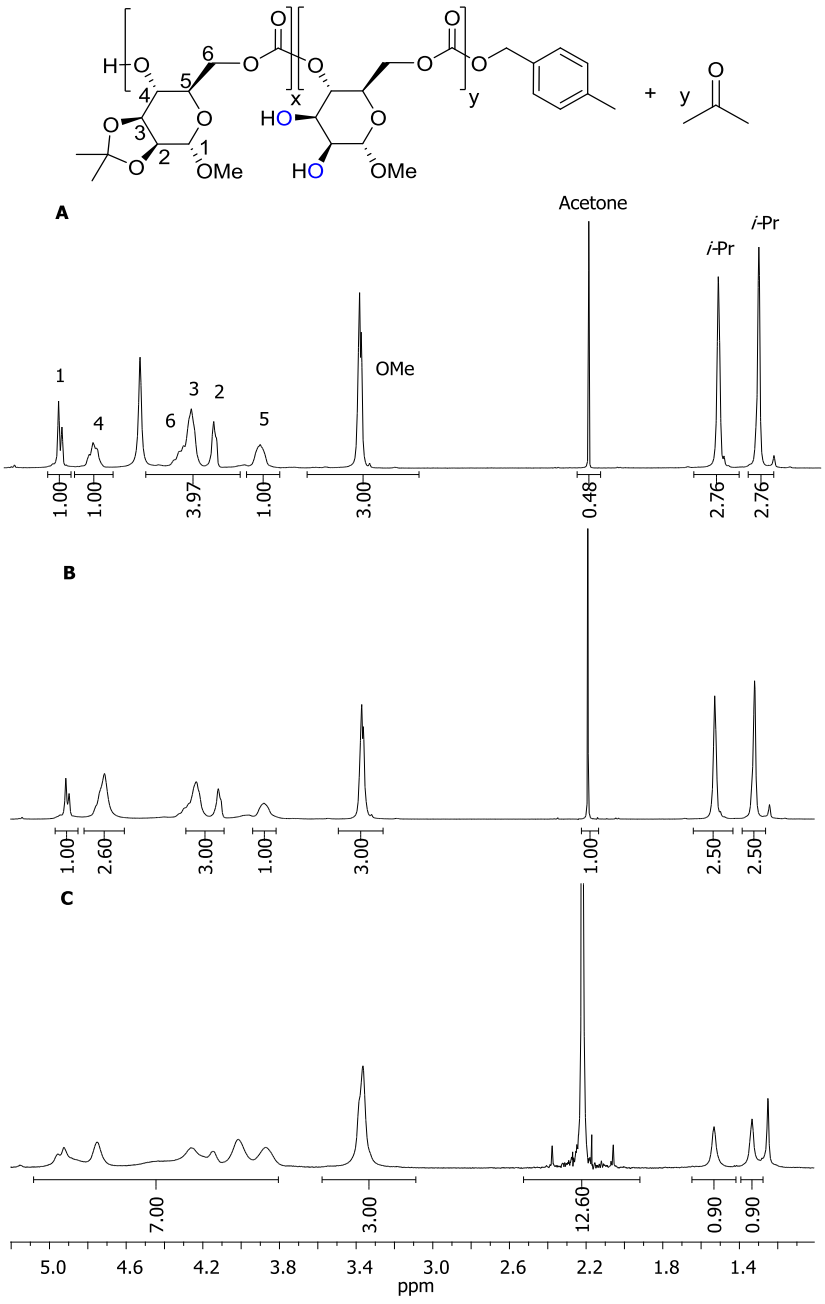

Figure 3.20. ^{1}H NMR spectra (400 MHz, $CDCl_3$) of polymer ($M_{n,SEC}$ 9330 g mol^{-1}, 1.15 Đ) treated with 80:20 CF_3COOH: H_2O showing (**A**) 8% removal of the ketal protecting group after 12 hours and associated acetone formation, (**B**) 17% removal after 24 hours ($M_{n,SEC}$ 9290 g mol^{-1}, Đ 1.15) and (**C**) 70% removal after 48 hours ($M_{n,SEC}$ 4370 g mol^{-1}, Đ 1.13). Further removal rendered the material insoluble in $CDCl_3$ and THF for analysis.

Overall, removal of 70% of the ketal groups was achieved whilst maintaining sufficient solubility in $CDCl_3$ for analysis (Figure 3.20C). SEC confirmed the soluble material to still be polymeric but with less than half the M_n (4370 g mol^{-1}, Đ 1.13), indicating cleavage of the polycarbonate backbone. Further deprotection yielded a material insoluble in $CDCl_3$, THF, D_2O and hexafluoroisopropanol. The fully-protected polycarbonates were also insoluble in water.

3.8. Conclusions and Further Work

In conclusion, the strategy for cyclic carbonate formation using CO_2 carbonylating agent with DBU reagent and tosyl leaving group (Chapter 2) has been successfully applied to the synthesis of a novel monomer from natural sugar, D-mannose. Following isopropylidene protection of the 1,2-diol in commercially available *O*-methyl-α-D-mannopyranoside, CO_2 insertion at 1 atm pressure occurred predominantly into the primary hydroxyl group. Under conditions of high dilution (0.1 mol L^{-1}) and on addition of tosyl chloride and triethylamine, *in situ* intramolecular cyclisation gave the six-membered *trans*-configured cyclic carbonate in a reasonable 57% yield (Figure 3.21).

The controlled ROP was demonstrated with 4-methylbenzyl alcohol initiator and TBD catalyst, to achieve high monomer conversions (>99%) and D-mannose derived polycarbonates with M_n up to 33 400 g mol^{-1} (Đ 1.19). NMR analysis supported by DFT calculations suggested a preference for unsymmetrical ring-opening to expose a secondary hydroxyl group for chain propagation and thus formation of regioregular APCs with predominantly head-tail linkages. The polycarbonates exhibited high glass transition temperatures (T_g~ 152 °C) and a low onset of thermal degradation (T_{on}~ 170 °C).

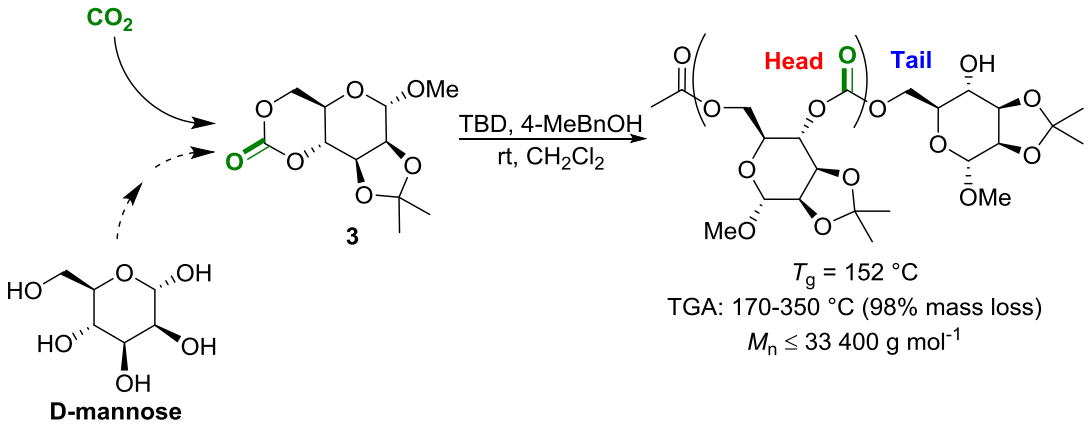

Figure 3.21. Synthesis of cyclic carbonate monomer **3** from D-mannose and CO_2. ROP with TBD organocatalyst and alcohol initiator yielded mannose-based APCs showing a preference for head-tail linkages.

Further to the use of TBD organocatalyst for the ROP of **3**, metal-based catalysts should also be investigated for achieving higher molecular weight polymers. Coordination of the chain end to a metal centre in a coordination-insertion ROP mechanism may reduce the backbiting reactions, which led to chain terminated macrocycles.

Further work is also required to optimise the post-polymerisation removal of the ketal protecting groups whilst minimising hydrolysis of the carbonate linkages to attain a greater percentage of mannose repeat units with free hydroxy groups. Spiro- 1,2-alkylidene protecting groups, such as that shown for mannose in **I** in Figure 3.22 are reported to undergo hydrolysis faster ($t_{1/2}$ = 8 hours for α-glucofuranose systems) compared to 1,2-*O*-isopropyliene groups ($t_{1/2}$ = 20 hours). This may allow for faster deprotection whilst causing less cleavage of the carbonate linkages.

There is also plenty of scope to introduce functionality through the choice of 2,3-protecting group itself. For example, attempts to form polymer thin films using a thermal press or solvent evaporation techniques revealed the highly brittle nature of the materials. The introduction of long alkyl chains as in **II** in Figure 3.22 could act as internal plasticisers, improving the polymer processing characteristics. Moreover, preliminary cell attachment studies (carried out by Bethan Charles, MRes, 2016) were promising, indicating good *in vitro* biocompatibility with cancer cell line MG-63. However, the introduction of functional groups that could render the films cationic, such as amines (**III** in Figure 3.22) may further enhance the cell attachment properties for tissue engineering scaffolds. Significantly increased cell attachment and spreading was reported by Sharma and coworkers[11] for bacterial cellulose films functionalised with quaternary ammonium groups compared to oxidised (anionic) and unfunctionalised cellulose.

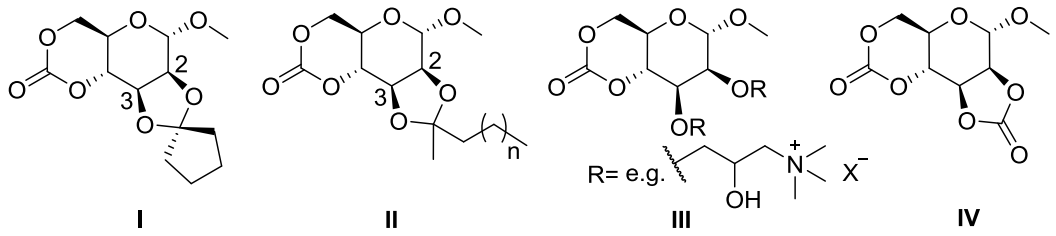

Figure 3.22. Mannose-based monomer targets. **I**: faster post-polymerisation removal of the 2,3-protecting group with less hydrolysis of the carbonate linkages; **II**: alkyl chain to act as an internal plasticiser improving the material properties; **III**: introduction of quaternary ammonium groups for tissue engineering scaffolds and **IV**: incorporation of more CO_2 to protect the 2,3-position.

The 1,2-diol could also be protected as the five-membered cyclic carbonate (**IV** in Figure 3.22) and moreover, the method utilising CO_2 used to carry out a "one-pot" dicarbonylation. ROP of the six-membered cyclic carbonate would be anticipated to occur selectively and

under mild reaction conditions in the presence of the more stable five-membered ring. Ring-opening of the latter could then be achieved under harsher reaction conditions or with amines to form polyether or polyurethane cross-linkages, respectively. Preliminary experiments using two equivalents of each of DBU, TsCl and triethylamine indicated the formation of a mixture of cyclic carbonate products. In the $^{13}C\{^{1}H\}$ NMR spectrum, carbonate environments typically of both five-membered (153 ppm) and six-membered cyclic carbonates (146 ppm) were observed. Under these conditions, known five-membered cyclic carbonate,[12] cyclic 2,3-*O*-carbonate-α-D-mannopyranoside with the 4,6-diol exposed, was isolated and characterised.

Finally, recent publications highlight the rapidly growing area of functionalised sugar-based polycarbonates. Following the completion of this work, Wooley an coworkers[13] built upon their D-glucose derived cyclic carbonate by further derivatising the 2- and 3- positions (Figure 3.23). The monomers containing ethyl carbonate groups and one bearing an additional alkyne functionality were prepared in 3 or 4 steps from commercially available methyl-4,6-*O*-benzylidene-α-D-glucopyranoside; the final cyclocarbonation was achieved using triphosgene in the presence of pyridine in yields of 51 and 56%, respectively. Sequential organocatalytic ROP of the two monomers and post-polymerisation modification *via* click chemistry of the segment containing the pendent alkyne groups afforded non-ionic, cationic, and anionic diblock copolymers. The well-defined (Đ< 1.1) amphiphilic copolymers underwent self-assembly into micelles and showed the same preference for head-tail regioselectivity in the polycarbonate backbone as reported for the D-mannose derived polycarbonates described in this chapter.

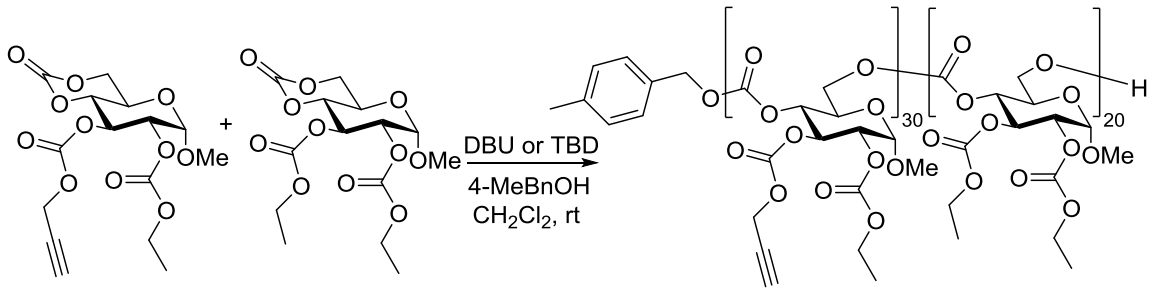

Figure 3.23. Functionalised D-glucose derived diblock copolycarbonates reported in 2017 by Wooley and coworkers.[13]

In 2017, Pati *et al.*[14] reported the D-glucose derived cyclic carbonate with triethylene glycol monomethyl ether groups (TEGM) at the 2- and 3- positions (Figure 3.24). Moreover, they did not resort to phosgene or its derivatives in the synthesis of the monomers with either

methyl or TEGM groups. From the bromoalcohol, cyclisation was achieved using CO_2 (10 bar) as the carbonylating agent with DBU reagent, albeit in DMF solvent to give yields of 40%. Diblock copolymers prepared by sequential copolymerisation of the hydrophobic *O*-methyl protected and hydrophilic *O*-TEGM functionalised monomers afforded amphiphilic linear and macrocyclic copolycarbonates, which showed self-assembly properties in water. Using TBD organocatalyst with 4-methylbenzyl alcohol initiator, linear homo- and copolymers were prepared whereas with DBU and thiourea (TU), macrocyclic polycarbonates were observed.

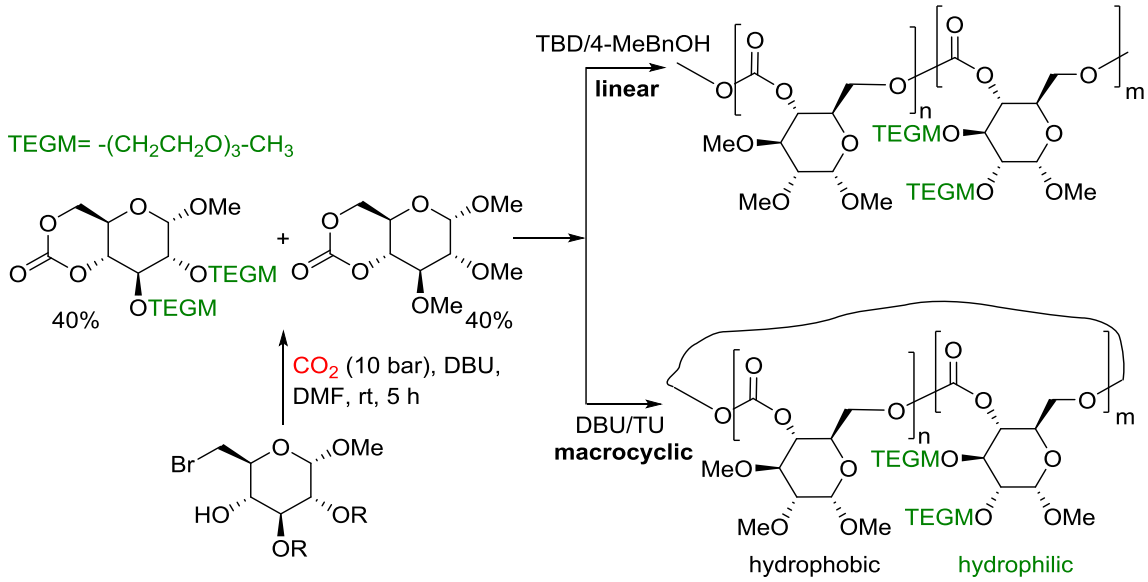

Figure 3.24. Organocatalytic ROP of D-glucose derived monomers to form amphiphilic diblock copolymers, reported by Pati *et al.*[14]

3.9. References

1. Y. Shen, X. Chen and R. A. Gross, *Macromolecules*, 1999, **32**, 2799-2802.
2. K. Mikami, A. T. Lonnecker, T. P. Gustafson, N. F. Zinnel, P. J. Pai, D. H. Russell and K. L. Wooley, *J. Am. Chem. Soc.*, 2013, **135**, 6826-6829.
3. D. Trimnell, W. M. Doane, C. R. Russell and C. E. Rist, *Carbohyd. Res.*, 1970, **13**, 301-305.
4. T. P. Gustafson, A. T. Lonnecker, G. S. Heo, S. Zhang, A. P. Dove and K. L. Wooley, *Biomacromolecules*, 2013, **14**, 3346-3353.
5. M. E. Evans and F. W. Parrish, *Carbohyd. Res.*, 1977, **54**, 105-114.
6. M. S. Chowdhary, R. K. Jain, S. S. Rana and K. L. Matta, *Carbohyd. Res.*, 1986, **152**, 323-328.
7. L. J. Farrugia, *J. Appl. Cryst.*, 2012, **45**, 849-854.
8. S. Sopeña, V. Laserna, W. Guo, E. Martin, E. C. Escudero-Adán and A. W. Kleij, *Adv. Synth. Catal.*, 2016, **358**, 2172-2178.
9. S. Venkataraman, V. W. L. Ng, D. J. Coady, H. W. Horn, G. O. Jones, T. S. Fung, H. Sardon, R. M. Waymouth, J. L. Hedrick and Y. Y. Yang, *J. Am. Chem. Soc.*, 2015, **137**, 13851-13860.
10. X. Chen and R. A. Gross, *Macromolecules*, 1999, **32**, 308-314.
11. J. C. Courtenay, M. A. Johns, F. Galembeck, C. Deneke, E. M. Lanzoni, C. A. Costa, J. L. Scott and R. I. Sharma, *Cellulose*, 2016, **24**, 253-267.
12. *Int. Pat.*, WO2016166682A1, 2016.
13. L. Su, S. Khan, J. Fan, Y.-N. Lin, H. Wang, T. P. Gustafson, F. Zhang and K. L. Wooley, *Polym. Chem.*, 2017, **8**, 1699-1707.
14. D. Pati, X. Feng, N. Hadjichristidis and Y. Gnanou, *Macromolecules*, 2017, **50**, 1362-1370.

Chapter 4

CO_2-Driven Stereochemical Inversion to Create Thymidine-Based Cyclic Carbonates for Ring-Opening Polymerisation

4. CO_2-Driven Stereochemical Inversion to Create Thymidine-Based Cyclic Carbonates for Ring-Opening Polymerisation

4.1. Introduction

4.1.1. Synthetic DNA analogues

The sugar components of DNA, 2'-deoxyribonucleosides are attractive and versatile building blocks owing to the hydrogen bonding interactions between complementary base pairs and scope for functionalisation *via* the nucleobase nitrogen atoms (Figure 4.01). As such, they have emerged as powerful tools in several fields.[1-8]

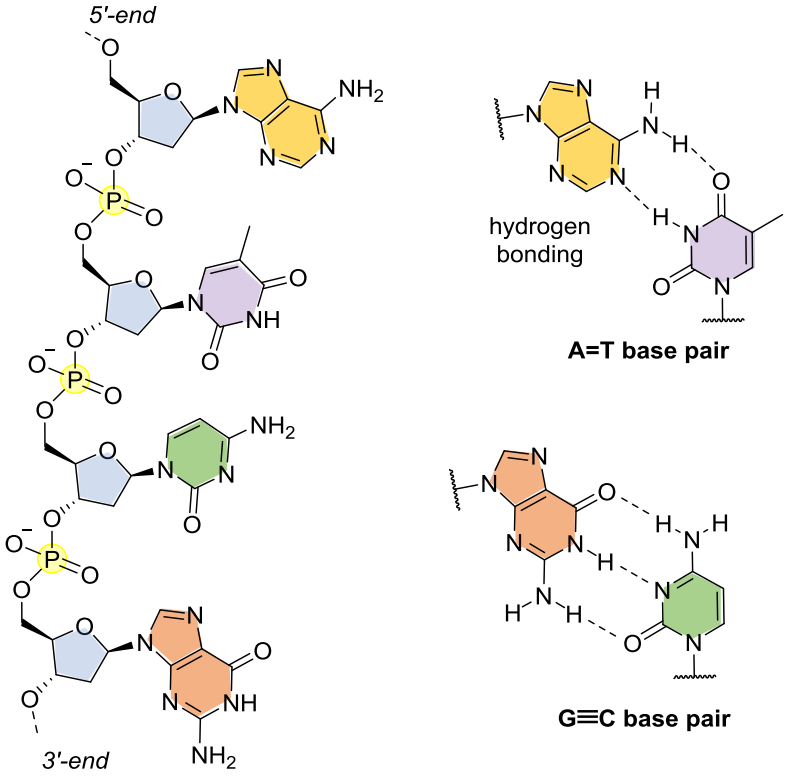

Figure 4.01. Sugar-phosphate backbone in DNA showing nucleobases (from the top): adenine (A), thymine (T), cytosine (C) and guanine (G). Watson-Crick base pairing between purine and pyrimidine nucleobases.

For example, in molecular recognition and diagnostics, nanoparticles imprinted with 2'- deoxyuridine were prepared for the detection of the complementary 2'- deoxyadenine nucleoside, a potential marker of several diseases.[5] The central role played by nucleosides and nucleotides in many cellular processes has led to a continual drive towards the development of chemically modified analogues, both for drug discovery and fundamental biological understanding.[9] A recent review by Seth and Wan[10] summaries the progress in

oligonucleotide-based therapeutics through modification of the backbone, sugar or nucleobase components. To address challenges in polymer synthesis, macromolecules bearing nucleobases have also been used for templated polymerisations, where the chain length and polydispersity of the parent template strand are copied to the daughter conjugate polymer.[6] The hydrogen-bonding capabilities can also impart self-assembly characteristics,[2, 4] leading to well-defined supramolecular architectures including mimicking the helical structure of double-stranded DNA.[11] Finally, the metal coordination chemistry of pyrimidine nucleobases such as thymine (T) offers the potential for unique polymer applications in metal detection and toxic metal removal (Figure 4.02).[12, 13]

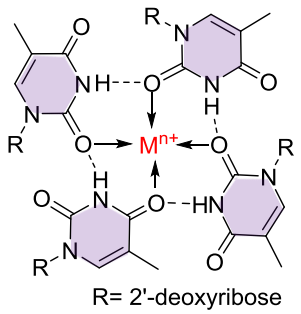

Figure 4.02. Metal coordination chemistry of the thymine nucleobase (*e.g.* M= Hg^{2+}, Cu^{2+}). Modified from Lippert and Sanz.[13]

Subsequently, extensive research has gone into the integration of nucleobases into the backbone of synthetic polymers[14] or as pendent or terminal groups,[15] either through direct polymerisation[16] or post-synthetic modification.[2, 7, 17-21] To date, there are several examples of DNA analogues, albeit mainly oligomers of 2'-deoxyribonucleosides, bearing carbonate,[22, 23] carbamate,[24] ester,[25] triazole,[11] ether [26] and silyl ether linkages.[27] The majority of these were prepared by condensation reactions except for the triazole-linked DNA analogue, which used click chemistry in a stepwise solid-phase synthesis to achieve 10 thymidine repeat units.

4.1.2. Cyclic carbonates from 2'-deoxyribonucleosides

The lack of reports on the synthesis of DNA-based polycarbonates by the ring-opening polymerisation (ROP) of 2'-deoxyribonucleoside-derived cyclic carbonates can be attributed to challenges in the cyclocarbonation of the *trans*-configured 1,3-diol of the five-membered furanose ring. Early work by Tittensor and Mellish[28] reported the attempted synthesis of the 3',5'- cyclic carbonate of thymidine *via* the trichloroethoxy- activated ester (Scheme 4.01).

They postulated the need for the carbonyl component at the 3'-position rather than 5'- hydroxyl group for cyclisation to occur and provided evidence for a 1:1 mixture of ethanol ring-opened cyclic carbonate suggesting a transient existence of the monomer.

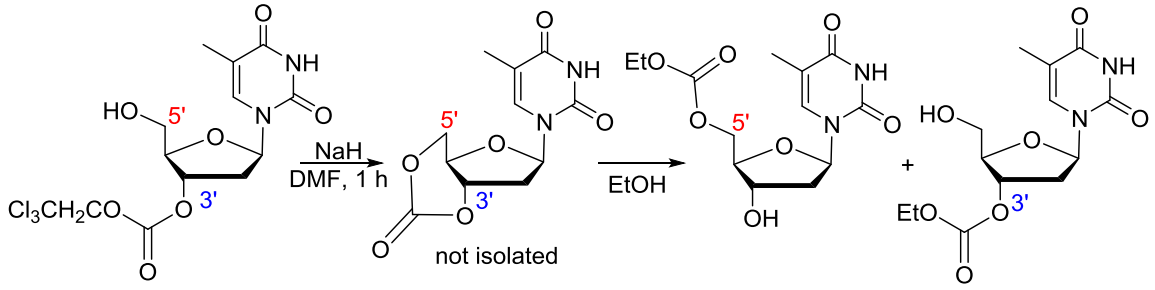

Scheme 4.01. Attempted synthesis of the *trans*-3',5'-cyclic carbonate of thymidine from the 3'-trichloroethoxy activated ester. A mixture of ethanol ring-opened products was isolated.

Subsequently in 2011, Suzuki *et al.*[23] used protecting group chemistry to selectively place a carbonyldimidazole (CDI) component at the 3'-position of thymidine and adenosine nucleosides (Scheme 4.02). However, on deprotection of the 5'-silyl protecting group, with a fluoride anion source, only polycondensation resulted leading to thymidine-based polycarbonates of low M_n (1700- 4700 g mol^{-1}, Đ 1.40-2.37). Unexpectedly, the polycondensates were not regioregular but showed the presence of 5'-5' and 3'-3'carbonate linkages in addition to the anticipated 3'-5' regiochemistry. This suggested that the alkoxide anion attacked the carbonate linkage of the polymer main chain as well as the carbonylimidazolide. For *N*-unprotected 2'-deoxyadenosine, undesired side reactions between the carbonylimidazolide and the amino group of the adenine nucleobase lead to carbamate linkages. Dynamic protection through complementary hydrogen bonding with the thymine nucleobase greatly reduced carbamate formation but still only gave oligomers (M_n 1000-1500 g mol^{-1}).

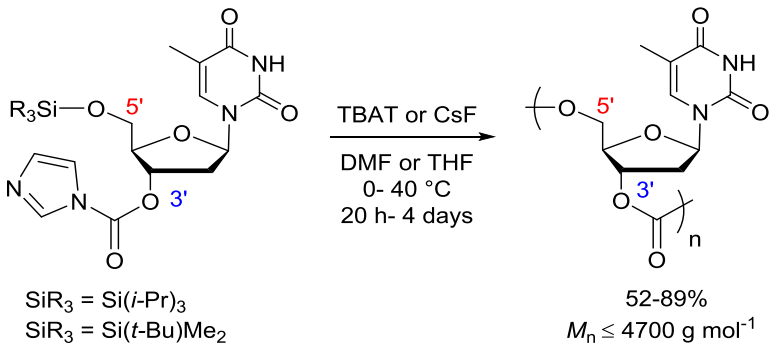

Scheme 4.02. Synthesis of low M_n thymidine-based polycarbonates by polycondensation on deprotection of the silyl group with a fluoride anion source. TBAT: $(n\text{-Bu})_4NPh_3SiF_2$.

4.2. Monomer Synthesis

4.2.1. Trans-3',5'-cyclic carbonate of thymidine

As expected given the literature attempts with activated esters, synthesis of the *trans*-3',5'-cyclic carbonate of thymidine was also unsuccessful by the nucleophilic addition-elimination method, developed in Chapter 2 and successfully applied to the D- mannopyranose sugar diol in Chapter 3 (Figure 4.03). This involved 1,8-diazabicyclo-[5.4.0]undece-7-ene (DBU)-facilitated CO_2 insertion coupled to a leaving group strategy at the carbonate. Firstly, solubility of the 2'-deoxynucleoside in solvents other than water and alcohols, which are not compatible with the DBU-aided CO_2 insertion step, proved problematic. Nevertheless, attempts in pyridine solvent and with 3-*N*-methyl thymidine, leading to improved solubility, were unsuccessful for cyclic carbonate formation. In both cases, CO_2 insertion was observed but following addition of the tosyl leaving group, only dimers and trimers were identified by mass spectrometry. For 3-*N*-methyl thymidine, the CO_2 insertion products were insoluble in the THF and acetonitrile solvents in which the diol was soluble and the reverse was found in $CHCl_3$ and CH_2Cl_2.

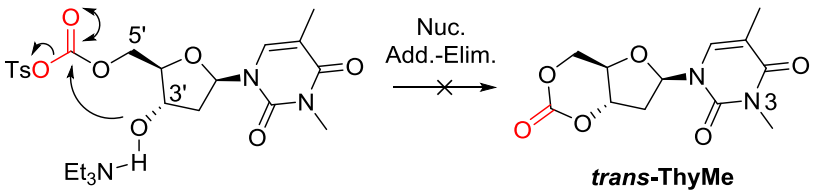

Figure 4.03. Attempted Synthesis of the 3',5'-*trans*-cyclic carbonate of thymidine by tosylation of the DBU-inserted carbonate and intramolecular cyclisation *via* a nucleophilic addition-elimination pathway.

DFT calculations at the rωb97xd/6-31+G(d)/cpcm=acetonitrile/298 K level of theory, suggested that both the ring-closing kinetics ($\Delta\Delta G^{\ddagger}$= +13.3 kcal mol^{-1}) and thermodynamic driving force ($\Delta\Delta G$= -20.8 kcal mol^{-1}) for cyclic carbonate synthesis *via* this pathway, should be accessible at ambient reaction conditions (Figure 4.04). Importantly, this was regardless of whether the carbonyl was at the 3'- or 5'- position, as CO_2 insertion occurs predominantly into the sterically less hindered primary 5'-position. The analogous parameters were also calculated for the reported *trans*-4,6-cyclic carbonate monomers derived from D-glucose and D-mannose.

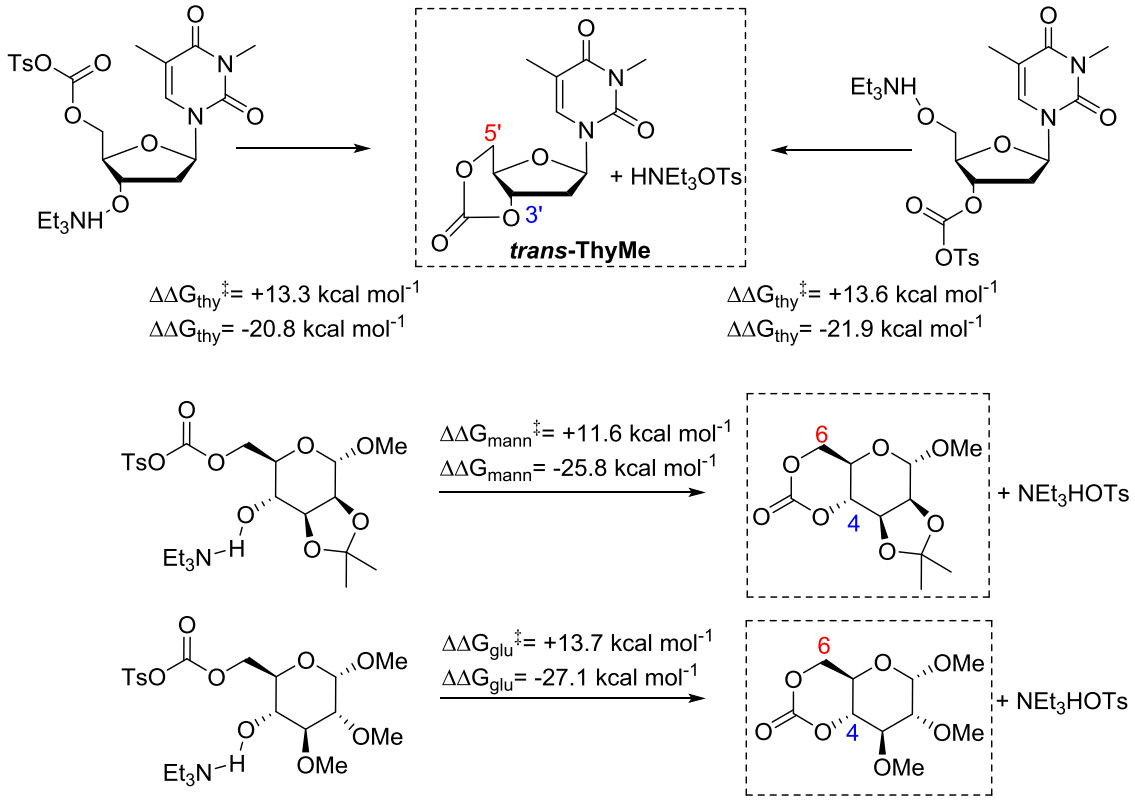

Figure 4.04. Comparison of the ring-closing kinetics (ΔΔG‡) and thermodynamics (ΔΔG) for the un-isolated *trans*-3',5'-cyclic carbonate of 3-*N*-methyl thymidine and the reported *trans*-4,6-cyclic carbonates derived from D-mannose and D-glucose calculated at the rωb97xd/6-31+G(d)/cpcm=acetonitrile/298 K level of theory.

The comparable ring-closing kinetics and thermodynamics for cyclocarbonation of the *trans*-1,3-diols in thymidine, glucose and mannose-based sugars led to a consideration of the cyclic carbonate ring-strain to provide insight into why synthesis of the thymidine monomer proved more challenging. The ring-strain was evaluated by calculating both the overall thermodynamics of ring-opening with primary and secondary alcohols (namely methanol and *iso*-propanol) as well as the enthalpy of the isodesmic reaction with dimethyl carbonate (DMC) (Figure 4.05). As the latter involves breaking and forming the same number and type of bonds, it is considered a more accurate evaluation of reaction thermodynamics though, the former is also commonly reported. Calculations were carried out at the rωb97xd/6-311++G(2d,p)/cpcm=dichloromethane/298 K level of theory for the hypothetical *trans*-configured cyclic carbonate of 3-*N*-methyl thymidine (***trans*-ThyMe**) as well as, for comparison, the analogous *cis*-fused cyclic carbonate (***cis*-ThyMe**) and the realised glucose, mannose and xylose (IPXTC) derived monomers (Figures 4.06 and 4.07).

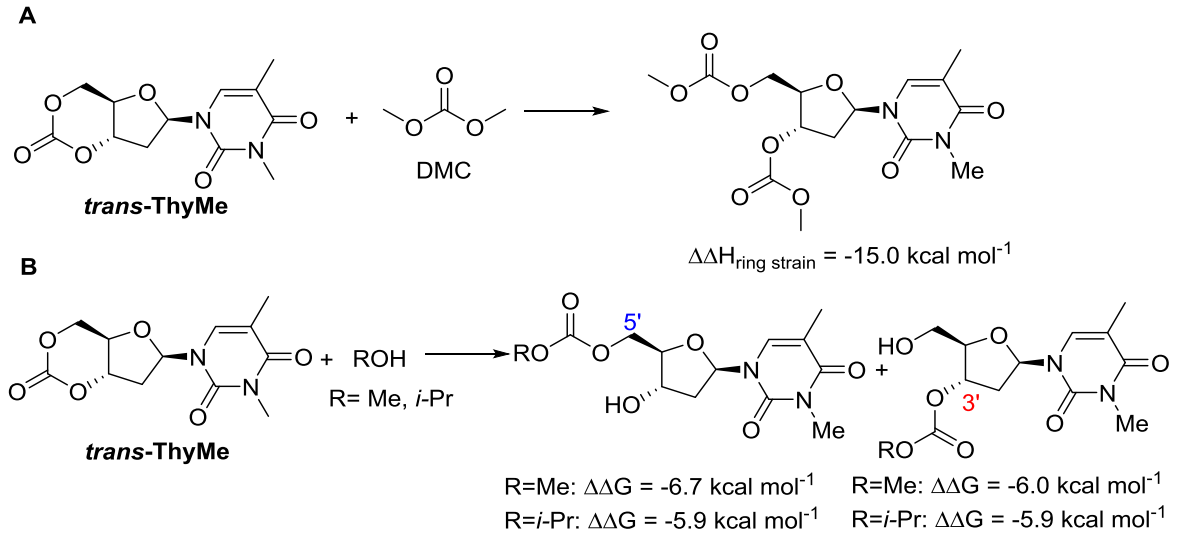

Figure 4.05. Ring strain calculations for ***trans*-ThyMe** carried out at the rωb97xd/6-311++G(2d, p)/cpcm=dichloromethane/298 K level of theory; **A:** Calculated enthalpy ($\Delta\Delta H_{ring\ strain}$) of the isodesmic ring-opening of the cyclic carbonate with dimethyl carbonate (DMC) and **B:** Calculated Gibbs free energy change (ΔΔG) on ring-opening of the cyclic carbonate with MeOH or *i*-PrOH.

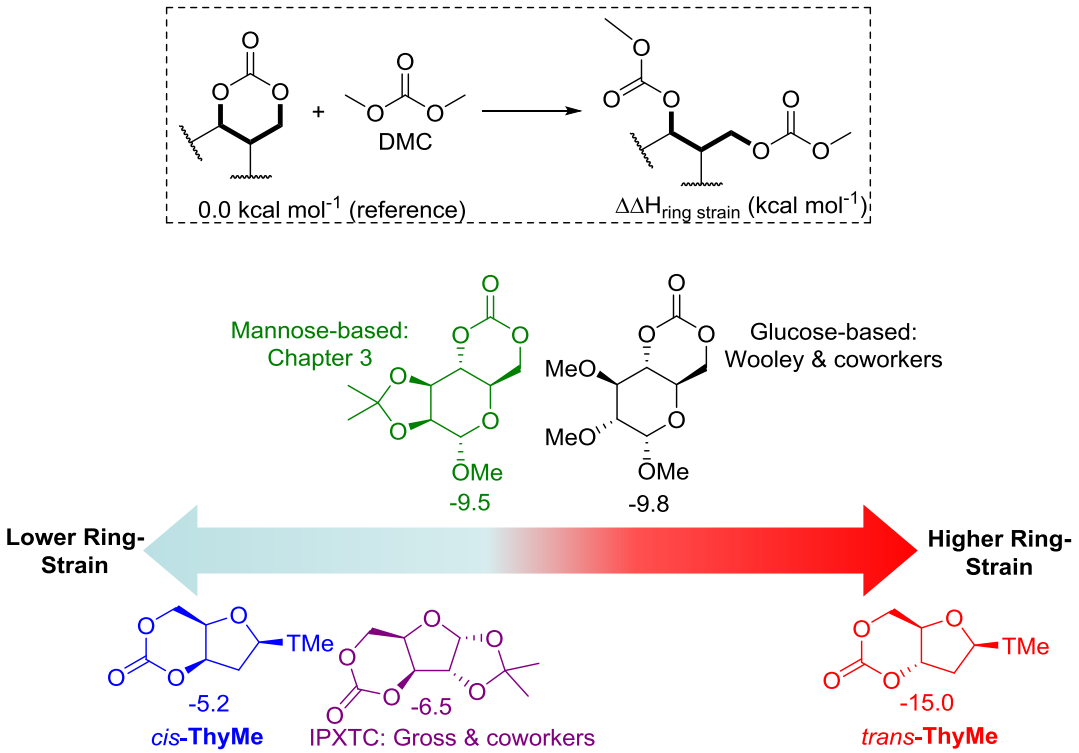

Figure 4.06. Calculated enthalpies ($\Delta\Delta H_{ring\ strain}$/ kcal mol^{-1}) for the isodesmic ring-opening reaction of sugar-derived cyclic carbonates with dimethyl carbonate (DMC) performed at the rωb97xd/6-311++G(2d,p)/cpcm=dichloromethane/298 K level of theory. The IPXTC monomer was reported by Gross and coworkers[29] and the protected D-glucose monomer by Wooley and coworkers.[30] Details of the synthesis of the mannose-based cyclic carbonate are given in Chapter 3.

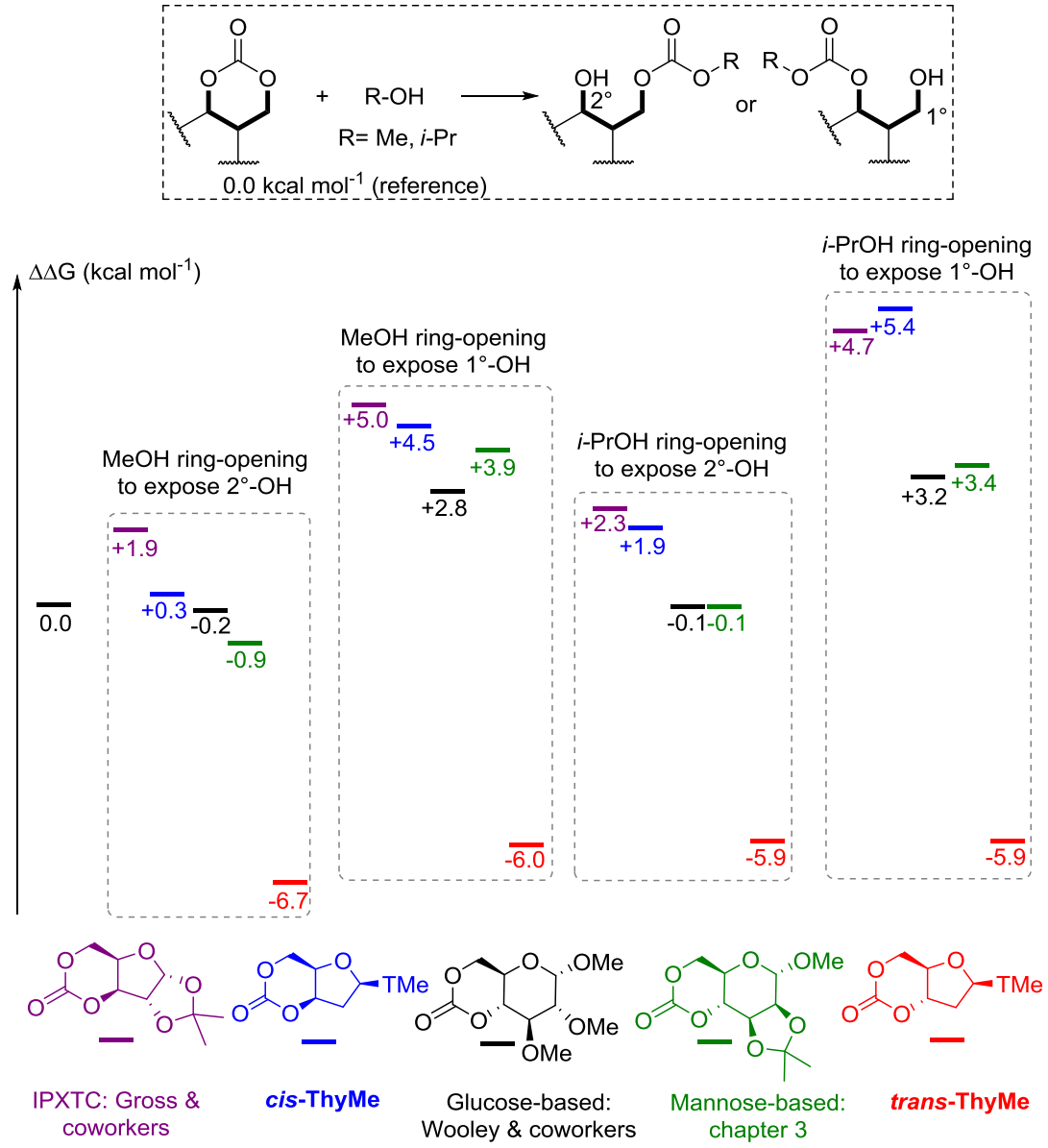

Figure 4.07. Calculated thermodynamics for ring-opening of sugar-based cyclic carbonates with MeOH and *i*-PrOH (ΔΔG/ kcal mol^{-1}) at the rωb97xd/6-311++G(2d,p)/cpcm=dichloromethane/298 K level of theory. The protected D-xylose based cyclic carbonate was prepared and polymerised by Gross and coworkers[29] and that from D-glucose by Wooley and coworkers.[30]

These calculations highlighted the more highly strained nature of the cyclic carbonate when *trans*-fused to the furanose ring in hypothetical ***trans*-ThyMe** compared to the six-membered pyranose sugar in synthesised D-mannose and D-glucose based monomers. For example, ring-opening with methanol (to expose a secondary hydroxyl group) was thermodynamically favourable by ΔΔG= -6.7 kcal mol^{-1} compared to -0.9 and -0.2 kcal mol^{-1} for mannose and glucose-derived monomers, respectively (Figure 4.07). The calculated enthalpy of ring-opening with dimethyl carbonate ($\Delta\Delta H_{ring\ strain}$) was also 5.5 kcal mol^{-1} more favourable for the *trans*-fused furanose monomer compared to the *trans*- configured D-mannopyranose

cyclic carbonate (Figure 4.06). The ability of the pyranose ring to adopt a chair conformation allows the *trans*-configuration of the cyclic carbonate to be accommodated compared to in the more conformationally restricted furanose sugar. ***Trans*-ThyMe** is most likely too highly strained to be isolated under these reaction conditions (especially, in the presence of alcohol).

It was demonstrated for 1,3-butanediol in Chapter 2, that ring-closing could also occur *via* a S_N2-type mechanism whereby, following tosylation of one of the alcohol groups, DBU-facilitated CO_2-insertion generated a carbonate nucleophile, leading to intramolecular cyclisation. For the thymidine diol, tosylation can occur at either the 5'- or 3'- hydroxyl groups. In the latter case, S_N2-like intramolecular displacement of the leaving group, with a 5'-carbonate nucleophile, would result in stereochemical inversion at the 3'-position yielding a *cis*-configured 3',5'- cyclic carbonate (Figure 4.08).

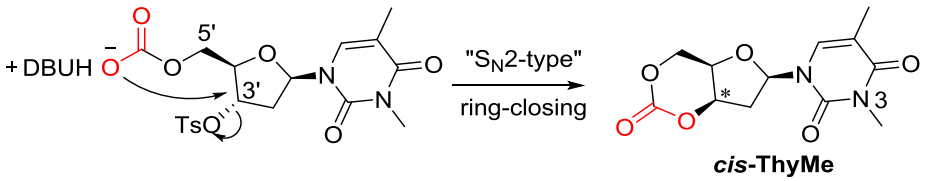

Figure 4.08. Ring-closing by an S_N2-type mechanism. Tosylation at the 3'-positon and intramolecular cyclisation with a CO_2-generated carbonate at the 5'-position would lead to stereochemical inversion and formation of ***cis*-ThyMe.**

As anticipated and following the literature procedure,[31] tosylation occurred selectively into the sterically less-hindered primary 5'-hydroxyl group (91% yield). Attempts to displace this leaving group with the 3'-carbonate, leading to the *trans*-configured cyclic product were unsuccessful. CO_2 insertion with DBU in $CDCl_3$ for the methylated derivative clearly showed the presence of a new resonance in the $^{13}C\{^1H\}$ NMR spectrum at 157 ppm consistent with formation of the DBUH carbonate salt. Heating to 40 and then 60 °C for 24 hours resulted in a loss of the CO_2 insertion resonance alongside the appearance of new tosyl environments, suggesting elimination. However, there was no evidence by mass spectrometry or NMR spectroscopy for formation of the cyclic product; only oligo-carbonate and -ether species from intermolecular reactions were detected. Similar observations were made for the reaction carried out in an autoclave at 60 °C and 8 bar CO_2 pressure.

Nevertheless, DFT calculations at the rωb97xd/6-31+G(d)/cpcm=acetonitrile/298 K level of theory supported more favourable cyclisation kinetics and thermodynamics for the S_N2-type ring-closing involving inversion of the natural stereochemistry in thymidine (Figure 4.09).

Compared to the formation of ***trans*-ThyMe**, the calculated thermodynamic driving force ($\Delta\Delta G$) was 13.0 kcal mol^{-1} greater and the kinetic barrier ($\Delta\Delta G^{\ddagger}$), 5.6 kcal mol^{-1} lower for formation of the analogous *cis*-configured 3',5'-cyclic carbonate (***cis*-ThyMe**).

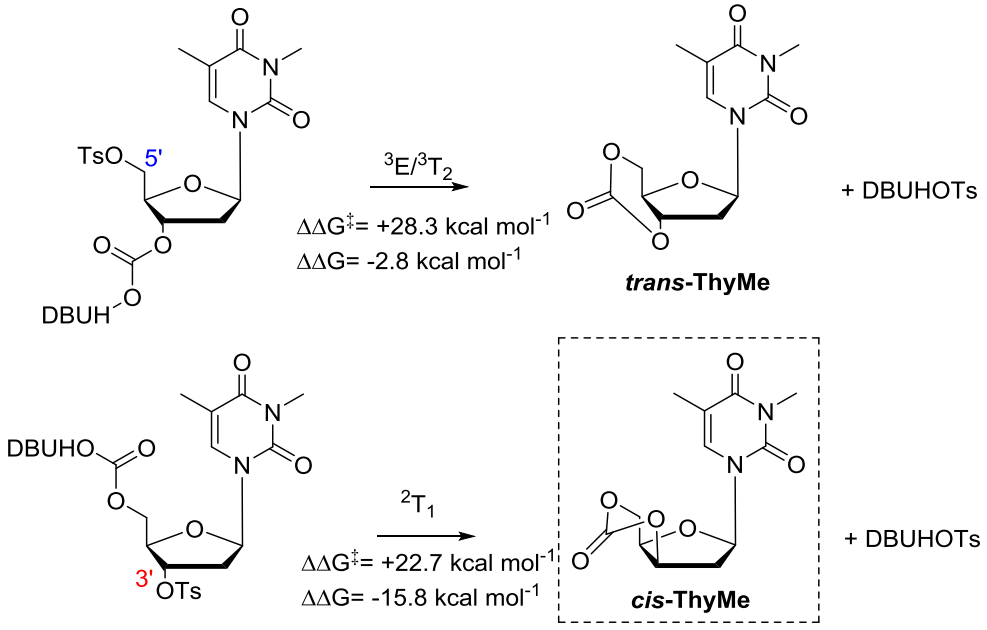

Figure 4.09. Calculated kinetics ($\Delta\Delta G^{\ddagger}$) and thermodynamics ($\Delta\Delta G$) at the rωb97xd/6-31+G(d)/cpcm=acetonitrile/298 K level of theory for ring-closing by intramolecular displacement of a tosyl leaving group with a carbonate nucleophile. $^2T_1$, $^3E/^3T_2$ refer to the twisted and envelope conformations of the furanose ring in the calculated transition states. Combined with the ring-strain calculations above, the favourable ring-closing kinetics and thermodynamics made ***cis*-ThyMe** a viable monomer target.

Moreover, ring strain calculations for ***cis*-ThyMe** (Figures 4.06 and 4.07) showed a comparable $\Delta\Delta H_{\text{ring strain}}$ and greater thermodynamic driving force for ring-opening with alcohols compared to the IPXTC monomer, successfully polymerised by Gross and coworkers.[29] This ROP potential combined with the feasibility of synthesis, meant that the *cis*-3,'5'-cyclic carbonate of thymidine became a viable monomer target.

4.2.2. Cis-3',5'-cyclic carbonate of thymidine

As shown in Scheme 4.03, selective tosylation of the 3'-hydroxyl position in thymidine was achieved in good yield by a sequential one-pot silylation followed by tosylation reaction. Subsequent deprotection of the 5'-silyl protecting group was carried out under mild reaction conditions with I_2 in methanol following the general procedure outlined by Vaino and Szarek.[32] This was a cheaper alternative to tetra-*n*-butylammonium fluoride (TBAF) or the use of fluoride on a polymer support. Less bulky, *tert*-butyl-dimethyl-silyl chloride

(TBDMSCl) was also used in preference to *tert*-butyl-diphenyl-silyl chloride as it was found to significantly reduce the deprotection reaction time from days to 2 hours. Unfortunately, protection of the 3-*N* position of the nucleobase was found to be necessary to avoid undesired side reactions during the cyclisation step and potentially during the ROP. Bases such as DBU are known to lead to the formation of 2,3'-anhydrothymidine by intramolecular ring-closing of the nucleobase with 3'-leaving groups (Scheme 4.04).[33-36] Even with several DBU equivalents, no CO_2 insertion into the nucleobase NH was apparent by $^{13}C\{^1H\}$ NMR spectroscopy, only formation of the 2,3'- anhydrothymidine was observed and confirmed by mass spectrometry and comparison with the literature NMR data.[35]

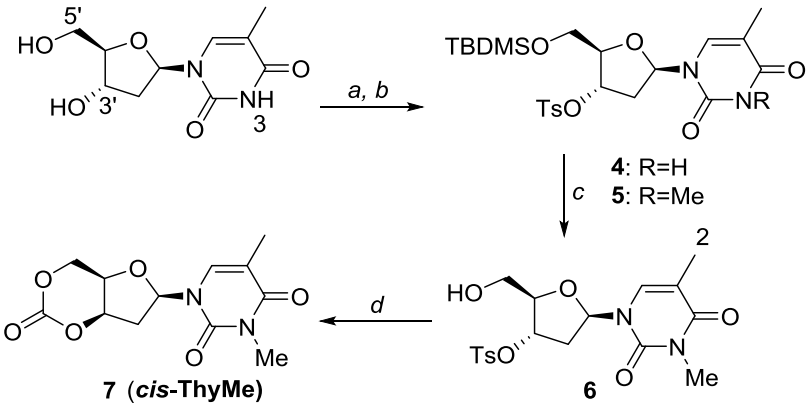

Scheme 4.03. Synthesis of ***cis*-ThyMe** (**7**) (a) i: *t*-BuMe$_2$SiCl, 4-(dimethylamino)pyridine (DMAP), pyridine, rt, 12 h; ii: TsCl, rt, 24 h, 84%; (b) MeI, K_2CO_3, acetone, 12 h, 93%; (c) 1 wt% I_2 in MeOH, reflux, 2 h, 95%; (d) DBU, CO_2 (1 atm), MeCN, 0- 40 °C, 24 h, 52%.

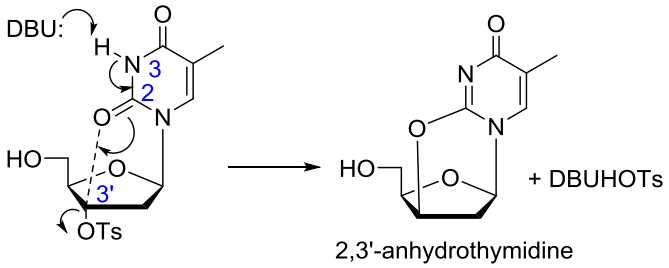

Scheme 4.04. Undesired side reaction observed with 3-*N*-unprotected thymidine: displacement of the tosyl leaving group by intramolecular ring-closing of the nucleobase with DBU base.

As an initial study and proof of concept of the monomer synthesis and ROP potential, the 3-*N*-position was irreversibly methylated. This could be carried out simply and in high yield with MeI and K_2CO_3 in acetone following a literature procedure.[37] 3-*N*-methyl-3'-tosyl-thymidine **6** was then reacted with DBU under 1 atm CO_2 pressure to form a transient amidinium alkyl 5'-carbonate salt, which underwent intramolecular nucleophilic cyclisation in 71% conversion. Although, the cyclic carbonate was observed at room temperature,

heating the reaction mixture to 40 °C enabled a shorter 24-hour reaction time. Isolation by column chromatography and purification by recrystallisation from dry toluene gave the monomer ***cis*-ThyMe** (now referred to as **7**) with polymerisation-grade purity and in a reasonable yield of 52%. For comparison, D-xylose (**2i**), D-glucose (**2j**) and D-mannose (**3**) derived cyclic carbonates, prepared (in Chapters 2 and 3) *via* the nucleophilic addition-elimination mechanism with CO_2 and TsCl, were isolated in yields of 67, 62 and 57%, respectively. The lower polarity of **7** compared to **2i**, **2j** and **3** made isolation by column chromatography more challenging and required a more unusual solvent system of 10% MeCN (rather than acetone) in $CHCl_3$.

The structure was confirmed by elemental analysis, NMR and FTIR spectroscopies, electrospray ionisation mass spectrometry (ESI-MS) and single-crystal X-ray diffraction. In the $^{13}C\{^1H\}$ NMR spectrum, a carbonyl environment (in addition to those of the nucleobase) was observed at 147 ppm, typical of a six-membered cyclic carbonate and a vicinal $^3J_{3'\text{-}4'}$ coupling constant in the ^1H NMR spectrum of 3.9 Hz was consistent with a *cis*-configuration. X-ray analysis of crystals grown from toluene (Figure 4.10) further corroborated stereochemical inversion at the 3'-carbon to form the 3',5'-*cis*-cyclic carbonate. The furanose ring adopts a 4'-endo-3'-exo twist ($^4T_3$) conformation, away from planarity, following the description of ring puckering given by Altona and Sundaralingam.[38, 39]

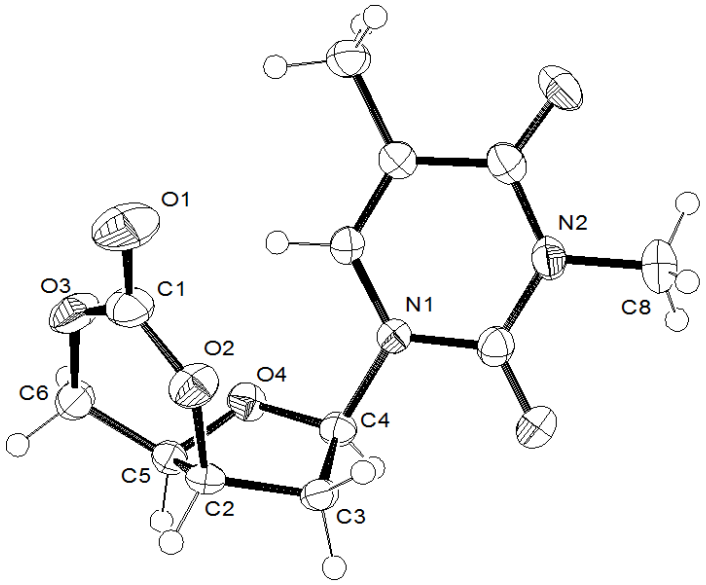

Figure 4.10. ORTEP[40] drawing of the crystal structure of **7** with thermal ellipsoids at the 50% probability level. Selected bond lengths (Å) and dihedral angles (°): C(2)-O(2) 1.466 (2), O(2)-C(1) 1.326 (3), O(1)-C(1) 1.202 (3), C(1)-O(3) 1.326(4), O(3)-C(6) 1.456(3); C(4)-C(3)-C(2)-C(5) -29.61 (19), C(3)-C(2)-C(5)-O(4) -36.87 (19), C(2)-C(5)-O(4)-C(4) 30.01 (2), C(5)-O(4)-C(4)-C(3) 10.5 (2), O(4)-C(4)-C(3)-C(2) 12.6 (2).

To further verify stereochemical inversion, single crystal X-ray diffraction analysis was also carried out of crystals grown from ethanol of the preceding 3-*N*-methyl-3'-tosyl thymidine intermediate **6**. In the solid-state structure, the unconstrained furanose ring adopts a 2'-endo (^{2}E) envelope conformation (Figure 4.11).

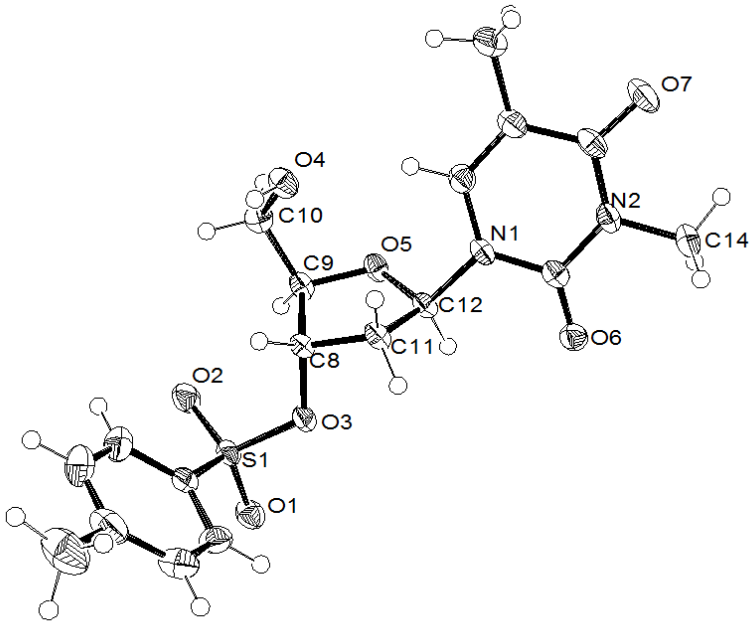

Figure 4.11. ORTEP[40] drawing of 3-*N*-methyl-3'-tosyl thymidine **6** with thermal ellipsoids at the 50% probability level. Selected bond lengths (Å) and angles (°): O(3)-C(8) 1.465(3), C(9)-C(10) 1.515(3), O(4)-C(10) 1.422(3), S(1)-O(3) 1.5859(16), C(8)-C(9) 1.531(3); O(3)-C(8)-C(9)-C(10) 147.36(18); C(12)-O(5)-C(9)-C(8) -4.2(2), C(11)-C(8)-C(9)-O(5) 22.1(2), C(9)-C(8)-C(11)-C(12) -30.5(2), C(9)-O(5)-C(12)-C(11) -15.5(2), C(8)-C(11)-C(12)-O(5) 28.7(2).

4.3. Ring-Opening Polymerisation

4.3.1. Concentration and temperature dependent equilibrium polymerisation

Initially, the ROP of **7** was explored with bifunctional organocatalyst, 1,5,7-triazabicyclo[4.4.0]dec-5-ene (TBD) and 4-methylbenzyl alcohol initiator. For a monomer-to-initiator feed ratio of 100 and a 1 mol L^{-1} initial monomer concentration, $[M]_0$, the polymerisation proceeded rapidly at 25 °C in CH_2Cl_2, reaching a plateau in monomer conversion at 80% after 1 hour. Further addition of monomer after 24 hours led to the reestablishment of a new higher equilibrium monomer conversion. This indicated no catalyst deactivation and a concentration dependent equilibrium polymerisation: at a $[M]_0$ of 2.5 mol L^{-1}, a higher equilibrium monomer conversion of 90% was achieved, which was reduced to 70% for an $[M]_0$ of 0.5 mol L^{-1} (Figure 4.12). Inset to Figure 4.12, a linear kinetic plot was

consistent with pseudo-first order kinetics, typical for ROP and from which a k_{app} of 1.39 ± 0.005 h^{-1} was determined. The limited solubility of the monomer as well as both its high melting point (204- 275 °C) and low thermal stability (178- 205 °C by TGA, 88% mass loss, T_{inf} 248 °C) prevented polymerisations from being carried out at higher concentrations or in the melt at higher temperatures.

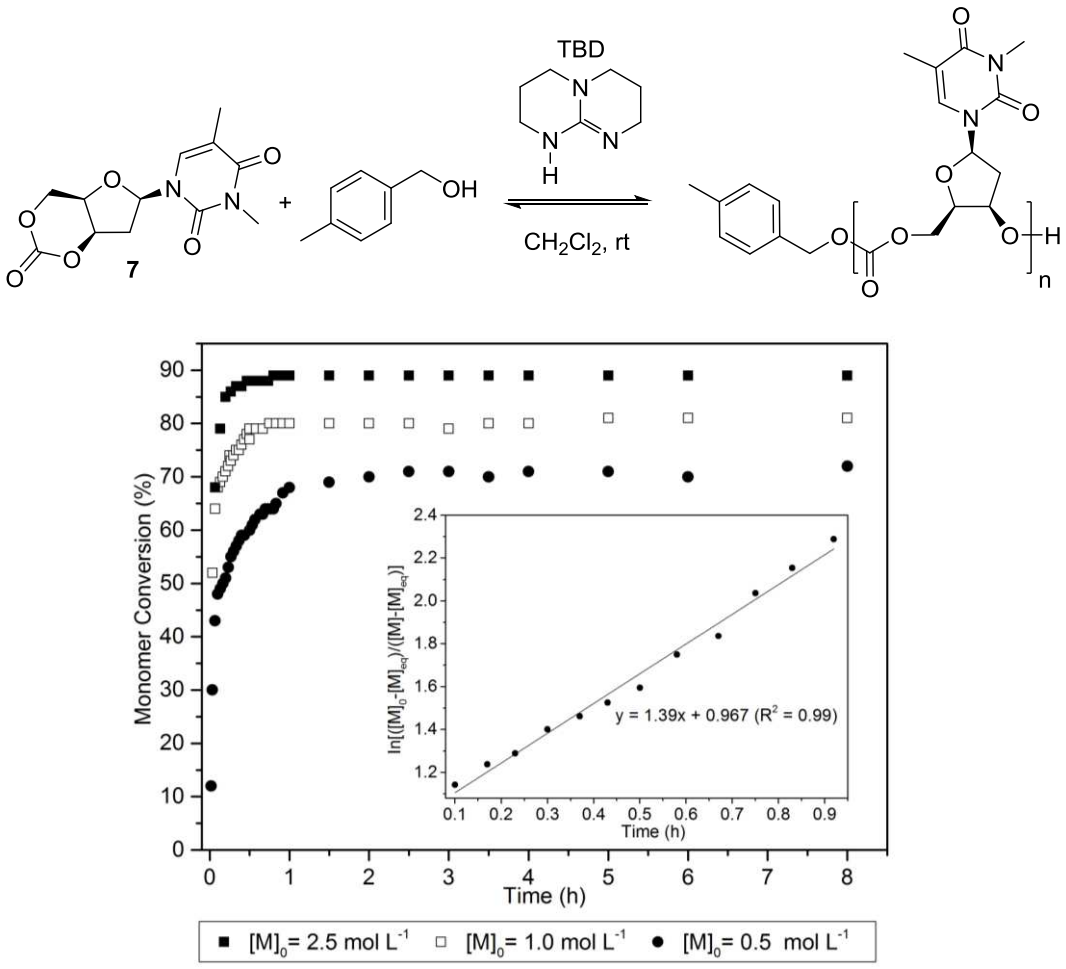

Figure 4.12. ROP of **7** with 4-MeBnOH and TBD catalyst showing the concentration dependence of the equilibrium polymerisation. Monomer conversion is plotted *versus* time for polymerisations carried out at 25 °C in CH_2Cl_2 for different $[M]_0$ and a $[M]_0$: $[TBD]_0$: $[4\text{-MeBnOH}]_0$ ratio of 100:1:1. Monomer conversion was determined (of aliquots taken and quenched with benzoic acid) by ^1H NMR spectroscopy ($CDCl_3$) by relative integration of the anomeric H-1' proton in the monomer (7.19 ppm) and polymer (7.39 ppm). **Inset:** Kinetic plot carried out under the same conditions for $[M]_0$= 0.5 mol L^{-1} and $[M]_{eq}$ = 0.16 mol L^{-1} (69% monomer conversion).

The temperature dependence of the equilibrium polymerisation was also investigated at fixed $[M]_0$, catalyst loading and initiator concentration in 1,2-dichloroethane solvent to access a wider temperature range of 0-80 °C. Colder temperatures resulted in higher equilibrium monomer conversions and from a plot of $\ln[M]_{eq}$ against the reciprocal of the absolute temperature, the polymerisation thermodynamic parameters were estimated (Figure 4.13):

ΔH_p = -12.3 ± 0.4 kJ mol^{-1} and ΔS_p = -29.2 ± 1.1 J mol^{-1} K^{-1}. For comparison, Endo and coworkers[41] reported an enthalpic driving force of -26.4 kJ mol^{-1} for the anionic polymerisation of unsubstituted trimethylene carbonate and accompanying -44.8 J mol^{-1} K^{-1} entropy decrease ($[M]_0$ = 1 mol L^{-1}). For substituted derivatives, a less favourable ΔH_p with increased steric bulk of the substituents was attributed to an unfavourable distortion of the polymer backbone leading to higher $[M]_{eq}$. To demonstrate the reversibility, heating the polymerisation equilibrated at 0 °C (72% monomer conversion), without quenching to 80 °C resulted in near quantitative recovery of the monomer (≤ 4% monomer conversion). This could have implications for monomer recyclability (Figure 4.14) though, may also limit the processability of the polymer.[42, 43]

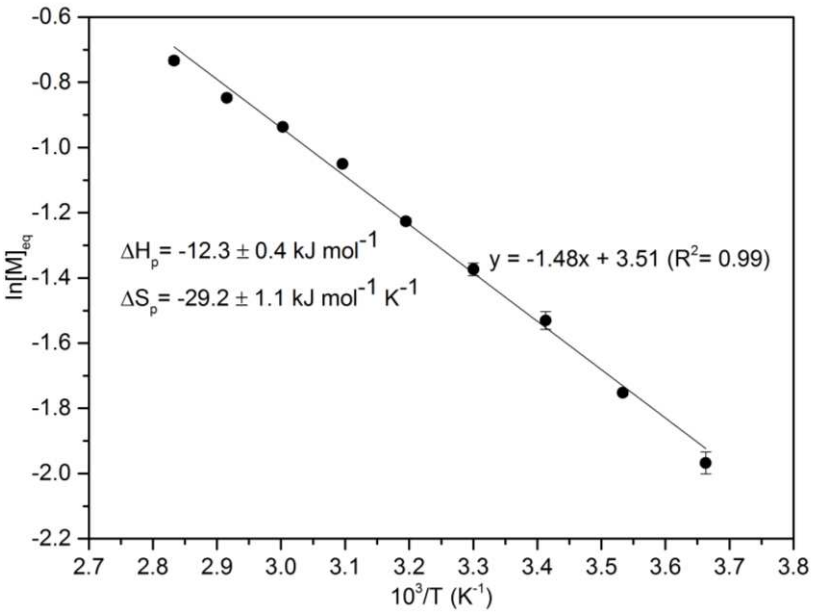

Figure 4.13. Calculation of the thermodynamic parameters from a plot of $\ln[M]_{eq}$ as a function of 1/T, where T is the absolute temperature. Polymerisations were carried out in 1,2-dichloroethane, over a temperature range of 0-80 °C for $[M]_0$ = 0.5 mol L^{-1} and $[M]_0$: $[TBD]_0$: $[4\text{-MeBnOH}]_0$ = 100:1:1. $[M]_{eq}$ was calculated based on the monomer conversion, determined by ^{1}H NMR spectroscopy. Three repeats were carried out at each temperature and an average taken. Error bars represent standard error.

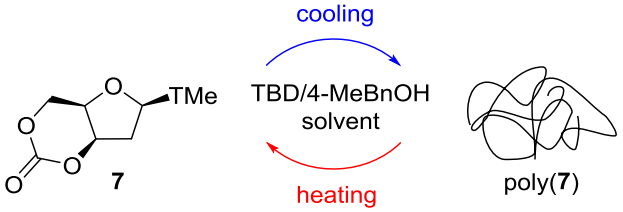

Figure 4.14. Temperature dependent polymerisation and depolymerisation of **7** in solution with TBD catalyst and 4-methyl benzyl alcohol initiator. This may have implications for monomer recyclability though repeated heating and cooling cycles could to lead to the formation of by-products and thus reduced monomer recovery.

4.3.2. Molecular weight control and end-group analysis

For a monomer-to-initiator feed ratio of 50, the M_n estimated by size elusion chromatography (SEC) *versus* polystyrene standards with $CHCl_3$ eluent, increased linearly with percentage monomer conversion whilst maintaining narrow dispersities (Đ 1.09- 1.18), indicating a controlled ROP (Figure 4.15). Good agreement was also observed with the predicted M_n up to 57% monomer conversion, where the SEC estimated M_n was 7650 g mol^{-1} (Đ 1.09) compared to the predicted 8170 g mol^{-1}. Under these polymerisation conditions (0 °C and $[M]_0$ = 2.5 mol L^{-1}), monomer conversion plateaued at 90%. As this thermodynamic equilibrium was approached, a slight decrease in the polymer M_n was observed alongside a broadening of the polymer molecular weight distribution to 1.29 and was attributed to transcarbonylation reactions.

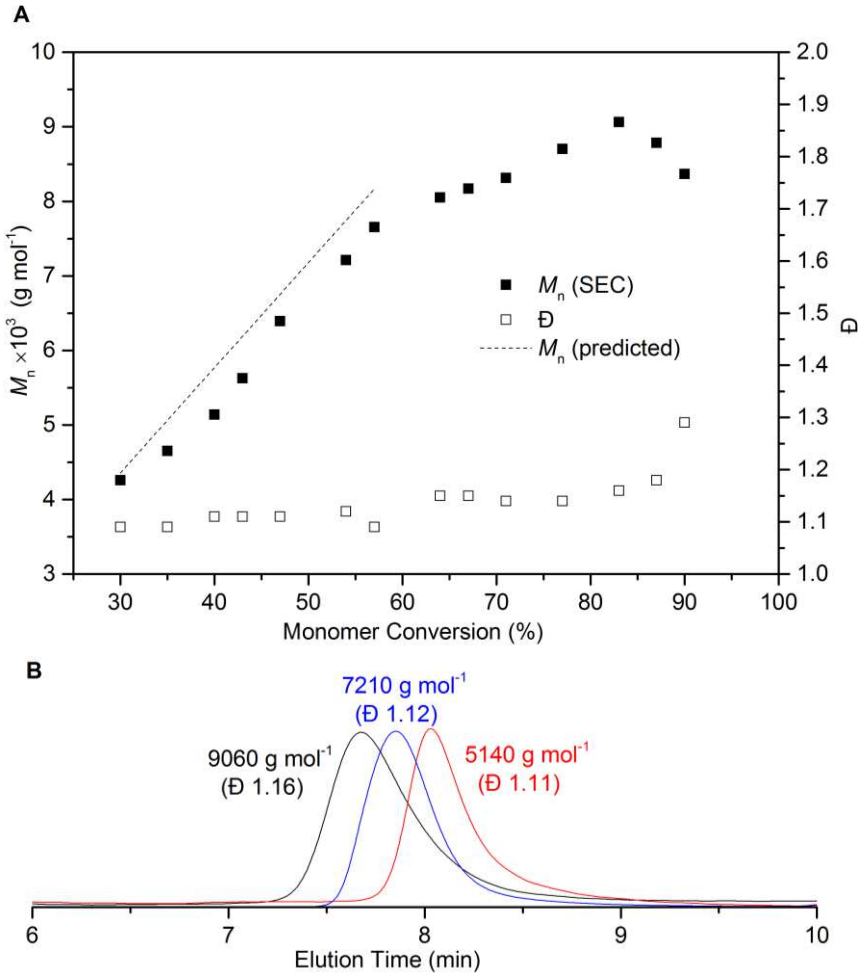

Figure 4.15. (A) Plot of M_n and Đ *versus* monomer conversion for a ROP carried out at 0 °C with $[M]_0$= 2.5 mol L^{-1} and 50:1:1 $[M]_0$: $[TBD]_0$: $[I]_0$. Conversion was determined by ^{1}H NMR spectroscopy of aliquots quenched with excess benzoic acid. M_n and Đ were estimated by SEC *versus* polystyrene standards using a refractive index (RI) detector and $CHCl_3$ eluent. Predicted M_n was calculated as: $M_r(I) + (M_r(M) \times conv./100\% \times [M]_0/[I]_0)$. **(B)** Selected SEC traces correlating to data points 3, 6 and 12.

MALDI-ToF mass spectrometry of the polymer ($M_{n,SEC}$ = 7210 g mol^{-1}, point 6 in Figure 4.15A) showed a major linear polymeric series of M_n 7120 g mol^{-1} with thymidine carbonate repeat unit ($\Delta m/z$ ~282.3) and expected 4-methylbenzyl alcohol and OH end groups (Figure 4.16). A minor (19%) cyclic species was also observed due to backbiting of the polymer chain. As the polymer chain grows and monomer concentration decreases, a greater rate of chain backbiting (leading to macrocycles) relative to chain propagation may account for deviations observed between the calculated and SEC estimated M_n at higher monomer conversions (>60% in Figure 4.15A).

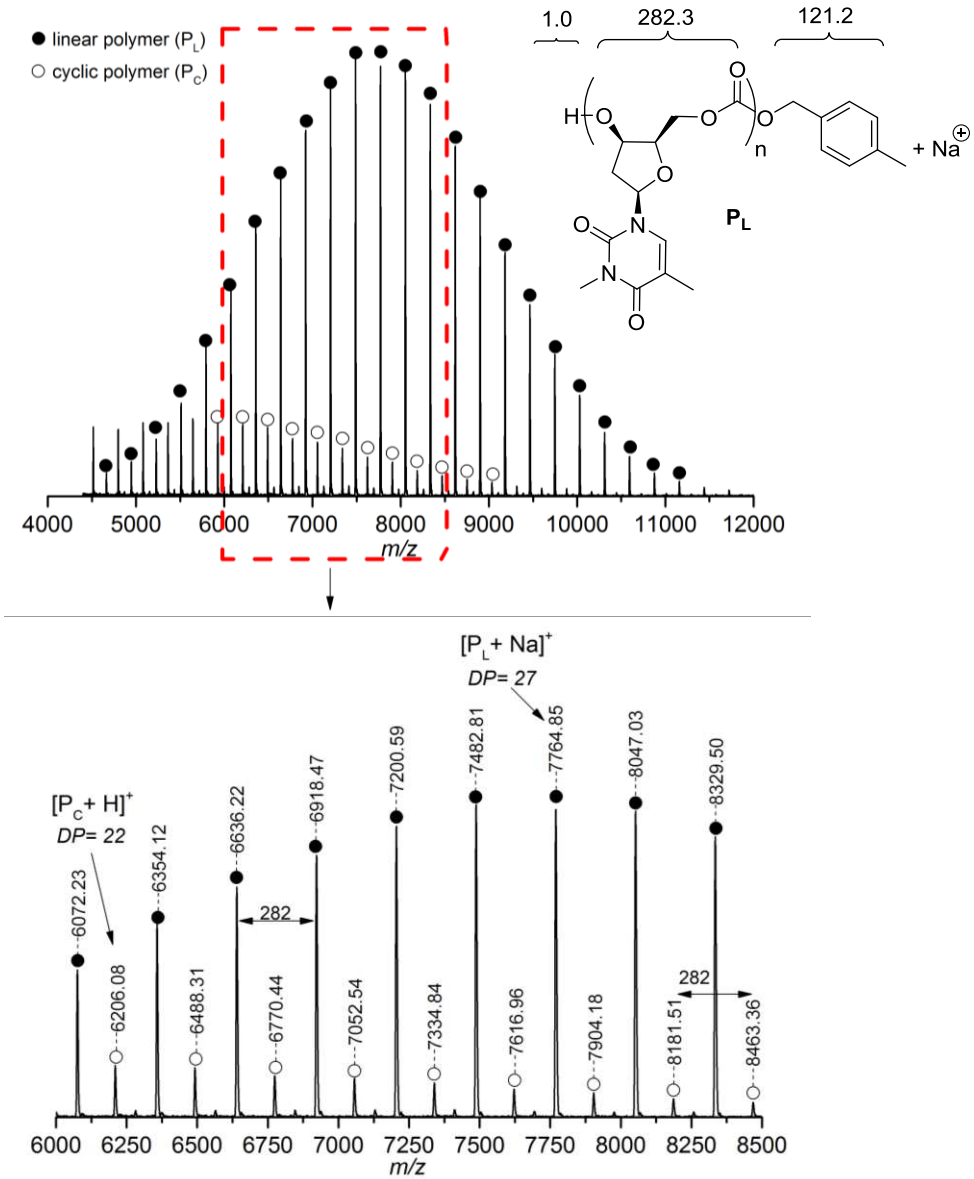

Figure 4.16. MALDI-ToF mass spectrum of polymer ($M_{n,SEC}$ 7210 g mol^{-1}, Đ 1.12) showing the sodium adduct of the linear polymer (P_L) with OH and 4-MeBnOH end-groups as the major series (81%, $M_{n,\,MALDI}$ 7120 g mol^{-1}, Đ 1.03). The minor series (19%) with thymidine repeat unit $\Delta m/z$ ~282.3 was assigned to the cyclic polymeric species ($M_{n,\,MALDI}$ 5250 g mol^{-1}, Đ 1.01). DP= degree of polymerisation.

Dilution of the reaction conditions to $[M]_0$ = 0.5 mol L^{-1} to favour macrocycle formation resulted in lower M_n (4260 g mol^{-1}) and more cyclic species by MALDI-ToF MS (Figure 4.17). Macrocycles are of interest in their own right and those derived from nucleosides are attractive for example, for the formation of supramolecular complexes with metal coordination characteristics.[25] The absence of chain ends in cyclic topologies can also give rise to properties distinct to those of linear polymers such as higher thermal decomposition temperatures.[44] They may also prevent reversion of the polymer back to the monomer by back-biting reactions at elevated temperatures. Though, complete thermal depolymerisation was reported for cyclic poly(γ-butyrolactone) by Chen and Hong[43] on heating the bulk material to 300 °C in the presence of $La[N(SiMe_3)_2]_3$ catalyst and an alcohol initiator.

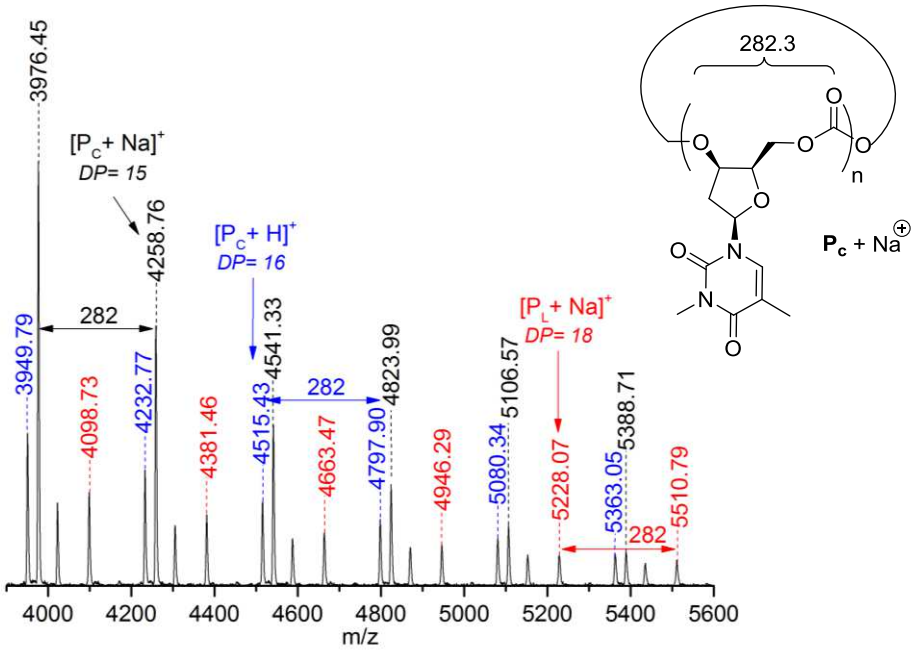

Figure 4.17. MALDI-ToF MS analysis of polymer ($M_{n,sec}$ 4260 g mol^{-1}, Đ 1.09) obtained under more dilute conditions ($[M]_0$ = 0.5 mol L^{-1}) showing the cyclic polymeric species (P_c) as the major series; $[P_c + Na]^+$ (DP= 15 gives *m/z* 4257.5) and $[P_c + H]^+$ (DP= 16 gives *m/z* 4517.8). The minor series corresponds to the linear polymer $[P_L+Na]^+$ (DP= 18 gives *m/z* 5226.6). DP= degree of polymerisation.

The largest molecular weights, up to 17 000 g mol^{-1} (Đ 1.30) were achieved at 0 °C and $[M]_0$ of 2.5 mol L^{-1} (Table 4.01, Entry 2). A greater disparity was observed between the theoretical M_n and those determined by SEC at higher $[M]_0/[I]_0$ ratios, most likely due to chain back-biting reactions. To explore the influence of the catalytic system on the control of M_n, metal complexes were also tested for the ROP of **7**. $Sn(Oct)_2$ catalyst with 4-MeBnOH initiator at 120 °C in toluene did not yield homopolymer. $Y(OiPr)_3$ or $Al(OTf)_3$ with alcohol initiator resulted in poor control and low M_n (1800-3910 g mol^{-1}, Đ 1.35-1.39) in CH_2Cl_2, dioxane

and toluene solvents at 0, 25, 70 and 120 °C. Although highly active for lactide ROP in CH_2Cl_2 at room temperature, the zinc (II) alkoxide catalyst (L1ZnOEt, Figure 4.18A) reported by Williams *et al.*[45] was slower compared to TBD for the ROP of **7**, as was the (BDI-1)ZnEt catalyst (Figure 4.18B)[46, 47] with 4-MeBnOH initiator (Table 4.01, Entries 3 and 4).

Table 4.01. ROP of **7**. [a]

Entry	Temp. (°C)	Cat.	$[M]_0$: $[C]_0$: $[I]_0$	Conv. (%)[b]	Time (h)	M_n [Đ] [c]
1[d]	0	TBD	100:1:1	68	4	4260 [1.09]
2	0	TBD	150:1:1	90	3	17 000 [1.30]
3[e]	25	L1ZnOEt	100:1	71	20	7250 [1.22]
4[f]	25	(BDI-1)ZnEt	100:1:1	60	24	5240 [1.15]
5	25	TBD	100:1:1	90	3	11 000 [1.27]
6	0	TBD	100:1:1	93	3	15 400 [1.28]

[a] All polymerisations were carried out at $[M]_0$ = 2.5 mol L^{-1} in CH_2Cl_2 unless stated otherwise; [b] Determined by ^1H NMR spectroscopy in $CDCl_3$; [c] Calculated by SEC with $CHCl_3$ eluent *versus* polystyrene standards (RI detector); [d] $[M]_0$ = 0.25 mol L^{-1}; [e] L1= 2,4-di-*tert*-butyl-6-{[(2'-dimethylaminoethyl)methylamino]-methyl}phenolate; [f] BDI-1= 2-((2,6-diisopropylphenyl)amido)-4-((2,6-diisopropylphenyl)-imino)-2-pentene].

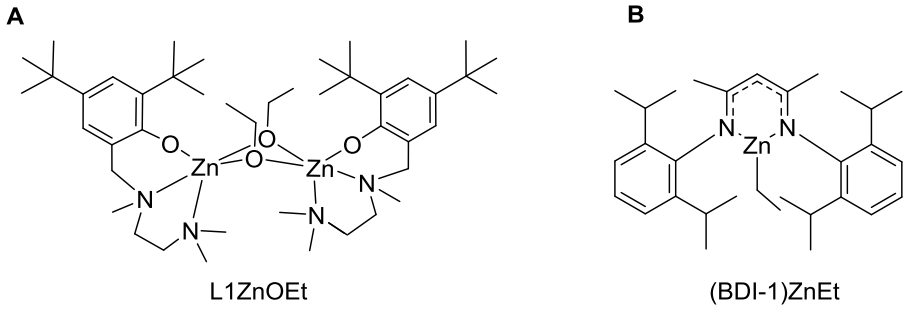

Figure 4.18. Literature zinc-based metal catalysts investigated for the ROP of **7**. L1ZnOEt is reported to exist as a dimmer in the solid state though, the monomeric form predominates in solution.[45]

4.4. Polycarbonate Structure

NMR spectroscopy gave an insight into the structure of the thymidine-based polycarbonates. Shown in Figure 4.19, a coalescing of the H-5' and H-4' proton environments in the ^1H NMR spectrum of the polymer compared to the monomer was consistent with loss of constraint upon ring-opening of the cyclic carbonate moiety. $^{13}C\{^1H\}$ NMR analysis revealed three carbonate environments centered at 154.4, 153.6 and 152.8 ppm assigned to

head-head (H-H), head-tail (H-T) and tail-tail (T-T) linkages in the polymer backbone (Figure 4.20). In contrast to the D-mannose derived polycarbonates (Chapter 3), which showed a preference for head-tail linkages, the ~1:2:1 integration ratio of these signals by quantitative $^{13}C\{^{1}H\}$ NMR spectroscopy, indicated a regiorandom polymer. Cleavage at either side of the asymmetric cyclic carbonate in **7** and propagation of the chain by attack of either a free secondary or primary hydroxy end-group gives rise to all three linkage types. Further splitting within each of the three carbonate environments may be attributed to long range sequence effects as also reported for the regiorandom D-xylose and D-glucose based polycarbonates.[29, 30]

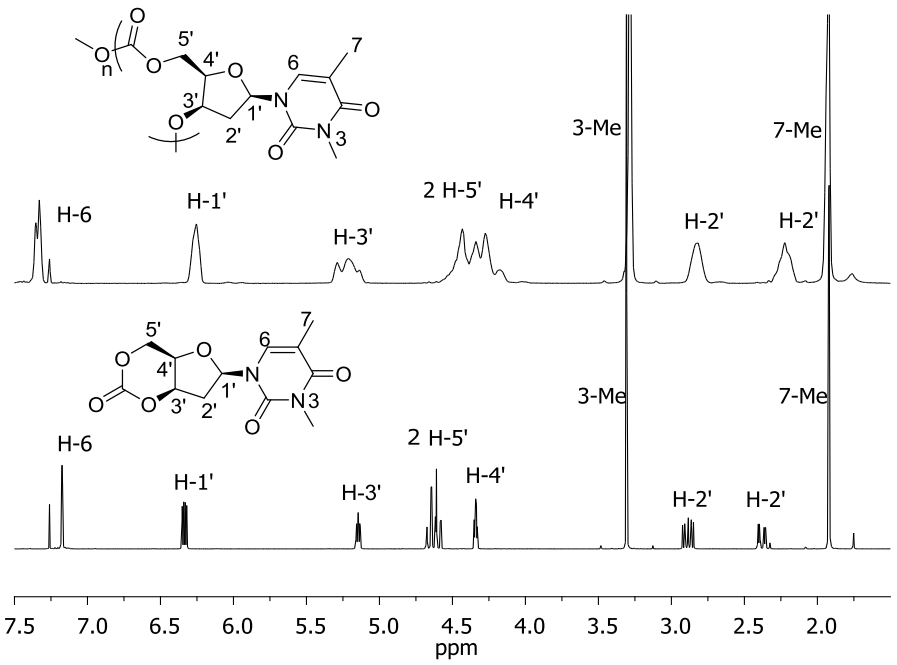

Figure 4.19. Comparison of the ^{1}H NMR spectra (400 MHz, $CDCl_3$) of monomer **7** (bottom) and its polymer (top,15 400 g mol^{-1}, Đ 1.28, Table 4.01, Entry 6).

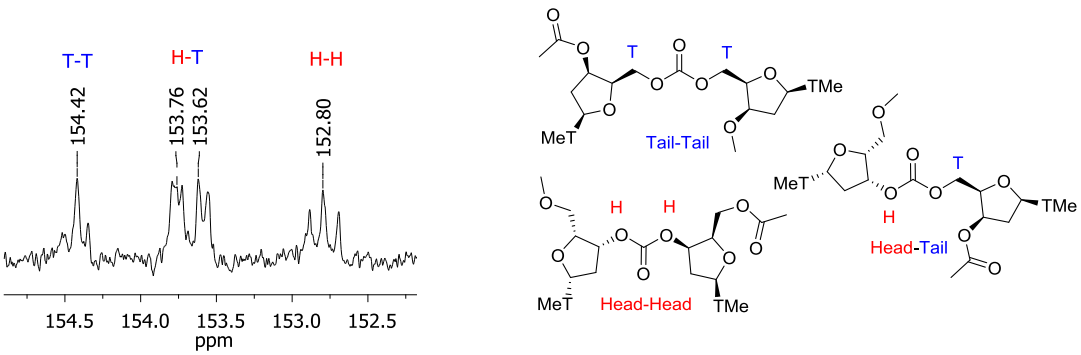

Figure 4.20. Carbonyl region of the $^{13}C\{^{1}H\}$ NMR spectrum (400 MHz, $CDCl_3$) of poly(**7**) (15 400 g mol^{-1}, Đ 1.28, Table 4.01, Entry 6) showing the different carbonate backbone regiochemistries, indicating a regiorandom polymer. Assignment was based on the 1:2:1 integration ratio (by quantitative $^{13}C\{^{1}H\}$ NMR) and on the work carried out by both Gross and coworkers[29] and Mikami *et al.*[30] on the D-xylose and D-glucose based polycarbonates, respectively.

In parallel, DFT modelling of the initiation step in the ROP of **7** with 4-MeBnOH and TBD catalyst (as detailed for **3** in Chapter 3) supported this lack of preference for ring-opening to expose either a free primary ($\Delta\Delta G$ = -5.6 kcal mol^{-1}) or secondary hydroxyl group ($\Delta\Delta G$ = -6.6 kcal mol^{-1}) for chain propagation (Figure 4.21). (At the same level of theory, ring-opening of the mannose derived monomer **3** to expose a secondary hydroxyl group was calculated to be 7.6 kcal mol^{-1} more favourable compared to ring-opening to expose a primary hydroxyl end-group).

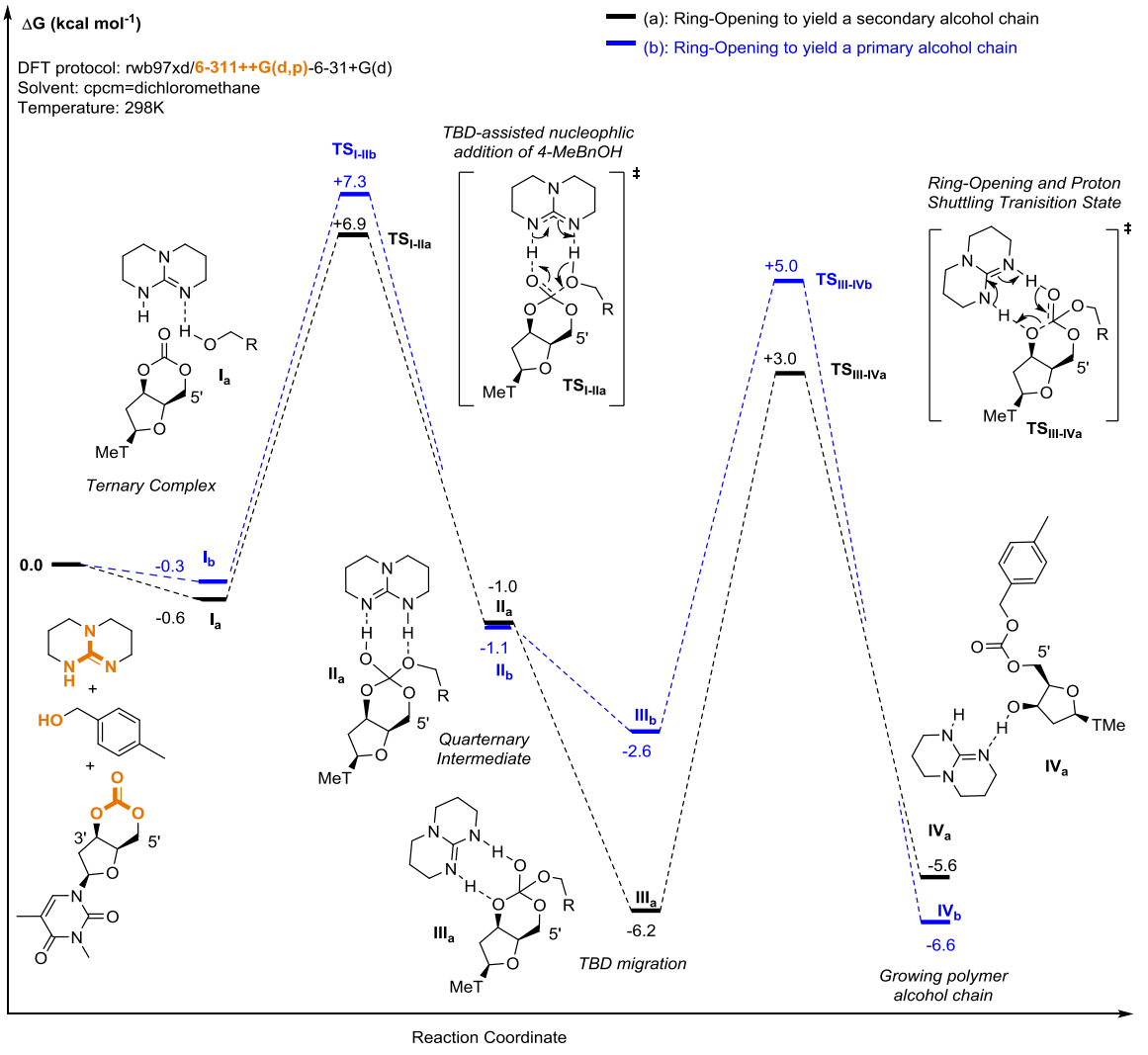

Figure 4.21. DFT computations for the initiation step in the ROP of **7** with 4-MeBnOH and TBD catalyst. Thermodynamically, an insignificant difference of 1 kcal mol^{-1} was calculated between ring-opening to expose either a free secondary (**IV$_a$**) or primary hydroxyl group (**IV$_b$**) for chain propagation.

4.5. Polycarbonate Properties

4.5.1. Thermal properties

Thermogravimetric analysis (TGA) of the thymidine-based polycarbonates with M_n 4650, 11 000 and 15 400 g mol^{-1} revealed the onset of thermal degradation occurred at relatively low temperatures of ~170 °C (Figure 4.22). A maximum rate of mass loss (T_{inf}) was observed at around 246 °C and mass losses of 91 to 94%, achieved by ~300 °C. The TG curves were similar for the polymers over this M_n range but a difference was observed compared to the monomer, which showed less overall mass loss (88%) and a slightly later onset of degradation (T_{on} = 178 °C).

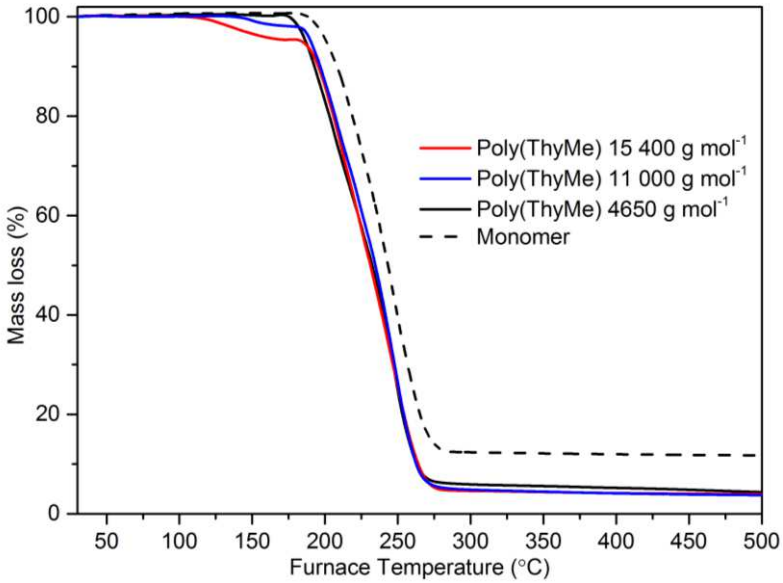

Figure 4.22. TGA analysis of thymidine-based polycarbonates of various M_n. For comparison, the TG of the monomer is also shown. Samples were heated from 30 to 500 °C at 5 K min^{-1}. The slight mass loss observed just prior to the main degradation profile for polymers of M_n 11 000 and 15 400 g mol^{-1} may be due to the loss of residual solvent.

Analysis of the gases evolved by tandem mass spectrometry confirmed the presence of *m/z* 44 attributed to the loss of CO_2^+ (Figure 4.23). Maximum detection was observed between 240 and 242 °C, coinciding with the T_{inf}, observed by TGA.

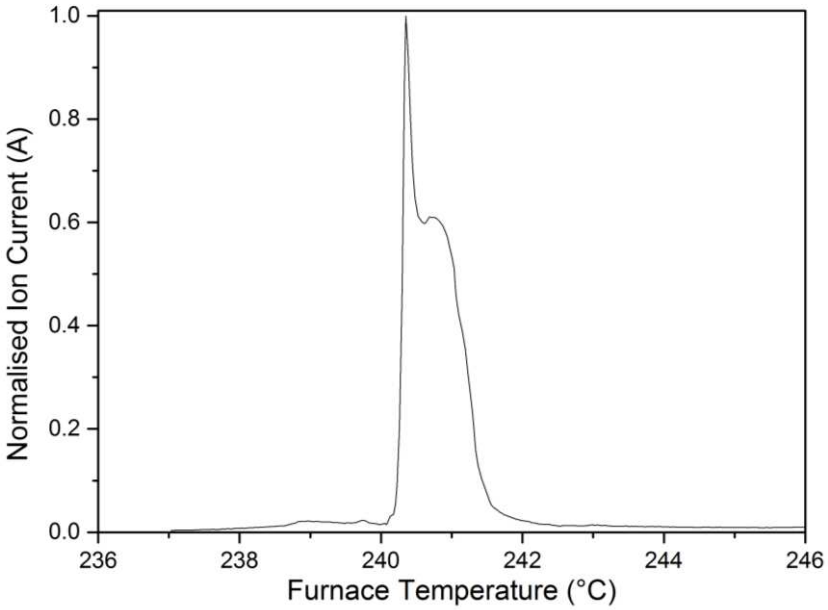

Figure 4.23. Normalised ion current as a function of furnace temperature (°C) for *m/z* 44 assigned to CO_2^+ evolved during the thermal decomposition of the thymidine derived polycarbonates (M_n 15 400 g mol^{-1}, Đ 1.28).

Micro Differential Scanning Calorimetry (DSC) of the polymer samples, carried out under argon at a heating rate of 1 K min^{-1}, revealed high glass transition temperatures (T_g). Namely, for the polycarbonate of M_n 15 400 g mol^{-1}, a T_g of 156 °C was measured (Figure 4.24A) and ~153 °C for polymers of M_n 4650 (Figure 4.24B) and 11 000 g mol^{-1}. The high values were attributed to restricted rotation about the furanose ring backbone and the bulky nucleobase substituent. Additional unassigned features observed in the DSC baseline were attributed to the slow heating rate and high sensitivity of the micro-DSC instrument. For comparison, furanose-cored isopropylidene-protected D-xylose derived polycarbonate exhibited a T_g of 128 °C (M_n 13 200 g mol^{-1})[29] and pyranose backboned D-mannose (Chapter 3) and D-glucose derived polycarbonates of 152 °C (M_n 13 600 g mol^{-1}) and 122 °C (M_n 14 700 g mol^{-1}),[30] respectively. No transitions associated with a melting domain were observed, indicating an amorphous polymer, which was further confirmed by powder X-ray diffraction (Appendix Figure A2).

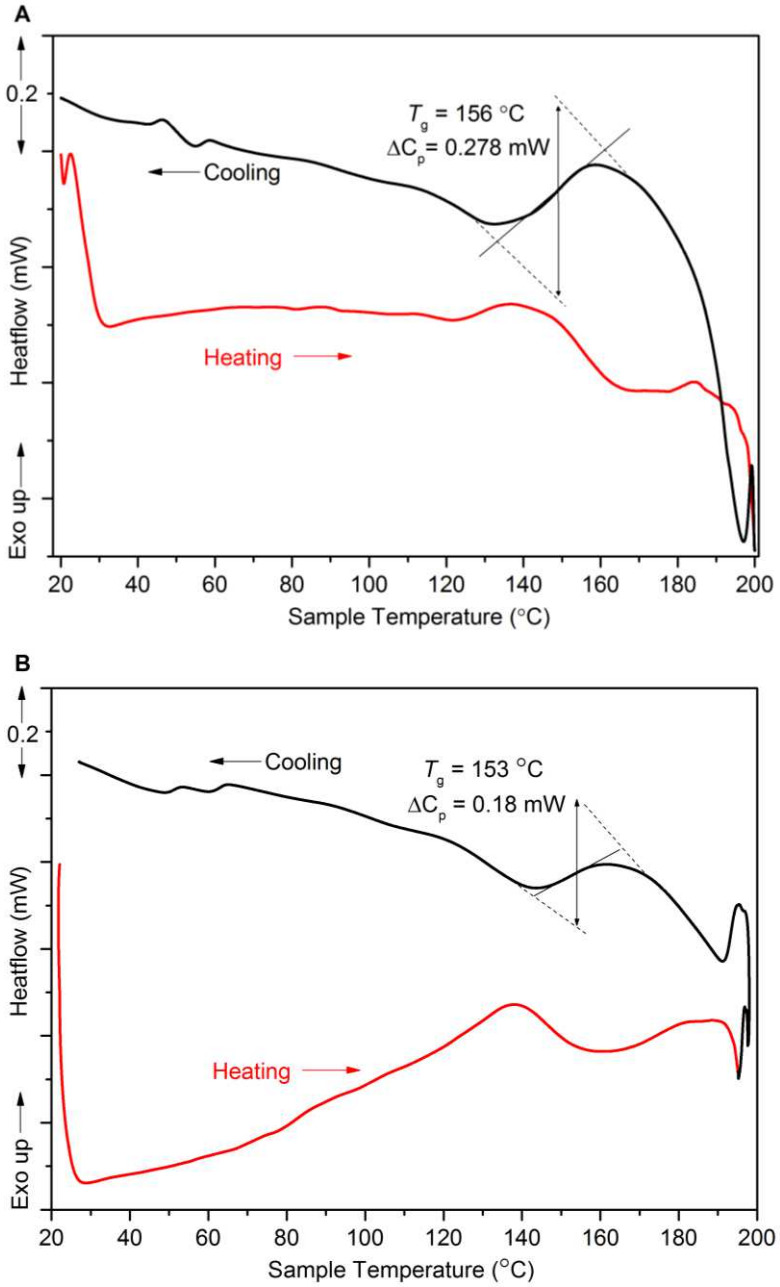

Figure 4.24. MicroDSC traces of thymidine-based polycarbonates; **A:** the first heating and cooling cycle of a polymer with M_n 15 400 g mol^{-1} (Đ 1.28) and **B:** the second heating and cooling cycle of polymer with M_n = 4650 g mol^{-1} (Đ 1.09). Samples were heated under an argon atmosphere from 20 to 200 °C at 1 K min^{-1} before being cooled at the same rate. For consistency, the T_g was taken at half height from the cooling curve. Additional features observed in the baseline are attributed to the slow heating rate (1 K min^{-1} compared to 10 K min^{-1} in traditional DSC) as well as the high sensitivity of the micro-DSC instrument.

4.5.2. Static water contact angle and hydrolytic stability

The hydrolytic stability of the water insoluble thymidine-based polycarbonates was investigated at room temperature with 0.25 wt% polymer (M_n 11 000 g mol^{-1}) in water, 1 mol L^{-1} HCl (aq) and 1 mol L^{-1} NaOH (aq) as well as in phosphate-buffered saline (PBS) solution at 37 °C with *Candida antartica* Lipase B. After 1 week, no solid had dissolved or

loss of mass observed by SEC for the neutral and acidic conditions. NMR analysis of the supernatant in D_2O revealed no environments. Under the alkali conditions, the polymer completely dissolved after 4 hours. ^1H NMR spectroscopy revealed environments consistent with the component *cis*-diol of 3-*N*-methyl thymidine by comparison with the product formed on dissolving the monomer in D_2O (Figure 4.25). Mass spectrometry further confirmed the presence of the diol and with no polymeric material detected by SEC, suggested hydrolytic degradation of the polymer to its constitute components. With Lipase B enzyme, unknown degradation products were detection in solution after one week.

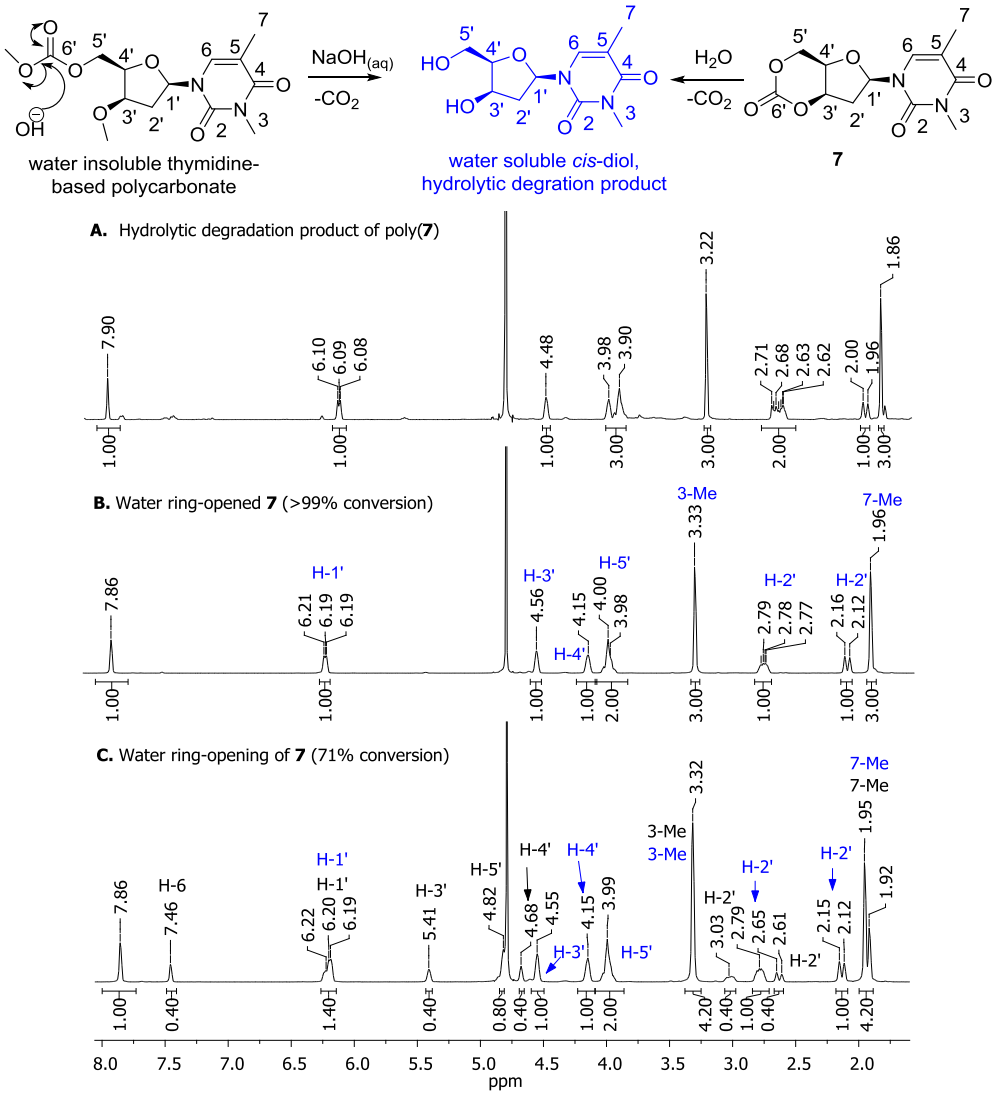

Figure 4.25. ^1H NMR spectra (400 MHz, D_2O) of **A:** the hydrolytic degradation products of poly(**7**) after 24 h at 4 wt% in 1 mol L^{-1} NaOH (a higher wt% enabled full visualisation of the signals); **B:** the *cis*-sugar diol (blue) formed on ring-opening and decarboxylation of **7** in D_2O (in the absence of a catalyst). Decarboxylation was confirmed by $^{13}C\{^1H\}$ NMR spectroscopy (loss of the C=O environment) as well as HR-MS (ESI). **C**: Evidence for ring-opening of **7** to the *cis*-diol; changes in the proton environments (*e.g.* H-3', H-4' and H-5') are consistent with the loss of ring strain in **7**. Conversion (after 12 h at rt) is based on relative integration of the alkene H-6 proton environments at 7.86 *versus* 7.46 ppm.

Static water contact angles were measured on thin films prepared by drop casting 1 wt% solutions of polymer in CH_2Cl_2 onto glass slides. An average angle of 48 ± 1° was more hydrophobic than films prepared of the monomer in the same way but less hydrophilic compared to the glass slide control (Figure 4.26). Polymer films prepared using a thermal press at 160 °C and 25 bar pressure* were too brittle for analysis of the mechanical properties and too inhomogeneous for reproducible static water contact angle measurements.

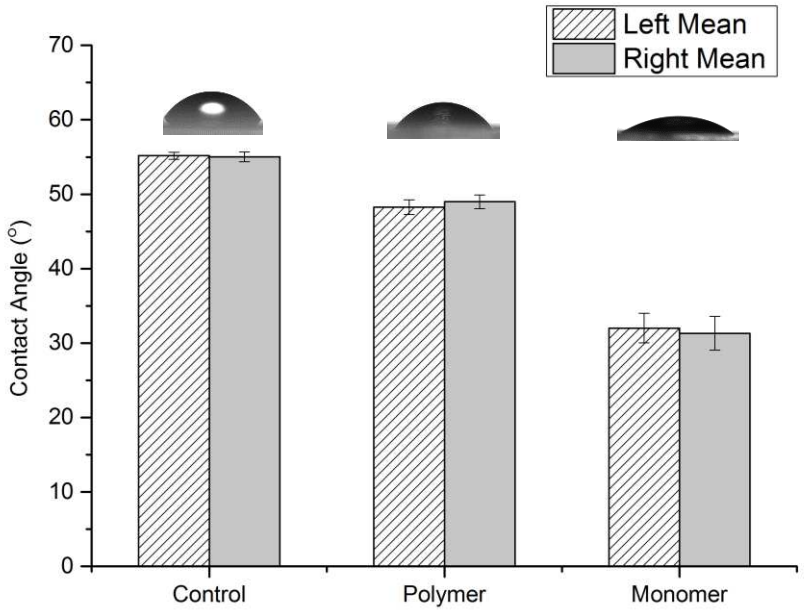

Figure 4.26. Right and left static water contact angle measurements (2 µL water droplets) for polymer thin films prepared by drop casting 1 wt% polymer solutions onto glass slides and allowing the solvent to evaporate before drying in a vacuum overnight at 40 °C. For comparison, contact angles were also measured for the glass cover slip as a control and thin films of the monomer prepared in the same way. Values represent an average of 10 measurements taken from three films and error bars the standard error of the mean (n=10). A greater error was observed for the monomer as the films were less even due to crystal formation**.**

4.6. Preliminary Cell Attachment Studies

Cell attachment studies were carried out with human osteoblast cancer cell line, MG-63 on polymer thin films drop cast onto glass slides (as above) at 0.25, 0.5, 0.75 and 1 wt% in CH_2Cl_2. After sterilisation of the films and fixing to a cell culture plate, cells were seeded in FBS^+ growth media at a density of 10, 000 live cells cm^{-2} (see Experimental Section). After either a 1 or 24-hour incubation period (at 37 °C in a 5% CO_2 atmosphere), the media containing any dead or unattached cells was removed and the films rinsed before attached

* Carried out on a Pressmasters 40T GEM series thermal press. The powdered polymer was placed between baking parchment and in turn, two stainless-steel plates at 160 °C and 25 bar for 5 minutes before being cooled to 25 °C and soaked overnight in acetone (to detached from the parchment).

live cells were fixed with formalin solution. Cell attachment was then measured by microscopy following fluorescent staining of the cells with 4,6-diamidino-2-phenylindole (DAPI). After a 1 hour incubation period, cell attachment was comparable to the empty well-plate (made of oxidised polystyrene) and glass controls and indicated that the thymidine-based materials did not have an adverse effect of the cells (Figures 4.27 and 4.28). After a longer 24-hour incubation period (Figure 4.29), less proliferation of the cells was observed compared to the empty well-plate control suggesting further modifications to the polymer surface are required for it to serve as an effective tissue engineering scaffold.

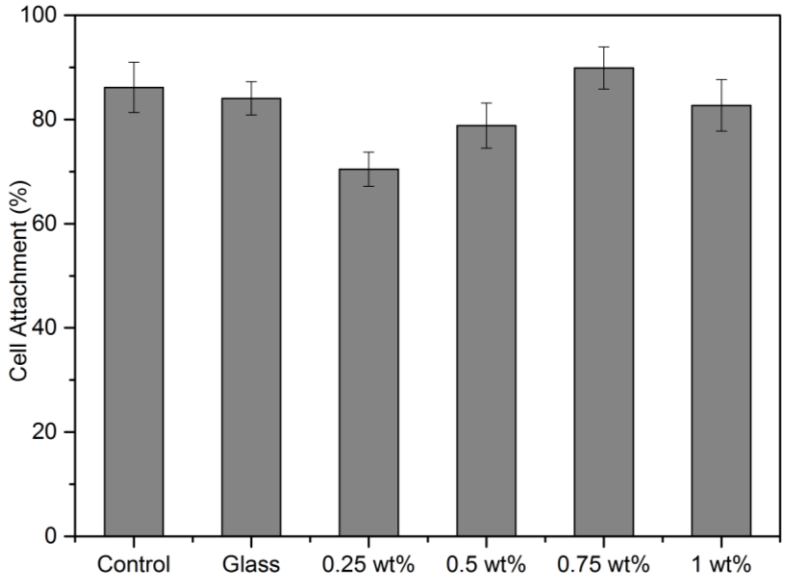

Figure 4.27. Number of MG-63 cells attached after a 1 hour incubation period (37 °C, 5% CO_2) expressed as a percentage of the seeding density (10,000 cells cm^{-2}) for polymer thin films prepared by drop casting solutions of different wt% onto glass slides and compared to the glass slide (glass) and empty culture plate well (control). Values are reported as an average with error bars representing standard error (n=18). Variation between different wt% of polymer solutions is attributed to the quality of the film formed, drop casting often results in non-uniform films. Polymer scaffolds prepared using a heat press were found to be too brittle for cell experiments.

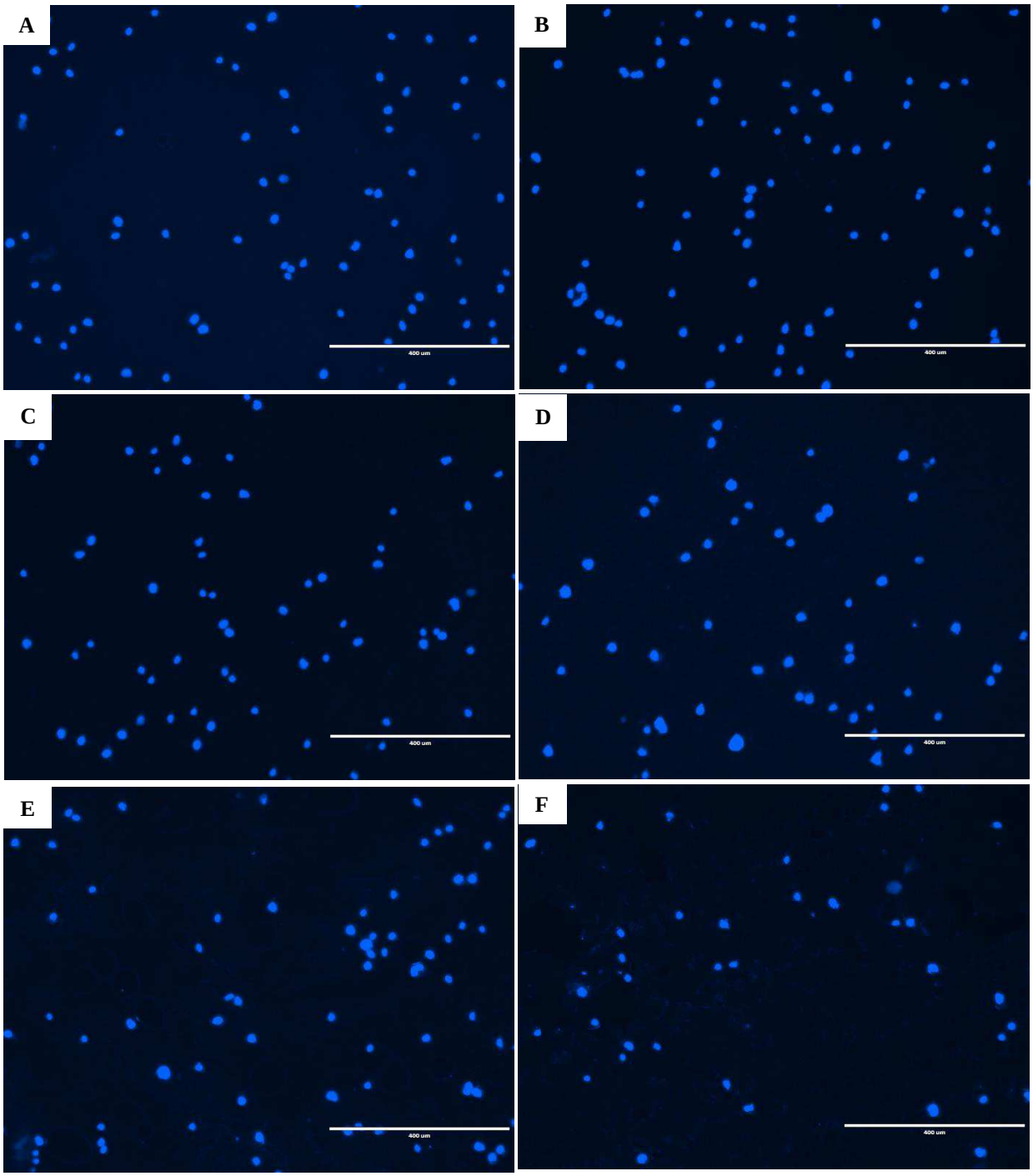

Figure 4.28. Confocal microscopy images of cells stained with 4,6-diamidino-2-phenylindole (DAPI) after the 1 hour incubation period for **(A)** the empty well-plate control, **(B)** the glass control and polymer films prepared by drop casting solutions of **(C)** 0.25 wt%, **(D)** 0.5 wt%, **(E)** 0.75wt% and **(F)** 1 wt %.

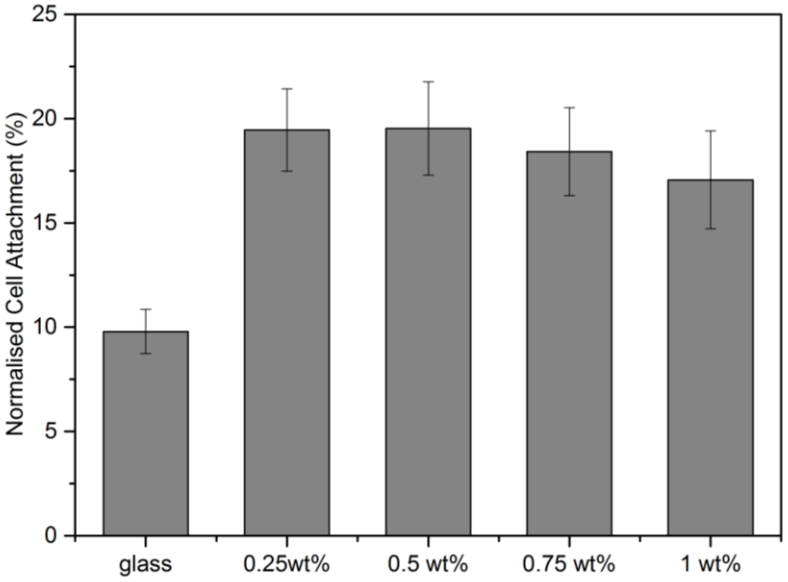

Figure 4.29. The number of MG-63 cells attached after a 24-hour incubation period (37 °C, 5% CO_2) as a percentage of the seeding density (10,000 cells cm^{-2}) and normalised to the empty polystyrene well-plate control. Values represent mean values and error bars standard error (n=18). Statistically more cells are attached to the polymer films compared to the glass slide control, which may be a result of the roughness of the polymer film surface due to the drop casting method.

4.7. Conclusions and Further Work

To conclude, for ROP to DNA-based polycarbonates, challenges in the isolation of the *trans*- 3',5'-cyclic carbonate of 2'-deoxyribonucleosides led to the development of a novel approach. Namely, the utilisation of CO_2 at 1 atm pressure, with DBU reagent, to form a 5'-carbonate nucleophile that affects intramolecular ring-closing by displacement of a tosyl leaving group at the 3'-position. This resulted in stereochemical inversion and formation of the *cis*-configured-3',5'-cyclic carbonate of 3-*N*-methyl thymidine. The strategy represents a generally applicable method to cyclic carbonate synthesis from natural furanose sugars bearing a *trans*-1,3-diol and extends the range of sugar-based cyclic carbonate monomers beyond those possible with classical reagents such as phosgene and its derivatives, which require a nucleophilic addition-elimination mechanism (Figure 4.30).

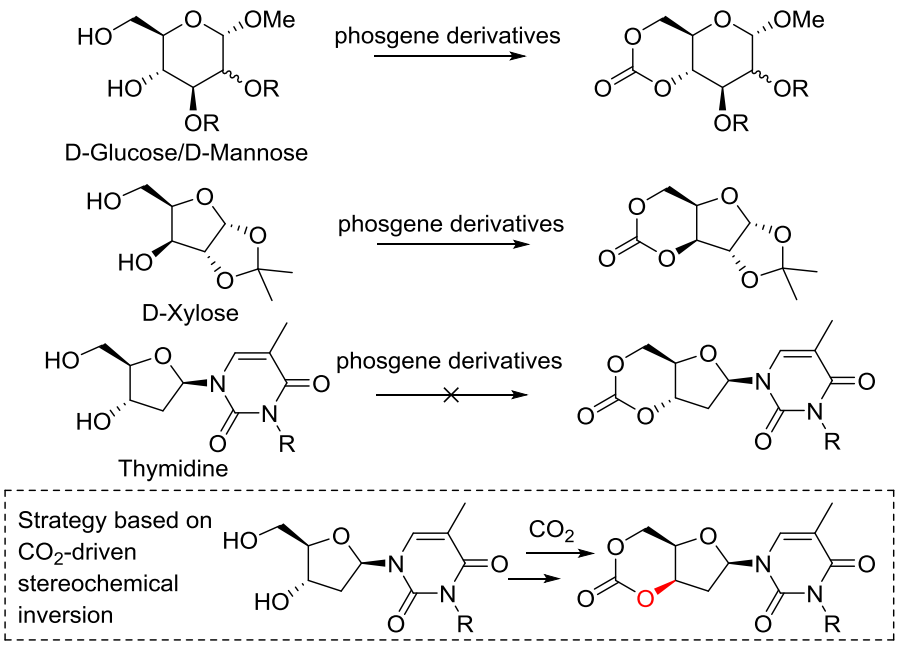

Figure 4.30. Cyclocarbonation of the *trans*-1,3-diols in protected D-gluco-/D-manno- pyranosides and *cis*-1,3-diol of protected D-xylofuranose sugar, with retention of the stereochemistry *via* a nucleophilic addition-elimination mechanism (for example, using phosgene derivatives). The *trans*-3',5'-cyclic carbonate of thymidine could not be isolated leading to a 4-step synthesis involving CO_2 driven stereochemical inversion at the 3'-position (by an S_N2-type mechanism) to form the *cis*-3',5'-cyclic carbonate monomer of 3-*N*-methyl thymidine.

The ROP of the *cis*-configured thymidine-based monomer was investigated and found to proceed under mild reaction conditions with organocatalyst TBD and 4-MeBnOH alcohol initiator. The kinetic and thermodynamic parameters of the established concentration and temperature dependent equilibrium polymerisation were determined and MALDI-ToF MS of the thymidine-based polycarbonates revealed both linear and cyclic topologies. Thermal analysis revealed high glass transition temperatures (T_g ~156 °C) and a low onset of thermal degradation (T_{on}~ 170 °C). Static water contact angle measurements on polymer thin films were carried out and cell attachment studies with MG-63 cell line indicated potentially biocompatible materials.

Nevertheless, the need to protect the 3-*N* position of the nucleobase for monomer synthesis (and potentially ROP) was somewhat limiting. Protecting groups that could be removed post-polymerisation such as *tert*-butoxy carbonyl (Boc) groups would allow the hydrogen bonding (and thus self-assembly) and metal coordination capabilities of the pyrimidine to be accessed. Initial work carried out by Elizabeth M. Hierons (NatSci, 2016) verified that the Boc- group could be readily used as a nucleobase protecting group. However, under the I_2 in methanol silyl deprotection conditions, which generates HI in solution removal of the acid-labile Boc- group also occurred. Work reported by Simeone *et al.*,[48] (Scheme 4.05) is

however promising for the selective removal of a 4,4'-dimethoxytrityl (DMTr) 5'-hydoxyl protecting group in in the presence of a thymidine 3-*N*-Boc group using 2 equivalents of anhydrous $ZnBr_2$ in dry CH_2Cl_2. The detritylated Boc- protected thymidine derivative was isolated in 84% yield with only trace amounts of the Boc- cleaved product.

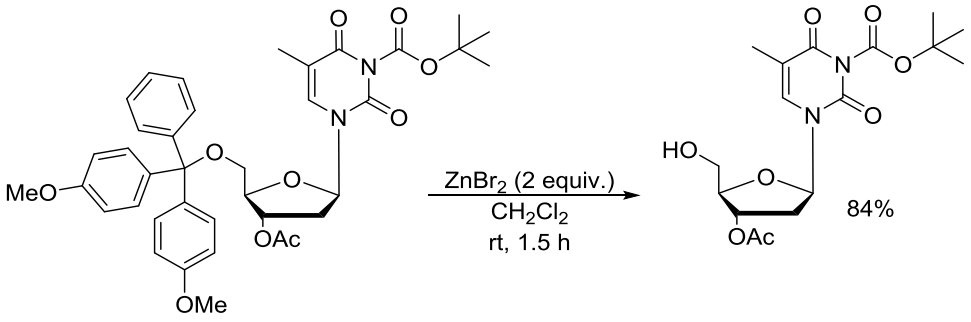

Scheme 4.05. DMTr- deprotection in the presence of a 3-*N*-Boc group reported by Simeone *et al*.[48] This exposes the 5'-OH group for CO_2 insertion and thus monomer synthesis. The acid labile Boc- group may be readily removed post-ROP.

The 3-*N*-position can also be protected as the benzoyl derivative, for which there is literature precedence for the post-polymerisation removal.[23] In fact, benzoylation carried out under the same reaction conditions used for the silylation and tosylation steps in the synthesis of **7** afforded **7-Bz** in fewer overall synthetic steps (Scheme 4.06). Preliminarily ROP experiments suggest that the added steric bulk of the benzoyl protecting group does not perturb the polymerisation with TBD catalyst and 4-MeBnOH alcohol initiator (M_n = 11 600 g mol^{-1}, Đ 1.33). A calculated $\Delta\Delta H_{ring\ strain}$ of -6.2 kcal mol^{-1} was comparable to the -5.2 kcal mol^{-1} computed for **7** at the same level of theory (rωb97xd/6-311++G(2d,p)/cpcm=dichloromethane/298 K).

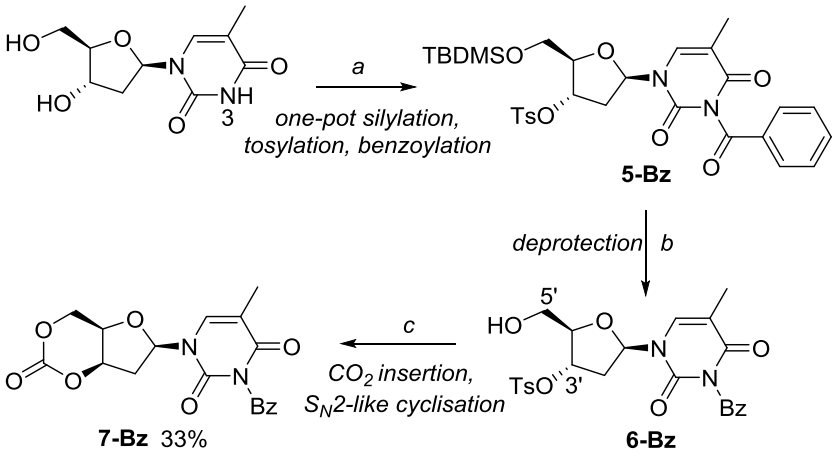

Scheme 4.06. Synthetic route to cyclic 3-*N*-benzoyl-3',5'-*O*-*cis*-carbonate-thymidine (**7-Bz**) carried out as part of this work: (a) i): TBDMSCl, pyr, DMAP, 12 h; ii: TsCl, 24 h; iii: BzCl, 12 h; (b) 1 wt% I_2 in MeOH, reflux, 2 h; (c) DBU, CO_2, MeCN, 0- 40 °C, 24 h. Carried out here to demonstrate the functionalisation potential of the 3-*N* nucleobase position.

In addition to groups that can be readily removed, the 3-*N*-position offers huge scope for functionalisation of the pendant arm with examples ranging from $Re(CO)_3$ complexes[49] to alkyne functionalities for click chemistry.[3, 50] Hence, future work will look to develop the functionalisation as well as protecting group strategies of the nucleobase and impart specific properties for targeted biomedical applications. For example, the introduction of a positive charge along the polymer backbone could improve cell attachment and spreading for tissue engineering scaffolds[51] as well as the binding of DNA plasmids for encapsulation and cell delivery.[52] Onofrio *et al.*[53] reported several examples of alkylation at the *N*-3 position with protected thymidine derivatives, including immobilisation of the thymidine to a solid support through the nucleobase (Figure 4.31A). This could be a simple means of introducing hydrophobicity and flexibility to the polycarbonates with long chain alkyl groups.

Aside from cyclic carbonates, there are reported examples of thymidine-derived *trans*-3',5'-cyclic species such as sultones[54] and boranophosphorothioates[55] (Figure 4.31B). Although this moves away from the utilisation of CO_2, the ROP of these cyclic species has not been investigated and may give rise to interesting polymer properties. Preliminary ring strain calculations for these potential monomers are comparable to those for **7**. The oxetane of thymidine has also been reported (Figure 4.31C),[56] formed by treatment of 3',5'-di-*O*-mesylthymidine with aqueous sodium hydroxide, and could be investigated for polycarbonate formation by the alternating copolymerisation with CO_2 in the presence of a suitable catalyst. Finally, scope should be widened to include other nucleosides (Figure 4.31D) and ultimately, base-paired polycarbonates may be envisaged.

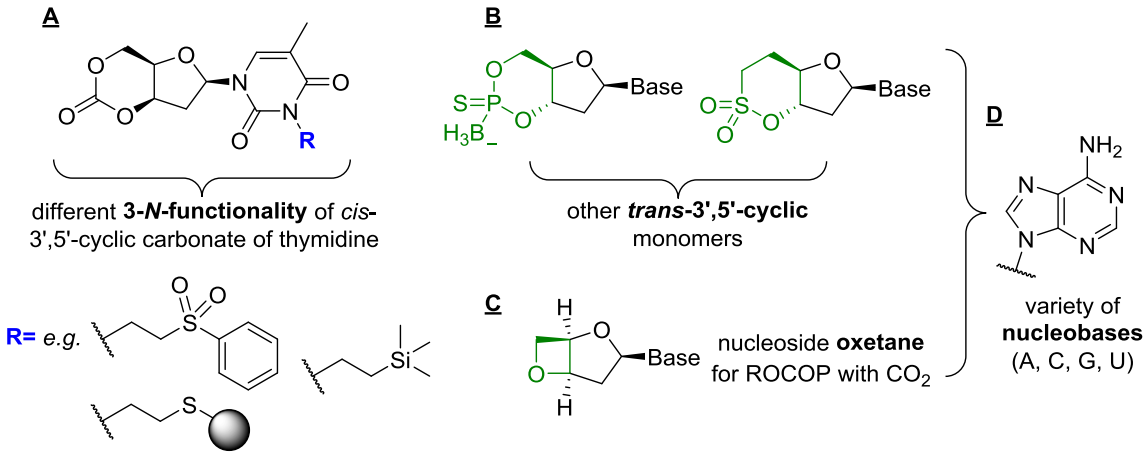

Figure 4.31. Future ideas for nucleoside derived cyclic monomers. **A:** Functionalisation at the 3-*N* position of thymidine with groups such as those shown based on work carried out by Onofrio *et al.* **B:** Different *trans*-configured 3',5'-cyclic monomers reported within the literature but not investigated for ROP. **C:** Oxetanes for ROCOP with CO_2. **D:** Cyclic monomers with adenine (A), cytosine (C), guanine (G) or uracil (U) nucleobases.

4.8. References

1. J. Shelton, X. Lu, J. A. Hollenbaugh, J. H. Cho, F. Amblard and R. F. Schinazi, *Chem. Rev.*, 2016, **116**, 14379-14455.
2. R. McHale and R. K. O'Reilly, *Macromolecules*, 2012, **45**, 7665-7675.
3. A. H. El-Sagheer and T. Brown, *Chem. Soc. Rev.*, 2010, **39**, 1388-1405.
4. S. Cheng, M. Zhang, N. Dixit, R. B. Moore and T. E. Long, *Macromolecules*, 2012, **45**, 805-812.
5. A. Poma, H. Brahmbhatt, J. K. Watts and N. W. Turner, *Macromolecules*, 2014, **47**, 6322-6330.
6. P. K. Lo and H. F. Sleiman, *J. Am. Chem. Soc.*, 2009, **131**, 4182-4183.
7. H. Kuang, S. Wu, Z. Xie, F. Meng, X. Jing and Y. Huang, *Biomacromolecules*, 2012, **13**, 3004-3012.
8. R. Bou Zerdan, P. Cohn, E. Puodziukynaite, M. B. Baker, M. Voisin, C. Sarun and R. K. Castellano, *J. Org. Chem.*, 2015, **80**, 1828-1840.
9. L. P. Jordheim, D. Durantel, F. Zoulim and C. Dumontet, *Nat. Rev. Drug. Discov.*, 2013, **12**, 447-464.
10. W. B. Wan and P. P. Seth, *J. Med. Chem.*, 2016, **59**, 9645-9667.
11. H. Isobe, T. Fujino, N. Yamazaki, M. Guillot-Nieckowski and E. Nakamura, *Org. Lett.*, 2008, **10**, 3729-3732.
12. C. Xing, H. Yuan, S. Xu, H. An, R. Niu and Y. Zhan, *ACS Appl. Mater. Interfaces*, 2014, **6**, 9601-9607.
13. B. Lippert and P. J. Sanz Miguel, *Acc. Chem. Res.*, 2016, **49**, 1537-1545.
14. G. S. Collier, L. A. Brown, E. S. Boone, B. K. Long and S. M. Kilbey, *ACS Macro Lett.*, 2016, **5**, 682-687.
15. A. S. Karikari, B. D. Mather and T. E. Long, *Biomacromolecules*, 2007, **8**, 302-308.
16. C. R. James, A. M. Rush, T. Insley, L. Vuković, L. Adamiak, P. Král and N. C. Gianneschi, *J. Am. Chem. Soc.*, 2014, **136**, 11216-11219.
17. I. H. Lin, C.-C. Cheng, C.-W. Huang, M.-C. Liang, J.-K. Chen, F.-H. Ko, C.-W. Chu, C.-F. Huang and F.-C. Chang, *RSC Adv.*, 2013, **3**, 12598-12603.
18. A. Jatsch, A. Kopyshev, E. Mena-Osteritz and P. Bäuerle, *Org. Lett.*, 2008, **10**, 961-964.
19. B. D. Mather, M. B. Baker, F. L. Beyer, M. A. G. Berg, M. D. Green and T. E. Long, *Macromolecules*, 2007, **40**, 6834-6845.
20. I. H. Lin, C.-C. Cheng, Y.-C. Yen and F.-C. Chang, *Macromolecules*, 2010, **43**, 1245-1252.
21. H. J. Spijker, F. L. van Delft and J. C. M. van Hest, *Macromolecules*, 2007, **40**, 12-18.
22. J. R. Tittensor, *J. Chem. Soc. (C)*, 1971, 2656-2662.
23. M. Suzuki, T. Sekido, S.-i. Matsuoka and K. Takagi, *Biomacromolecules*, 2011, **12**, 1449-1459.
24. J. M. Coull, D. V. Carlson and H. L. Weith, *Tetrahedron Lett.*, 1987, **28**, 745-748.
25. N. Calcerrada-Muñoz, I. O'Neil and R. Cosstick, *Nucleosides, Nucleotides and Nucleic Acids*, 2001, **20**, 1347-1350.
26. J. Sengupta and A. Bhattacharjya, *J. Org. Chem.*, 2008, **73**, 6860-6863.
27. K. K. Ogilvie and J. F. Cormier, *Tetrahedron Lett.*, 1985, **26**, 4159-4162.
28. J. R. Tittensor and P. Mellish, *Carbohyd. Res.*, 1972, **25**, 531-534.
29. Y. Shen, X. Chen and R. A. Gross, *Macromolecules*, 1999, **32**, 2799-2802.
30. K. Mikami, A. T. Lonnecker, T. P. Gustafson, N. F. Zinnel, P. J. Pai, D. H. Russell and K. L. Wooley, *J. Am. Chem. Soc.*, 2013, **135**, 6826-6829.
31. A. M. Michelson and A. R. Todd, *J. Chem. Soc.*, 1955, 816-823.
32. A. R. Vaino and W. A. Szarek, *Chem. Commun.*, 1996, 2351-2352.
33. W. Hua, C. Changmei, Z. Hongchao, L. Xiaohong, F. Chang, X. Shanshan and Z. Yufen, *Chem. Lett.*, 2005, **34**, 432-433.
34. I. Krizmanić, A. Višnjevac, M. Luić, L. Glavaš-Obrovac, M. Žinić and B. Žinić, *Tetrahedron*, 2003, **59**, 4047-4057.
35. J. Hiebl, E. Zbiral, J. Balzarini and E. De Clercq, *J. Med. Chem.*, 1990, **33**, 845-848.

36. T. S. Rao and C. B. Reese, *J. Chem. Soc., Chem. Commun.*, 1989, 997-998.
37. J. Adams, M. David and R. W. Giese, *Anal. Chem.*, 1986, **58**, 345-348.
38. C. Altona and M. Sundaralingam, *J. Am. Chem. Soc.*, 1972, **94**, 8205-8212.
39. C. Altona and M. Sundaralingam, *J. Am. Chem. Soc.*, 1973, **95**, 2333-2344.
40. L. J. Farrugia, *J. Appl. Cryst.*, 2012, **45**, 849-854.
41. J. Matsuo, K. Aoki, F. Sanda and T. Endo, *Macromolecules*, 1998, **31**, 4432-4438.
42. D. Myers, A. Cyriac and C. K. Williams, *Nat. Chem.*, 2016, **8**, 3-4.
43. M. Hong and E. Y. X. Chen, *Nat Chem*, 2016, **8**, 42-49.
44. S. Honda and H. Sugimoto, *J. Polym. Sci., Part A: Polym. Chem.*, 2016, **54**, 3336-3342.
45. C. K. Williams, L. E. Breyfogle, S. K. Choi, W. Nam, V. G. Young, M. A. Hillmyer and W. B. Tolman, *J. Am. Chem. Soc.*, 2003, **125**, 11350-11359.
46. B. M. Chamberlain, M. Cheng, D. R. Moore, T. M. Ovitt, E. B. Lobkovsky and G. W. Coates, *J. Am. Chem. Soc.*, 2001, **123**, 3229-3238.
47. M. Cheng, A. B. Attygalle, E. B. Lobkovsky and G. W. Coates, *J. Am. Chem. Soc.*, 1999, **121**, 11583-11584.
48. L. Simeone, L. D. Napoli and D. Montesarchio, *Chem. Biodivers.*, 2012, **9**, 589-597.
49. M. D. Bartholoma, A. R. Vortherms, S. Hillier, J. Joyal, J. Babich, R. P. Doyle and J. Zubieta, *Dalton Trans.*, 2011, **40**, 6216-6225.
50. K. Liu, L. Zheng, Q. Liu, J. W. de Vries, J. Y. Gerasimov and A. Herrmann, *J. Am. Chem. Soc.*, 2014, **136**, 14255-14262.
51. J. C. Courtenay, M. A. Johns, F. Galembeck, C. Deneke, E. M. Lanzoni, C. A. Costa, J. L. Scott and R. I. Sharma, *Cellulose*, 2016, **24**, 253-267.
52. S. Jung, T. P. Lodge and T. M. Reineke, *J. Phys. Chem. B*, 2017, **121**, 2230-2243.
53. J. D'Onofrio, L. De Napoli, G. Di Fabio and D. Montesarchio, *Synlett*, 2006, **2006**, 845-848.
54. P. A. Crooks, R. C. Reynolds, J. A. Maddry, A. Rathore, M. S. Akhtar, J. A. Montgomery and J. A. Secrist, *J. Org. Chem.*, 1992, **57**, 2830-2835.
55. P. Li and B. Ramsay Shaw, *Chem. Commun.*, 2002, 2890-2891.
56. J. P. Horwitz, J. Chua, M. A. D. Rooge, M. Noel and I. L. Klundt, *J. Org. Chem.*, 1966, **31**, 205-211.

Chapter 5

Ring-Opening Polymerisation and Copolymerisation of Cyclic Carbonates Derived from 2-Deoxy-D-Ribose and CO_2

5. Ring-Opening Polymerisation and Copolymerisation of Cyclic Carbonates Derived from 2-Deoxy-D-Ribose and CO_2

5.1. Introduction

Many natural sugars bear multiple hydroxyl groups and although this offers advantages for introducing functionality and modifying polymer properties, protecting group chemistry is often required to avoid undesired side reactions during monomer synthesis and ring-opening polymerisation (ROP). The need for multiple protection-deprotection sequences to selectively expose primary, secondary or anomeric hydroxyl groups entails extra synthetic steps and can reduce the overall efficiency and scalability of the monomer and polymer synthetic routes.[1, 2] 2-Deoxy-D-ribose is a readily accessible and simple pentose sugar consisting of a single anomeric hydroxy group, in addition to those required for cyclic carbonate formation. Further to the functionalisation potential, the chirality of this anomeric centre coupled to the rigid monosaccharide ring is attractive for imparting tacticity as well as stiffness to the polymer backbone. The impact of tacticity on polymer properties is well-known for example with poly(methylmethacrylate) (PMMA), polypropylene[3] and poly(lactic acid).[4, 5] Whereas isotactic poly(lactic acid) is crystalline with a melting point of 170-180 °C and a glass transition temperature (T_g) of ~60 °C, the atactic equivalent is amorphous with a T_g of ~50 °C.

In its thermodynamically favoured six-membered pyranose ring form, 2-deoxy-D-ribose consists of a *cis*-1,2-diol, the cyclocarbonation of which would yield a five-membered cyclic carbonate *cis*-fused to the pyranose ring (Figure 5.01). The low ring strain of five-membered cyclic carbonates often means that forcing ROP conditions are required that result in decarboxylation and subsequently ether linkages in the polymer backbone. This can have a detrimental effect on the polymer properties.[6] Reports of five-membered cyclic carbonates that undergo ROP under mild reaction conditions and without the elimination of CO_2 consist of bicyclic structures where the carbonate is *trans*-fused to for example, a cyclohexane[7] or cyclohexene ring.[8]

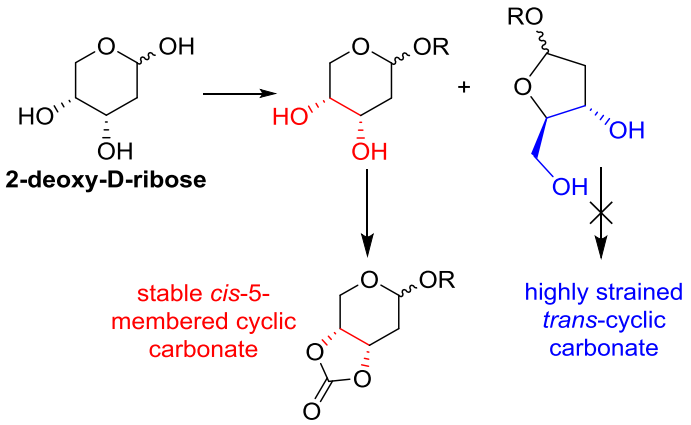

Figure 5.01. Challenges in the synthesis of cyclic carbonate monomers from 2-deoxy-D-ribose. In its pyranose ring form, 2-deoxy-D-ribose, protected or functionalised at the anomeric position consists of a *cis*- configured vicinal diol for cyclic carbonate formation. Such bicyclic *cis*-fused cyclic carbonates often require forcing conditions for ROP. In its furanose ring form, 2-deoxy-D-ribose consists of a *trans*- 1,3-diol, cyclocarbonation of which is notoriously challenging.

Endo and co-workers[9, 10] reported the anionic ROP of the *trans*-configured five-membered cyclic carbonate of methyl-4,6-*O*-benzylidene-α-D-glucopyranoside (MBCG, Figure 5.02) using alkoxide and 1,8-diazabicyclo[5.4.0]undec-7-ene (DBU) initiators at temperatures below 30 °C without any evidence of decarboxylation. For a polymerisation carried out at room temperature in THF solvent with sodium *tert*-butoxide initiator, a high conversion (>99%) was reported within 30 seconds, yielding a polycarbonate with number average molecular weight (M_n) of 16 000 g mol^{-1} and polydispersity (Đ) of 1.99. Tezuka *et al.*[11] later showed that the five-membered cyclic carbonate *trans*-fused to the pyranose ring in α-D-galactose (MBCGa, Figure 5.02) also underwent ROP, in DMF at 90 °C with DBU and BnOH initiator or using *t*-BuOK, to yield polycarbonates of M_n 4 000 g mol^{-1} (Đ 1.68). However, the analogous *cis*-fused monomer of mannopyranose (MBCM, Figure 5.02) had insufficient ring strain and gave quantitative recovery of the cyclic carbonate under the range of anionic ROP conditions investigated. Cyclocarbonation of the protected pyranosides was carried out using ethyl chloroformate and triethylamine following the method reported for D-glucose by Rist and coworkers.[12]

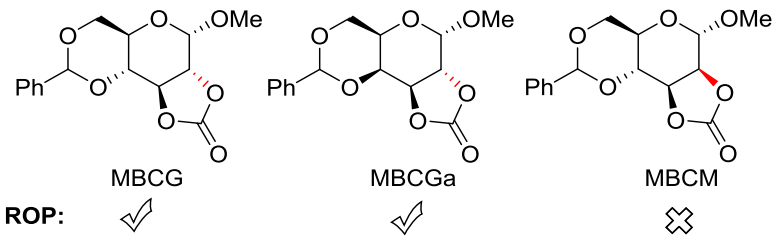

Figure 5.02. Five-membered cyclic carbonates prepared from protected glucose, galactose, and mannose pyranose sugars. Only the *trans*-configured cyclic carbonates had sufficient ring strain to undergo anionic ROP to polycarbonates under mild reaction conditions (≤ 90 °C). For MBCM, quantitative recovery of the monomer was observed.[9-11]

In its five-membered furanose form (Figure 5.01), 2-deoxy-D-ribose would expose a *trans*-1,3-diol for six-membered cyclic carbonate formation. However, cyclocarbonation of this motif, with retention of stereochemistry, is notoriously challenging due to the highly strained and unstable nature of the cyclic carbonate *trans*-fused to the furanose ring (see Chapter 4).

5.1.1. Copolymers of sugar-based cyclic carbonates

Copolymerisation provides a means of tailoring polymer properties such as degradation rates and T_g for designing materials with wider potential applications. For example, poly(trimethylene carbonate) (PTMC), prepared by the ROP of trimethylene carbonate (TMC), is a flexible, hydrophobic and non-crystalline polymer exhibiting a T_g between -20 and -30 °C.[13, 14] The fine-tuning of these properties has been extensively studied through copolymerisation with for example 2,2-dimethyltrimethylene carbonate,[15] lactide,[16, 17] glycolide[18] and caprolactone.[19] The rigid furanose and pyranose rings of some carbohydrate-derived monomers (when retained on polymerisation) alongside the functionality and stereochemistry of substituents about the ring can be well placed to impart stiffness, chirality, and functionality into the backbone of copolymers.[1] In addition, some sugar-derived monomers, such as the tetra-substituted-1,6-lactones from D-galactose or D-glucose, described in Chapter 1 (Section 1.5.2), do not readily undergo homopolymerisation and can only be incorporated into polymer chains through copolymerisation.[20, 21]

In 1999, Gross and coworkers reported the copolymerisation of the D-xylose derived cyclic carbonate (IPXTC) with both TMC[22] and L-lactide[23] (Figure 5.03). Of the organometallic catalysts evaluated for the copolymerisation with L-lactide, tin(II) 2-ethylhexanoate ($Sn(Oct)_2$) gave the highest molecular weight copolymers. After 6 hours at 120 °C in toluene, molecular weights of 78 400 g mol^{-1} (Đ 1.9) were reported for a 200:1 total monomer-to-initiator feed ratio. However, the lactide showed a much higher (20-fold) reactivity compared to IPXTC and the copolymer contained only 7% xylose content, less than half of that in the monomer feed. Higher xylose content, up to 39 mol% was achieved with a greater ratio of IPXTC to lactide in the feed (64:36) but in lower 48% yield (compared to 82% above) and with a significantly decreased M_n (13 900 g mol^{-1}, Đ 1.7). This greater IPXTC content did however, result in a higher T_g of 89 °C compared to 63 °C for the 7 mol% random copolymer. Partial deprotection of the ketal groups, to introduce free hydroxyl groups along the copolymer backbone was achieved with aqueous trifluoroacetic acid. For poly(L-lactide-

co-8mol%-IPXTC) of starting M_n 70 200 g mol^{-1} (Đ 2.3), removal of 62 mol% of the protecting groups gave a polymeric material of M_n 64 700 g mol^{-1} (Đ 2.2) but further removal (86 mol%) resulted in hydrolysis of the ester linkages and a decrease in the copolymer molecular weight to 33 200 g mol^{-1} (Đ 3.0).

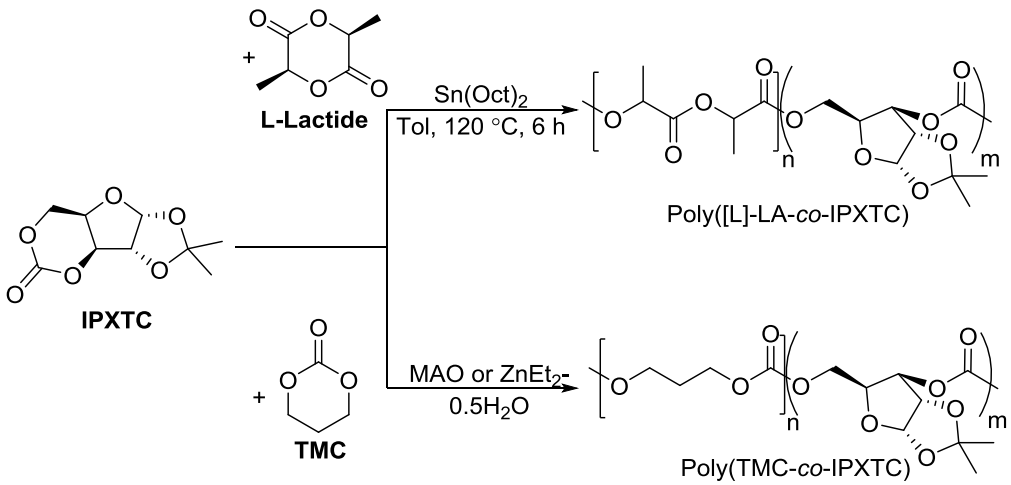

Figure 5.03. Ring-opening copolymerisation of 1,2-*O*-isopropylidene-D-xylofuranose-3,5-cyclic carbonate (IPXTC) with L-lactide using tin(II) octanoate and trimethylene carbonate (TMC) with methylaluminoxane (MAO) or $ZnEt_2$-0.5H_2O catalysts.[22, 23]

In contrast, $Sn(Oct)_2$ showed poor activity for the copolymerisation of IPXTC with TMC, where methylaluminoxane (MAO) and $ZnEt_2$-0.5H_2O catalysts were found to give the most promising results in terms of polymer molecular weights and yields (though lower than for the copolymerisation with L-lactide). For a $ZnEt_2$-0.5H_2O catalysed polymerisation at 90 °C, with 32 mol% IPXTC content in the feed, conversions of 98% were reported (after 4 hours) for both comonomers giving a copolymer of M_n 19 300 g mol $^{-1}$ (Đ 2.0). For a MAO-catalysed polymerisation carried out at the same temperature, with a 50:50 feed ratio of comonomers, an M_n of 20 600 g mol^{-1} (Đ 2.7) was reported with 43 mol% IPXTC repeat units. A single T_g was reported for all copolymers, ranging from 3 to 109 °C with varying copolymer composition from 8 to 83 mol% IPXTC content, respectively.

Gross and coworkers[24] also reported the synthesis and copolymerisation of the spiro six-membered cyclic carbonate derived from D-glucose in its furanose form (Scheme 5.01).[25*] The monomer 1,2-*O*-isopropylidene-3-benzyloxy-pentofuranose-4,4'-cyclic carbonate (IPPTC) was prepared in 65% yield using ethyl chloroformate carbonylating agent.

[*] By oxidation of 1,2-*O*-isopropylidene-α-D-glucofuranose to the aldehyde and subsequent reaction with formaldehyde and NaOH to form the spiro diol.[25]

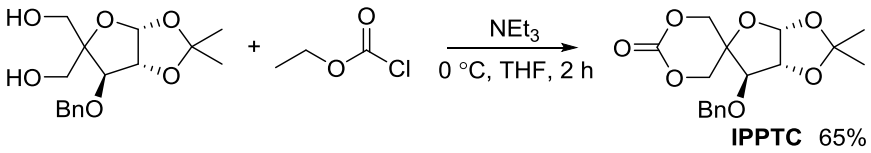

Scheme 5.01. Synthesis of IPPTC monomer from benzyl ether and ketal-protected D-glucofuranose derivative, as reported by Gross and coworkers.[24]

Following copolymerisation with L-lactide, in the bulk at 130 °C using $Sn(Oct)_2$, removal of the ketal- or benzyl ether protecting groups could be carried out selectively to strategically introduce one, two or three hydroxyl groups along the copolymer backbone (Scheme 5.02).

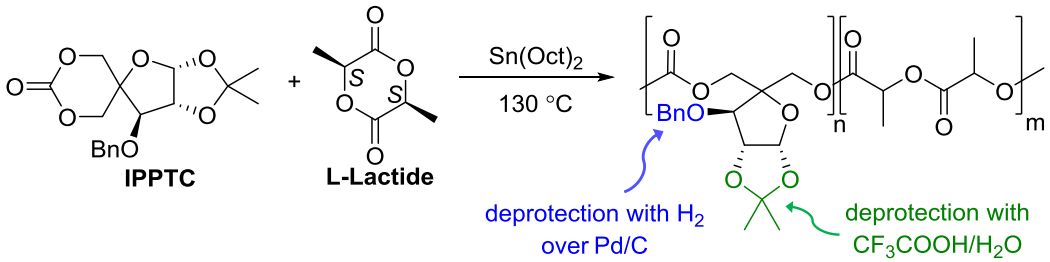

Scheme 5.02. Copolymerisation of IPPTC with L-lactide in the bulk at 130 °C using $Sn(Oct)_2$. Removal of the benzyl ether alcohol protecting group or ketal-diol protecting group was carried out selectivity to introducing different numbers of free hydroxyl groups into the IPPTC segment of the "blocky" copolymers.[24]

Under these polymerisation conditions ($[M]_0/[C]_0$=400), blocky copolymers composed of 4 to 21 mol% pentofuranose glucose content were prepared. As for the D-xylose derived cyclic carbonate (IPXTC), IPPTC showed a lower reactivity compared to the L-lactide comonomer and after 6 hours with 9 mol% IPPTC in the feed, near quantitative conversion of L-lactide was observed compared to 32% for IPPTC. Longer reaction times of up to 18 hours led to higher IPPTC conversions (49%) but resulted in lower M_n (51 500 compared to nearly 80 000 g mol^{-1} after just 6 hours). Alongside a broadening of the molecular weight distribution from 1.9 to 2.3, these observations were attributed to thermal depolymerisation and intermolecular transesterification reactions with the poly(L-lactic acid) segments.

Compared to poly(L-lactic acid) (M_n 84 400 g mol^{-1}, Đ 2.14), which exhibited a melting temperature (T_m) of 175 °C, a T_g of 58 °C and the onset of thermal degradation (T_{on}) at ~258 °C, incorporation of IPPTC into the backbone, resulted in both higher thermal stabilities (T_{on}= 290 °C for 4 mol%) and glass transition temperatures (T_g= 61 °C for 14 mol%) but lower melting temperatures (T_m= 112 °C for 14 mol%). For a copolymer (M_n 77 800 g mol^{-1}, Đ 1.95) composed of 4 mol% IPPTC content, selective debenzylation by hydrogenation with

Pd/C removed 90% of the benzyl ether groups (M_n 74 700 g mol^{-1}, Đ 2.26) and reduced the onset of thermal degradation from 290 to 275 °C. The debenzylated derivative however, had minor impact on both the copolymer melting (T_m= 160 °C) and glass transition temperatures (T_g= 58 °C) compared to the fully protected copolymer. Complete exposure of the vicinal diols in the IPPTC segments of the same copolymer, using TFA and H_2O (M_n 66 000 g mol^{-1}, Đ 1.62), also lowered the thermal stability (T_{on}= 193 °C) and had insignificant impact on the melting and glass transition temperatures. Deprotection of the ketal or benzyl ether groups was also reported to affect the crystallisation kinetics of the copolymers.

5.2. Monomer Synthesis

5.2.1. Trans-3,5-cyclic carbonate of 2-deoxy-D-ribofuranose

The methyl- and benzyl- furanosides of 2-deoxy-D-ribose (**8-Me** and **8-Bn**, Scheme 5.03) were prepared under acid catalysed and kinetically controlled reaction conditions according to the literature procedures.[26, 27] Both methyl- and benzyl- protected 1,3-diols were isolated as a roughly 50:50 mixture of α- and β- anomers and consisted of 10-11% of the thermodynamically more favoured pyranosides (**8'-Me** and **8'-Bn**). Commercially available 1-*O*-methyl-2-deoxy-D-ribofuranoside (**8-Me**) was also found to consist of ~11% of the 6-membered ring impurity. This could be reduced (to around 6%) over several days following a patented procedure[28] that takes advantage of the selective oxidative cleavage of 1,2-diols in the presence of sodium periodate to form a di-aldehyde and sodium salt, which was readily removed by filtration.

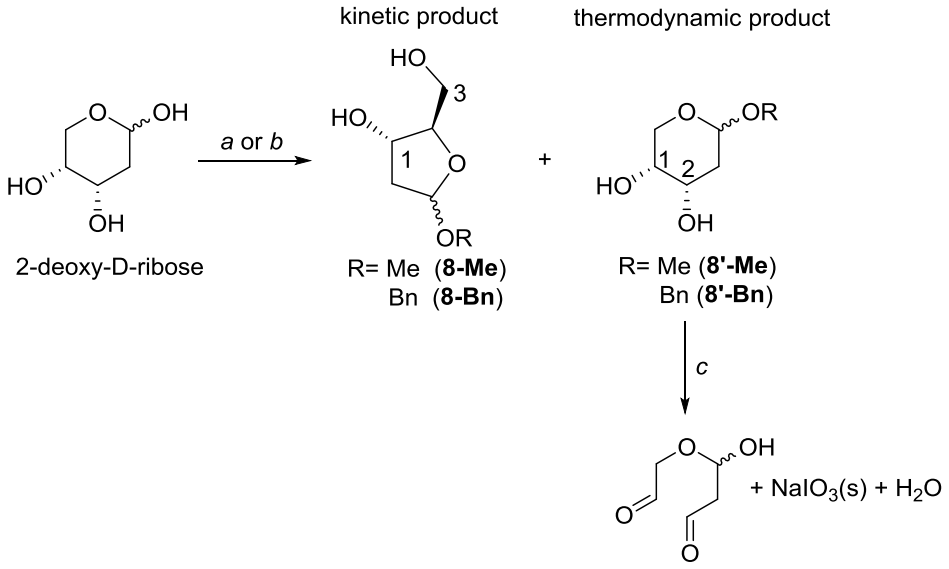

Scheme 5.03. Synthesis of the *O*-methyl and *O*-benzyl furanosides of 2-deoxy-D-ribose (kinetic product) with *a*: CH_3COCl, MeOH, -18 °C, 12 h[26] or *b*: BnOH, HCl, rt, 10 mins.[27] Removal of the pyranoside thermodynamic by-product by selective oxidative cleavage of the 1,2- diol in the presence of the 1,3-diol with *c*: $NaIO_4$ (2 equiv.), MeCN, rt, 5 days.[28]

Cyclocarbonation of the methyl and benzyl ribofuranosides (**8-Me** and **8-Bn**), with retention of the *trans*-stereochemistry, was attempted *via* the nucleophilic addition-elimination pathway outlined in Chapter 2, involving DBU-facilitated CO_2 insertion followed by tosylation and intramolecular cyclisation (Scheme 5.04). Only the five-membered cyclic carbonates *cis*- fused to the ribopyranose ring (**9'-Me** and **9'-Bn**) were isolated and in low yield (~11%).[†] This was confirmed by NMR spectroscopy and for the *O*-benzyl anomeric substituent by single-crystal X-ray diffraction.

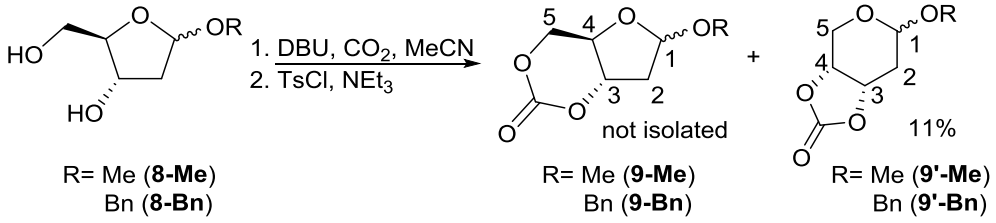

Scheme 5.04. Attempted synthesis of the *trans*-3,5-cyclic carbonate of 1-*O*-methyl/benzyl-2-deoxy-D-ribofuranoside, with CO_2 and TsCl in the presence of DBU and NEt_3 bases, led to the isolation of the undesired *cis*-3,4-cyclic carbonates (**9'-Me** and **9'-Bn**).

Characteristic of a five-membered cyclic carbonate, the carbonyl resonance in **9'-Bn** and **9'- Me** appeared at 154 ppm in the $^{13}C\{^1H\}$ NMR spectra. In addition, carbon environments consistent with a pyranose ring were also observed at ~95, 71-74, 59 and 30 ppm, assigned

[†] From **8'-Bn** (prepared under thermodynamic reaction conditions) the five-membered cyclic carbonate (**9'-Bn**), was prepared in 72% yield *via* this method.

to the anomeric carbon (C-1), C-3 or C-4, and the two pyranose ring methylene carbons (C-5 and C-2), respectively. For comparison, six-membered cyclic carbonates typically give rise to a carbonate environment at ~147 ppm and the carbon environments in furanose rings generally appear at about 105 (C-1), 70-80 (C-3, C-4), 67 (C-5) and 42 (C-2) ppm. Single-crystal X-ray diffraction of crystals of **9'-Bn**, grown by layering hexanes over $CDCl_3$, confirmed the pyranose ring structure and *cis*-configured 5-membered cyclic carbonate. Shown in Figure 5.04, the twist-boat conformation of the pyranose ring results in an almost eclipsing interaction of H-3 and H-4, which may (if retained in solution) account for the $^3J_{34}$ coupling constant of 8.2 Hz observed in the ^{1}H NMR data (Karplus equation). Attempts at ROP with acid catalyst (HCl), organocatalyst TBD and $Sn(Oct)_2$ were unsuccessful and supported the anticipated low ring-strain of the cyclic carbonate. DFT computations (rωb97xd/6-311++G(2d,p)/cpcm=dichloromethane/298 K protocol) of the enthalpy of ring-opening with dimethyl carbonate (DMC) gave a $\Delta\Delta H_{ring\ strain}$ of -3.6 kcal mol^{-1} for **9'-Bn** compared to, at the same level of theory, -9.5 and -5.2 kcal mol^{-1} for the ring-opened D-mannose and thymidine derived six-membered cyclic carbonates (Chapters 3 and 4), respectively. Formation of **9'-Me** or **9'-Bn** was observed despite the near complete removal of the pyranose impurity in the starting material and suggested that interconversion of the furanose to the pyranose ring form may be occurring to some extent under the reaction conditions.

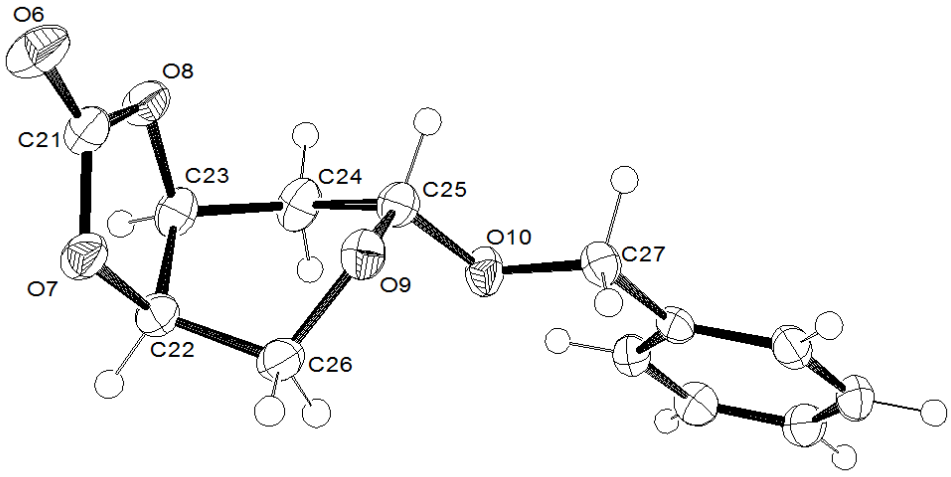

Figure 5.04. ORTEP[29] drawing of the crystal structure of the *cis*- configured five-membered cyclic carbonate of 1-*O*-benzyl-2-deoxy-D-ribopyranoside (**9'-Bn**) with thermal ellipsoids at the 50% probability level and key atoms labelled. Selected bond lengths (Å) and angles (°): O(8)-C(23) 1.458(2), O(7)-C(22) 1.4529(19), O(7)-C(21) 1.336(2), O(8)-C(21) 1.339(2), O(6)-C(21) 1.195(2), C(22)-C(23) 1.534(3), O(10)-C(25) 1.4115(19), C(23)-C(24)-C(25)-O(9) 20.7(2), C(26)-O(9)-C(25)-C(24) 38.61(18), C(26)-C(22)-C(23)-C(24) 16.8(2), C(25)-O(9)-C(26)-C(22) -72.56(17), C(23)-C(22)-C(26)-O(9) 40.61(19).

Experimental evidence for formation of the desired six-membered cyclic carbonate, **9-Me** was tentatively observed by $^{13}C\{^{1}H\}$ NMR spectroscopy of column fractions isolated in ~13% yield but composed of at least 50% of the inseparable **9'-Me** by-product. Furthermore, high resolution electrospray ionisation mass spectrometry (HR-MS(ESI)) in methanol of the crude reaction mixture showed ions assigned to the unreacted sugar, dimeric, trimeric and tetrameric carbonate species as well as a methanol ring-opened cyclic carbonate. The latter was not observed in the HR-MS(ESI) of the isolated five-membered cyclic carbonate but was a common occurrence of the six-membered cyclic carbonates synthesised throughout this work. However, variation of the reaction conditions to include temperature, time, choice of solvent, DBU equivalents and the order of addition of reagents, led to no further improvements in the occurrence or isolation of the suspected **9-Me** product, which could not be separated from the five-membered cyclic species. Attempts with other carbonylating agents namely, carbonyldiimidazole (CDI) in CH_2Cl_2 at room temperature or THF at 60 °C, bis(pentaflurophenyl) carbonate with CsF in THF at 60 °C as well as the CeO_2/2-cyanopyridine method reported by Honda *et al*.[30] with CO_2 at 8 bar pressure and 100 °C, gave no evidence for formation of the desired product.

5.2.2. Cis-3,5-cyclic carbonate from 2-deoxy-D-ribose

In a similar fashion to the synthesis of the *cis*-thymidine based monomer in Chapter 4, and following kinetic trapping of the sugar ring in its furanose form by methylation of the anomeric hydroxyl group, sequential silyl protection of the 5-position and tosylation of the 3-position was carried out in the same reaction pot (Step *a*, Scheme 5.05).[31] The minor protected pyranose ring impurity was removed *via* a silica plug with CH_2Cl_2 eluent. Subsequent removal of the silyl group in **10** by refluxing with I_2 in MeOH gave a 78% yield of the deprotected 3-tosyl product **11** (Step *b*, Scheme 5.05). The high sensitivity of the furanose ring (particularly regarding conversion to the pyranose form) meant harsher reagents namely, *n*-Bu_4NF (TBAF) resulted in substantially lower isolated yields (<30%). Under the deprotection conditions used and for an anomerically pure sample of **10**, mutarotation of the α- to the β- anomer (and *vice versa*) was observed and for the *O*-benzyl furanosides, interchange of the -OBn group with the methanol solvent.

Monomer (**12**) was then prepared as a roughly 50:50 mixture of α- and β- anomers following CO_2 insertion (at 1 atm pressure) using DBU reagent into the then exposed primary hydroxyl

group (Step *c*, Scheme 5.05). *In situ* cyclisation proceeded at room temperature (rt) by an intramolecular S_N2-like displacement of the tosyl leaving group with the carbonate nucleophile, resulting in stereochemical inversion at the 3-position. The α- and β- anomers of the subsequently *cis*-configured six-membered cyclic carbonates, were separated by column chromatography into α- and β-rich fractions and purified by recrystallisation from either dry ether or toluene, respectively.

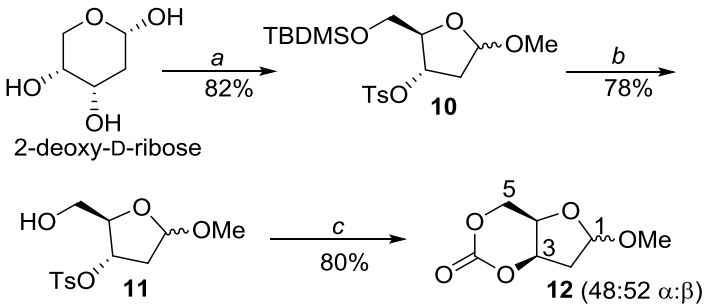

Scheme 5.05. Synthesis of **12α** and **12β** from 2-deoxy-D-ribose: *a*: i) MeOH, HCl, 0.5 h ii) TBDMSCl (1.1 equiv.), pyridine, cat. DMAP (0.1 equiv.), 2 h iii) TsCl (1.1 equiv.), 12 h; *b*: 1 wt% I_2 in MeOH, reflux, 4 h; *c*: DBU (1 equiv.), CO_2 (1 atm), MeCN, 0° to rt, 24 h.

Both **12α** and **12β** were fully characterised by elemental analysis, NMR and FTIR spectroscopies, HR-MS(ESI) and single-crystal X-ray diffraction. *J*-coupling constants ($^3J_{34}$) in the ^{1}H NMR spectra of 4.9 and 5.7 Hz for the α- and β- anomers, respectively was consistent with a *cis*- configured six-membered cyclic carbonate. This was further confirmed by single crystal X-ray diffraction of crystals grown by layering hexanes over chloroform. The furanose ring in **12β** adopts a 2-exo (E_2) envelope conformation whereby C5 puckers below the plane formed by C4-C3-O4-C6 (dihedral angle ~2°) (Figure 5.05, right). In contrast, the α-anomer adopts a more twisted conformation ($^0T_1/E_1$), with C6 below and O4 above the plane formed by C5-C4-C3 (Figure 5.05, left). This difference in conformation of the ribofuranose ring later proved to have a marked impact on the ring strain and thus ROP reactivity of the fused cyclic carbonate.

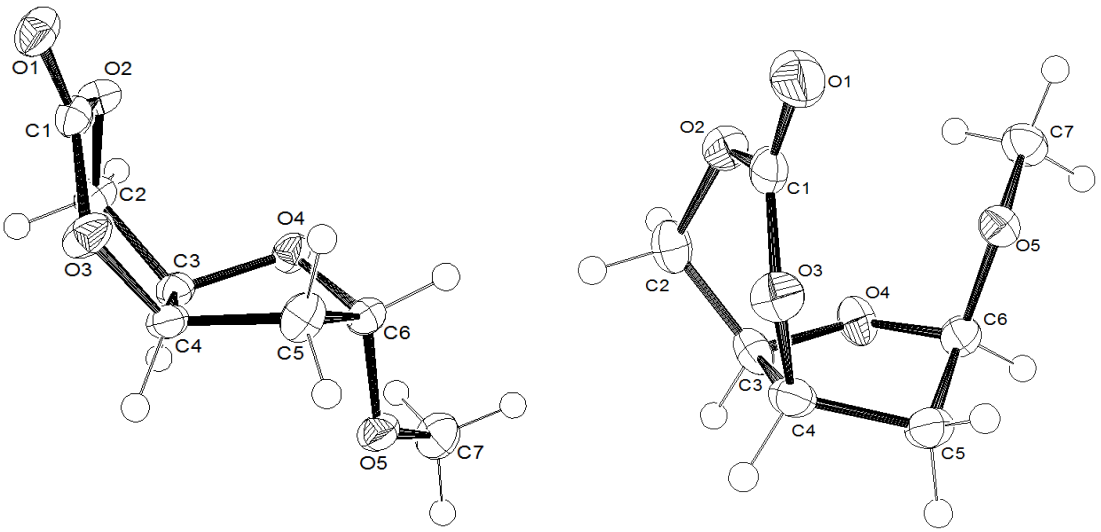

Figure 5.05. ORTEP[29] drawings with thermal ellipsoids at the 50% probability level for **12α** (left); selected bond lengths (Å) and torsion angles (°): C(1)-O(1) 1.1985(19), C(1)-O(2) 1.3325(19), C(1)-O(3) 1.342(2), O(4)-C(3)-C(4)-C(5) -9.34(15), C(3)-C(4)-C(5)-C(6) -14.60(15), C(4)-C(5)-C(6)-O(4) 34.21(15), C(5)-C(6)-O(4)-C(3) -41.74(15), C(4)-C(3)-O(4)-C(6) 31.81(15) and **12β** (right); selected bond lengths (Å) and torsion angles(°): O(2)-C(1) 1.333(2), O(1)-C(1) 1.1995(19), O(3)-C(1) 1.333(2), C(3)-O(4)-C(6)-C(5) 22.07(16), C(6)-O(4)-C(3)-C(4) -1.96(17), O(4)-C(3)-C(4)-C(5) -18.81(17), C(3)-C(4)-C(5)-C(6) 31.09(16), O(2)-C(6)-C(5)-C(4) -32.95(16).

5.3. Homopolymerisation

The ROP of **12α** was carried out with 1,5,7-triazabicyclo[4.4.0]dec-5-ene (TBD) organocatalyst and benzyl alcohol initiator (Scheme 5.06). Over a range of initial monomer concentrations ($[M]_0$ = 1-5 mol L^{-1}), catalyst loadings (0.1-2 mol%) and monomer-to-initiator feed ratios ($[M]_0/[I]_0$ = 50-1000), the polymer precipitated from the polymerisation solution and was found to be highly insoluble in many common organic solvents as well as water, DMF and DMF/LiBr. Solubility in hexafluoroisopropanol (HFIP) however, enabled estimation of the M_n and polydispersity by size-exclusion chromatography (SEC). For a polymerisation with $[M]_0$ of 5 mol L^{-1} in CH_2Cl_2, $[M]_0/[I]_0$ of 400 and 0.25 mol% catalyst loading, the polymer precipitated after 1 hour and had an M_n of 25 600 g mol^{-1} (Đ 1.41) relative to PMMA standards.

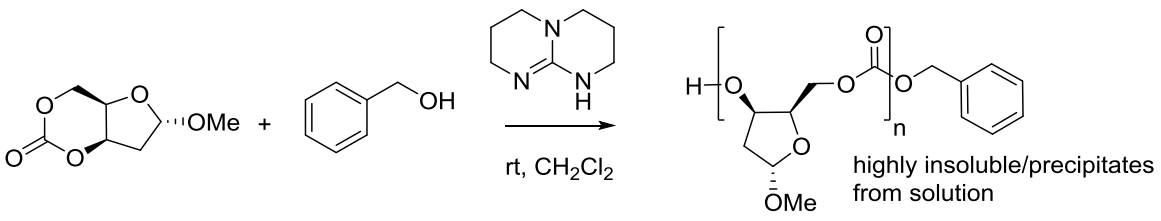

Scheme 5.06. ROP of **12α** with benzyl alcohol initiator and TBD catalyst carried out room temperature in CH_2Cl_2 solvent. The polymer was insoluble in common organic solvents, water and DMF but soluble in HFIP.

MALDI-ToF mass spectrometry of this polymer revealed a ~46:54 mixture of both linear and cyclic polycarbonate species, respectively but of much lower M_n (Figure 5.06). This may be due to PMMA being a poor standard for the ribose-based polycarbonates or difficulties in ionising higher M_n species during the MALDI process.

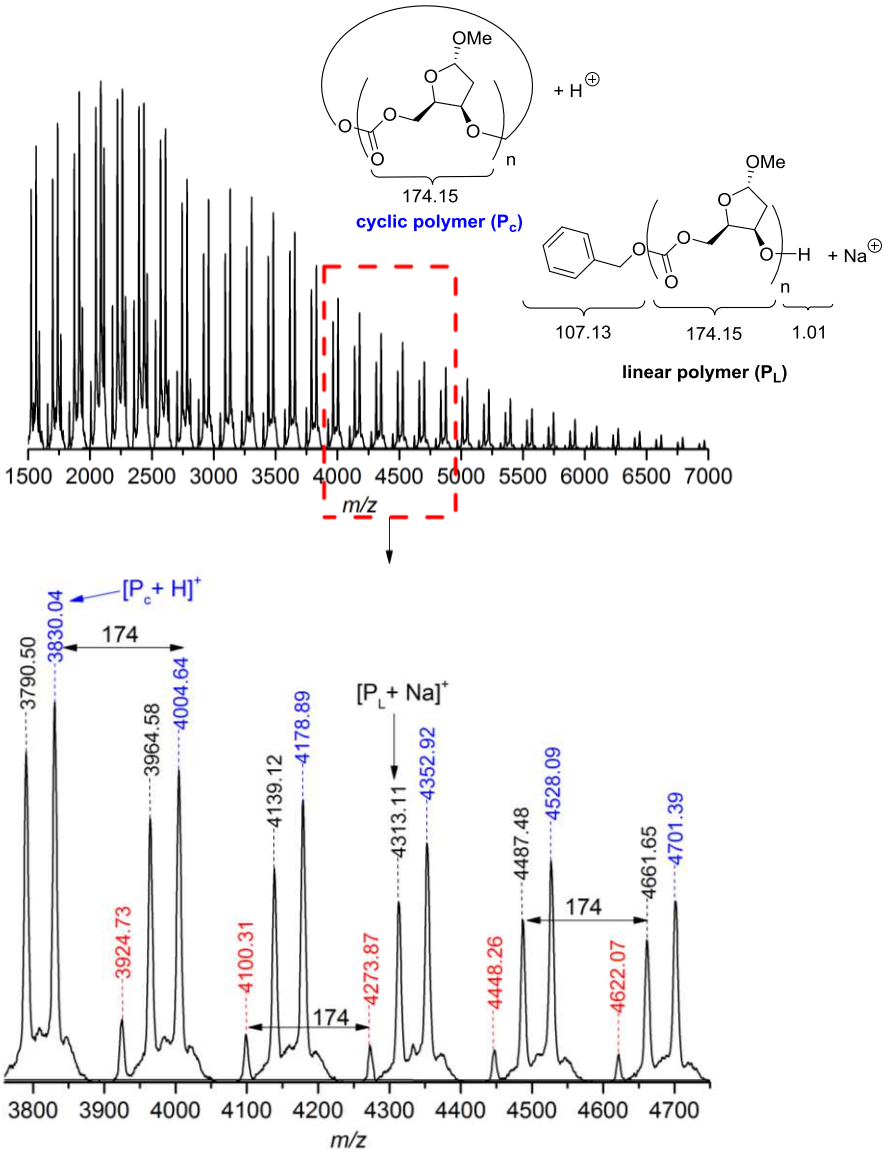

Figure 5.06. MALDI-ToF MS of poly(**12*α***) showing cyclic polymeric series $[P_c + H]^+$ (e.g. DP = 26 gives *m/z* 4528.91) and linear polymer series with benzyl alcohol and -OH end-groups, $[P_L + Na]^+$ (e.g. DP = 24 gives *m/z* 4310.73). The less intense red series may be assigned to the sodium adduct of the linear polymer with the loss of 1 CO_2 molecule.

NMR and SEC analysis of the supernatant of the polymerisation reaction mixture revealed unreacted monomer and lower molecular weight oligomers (M_n ~1150 g mol^{-1}). At a lower catalyst and initiator loading ($[M]_0$:$[TBD]_0$:$[BnOH]_0$ = 1000:1:1; $[M]_0$ = 5 mol L^{-1}), monomer conversion could be monitored before polymer precipitation, by integration of the ^{1}H NMR spectra in $CDCl_3$ of aliquots taken and quenched with benzoic acid. A plateau was

reached at 60% **12α** conversion (Figure 5.07), to which the addition of further monomer led to the establishment of a new equilibrium monomer conversion. This indicated no catalyst deactivation and suggested a concentration dependent equilibrium polymerisation (as also observed for the thymidine-based monomer in Chapter 4).

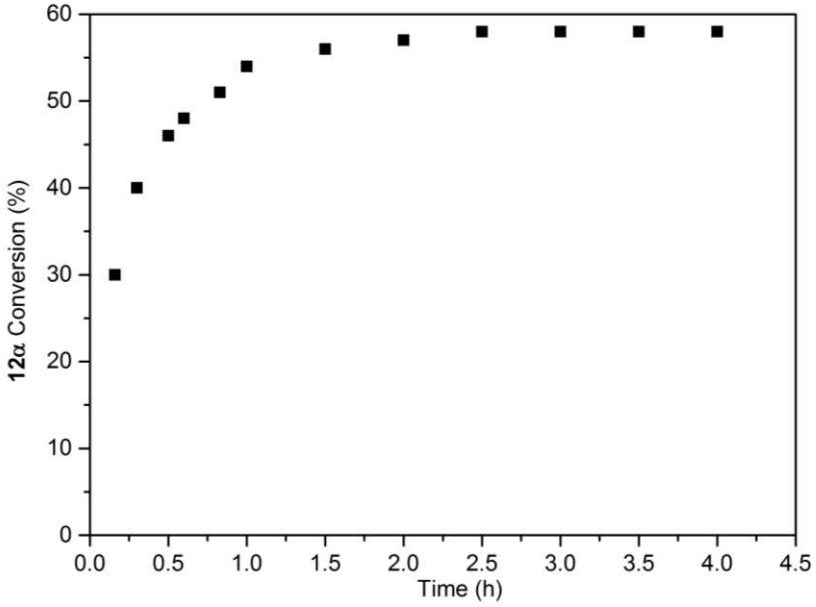

Figure 5.07. Monomer conversion as a function of time prior to precipitation of the polymer from the reaction solution. The polymerisation was carried out at rt with $[M]_0$= 5 mol L^{-1} and $[M]_0$: $[TBD]_o$: $[BnOH]_0$ of 1000:1:1. Monomer conversion was determined by relative integration of the ring methylene H-2 protons (2.41 ppm in the monomer *versus* 2.31 ppm in the polymer) in the ^{1}H NMR spectra (400 MHz, $CDCl_3$) of aliquots taken at specific time intervals and quenched with benzoic acid.

Under melt conditions (T_m **12α** = 67-68 °C) and with a 0.25 mol% catalyst and initiator loading, an equilibrium monomer conversion of 51% was observed and an M_n of 22 300 g mol^{-1} (Đ 1.21) determined by SEC *versus* PMMA standards. Reliable determination of the ROP thermodynamic parameters however, was complicated by the precipitation of the polymer from solution, especially at low temperatures.

Comparison of the ^{1}H NMR spectra of the monomer (Figure 5.08A) to that of the polymer in HFIP-d_2 (Figure 5.08B), showed a characteristic broadening of the proton signals on ROP to the polymer alongside a coalescing of the methylene environments in the furanose ring (H-2 and H-2') and cyclic carbonate (H-5 and H-5'). This was attributed to the release of ring-strain in the monomer and subsequent conformational reorganisation in the polymer. Estimation of the molecular weight by relative integration of the H-2 signals to those of the benzyl alcohol end-group gave an M_n (87 200 g mol^{-1}) much larger than that predicted based

on the monomer-to-initiator feed ratio ($M_{n,\,calc}$ = 41 900 g mol^{-1}) and is consistent with the presence of cyclic polymeric species bearing no end-group functionality. The carbonate region of the $^{13}C\{^{1}H\}$ NMR spectrum (Figure 5.08C) revealed three carbonate signals at 154.3, 154.0 and 153.6 ppm assigned to ring-opening at either side of the unsymmetrical monomer leading to tail-tail (T-T), head-tail (H-T) and head-head (H-H) linkages, respectively. Quantitative $^{13}C\{^{1}H\}$ NMR spectroscopy revealed a roughly 1:2:1 ratio of these signals, indicating a regiorandom polymer as also observed for the D-glucose,[32] D-xylose[33] and thymidine-based polycarbonates (Chapter 4).

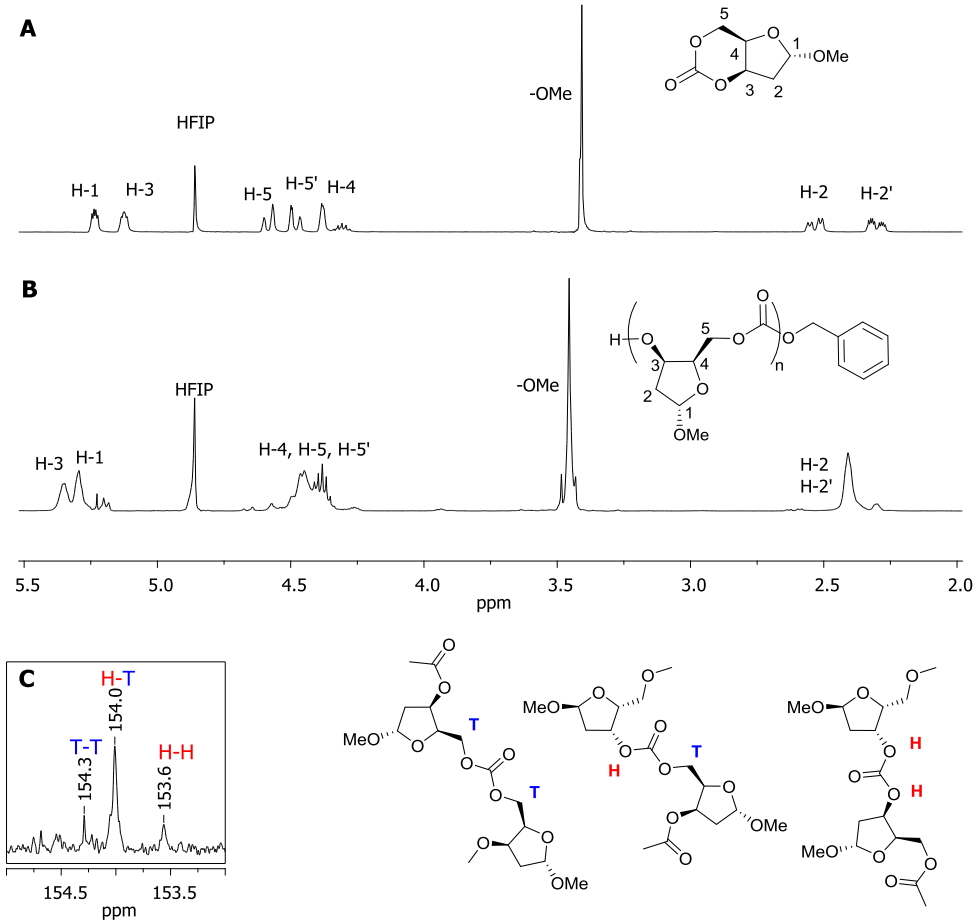

Figure 5.08. Comparison of the ^{1}H NMR spectra (400 MHz, HFIP-d_2) of **(A) 12*α*** and **(B)** poly(**12*α***). **(C)** The carbonate region of the $^{13}C\{^{1}H\}$ NMR spectrum (400 MHz, HFIP-d_2) of the homopolymer with assigned tail-tail (T-T), head-tail (H-T) and head-head (H-H) regiochemistries.

In contrast, **12β** did not undergo homopolymerisation with organic bases (TBD, DBU and DBU/thiourea combination) or metal-based catalysts: $Al(OTf)_3$, $Y(OiPr)_3$ and $Sn(Oct)_2$ in CH_2Cl_2, toluene, dioxane and THF solvents over a temperature range of -78- 120 °C as well as under melt conditions (T_m **12β** = 106-108 °C). With $Al(OTf)_3$ catalyst and BnOH initiator, mutarotation of **12β** to the equilibrium ratio of **12α**:**12β** was observed with no

polymerisation. A 50:50 feed ratio of both anomers, as an oil or in CH_2Cl_2 ($[M]_t$ = 5 mol L^{-1}) led to only polymerisation of the α-anomer with no evidence by NMR spectroscopy of incorporation of **12β.**

DFT modelling of the ROP initiation step was carried out at the rωb97xd/6-311+G(d,p)/6-31+G(d)/cpcm=dichloromethane/298 K level of theory (as for Chapter 3, Section 3.5) to provide an insight into the different behaviour of the two anomers (Figure 5.09).

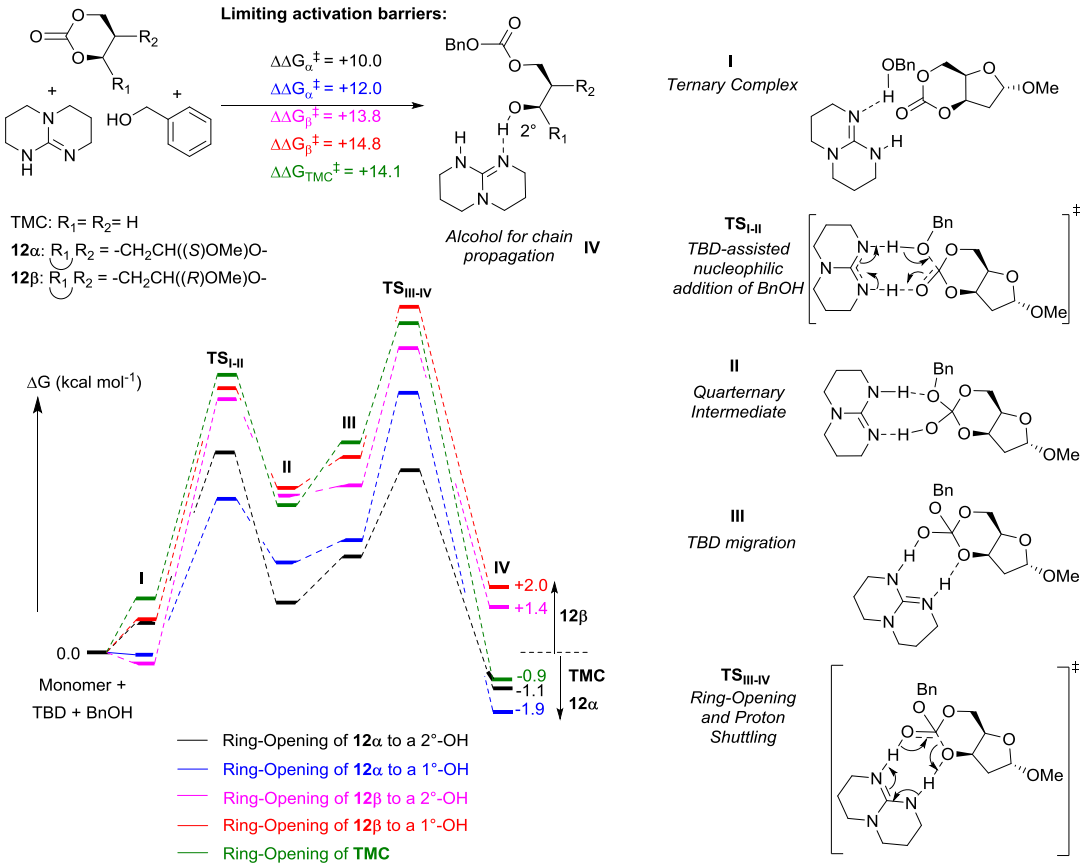

Figure 5.09. DFT modelling (rωb97xd/6-311+G(d,p)/6-31+G(d)/cpcm=DCM/298 K protocol) for the initiation step in the ROP of **12α**, **12β** and TMC with TBD catalyst and BnOH initiator involving formation of ternary complex **I**, nucleophilic addition of BnOH (**TS$_{I-II}$**) to form quaternary intermediate **II**, TBD migration **III** for ring-opening (**TS$_{III-IV}$**) to expose a primary (1°-OH) or secondary alcohol (2°-OH) in **IV** (see Appendix for calculated energies of all intermediates and TS).

The lowest kinetic energy barriers ($\Delta\Delta G^‡$) calculated for **12α** and **12β** were +10.0 and +13.8 kcal mol^{-1}, respectively. These are both low and for comparison, at the same level of theory, $\Delta\Delta G^‡$ for TMC initiation with TBD and BnOH was +14.1 kcal mol^{-1}. The different ROP behaviour was thus attributed to the overall thermodynamics of ring-opening. Whereas, ring-opening of TMC and (to either side) of unsymmetrical **12α**, was favourable by ΔΔG of -0.9 to -1.9 kcal mol^{-1}, benzyl alcohol ring-opening of **12β** was calculated to be unfavourable by

+1.4 or +2.0 kcal mol^{-1} to expose either a secondary or primary alcohol group for chain propagation, respectively. For the ROP of **12β**, the equilibrium must lie well over to the monomer. In accordance with the experimentally observed random cleavage at either side of the carbonate in **12α**, yielding all three linkage types in the polymer backbone, little preference is calculated for ring-opening to expose either a primary or secondary growing alcohol chain. The difference in ring strain of **12α**, **12β** and TMC was also evaluated by calculation of the enthalpy of isodesmic ring-opening with DMC and thermodynamics of ring-opening with primary and secondary alcohols (see Chapter 4, Section 4.2.1). Both support the more highly strained nature of **12α** compared to **12β** and reveal a similar ring stain for TMC to that of **12α** (Figure 5.10). For example, for the isodesmic reaction, values of $\Delta\Delta H_{ring\ strain}$ of -6.6, -6.5 and -4.6 kcal mol^{-1} were calculated for **12α**, TMC and **12β**, respectively.

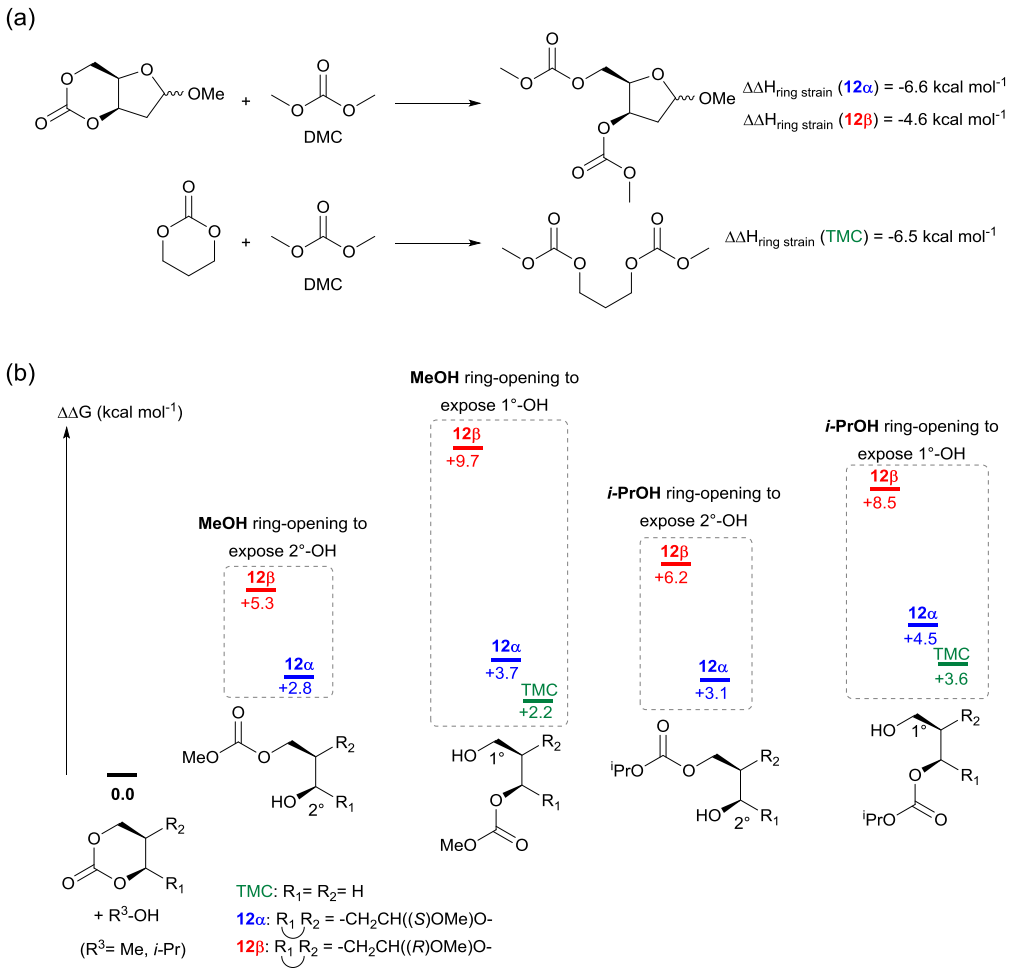

Figure 5.10. DFT calculations at the rωb97xd/6-311+G(2d,p)/cpcm=DCM/298 K level of theory for (a) the enthalpy of ring-opening ($\Delta\Delta H_{ring\ strain}$) of **12α**, **12β** and **TMC** with dimethyl carbonate (DMC) and (b) the overall Gibbs Free energy ($\Delta\Delta G$) for the ring-opening of **12α** (blue), **12β** (red) and TMC (green) with MeOH and *i*-PrOH to expose a primary (1°- OH) or secondary (2°-OH) alcohol.

5.4. Copolymerisation with TMC

For a 50:50 feed ratio of **12α**: TMC, the copolymerisation could be carried out in the absence of solvent at room temperature with TBD organocatalyst and benzyl alcohol initiator. A similar eutectic melt formation was also reported on mixing L-lactide with TMC.[34] After 3 hours with 0.1 mol% catalyst and $[M_t]_0/[I]_0$ of 1000, stirring was significantly perturbed because of the increased viscosity and the polymerisation quenched. Conversely to the homopolymerisation of **12α**, the resulting polymeric material was soluble in common organic solvents and SEC analysis in $CHCl_3$ eluent *versus* polystyrene standards revealed a single polymer distribution with a M_n of 64 000 g mol^{-1} (Table 5.01, Entry 1). DOSY NMR spectroscopy also showed a unique diffusion coefficient supporting the formation of a copolymer rather than two homopolymers.

Table 5.01. Copolymerisation of **12α** and TMC with TBD catalyst and BnOH initiator.[a]

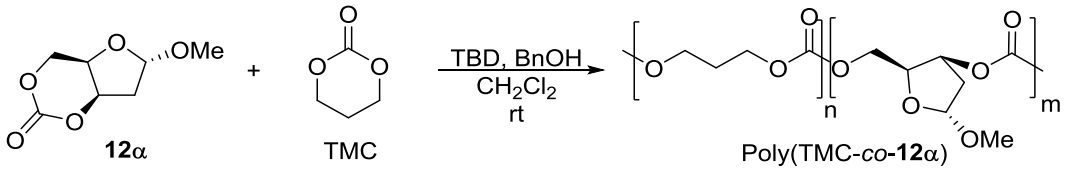

Entry	$[M_t]_0$: $[C]_0$: $[I]_0$	Time (h)	Conv. 12α (%)[b]	Conv. TMC (%)[b]	Yield (%)[c]	$M_{n,SEC}$ (g mol^{-1}) [Đ] [d]	$M_{n,calc}$ (g mol^{-1}) [e]	$M_{n,NMR}$ (g mol^{-1}) [f]	F_α/ F_{TMC} [g]	L_α/ L_{TMC} [h]
1[i]	1000:1:1	3	66	46	64	64 000 [1.33]	81 100	101 000	56/44	3.03/ 1.41
2	100:1:2	0.5	99	96	76	6380 [1.19]	6870	7320	47/53	1.23/ 1.46
3	100:1:1	0.16	69	44	72	8870 [1.11]	9120	9150	63/37	2.40/ 1.60
4	400:1:1	1	97	99	59	43 500 [1.63]	54 100	53 300	53/47	1.98/ 1.78
5	800:1:1	3	96	89	75	59 100 [1.44]	103 000	107 000	54/46	2.13/ 1.85

[a] Polymerisation conditions: f_α/f_{TMC} =50/50, $[M_t]_0$ = 5 mol L^{-1} in CH_2Cl_2, rt. [b] Determined by relative integration of the crude ^{1}H NMR spectra ($CDCl_3$); for **12α** conversion: integration of H-2 at 2.41 ppm in the monomer to 2.31 ppm in the polymer; for TMC: integration of H-7 at 2.14 ppm in the monomer to 2.05 ppm in the polymer. [c] Ether-insoluble copolymer (g)/monomer feed (g) × 100. [d] Estimated by SEC (RI detector) *versus* polystyrene standards with $CHCl_3$ eluent. [e] Calculated as: $[M]_0/[I]_0 \times [(M_r(\mathbf{12\alpha}) \times \mathbf{12\alpha}$ conv./100 × $f_\alpha)$+ (Mr(TMC)× TMC conv./100 × $f_{TMC})] + M_r(I)$. [f] Assuming a linear polymer with benzyl alcohol and OH end-groups. Based on the relative integration of the aromatic resonances of the benzyl alcohol initiator (~7.37 ppm) to the methylene protons of the **12α** (H-2, 2.31 ppm) and TMC (H-7, 2.05 ppm) repeat units in the ^{1}H NMR spectra (400 MHz, $CDCl_3$) of the copolymer precipitated from ether. [g] Copolymer compositions determined by integration of the ^{1}H NMR spectra of the purified copolymer. [h] $L_\alpha = [I_{\alpha\text{-}\alpha}(I_{154.81ppm} + I_{154.35} + I_{154.04}) + I_{\alpha\text{-}TMC}(I_{154.47})]/I_{\alpha\text{-}TMC}(I_{154.47})$ and $L_{TMC} = [I_{TMC\text{-}TMC}(I_{154.99ppm}) + I_{TMC\text{-}\alpha}(I_{154.89})]/I_{TMC\text{-}\alpha}(I_{154.89})$ where I = integration of the subscripted carbonate signal in the quantitative $^{13}C\{^1H\}$ NMR spectra. [i] No solvent.

Monomer conversion was then monitored as a function of time for a polymerisation carried out at room temperature with the same catalyst and initiator loadings (0.1 mol%) but with an initial total monomer concentration ($[M_t]_0$) of 5 mol L^{-1} in CH_2Cl_2. This allowed aliquots to be taken, quenched, and conversion evaluated by ^1H NMR spectroscopy (Figure 5.11A).

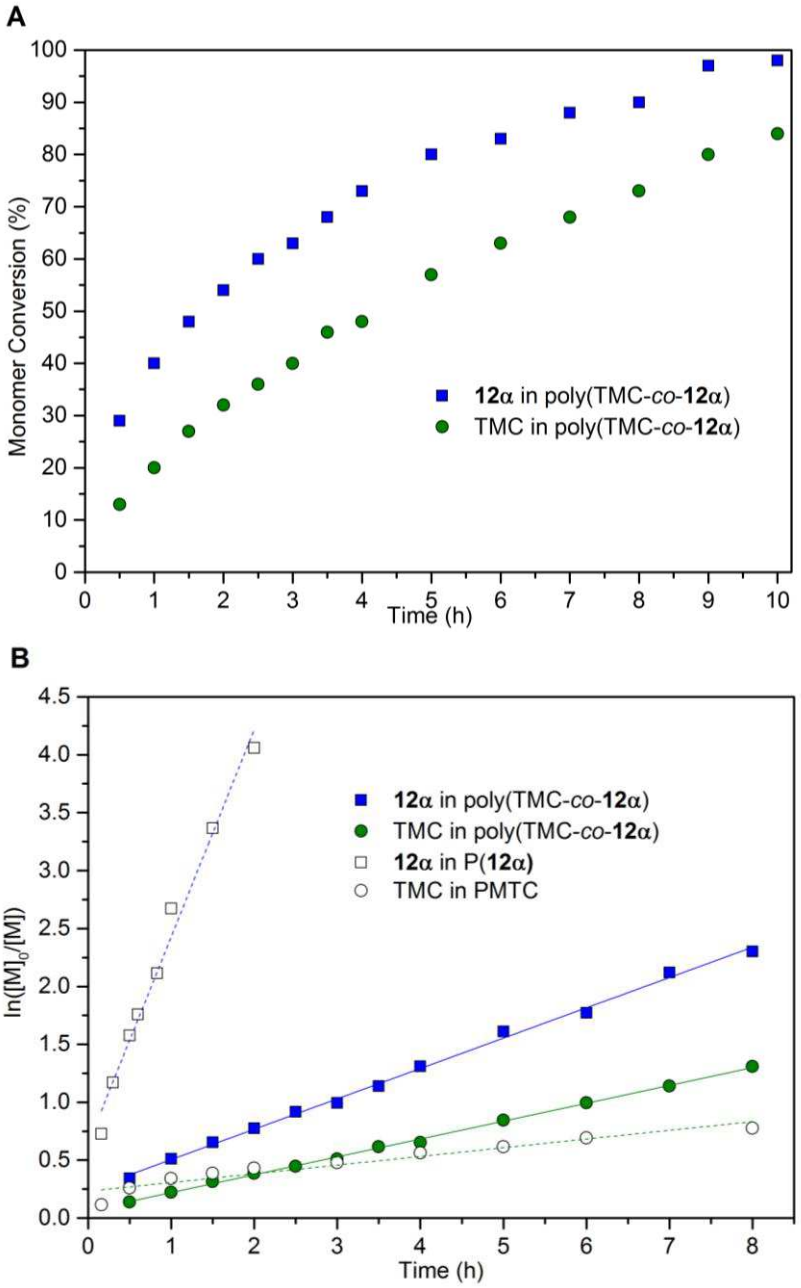

Figure 5.11. (A) Monomer conversion as a function of time for **12*α*** and TMC copolymerisation at f_ω/f_{TMC}= 50/50, $[M_t]_0$:$[TBD]_0$:$[BnOH]_0$= 1000:1:1, rt and $[M_t]_0$ = 5 mol L^{-1} in CH_2Cl_2. **(B)** Corresponding kinetic plot for **12*α*** (y= 0.262x+ 0.243, R^2 =0.97) and TMC (y= 0.154x + 0.0664, R^2= 0.98) in the copolymer. The kinetic plots for the homopolymerisation of **12*α*** (y=1.79x+ 0.64, R2 = 0.98) and TMC (y= 0.0751x+ 0.232, R^2= 0.96) are also shown for the same reaction conditions. For the homopolymerisation of **12*α***, time is plotted against ln{($[M]_0$-$[M]_{eq}$)/($[M]$-$[M]_{eq}$)} where $[M]_{eq}$ = 2.1 mol L^{-1}. All conversions were determined by ^1H NMR spectroscopy from aliquots quenched with benzoic acid.

12α was consumed faster than the TMC co-monomer, reaching 98% conversion after 10 hours compared to 84% for TMC. Thus, the thermodynamically limited conversion of **12α** in the homopolymerisation (which plateaued at 60%) was overcome in the copolymerisation and suggested blocks of **12α** were not being formed. Kinetic plots (Figure 5.11B) showed pseudo first-order kinetics, typical of ROP, from which k_{app} values of 0.262 ± 0.004 h^{-1} and 0.154 ± 0.002 h^{-1} were determined for **12α** and TMC, respectively. The kinetics for the homopolymerisation of **12α** (k_{app} = 1.79 ± 0.09 h^{-1}) and TMC (k_{app} = 0.0751 ± 0.007 h^{-1}) under the same reaction conditions are shown for comparison. The difference in kinetics of the monomers in the copolymer formation compared to during homopolymerisation further hinted at the formation of a random or alternating copolymer, instead of block copolymers.

For the same 50:50 feed ratio, the catalyst and initiator loadings were varied (Table 5.01 above, Entries 2-5). Generally, good agreement was observed between the SEC estimated and calculated M_n values as for example, in Entries 2 and 3. A plot of M_n and Đ (estimated by SEC) as a function of conversion for a copolymerisation carried out with 0.1 mol% TBD and $[M_t]_0/[I]_0$ of 50 showed a linear increase in molecular weight with total monomer conversion whilst maintaining relatively narrow dispersities (Đ<1.2) (Figure 5.12). This indicated a controlled polymerisation under optimised conditions. At lower catalyst and initiator loading (0.125 mol%), a greater disparity between the theoretical M_n and the one determined by SEC was observed (Table 5.01 above, Entry 5).

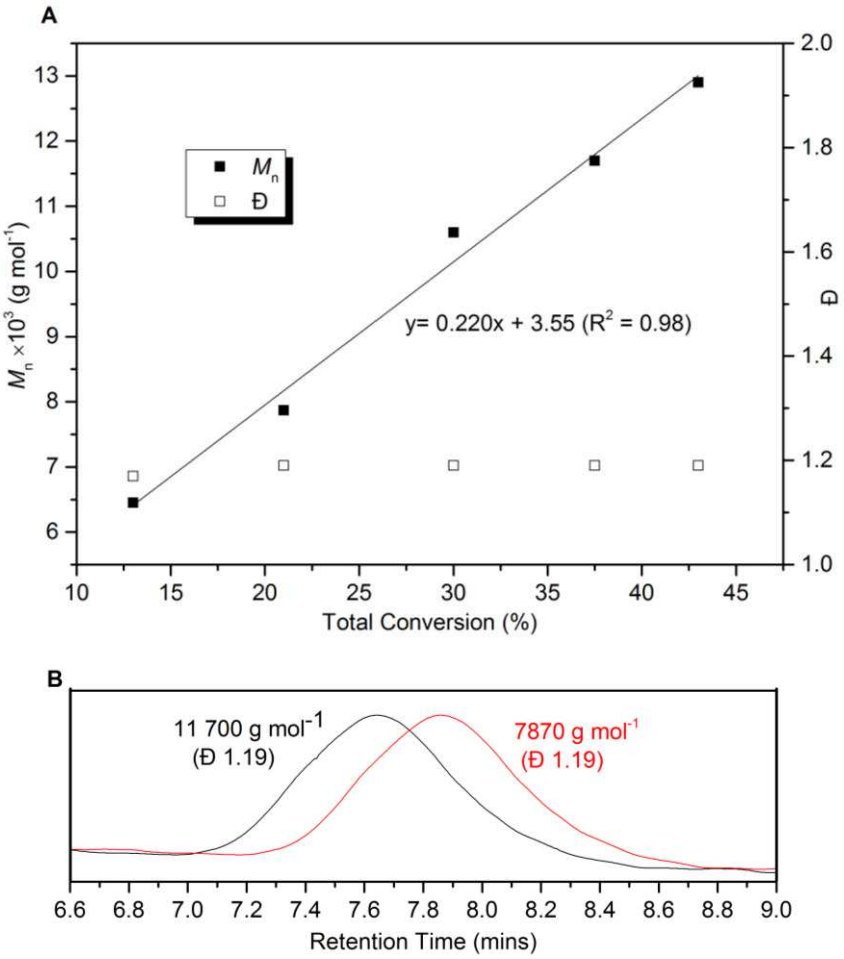

Figure 5.12. (A) Linear increase in M_n with monomer conversion whilst maintaining a relatively narrow dispersity (Đ < 1.2) for a copolymerisation with **12α**: TMC feed ratio of 50:50, 1000:1:20 $[M]_0$: $[TBD]_0$: $[BnOH]_0$, $[M_t]_0$ = 5 mol L^{-1} in CH_2Cl_2 at rt. Monomer conversion was determined by integration of the ^{1}H NMR spectra of aliquots taken at specific times and quenched with benzoic acid. For these aliquots, M_n and Đ were estimated by SEC (RI detector) with $CHCl_3$ eluent *versus* polystyrene standards. **(B)** SEC traces corresponding to data points 2 (21% conversion) and 4 (38% conversion).

Subsequently, the feed ratio of the two co-monomers was varied for $[M_t]_0/[I]_0$ of 400 (Table 5.02). The copolymers were all soluble in typical organic solvents, namely $CHCl_3$, CH_2Cl_2 and THF, though this solubility was reduced for copolymers of higher **12α** content of 85 and 93 mol%. Monomer conversion and the resulting copolymer composition were determined by relative integration of the methylene H-2 proton environments of **12α** and TMC. Nearly full conversion (>96%) was observed for the TMC co-monomer in all cases. For **12α**, full or high conversion (>88%) was observed within the 1 hour reaction time for **12α** and TMC feed ratios (f_{α}/f_{TMC}) up to 70/30. At higher ratios (Table 5.02, Entries 2 and 3), the polymerisation solution became cloudy as for the **12α** homopolymerisation. Nevertheless, ^{1}H NMR spectroscopy of the polymers purified by precipitation from ether revealed copolymer compositions well correlated to the input ratio of co-monomers, which is promising for polymer design and tunability. High M_n (up to 46 500 g mol^{-1}, Đ 1.65) were

achieved after 1 hour, with generally good agreement with the M_n predicted from the monomer conversion.

Table 5.02. Synthesis of poly(TMC-*co*-**12α**) of different compositions.[a]

Entry	f_α/f_{TMC}	**12α conv. (%)**[b]	**TMC conv. (%)**[b]	$M_{n,\,SEC}$ (g mol^{-1}) [c]	Đ [c]	$M_{n,\,calc}$ (g mol^{-1}) [d]	Yield (%)[e]	F_α/F_{TMC}[f]	L_α/L_{TMC} [g]
1	100/0	60	-	25 600[h]	1.41	41 900	48	-	-
2	90/10	73	99	33 200	1.74	49 900	57	93/7	-
3	80/20	81	99	36 100	1.61	53 300	69	85/15	3.30/0.80
4	70/30	88	97	39 300	1.64	54 900	54	66/34	1.97/1.13
5	60/40	98	99	36 700	1.46	57 200	43	60/40	2.03/1.64
6	50/50	97	99	43 500	1.63	54 100	59	53/47	1.98/1.78
7	40/60	99	98	30 200	1.75	51 700	66	39/61	1.65/2.79
8	30/70	99	96	26 100	1.39	48 200	53	31/69	1.27/2.91
9	20/80	99	99	46 500	1.65	46 200	76	23/77	-
10	10/90	99	99	40 900	1.37	43 400	69	14/86	-
11	0/100	-	99	42 500	1.55	40 500	72	-	-

[a] Polymerisation conditions: $[M_t]_0$ = 5 mol L^{-1} in CH_2Cl_2, $[M_t]_0$: $[TBD]_0$: $[BnOH]_0$= 400:1:1, 1 h, rt. [b] Determined by integration of the crude ^{1}H NMR spectra ($CDCl_3$). [c] Estimated by SEC (RI detector) *versus* polystyrene standards in $CHCl_3$ eluent. [d] Calculated as: $[M]_0/[I]_0 \times [(M_r(\mathbf{12\alpha}) \times \mathbf{12\alpha}\text{ conv.}/100 \times f_\alpha) + (M_r(TMC) \times TMC\text{ conv.}/100 \times f_{TMC})] + M_r(I)$. [e] Ether-insoluble copolymer (g)/monomer feed (g) × 100. [f] Copolymer compositions determined by integration of the ^{1}H NMR spectra of the purified copolymer. [g] $L_\alpha = [I_{\alpha\text{-}\alpha}(I_{154.81ppm} + I_{154.35} + I_{154.04}) + I_{\alpha\text{-}TMC}(I_{154.47})]/I_{\alpha\text{-}TMC}(I_{154.47})$ and $L_{TMC} = [I_{TMC\text{-}TMC}(I_{154.99ppm}) + I_{TMC\text{-}\alpha}(I_{154.89})]/I_{TMC\text{-}\alpha}(I_{154.89})$ where I = integration of the subscripted carbonate signal in the quantitative ^{13}C NMR spectra. [h] Estimated by SEC (RI detector) *versus* PMMA standards with HFIP eluent.

5.4.1. Copolymer structure

^{1}H NMR analysis of poly(TMC-*co*-53mol%-**12α**) (Table 5.02, Entry 6) revealed proton environments analogous to those observed in the NMR spectra of PTMC and poly(TMC-co-93mol%-**12α**) (Figure 5.13).

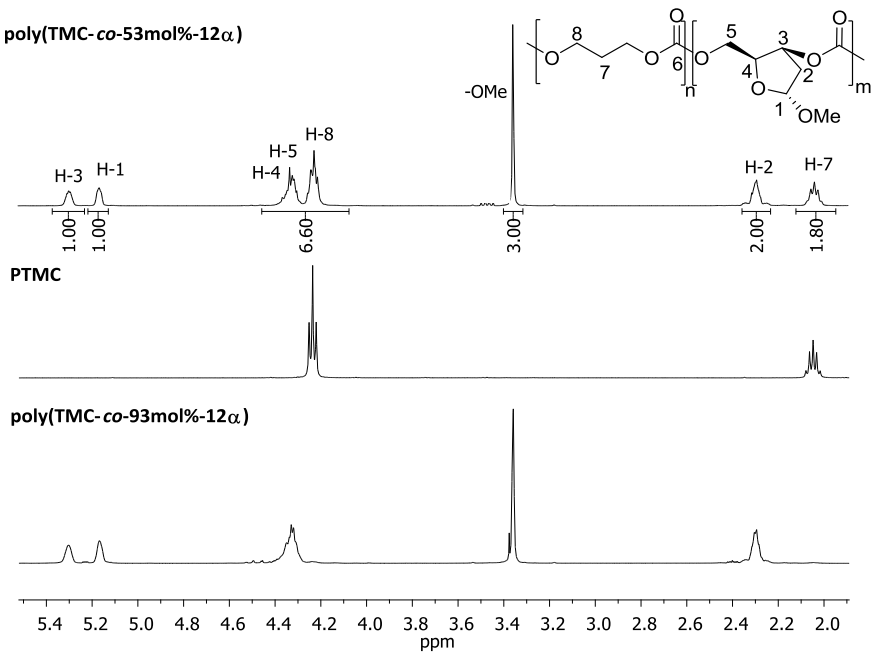

Figure 5.13. ^{1}H NMR spectra (400 MHz, $CDCl_3$) of poly(TMC-co-53mol%-**12α**), poly(TMC-co-93mol%-**12α**) and PTMC.

Detailed analysis of the carbonyl region in the $^{13}C\{^{1}H\}$ NMR spectra of the copolymers revealed the presence of 6 carbonate environments in the backbone (Figure 5.14). These were assigned based on comparison with the homopolymer NMR data and their relative intensity depending upon the comonomer content. Carbonate environments at 154.89 and 154.47 ppm were assigned to alternating TMC-α and α-TMC linkages, respectively and were most intense for the copolymer with 53mol% **12α** content (Figure 5.14B). The presence of TMC-TMC carbonate environments and the T-T, H-T and H-H regiochemistries characteristic of **12α** diads also indicated the presence of segments of **12α** and TMC repeat units. Thus, the copolymers were not perfectly alternating, which was consistent with the slightly faster consumption of **12α.**

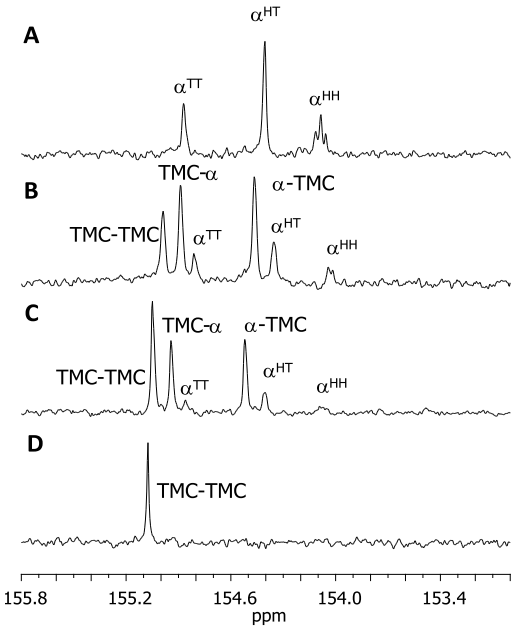

Figure 5.14. Carbonate region of the $^{13}C\{^{1}H\}$ NMR spectra (400 MHz, $CDCl_3$) of **(A)** poly(TMC-co-93mol%-**12α**), **(B)** poly(TMC-co-53mol%-**12α**), **(C)** poly(TMC-co-31mol%-**12α**) and **(D)** PTMC.

The average lengths of these segments (L_α and L_{TMC}) were estimated based on the relative integration of the carbonyl signals by quantitative $^{13}C\{^{1}H\}$ NMR spectroscopy (Tables 5.01 and 5.02). Short L_α lengths, even at 85 mol% **12α** content (L_α =3.30, Table 5.02, Entry 3), indicated that blocky copolymers were not being formed. Estimation of the reactivity ratios using the Finemann-Ross method[35] for polymerisations with monomer conversions less than 15% gave values for **12α** and TMC, respectively of r_α =0.54 ± 0.08 and r_{TMC} = 0.41 ± 0.01 (Figure 5.15). These values, both less than 1 suggest a random copolymer (*rr* = 1) tending towards alternating (*rr* = 0). Attempts to synthesise di-, tri- and tetra- block copolymers by sequential addition of monomers proved challenging due to the lack of copolymer solubility when blocks of **12α** were present. Further complexity arose from the thermodynamically limited equilibrium homopolymerisation of **12α**, which resulted in less than full conversion and prevented clean **12α**-TMC block sequences.

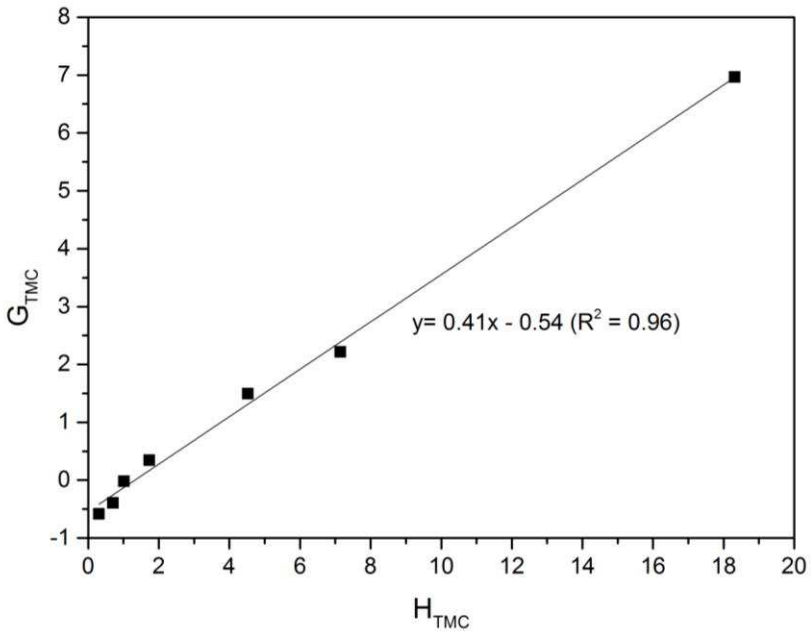

Figure 5.15. Calculation of reactivity ratios: r_α and r_{TMC} using the Finemann-Ross method.[35] Polymerisations were carried out at rt with $[M_t]_0$: $[TBD]_0$: $[BnOH]_0$ ratio of 1000:1:1 and $[M_t]_0$ = 5 mol L^{-1} in CH_2Cl_2 for different feed ratios of **12α** and TMC (f_α and f_{TMC}). Polymerisations were quenched below 15% monomer conversion (<10 minutes) and the copolymer compositions of **12α** and TMC (F_α and F_{TMC}) determined by ^{1}H NMR spectroscopy. $G_{TMC} = H_{TMC}\, r_{TMC} - r_\alpha$ where $\mathbf{G} = \frac{f_{TMC}(2F_{TMC}-1)}{(1-f_{TMC})F_{TMC}}$ and $\mathbf{H} = \frac{f_{TMC}^2(1-F_{TMC})}{(1-f_{TMC})^2F_{TMC}}$

5.4.2. MALDI-ToF mass spectrometry

MALDI-ToF MS (Figures 5.16 and 5.17) of poly(TMC-co-47mol%-**12α**) (Table 5.01, Entry 2) showed multiple polymer series consisting of **12α** and TMC repeat units (Δ*m/z* 174 and 102, respectively). All peaks were consistent with the sodium adducts of copolymers with benzyl alcohol and OH end-groups. The majority had roughly equal numbers of **12α** and TMC units as expected based on the copolymer composition determined by NMR spectroscopy. In Figure 5.17, polymer series have been differentiated and labelled so that each contains the same number of **12α** units (m = 11-18) but different numbers of TMC co-monomer (n =11-22). This is arbitrary and not representative of the polymerisation process, as from most signals, a higher *m/z* species can be found that corresponds to the addition of either a TMC or **12α** unit. For example, the species at *m/z* ~ 4100 (consistent with a polymer chain with 15 TMC and 14α units) could grow by a **12α** unit to *m/z* ~ 4275 (15T, 15α) or by a TMC unit to *m/z* ~ 4200 (16T, 14α). The presence of all possible combinations supports the random, statistical nature of the copolymer.

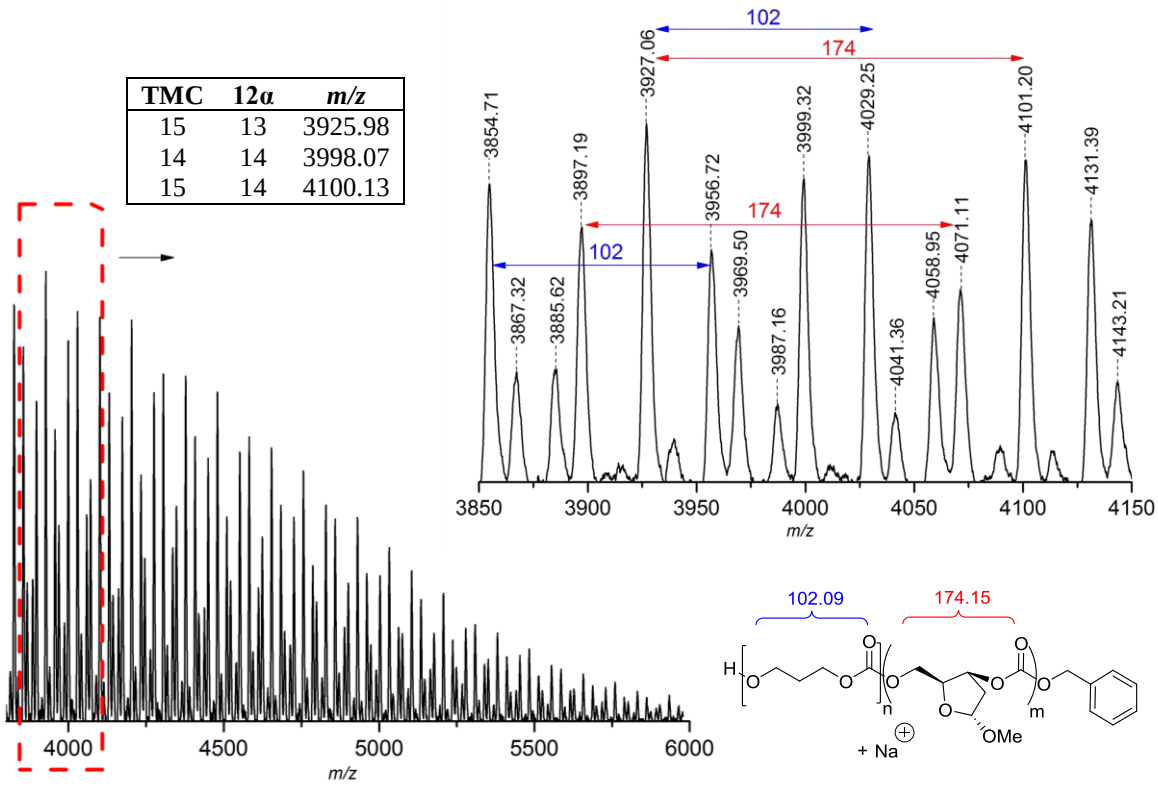

Figure 5.16. MALDI-ToF MS of poly(TMC-*co*-47mol%-**12α**) (Table 5.01, Entry 2) with peaks labelled in the *m/z* region from 3850 to 4150 showing TMC and ribose repeat units. *m/z* values are consistent with the sodium adduct of the linear copolymer with benzyl alcohol and -OH end groups.

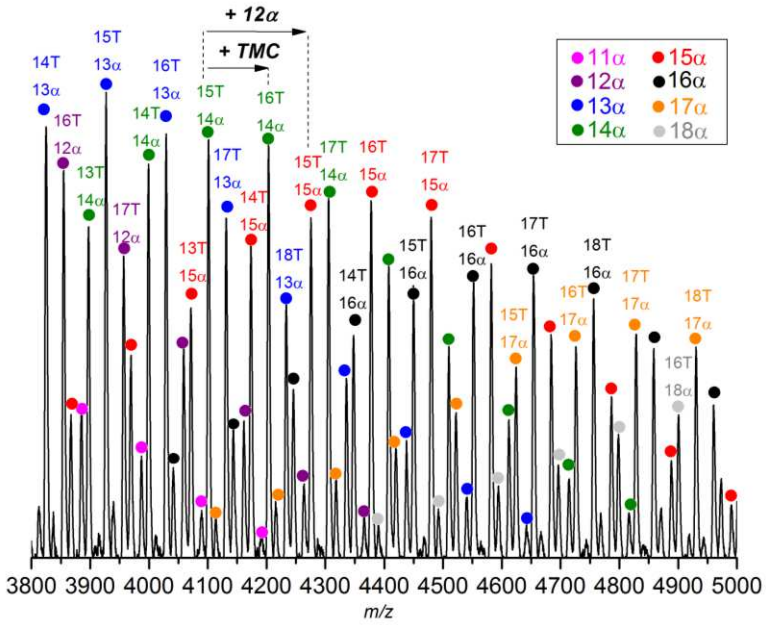

Figure 5.17. MALDI-ToF MS of poly(TMC-*co*-47mol%-**12α**) (Table 5.01, Entry 2) in the region from *m/z* 3800 to 5000 where polymeric series have been labelled which contain the same number of **12α** units (11-18) but different amounts of TMC (T).

5.4.3. Copolymerisation of 12β and TMC

Despite not undergoing homopolymerisation with TBD catalyst and benzyl alcohol initiator, **12β** did copolymerise under these conditions with TMC, at room temperature and an $[M_t]_0$ of 5 mol L^{-1} in CH_2Cl_2. For a 50:50 feed ratio of **12β**: TMC, complete TMC conversion was achieved though, conversely to the copolymerisation of **12α** with TMC, the conversion of **12β** did not proceed above 40%. Monitoring conversion as a function of time (Figure 5.18), for a polymerisation carried out with 0.1 mol% TBD and $[M_t]_0/[I]_0$ of 1000, showed the faster consumption of TMC comonomer compared to the **12β**. The corresponding kinetic plot (Figure 5.19) gave significantly lower values for k_{app} of 0.0145 ± 0.0009 h^{-1} and 0.0621 ± 0.002 h^{-1} for **12β** and TMC, respectively compared to the copolymerisation of TMC with the α-anomer.

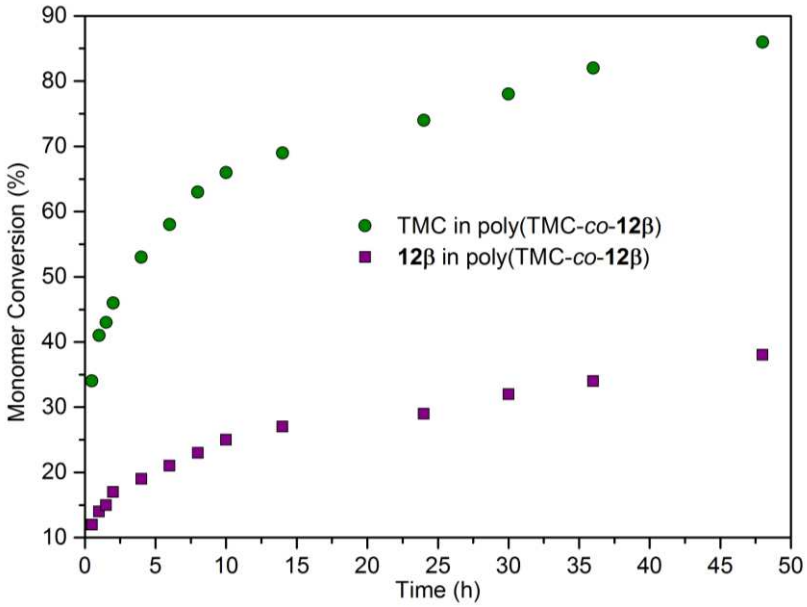

Figure 5.18. Monomer conversion versus time for the copolymerisation of **12β** and TMC under the following reaction conditions: f_β/f_{TMC} = 50/50, $[M_t]_0$ = 5 mol L^{-1} in CH_2Cl_2, [**12β** + TMC]$_0$: [TBD]$_0$: [BnOH]$_0$ = 1000:1:1. Aliquots were taken at specific times, quenched with excess benzoic acid and monomer conversion determined by integration of the ^{1}H NMR spectra ($CDCl_3$); for TMC conversion, by relative integration of the H-7 methylene environments at 2.14 ppm in the monomer and 2.05 ppm in the copolymer; for **12β** conversion, by relative integration of the H-2 proton at 2.44 ppm in the monomer and 2.17 ppm in the copolymer.

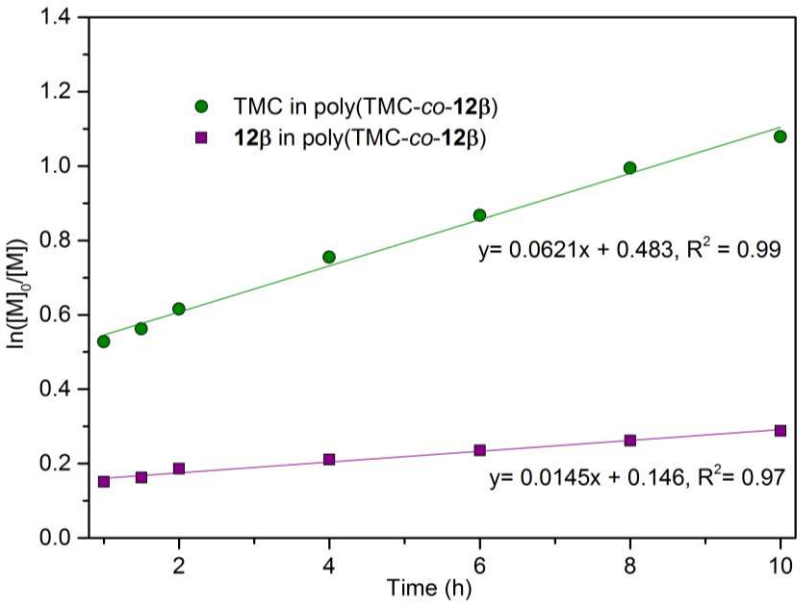

Figure 5.19. Kinetic plot (corresponding to Figure 5.18 above) for the copolymerisation of **12β** and TMC under the following reaction conditions: f_{β}/f_{TMC} = 50/50, $[M_t]_0$ = 5 mol L^{-1} in CH_2Cl_2, [**12β** + TMC]$_0$: [TBD]$_0$: [BnOH]$_0$ = 1000:1:1, aliquots were taken at specific times, quenched with excess benzoic acid and monomer conversion determined by integration of the ^{1}H NMR spectra ($CDCl_3$).

In Figure 5.20A, proton environments attributed to the β-ribose monomer can be seen in the ^{1}H NMR spectrum of the copolymer (F_{β}/F_{TMC} = 32/68, $M_{n,SEC}$ = 43 200 g mol^{-1}, Đ 1.39) precipitated from ether. Loss of the doublet of doublets for each of the methylene H-5 environments of the cyclic carbonate was observed on ring-opening **12β** in the copolymer NMR spectrum as well as a separating of the overlapping H-3 and H-1 environments. Analysis of the ^{13}C{^{1}H} NMR spectrum in the carbonyl region (Figure 5.20B) revealed no signals due to the H-H, H-T and T-T linkages of repeating **12β** units. This is consistent with no homopolymerisation of **12β** being observed under these reaction conditions. Thus, **12α** can ring-open **12α** and TMC but will not polymerise with **12β,** whereas TMC will copolymerise with both **12β** and **12α**.

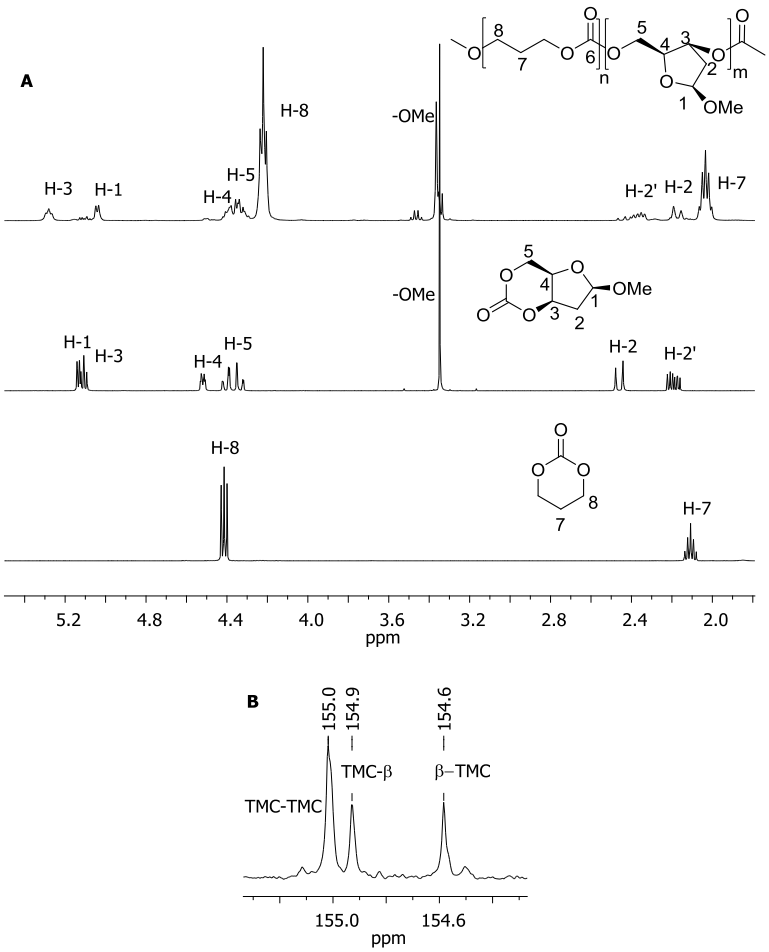

Figure 5.20. A: Comparison of the ^{1}H NMR spectra ($CDCl_3$) of poly(TMC-co-32mol%-**12β**), TMC and **12β**. **B:** $^{13}C\{^{1}H\}$ NMR spectrum ($CDCl_3$) of the copolymer in the carbonyl region showing TMC-TMC and TMC-β carbonate environments.

5.5. Copolymer Thermal Properties

5.5.1. Glass transition temperature

Differential scanning calorimetry (DSC) of the copolymers showed a single T_g supportive of random or alternating rather than block copolymers. The homopolymer of **12α** exhibited a significantly lower T_g of ~58 °C, compared to the sugar-based polycarbonates derived from D-xylose (T_g= 128 °C),[33] D-glucose (T_g= 122 °C),[32] D-mannose (T_g= 152 °C, Chapter 3) and 3-*N*-methyl thymidine (T_g=156 °C, Chapter 4). In addition to the pyranose or furanose rings in the polymer backbone, these contain pendent methoxy or ketal protecting groups and in the latter, a bulky nucleobase side-arm, that may further restrict rotation about the main chain, leading to enhanced T_g values. For further comparison, completely unfunctionalised poly(cyclopentene carbonate), produced by the copolymerisation of cyclopentene oxide with CO_2, has a reported T_g of 84.5 °C.[36] Greater **12α** content in the copolymers, ranging from 0 to 93 mol%, led to increasing T_g values from -25 to +50 °C and in general, good agreement

was observed with the values predicted by the Fox equation[‡] (Table 5.03). Small exotherms at ~137 °C were also detected in the cooling curves (and corresponding endotherms in the heating curve) for copolymers with greater than 23 mol% **12α** (Figure 5.21). These are potentially due to crystallisation (and melting) of crystalline domains though, no crystallinity was observed by powder X-ray diffraction. As the onset of degradation occurred close to T_c, heating until the endotherms were observed may also have induced some thermal degradation.

Table 5.03. T_g values measured by DSC and predicted by the Fox equation for poly(TMC-*co*-**12α**) of different compositions.

Entry	12α mol%	T_g (°C)	T_g^{calc}(°C)	T_c (°C)	ΔH_c (J g^{-1})
1	100	58	-	137.3	0.301
2	93	50	51	137.0	0.512
3	85	46	48	-	-
4	66	38	34	137.1	1.96
5	53	30	24	138.4	0.786
6	37	9	11	137.0	0.937
7	31	3	5	137.2	2.46
8	23	-3	-2	137.6	1.50
9	14	-11	-11	-	-
10	0	-25	-	-	-

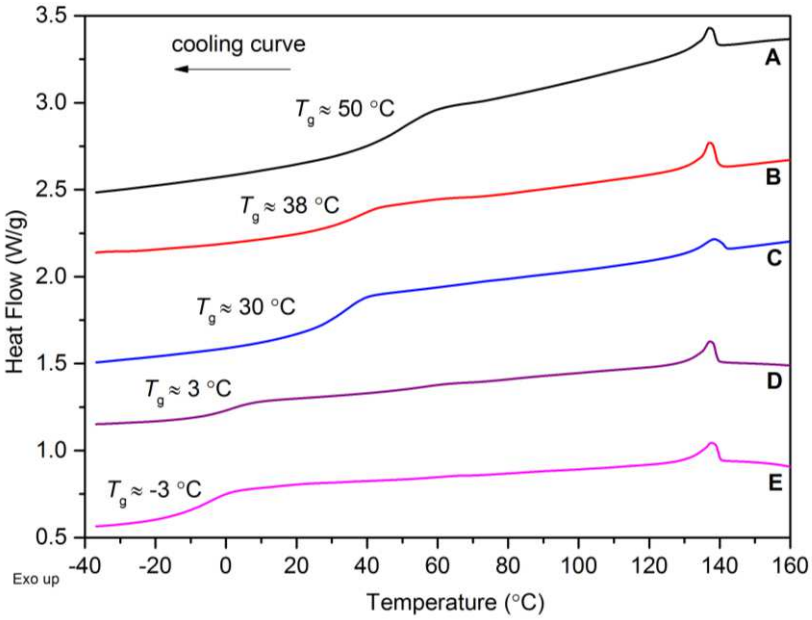

Figure 5.21. Selected DSC traces of **12α** and TMC copolymers showing the cooling curve from 160 to -40 °C (10 K min^{-1}) of the first heating cycle. **A:** poly(TMC-*co*-93mol%-**12α**); **B:** poly(TMC-*co*-66mol%-**12α**); **C:** poly(TMC-*co*-53mol%-**12α**); **D:** poly(TMC-*co*-31mol%-**12α**); **E:** poly(TMC-*co*-23mol%-**12α**).

[‡] Fox equation: $\frac{1}{T_g} = \frac{w_{12\alpha}}{T_{g,12\alpha}} + \frac{w_{TMC}}{T_{g,TMC}}$, where w = weight fraction of **12α** or TMC.

5.5.2. Thermal degradation

Thermogravimetric analysis (TGA) of the copolymers revealed a general trend towards lower thermal stability with higher **12α** content (Figure 5.22). For example, the temperature at which the maximum percentage mass loss was observed (T_{inf}) decreased from ~212 °C for the copolymer with just 14 mol% **12α** to ~195 °C with 93 mol% **12α** content (Table 5.04, Entries 2 and 8). The onset of thermal degradation (T_{on}) occurred at ~170 °C for copolymers of higher sugar composition (66-93 mol%) and showed less stepwise degradation profiles compared to copolycarbonates of 53 mol% or less **12α** content (T_{on} ~ 200 °C). For all copolymers, mass losses of 90% or over were observed and analysis of the degradation products by tandem mass spectrometry revealed ions of *m/z* 44 consistent with the loss of CO_2^+. In Figure 5.23, this can be seen to coincide with the mass loss during thermal degradation.

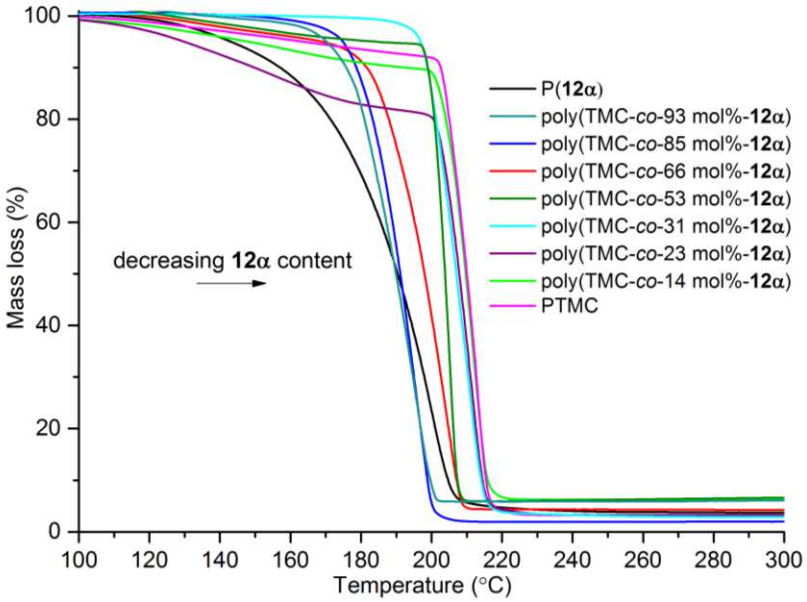

Figure 5.22. TGA analysis of poly(TMC-*co*-**12α**) of various composition. Copolymers were heated from 30- 500 °C at 5 K min^{-1}.

Table 5.04. TGA data for copolymers of TMC and **12α** with different compositions.

Entry	12α mol%	T_{on} (°C) [a]	T_{inf} (°C) [b]	% mass loss [c]
1	100	125	200	94
2	93	156	195	93
3	85	160	196	98
4	66	168	204	91
5	53	196	205	97
6	31	194	210	98
7	23	197	212	97
8	14	196	212	90
9	0	197	213	96

[a] Onset of thermal degradation. [b] Temperature at which maximum mass loss was observed. [c] Total mass loss.

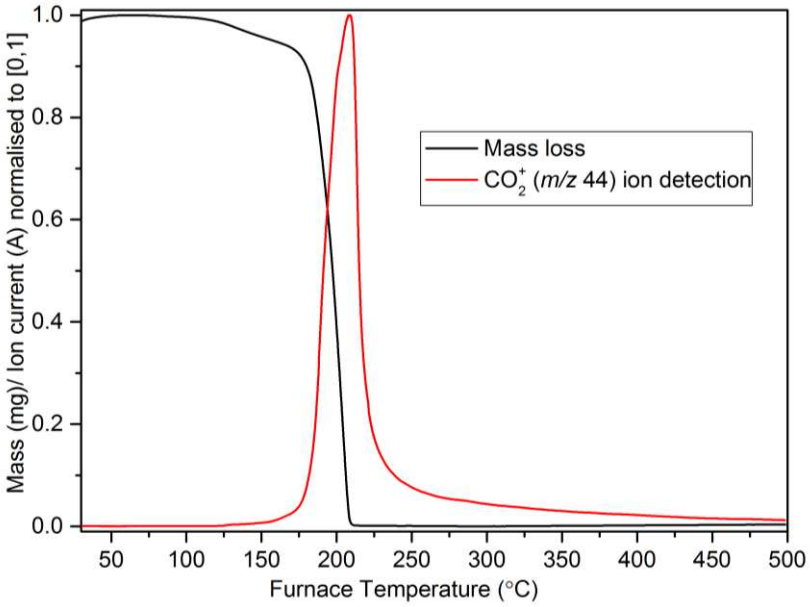

Figure 5.23. TGA-mass spectrometry of poly(TMC-*co*-66mol%-**12α**). The sample mass (mg) and detected *m/z* 44 ion current (A), both normalised to [0,1], are plotted against the furnace temperature

5.6. Looking Forward: Polymers from Carbon Disulfide and Sugars

5.6.1. Sulfur-containing polymers

Substitution of the oxygen atoms in polymer backbones with sulfur can result in enhanced thermal properties. For example, higher melting temperatures (T_m) of 105 °C were observed for poly(ε-thiocaprolactone) with a sulfur atom in the ester linkage (Figure 5.24A) compared to poly(caprolactone) (T_m ~ 60 °C).[37-39] Replacement of the oxygen with sulfur in PTMC to

form poly(trimethylene monothiocarbonate) (PTMMTC), reported by Darensbourg and coworkers[40] (Figure 5.24B), led to crystallisation behaviour similar to high-density polyethylene. Namely, a degree of crystallinity up to 71% and T_m of 127.5 °C. The semicrystalline poly(monothiocarbonate) also exhibited higher thermally stability than amorphous PMTC, showing only 5% mass loss at ~230 °C.

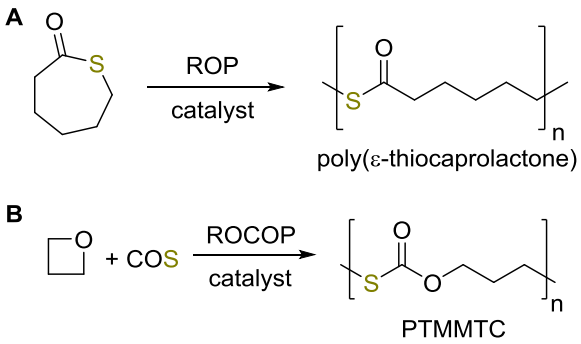

Figure 5.24. A: Formation of poly(thioester) by ROP of ε-thiocaprolactone[38] and **B:** alternating copolymerisation of oxetane and COS to form semicrystalline poly(trimethylene monothiocarbonate).[40]

In addition to enhanced thermal properties, sulfur-containing polymers are also reported to show good mechanical, electrical and optical properties as well as advanced characteristics such as adhesion to metals, biological and chemical resistance, and biocompatibility.[41] In particular, the thiocarbonate linkages in poly(thiocarbonate) backbones are attractive for imparting further biodegradability characteristics.[42, 43]

Both carbonyl sulfide (COS) and carbon disulfide (CS_2) have been used as sulphur-containing C1 building blocks to introduce sulfur into polymer chains.[43, 44] Darensbourg and coworkers observed scrambling of the oxygen and sulfur atoms, in the copolymerisation of CS_2 with propylene oxide,[45] cyclohexene oxide,[46] cyclopentene oxide [47] and oxetane[48] using various metal-based catalysts, leading to irregular chain structure (Figure 5.25). Diebler *et al.*[49] however, reported the formation of highly regioregular and alternating poly(thiocarbonate)s from the coupling of CS_2 with terminal epoxides using lithium *tert*- butoxide at 25 °C. Further to the preparation of PTMMTC by the alternating copolymerisation of COS (an air pollutant) with oxetane,[40] Darensbourg and coworkers also reported the synthesis of well-defined poly(monothiocarbonates) by copolymerisation of COS with epoxides.[42]

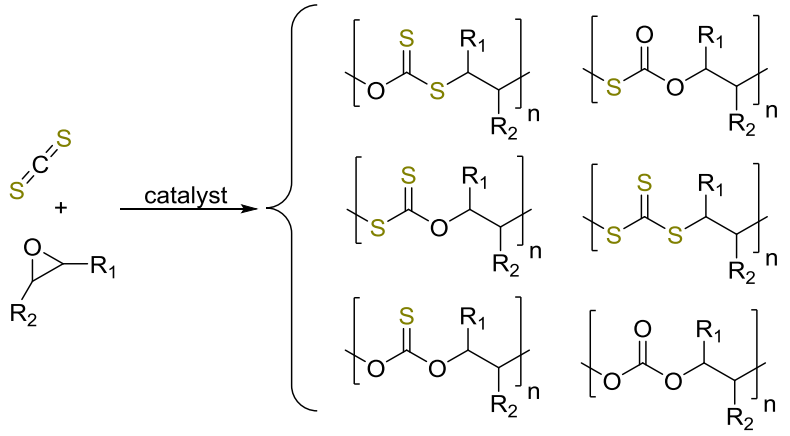

Figure 5.25. Scrambling of the O and S atoms, reported by Darensbourg and co-workers,[33] in the copolymerisation of CS_2 with epoxides to form sulphur containing APCs. O/S- scrambling was also observed in the 5-membered cyclic by-products formed by chain backbiting.

Accordingly, the synthesis of sulfur analogues of cyclic carbonates (Figure 5.26) has attracted attention for ROP to sulfur-containing polycarbonates. Examples exist for the ROP of cyclic trithiocarbonates (–S–CS–S–),[48] cyclic 1,3-oxathiolane-2-thiones (–S–CS–O–),[50] cyclic thione carbonates (–O–CS-O–),[51, 52] cyclic monothiocarbonates (-S-CO-O-)[53] and cyclic dithiocarbonates (–S–CO–S–).[54]

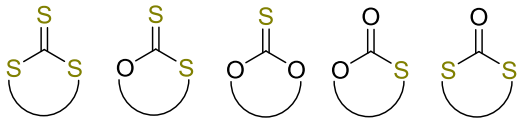

Figure 5.26. Sulfur-containing analogues of cyclic carbonates for ROP to sulfur-containing polymers.

Sulfur-containing cyclic carbonate analogues of sugar-based diols have also been reported (Figure 5.27).[55-59] Many of these were synthesised using $CSCl_2$ or Im_2CS (Im = imidazole) reagents and investigated as useful intermediates in organic synthesis owing to their tendency to undergo O-S rearrangements. No polymerisation studies have been reported.

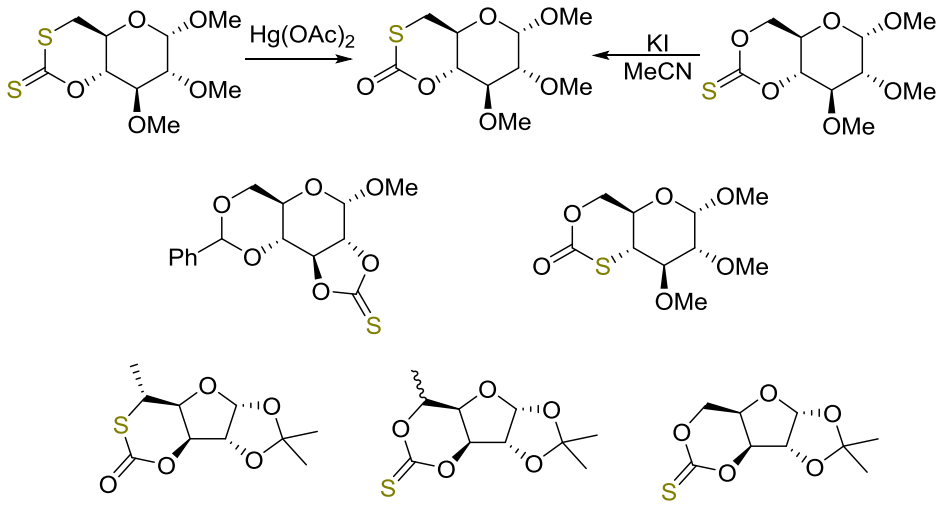

Figure 5.27. Reported sulfur-analogues of cyclic carbonates derived from D-glucose and D-xylose sugar diols. No polymerisation studies have been reported.[54-58]

5.6.2. CS_2 as a CO_2 analogue

Using liquid CS_2 in place of CO_2 gas in the method for cyclic carbonate synthesis from *O*- methyl-2,3-*O*-isopropylidiene-α-D-mannose (Chapter 3), with DBU reagent and TsCl in the presence of triethylamine, led to the formation of **13** + **14** as an inseparable mixture (Scheme 5.08).

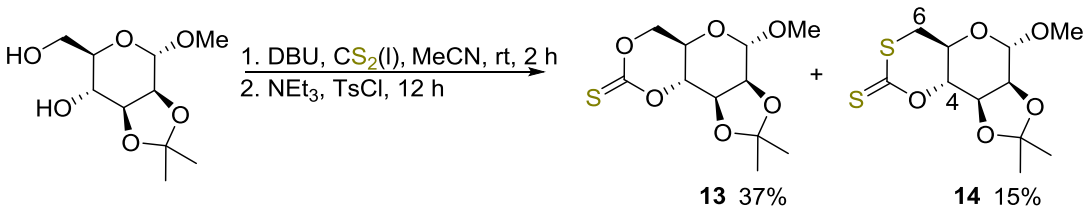

Scheme 5.07. Reaction of CS_2 with protected D-mannose-based diol and DBU followed by addition of NEt_3 and TsCl.

The presence of two species containing either one or two sulfur atoms in place of oxygen was confirmed by HR-MS(ESI). Cyclic monomer **13** showed similar ^{1}H and $^{13}C\{^{1}H\}$ NMR environments to the corresponding cyclic carbonate but with a C=S environment at 188.4 ppm and typically of a cyclic thione carbonate.[48] In contrast, cyclic monomer **14** displayed a C=S resonance at 206.0 ppm. The unexpected presence of the sulfur atom at the 6-position in **14** was indicated by the very upfield shift of the attached methylene (H-6) protons at 3.20 and 3.03 ppm compared to 4.50 and 4.26 ppm in the ^{1}H NMR spectrum of the cyclic carbonate. In the $^{13}C\{^{1}H\}$ NMR data, the C-6 environment adjacent to the sulfur atom appeared at 34.0 ppm, significantly shielded compared to 69.3 ppm when attached to the

more electronegative oxygen atom in the cyclic carbonate. The identity of the cyclic species was further corroborated by single-crystal X-ray diffraction analysis of orange crystals grown by layering hexanes over $CDCl_3$ (Figure 5.28). In **14**, the C1-O6 bond length is shorter by 0.43 Å compared to the C1-S2 bond, consistent with poorer C(2p)-S(3p) orbital overlap as opposed to C(2p)-O(2p).

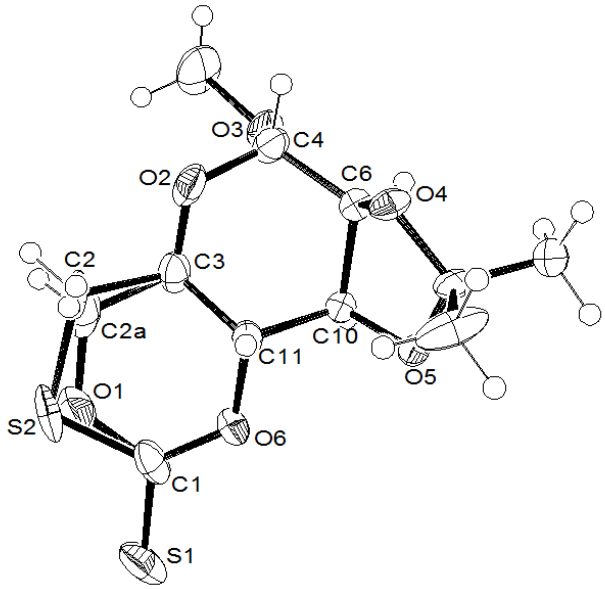

Figure 5.28. ORTEP[29] drawings with thermal ellipsoids at the 50% probability level for **13+14;** selected bond lengths (Å) and torsion angles (°): S(1)-C(1) 1.651(3), S(2)-C(1) 1.744(5), S(2)-C(2) 1.83(3), O(6)-C(1) 1.318(3), O(1)-C(1) 1.372(8), O(6)-C(1) 1.318(3), O(6)-C(11) 1.464(3), C(1)-O(6)-C(11)-C(3) -42.1(3), C(1)-S(2)-C(2)-C(3) 17.6(15), C(1)-O(1)-C(2A)-C(3) 18.8(16).

The isolation of **13** was expected following a nucleophilic addition-elimination ring-closing pathway, as observed for the corresponding cyclic carbonate. However, assuming no O-S rearrangements, **14** is postulated to arise from CS_2 insertion at the 4-position and subsequent S_N2-type ring-closing, eliminating a tosyl leaving group at the 6-position. In parallel with this, for the reaction carried out with *O*-methy-2-deoxy-D-ribofuranoside (**8-Me**), six-membered cyclic monomer **15** was isolated, albeit in low 10% yield, bearing the sought after 3,5-*trans*-cyclic configuration (Scheme 5.09).

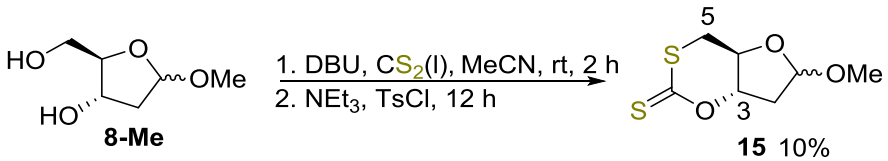

Scheme 5.08. Reaction of CS_2 with ribose-based diol and DBU followed by addition of NEt_3 and TsCl.

Presumably, the longer C-S bond length (155.3 pm in CS_2) compared to the typical C-O bond length (116.3 pm in CO_2) enabled formation of this *trans*-fused furanose monomer where the analogous cyclic carbonate could not be formed. As for **14**, the sulfur atom at the 5-position, negating any O-S scrambling, would suggest cyclisation *via* an S_N2-type mechanism.

In contrast to the previous *cis*-configured cyclic carbonates, **12α** and **12β**, which could be separated by column chromatography and displayed different solubilities and melting points, both anomers of **15** eluted during column chromatography with a single R_f value, for which ^{1}H NMR spectroscopy confirmed a 1:1 mixture. The mixture displayed a sharp melting point at 90 °C. Shown in Figure 5.29, the H-5 methylene protons adjacent to the sulfur atom, appeared significantly upfield at 3.21 to 3.28 ppm compared to in the cyclic carbonates. The H-3 environments also appear at lower chemical shifts compared to in **12α** and **12β** where the stereochemistry at this position was inverted.

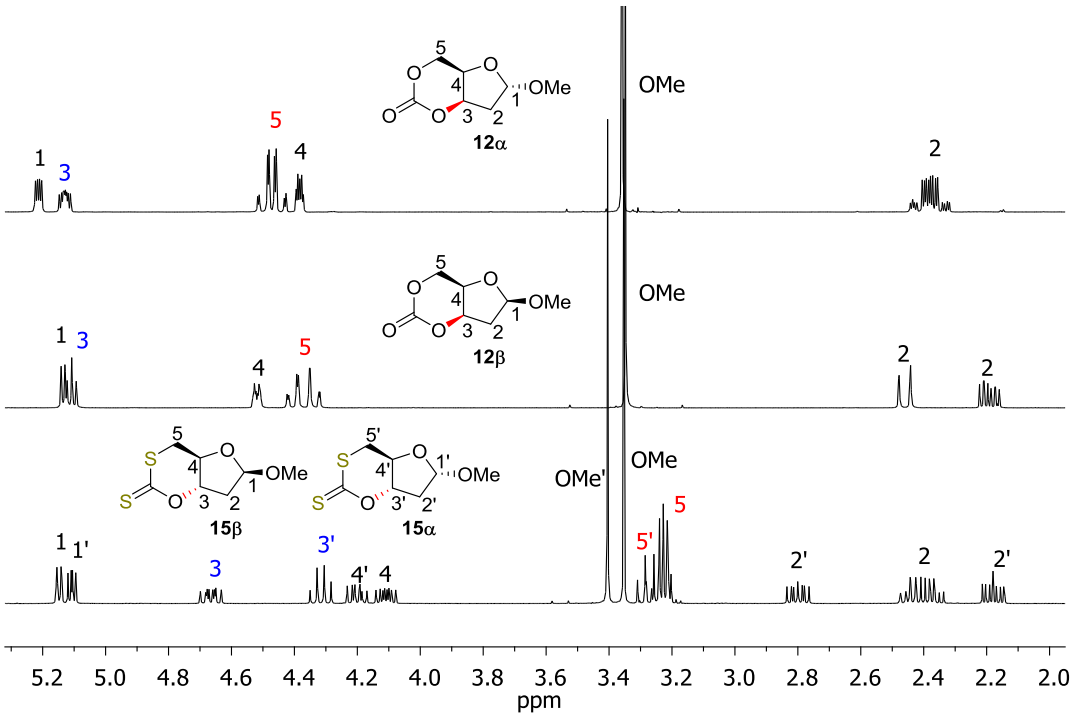

Figure 5.29. Comparison of the ^{1}H NMR spectra (400 MHz, $CDCl_3$) for *cis*-configuration cyclic carbonates **12α** and **12β** with the *trans*-configured CS_2 analogues **15(α+β)**, where the ring sulfur is at the 5-position.

In the β-anomer of **12**, the H-2 furanose ring methylene protons are in distinct chemical environments whereas in **12α** the environments overlap. This is reversed for the α- and β-anomers of **15** owing to stereochemical retention at the 3-position. In **15β**, the configuration

of the oxygen substituents either side of the equatorial and axial H-2 protons are *anti*- (1-axial, 3-equatorial) leading to a greater chemical inequivalence compared to in **15α** were the substituents either side are both in the axial position. Consistent also with a *trans*-configured cyclic carbonate, was the larger $^{3}J_{34}$ coupling constant of 8.7-8.8 Hz observed for **15** compared to 4.9 or 5.7 Hz for the *cis*-configured cyclic monomers. Analogous to **14**, the $^{13}C\{^{1}H\}$ NMR data showed the C-5 environments in **15** at significantly lower chemical shifts (37-38 ppm) compared to in the cyclic carbonates (67 ppm), where the carbon was adjacent to the more electronegative oxygen. Finally, the thione (-S-CS-O-) environment in the cyclic xanthates were observed at ~208 ppm.

Single crystal X-ray diffraction analysis of crystals grown by layering hexanes over $CDCl_3$ confirmed the structure and co-crystallisation of both anomers (Figure 5.30). For the β-anomer (left) the C1-S2 bond length was 1.74 Å compared to 1.33 Å for the neighbouring C1-O3 bond; it showed some double bond character based on comparison to the S2-CS single bond (1.83 Å) but less than C1=S1 (1.65 Å). The furanose ring adopts a 3-endo (^{3}E) conformation whereby, C7 in Figure 5.30 puckers above the plane (by 24 to 27°) formed by C3-O1-C4-C6 (dihedral angle ~1.5°). Similar observations for the bond lengths were made for the α-anomer (right, Figure 5.30), where the furanose ring adopts a 4-exo-3-endo twist conformation ($^{3}T_{4}$). (**12α** and **12β** adopted $^{0}T_{1}$ and E_{2} conformations, respectively).

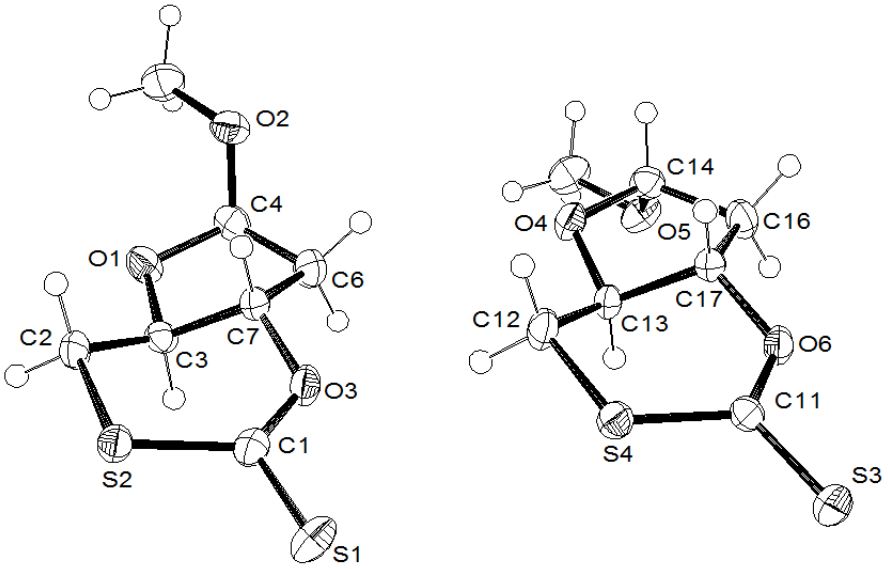

Figure 5.30. ORTEP[29] drawings of crystals of **15** with thermal ellipsoids at the 50% probability level for the co-crystallised β-anomer (top); selected bond lengths (Å) and torsion angles (°): S(1)-C(1) 1.645(2), S(2)-C(1) 1.742(2), S(2)-C(2) 1.831(2), O(3)-C(1) 1.329(3), O(3)-C(7) 1.447(2), C(4)-C(6)-C(7)-C(3) 39.3(2), O(1)-C(3)-C(7)-C(6) -41.6(2), C(4)-O(1)-C(3)-C(7) 27.0(2), C(3)-O(1)-C(4)-C(6) 1.5(2), O(1)-C(4)-C(6)-C(7) -24.1(2) and the α-anomer (bottom); selected bond lengths (Å) and torsion angles (°): S(3)-C(11) 1.642(2), S(4)-C(11) 1.742(2), S(4)-C(12) 1.823(2), C(14)-C(16)-C(17)-C(13) 33.5(2), O(4)-C(13)-C(17)-C(16) -45.4(2), C(14)-O(4)-C(13)-C(17) 39.5(2), C(13)-O(4)-C(14)-C(16) -18.0(2), O(4)-C(14)-C(16)-C(17) -10.7(2).

5.6.3. DFT modelling

The kinetics and thermodynamics of ring-closing *via* an S_N2-type pathway, involving DBU facilitated CS_2 or CO_2 insertion at the 3-position and elimination of a 5-tosyl leaving group were carried out for **8-Me** with the rωb97xd/6-31+G(d)/cpcm=acetonitrile/298 K protocol (Figure 5.31). The calculated barriers to cyclisation ($\Delta\Delta G^{\ddagger}$) were similar for both carbonate and sulfate nucleophiles, but the thermodynamic driving force ($\Delta\Delta G$) was greater for formation of the sulfur-containing *trans*-fused monomer **15** compared to the higher energy *trans*-3,5-cyclic carbonate. This suggested mechanism entails xanthate formation at the 3-position though, in a one-pot reaction and based on the CO_2 work, insertion would be anticipated to occur preferentially into the less sterically hindered primary hydroxyl group. This may account for the low isolated yield of **15** and improved yields may then be obtained by addition of the TsCl to the reaction mixture first, to target the 5-tosyl species before DBU facilitated CS_2 insertion and *in situ* cyclisation. An excess of CS_2 in the reaction mixture and heating may also lead to improvements in the yield. The calculated kinetic barrier is still relatively high compared to for example, +22.2 kcal mol^{-1} computed for the S_N2-type ring-closing, proceeding with inversion of stereochemistry, to form **12β**.

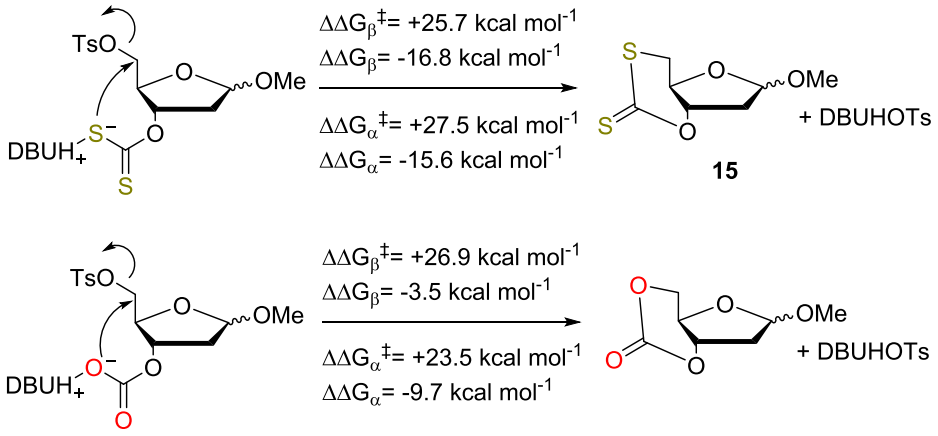

Figure 5.31. DFT modelling at the rωb97xd/6-31+G(d)/cpcm=acetonitrile/298 K level of theory for S_N2-type ring-closing with xanthate (OCS_2^-) or carbonate nucleophiles.

Nevertheless, calculations carried out at the same level the theory (Figure 5.32) and assuming a trimolecular mechanism for the reaction between CS_2, DBU and the sugar diol (as for CO_2 insertion) suggested little preference for insertion into either the 3- or 5-positions. Reaction of DBU with CS_2 is also plausible however, $^{13}C\{^1H\}$ NMR experiments in MeCN-

d_3 indicated no interaction; the C=S environment remained as reported for CS_2 in the absence of DBU base (δ_C = 193.6 ppm). This is in contrast to TBD, where the CS_2 adduct was isolated from THF by Thibault and coworkers.[60] An intense colour change from colourless to yellow was observed, only on addition of the DBU base to the mixture of sugar diol and CS_2.

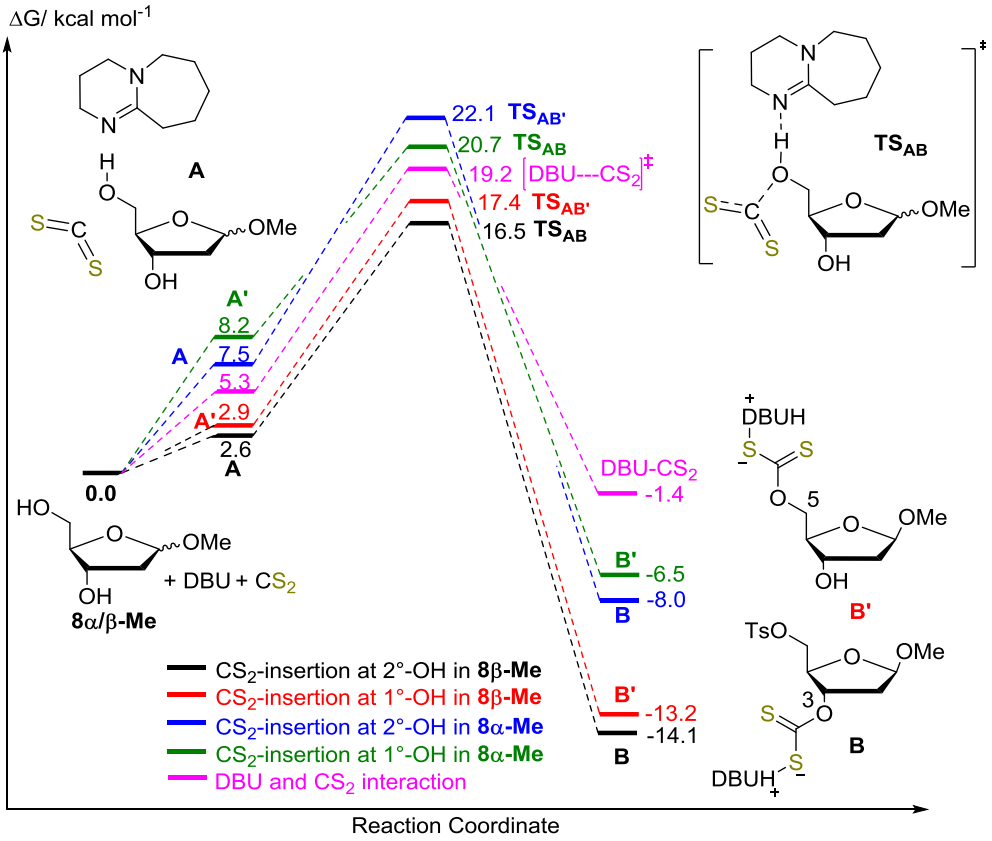

Figure 5.32. DFT modelling of the DBU-facilitated CS_2 insertion into *O*-methy-2-deoxy-D-ribofuranoside (**8-Me**) calculated at the ωb97xd/6-31+G(d)/cpcm=acetonitrile/298 K level of theory.

5.6.4. Ring strain

Preliminary ROP experiments of **15**, carried out by Eva M. López-Vidal suggest both anomers readily undergo organocatalytic ROP at room temperature and are corroborated by initial DFT calculations, assessing the ring stain (Figure 5.33).

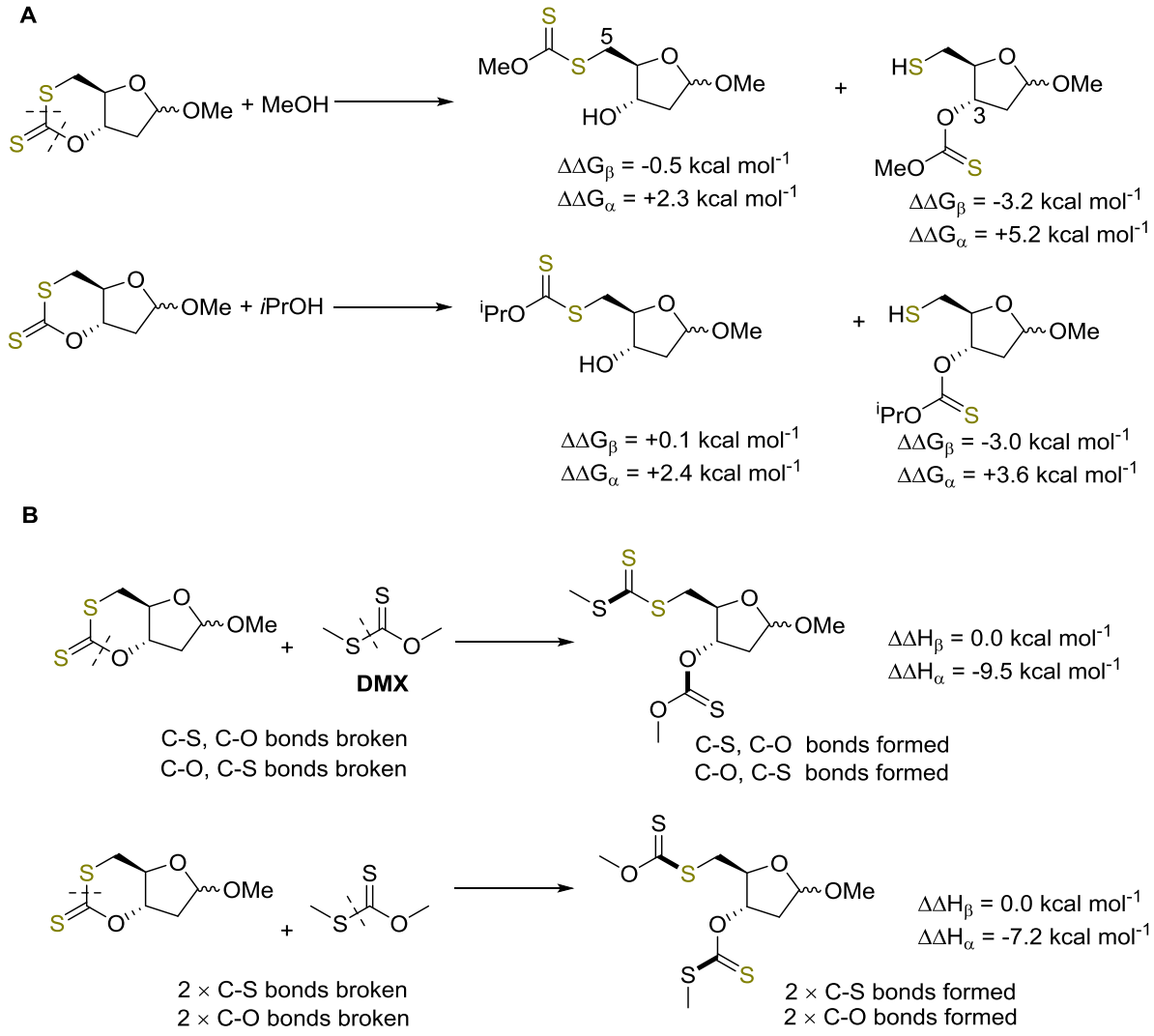

Figure 5.33. DFT calculations carried out at the rωb97xd/6-311++G(2d,p)/cpcm=dichloromethane/298 K level of theory for **A:** Ring-opening of **15** with MeOH or *i*-PrOH and **B:** isodemisc ring-opening of **15** with dimethyl xanthate (**DMX**).

5.7. Conclusions and Future Work

To conclude, six-membered cyclic carbonates can be prepared in 3 high-yielding steps from natural pentose sugar, 2-deoxy-D-ribose. Kinetic trapping of the sugar in its furanose ring form as the methyl glycoside and utilising CO_2 as a carbonylating agent (at room temperature and 1 atm pressure) leads to inversion of the stereochemistry at the 3-position (Figure 5.34). The α- and β- anomers of the *cis*-configured bicyclic monomers resulted in markedly different ROP behaviour. Whereas, the β-anomer did not undergo homopolymerisation with TBD catalyst and benzyl alcohol initiator, the α-anomer polymerised readily at room temperature to form highly insoluble ribose-based polycarbonates. DFT calculations suggested that the different polymerisablity of the anomers under these conditions had a thermodynamic rather than kinetic origin.

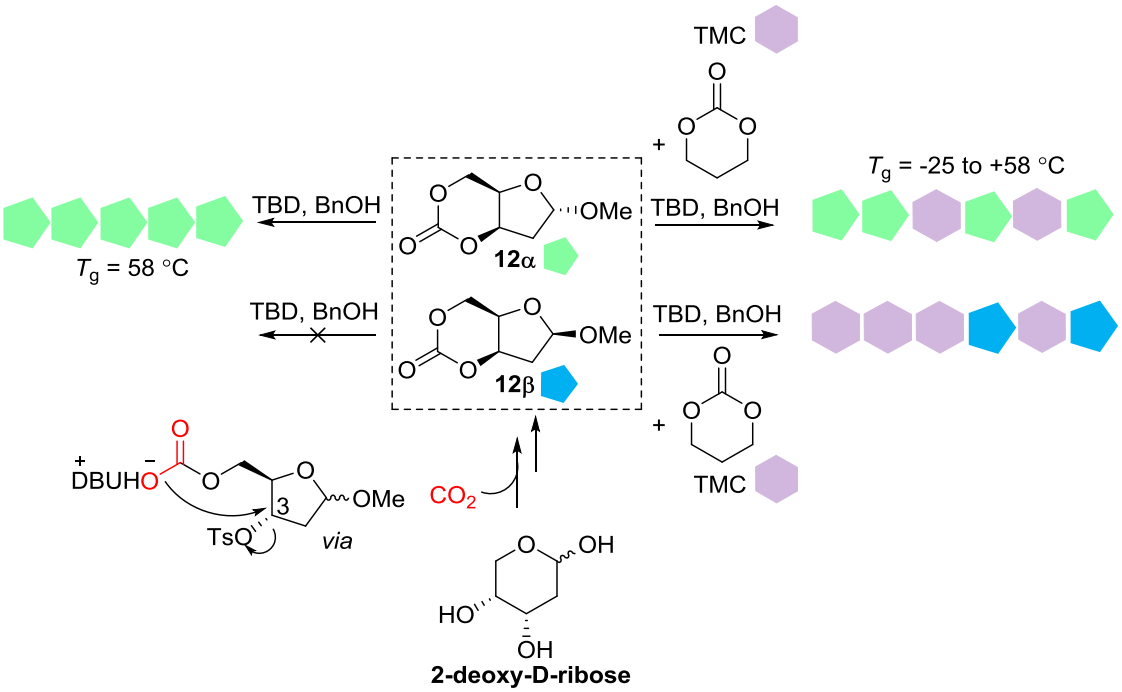

Figure 5.34. Cyclic carbonates from 2-deoxy-D-ribose and CO_2 showing different ROP behaviour for the α-and β-anomers with TBD organocatalyst and BnOH initiator. Copolymerisation with trimethylene carbonate (TMC) afforded APCs with T_g and thermal degradation properties tuneable through the comonomer composition.

Copolymerisation with TMC, resulted in high conversions (>99%) for the α-anomer and based on the input ratio of comonomers, copolymers could be prepared with controlled composition, leading to T_g values tuneable over a window of -25 to +58 °C. Relative to PTMC, copolycarbonates with α-content greater than 53 mol% also showed enhanced thermal degradation.

Further work might investigate macro-initiators for retaining the growing α-monomer segment in solution as well as for imparting amphiphilic properties. For example, diblock copolymers of the methoxy-protected D-glucose-based cyclic carbonate were prepared using polyphosphoester (PPE) macroinitiator (Scheme 5.09).[61] The alkyne functionality along the PPE segment was subsequently transformed through thiol-yne reactions to impart amphiphilic properties. Below a lower critical solution temperature (LCST), self-assembly into micelles was observed.

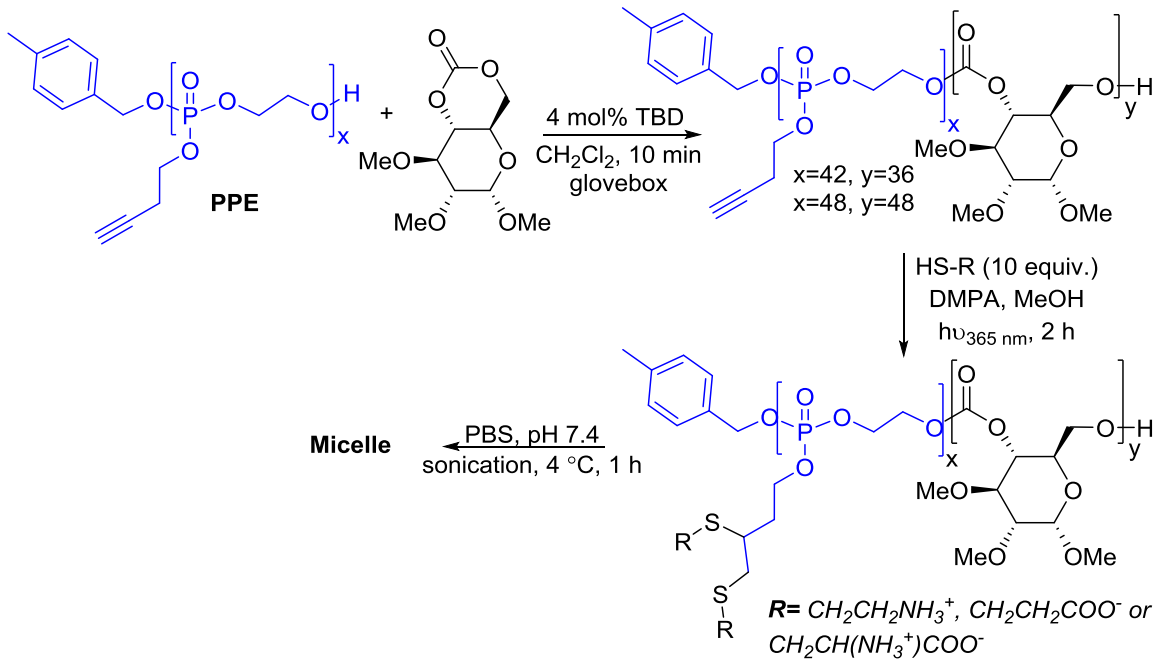

Scheme 5.09. Organocatalytic ROP of glucose-based cyclic carbonate with polyphosphoester (PPE) macroinitiator to form diblock copolymers, PPE-*b*-poly(D-glucose carbonate). Transformation of the alkyne functionality of the PPE segment imparted amphiphilic properties leading to micelle formation.[61]

An initial experiment with PEG macroinitiator and TBD catalyst for the ROP of **12α** was promising for preventing precipitation of the polymer. Moreover, selective functionalisation of the anomeric position in 2-deoxy-D-ribofuranose could introduce the alkyne group into the polycarbonate repeat units of block or random copolymers.

Under the ROP conditions investigated, the lack of polymerisation observed for **12β** was surprising considering the readily polymerisable nature of the thymidine derived and similarly furanose-cored cyclic carbonate in Chapter 4, where the nucleobase is also in the β-configuration. Thus, future work should also look to investigate the impact of the anomeric substituent on the ring-strain of the sugar-fused cyclic carbonate. Bulkier groups may give rise to both α- and β- anomers undergoing ROP. In turn, different polymerisation behaviour under changing ROP conditions of temperature or choice of catalyst, for example could lead to controlled incorporation of stereocentres and functionality.

Although they may be too far removed from the carbonate moiety, bulkier anomeric substituents may also lead to a preference for one linkage type in the polycarbonate backbone. Regiorandom polymers were observed for poly(**12α**) and the thymidine-based monomer in Chapter 4 yet, a preference for head-tail linkages was supported in the D-mannose derived polycarbonates (Chapter 3) and attributed to the bulky side-groups on the

pyranose ring. For a single anomer and either through the choice of anomeric substituent or use of a specifically design catalyst, a preference for asymmetric ring-opening to expose a secondary alcohol, leading to head-tail linkages would result in syndiotacticity [Figure 5.35(a)]. For a perfectly alternating copolymer of α- and β- anomers with the same or different anomeric functionality, isotacticity may be achieved [Figure 5.35(b)].

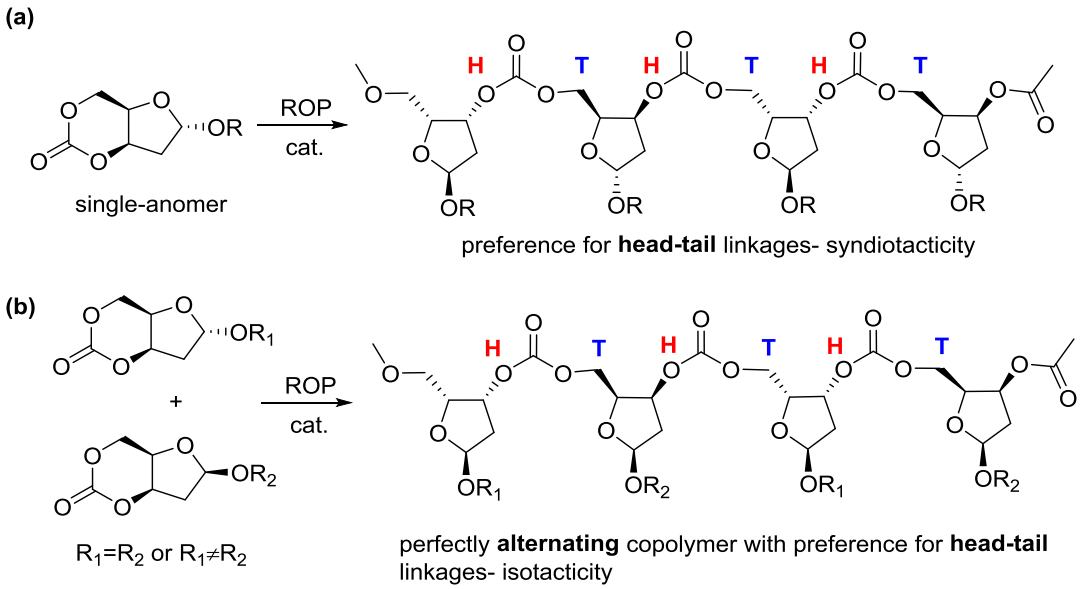

Figure 5.35. Tacticity in ribose-derived polycarbonates showing a preference for head-tail linkages.

Finally, the synthesis of *trans*-configured six-membered cyclic monomers from 2-deoxy-D-ribose using CS_2 as a CO_2 analogue is promising for the synthesis of sulfur-containing sugar-based polymers that may show enhanced thermal properties. Further work is required to improve the yield of the cyclic monomer with *O*-methyl-2-deoxy-D-ribofuranoside for subsequent investigations into the ROP and resulting polymer properties.

5.8 References

1. J. A. Galbis, M. d. G. García-Martín, M. V. de Paz and E. Galbis, *Chem. Rev.*, 2015, **116**, 1600-1636.
2. G. L. Gregory, E. M. Lopez-Vidal and A. Buchard, *Chem. Commun.*, 2017, **53**, 2198-2217.
3. G. W. Coates, *Chem. Rev.*, 2000, **100**, 1223-1252.
4. G. L. Baker, E. B. Vogel and M. R. Smith, *Polym. Rev.*, 2008, **48**, 64-84.
5. Y. Liu, W.-M. Ren, W.-P. Zhang, R.-R. Zhao and X.-B. Lu, *Nat. Commun.*, 2015, **6**.
6. G. Rokicki and P. G. Parzuchowski, in *Polymer Science: A Comprehensive Reference*, eds. K. Matyjaszewski and M. Möller, Elsevier, Amsterdam, 2012, pp. 247-308.
7. K. Tezuka, K. Komatsu and O. Haba, *Polym. J.*, 2013, **45**, 1183-1187.
8. A. K. Diallo, E. Kirillov, M. Slawinski, J.-M. Brusson, S. M. Guillaume and J.-F. Carpentier, *Polym. Chem.*, 2015, **6**, 1961-1971.
9. O. Haba, H. Tomizuka and T. Endo, *Macromolecules*, 2005, **38**, 3562-3563.
10. M. Azechi, K. Matsumoto and T. Endo, *J. Polym. Sci. Part A: Polym. Chem.*, 2013, **51**, 1651-1655.
11. K. Tezuka, K. Koda, H. Katagiri and O. Haba, *Polym. Bull.*, 2015, **72**, 615-626.
12. W. M. Doane, B. S. Shasha, E. I. Stout, C. R. Russell and C. E. Rist, *Carbohydr. Res.*, 1967, **4**, 445-451.
13. K. Fukushima, *Biomater. Sci.*, 2016, **4**, 9-24.
14. J. M. W. Chan, X. Zhang, M. K. Brennan, H. Sardon, A. C. Engler, C. H. Fox, C. W. Frank, R. M. Waymouth and J. L. Hedrick, *J. Chem. Educ.*, 2015, **92**, 708-713.
15. M. Pastusiak, P. Dobrzynski, J. Kasperczyk, A. Smola and H. Janeczek, *J. Appl. Polym. Sci.*, 2014, **131**, 40037.
16. C. Fliedel, S. Mameri, S. Dagorne and T. Avilés, *Appl. Organomet. Chem.*, 2014, **28**, 504-511.
17. K. Kobayashi, S. Kanmuri, Y. Kimura and K. Masutani, *Polym. Int.*, 2015, **64**, 641-646.
18. P. Dobrzynski and J. Kasperczyk, *J. Polym. Sci. Part A: Polym. Chem.*, 2006, **44**, 98-114.
19. A. Couffin, D. Delcroix, B. Martín-Vaca, D. Bourissou and C. Navarro, *Macromolecules*, 2013, **46**, 4354-4360.
20. C. L. Romero Zaliz and O. Varela, *Carbohydr. Res.*, 2006, **341**, 2973-2977.
21. I. M. Pinilla, M. B. Martínez and J. A. Galbis, *Carbohydr. Res.*, 2003, **338**, 549-555.
22. Y. Shen, X. Chen and R. A. Gross, *Macromolecules*, 1999, **32**, 3891-3897.
23. X. Chen and R. A. Gross, *Macromolecules*, 1999, **32**, 308-314.
24. R. Kumar, W. Gao and R. A. Gross, *Macromolecules*, 2002, **35**, 6835-6844.
25. R. D. Youssefyeh, J. P. H. Verheyden and J. G. Moffatt, *J. Org. Chem.*, 1979, **44**, 1301-1309.
26. M. Quintiliani, J. Balzarini and C. McGuigan, *Tetrahedron*, 2013, **69**, 9111-9119.
27. O. R. Ludek and V. E. Marquez, *Tetrahedron*, 2009, **65**, 8461-8467.
28. *Int. Pat.*, WO2012/71508 A1, 2012
29. L. J. Farrugia, *J. Appl. Cryst.*, 2012, **45**, 849-854.
30. M. Honda, M. Tamura, K. Nakao, K. Suzuki, Y. Nakagawa and K. Tomishige, *ACS Catal.*, 2014, **4**, 1893-1896.
31. E. Larsen, T. Kofoed and E. B. Pedersen, *Synthesis*, 1995, **1995**, 1121-1125.
32. K. Mikami, A. T. Lonnecker, T. P. Gustafson, N. F. Zinnel, P. J. Pai, D. H. Russell and K. L. Wooley, *J. Am. Chem. Soc.*, 2013, **135**, 6826-6829.
33. Y. Shen, X. Chen and R. A. Gross, *Macromolecules*, 1999, **32**, 2799-2802.
34. O. Coulembier, V. Lemaur, T. Josse, A. Minoia, J. Cornil and P. Dubois, *Chem. Sci.*, 2012, **3**, 723-726.
35. M. Fineman and S. D. Ross, *J. Polym. Sci., Part A: Polym. Chem.*, 1950, **5**, 259-262.
36. D. J. Darensbourg, W.-C. Chung and S. J. Wilson, *ACS Catal.*, 2013, **3**, 3050-3057.
37. C. G. Overberger and J. Weise, *J. Polym. Sci., Part B: Polym. Lett.*, 1964, **2**, 329-331.
38. T. J. Bannin and M. K. Kiesewetter, *Macromolecules*, 2015, **48**, 5481-5486.
39. C. G. Overberger and J. K. Weise, *J. Am. Chem. Soc.*, 1968, **90**, 3533-3537.

40. H.-L. Wu, J.-L. Yang, M. Luo, R.-Y. Wang, J.-T. Xu, B.-Y. Du, X.-H. Zhang and D. J. Darensbourg, *Macromolecules*, 2016.
41. A. Kultys, in *Encyclopedia of Polymer Science and Technology*, John Wiley & Sons, Inc., 2002.
42. M. Luo, X. H. Zhang and D. J. Darensbourg, *Acc. Chem. Res.*, 2016, **49**, 2209-2219.
43. M. Luo, Y. Li, Y.-Y. Zhang and X.-H. Zhang, *Polymer*, 2016, **82**, 406-431.
44. B. Ochiai and T. Endo, *Prog. Polym. Sci.*, 2005, **30**, 183-215.
45. X.-H. Zhang, F. Liu, X.-K. Sun, S. Chen, B.-Y. Du, G.-R. Qi and K. M. Wan, *Macromolecules*, 2008, **41**, 1587-1590.
46. D. J. Darensbourg, J. R. Andreatta, M. J. Jungman and J. H. Reibenspies, *Dalton Trans.*, 2009, 8891–8899.
47. D. J. Darensbourg, S. J. Wilson and A. D. Yeung, *Macromolecules*, 2013, **46**, 8102-8110.
48. M. Luo, X.-H. Zhang and D. J. Darensbourg, *Macromolecules*, 2015, **48**, 5526-5532.
49. J. Diebler, H. Komber, L. Häußler, A. Lederer and T. Werner, *Macromolecules*, 2016, **49**, 4723-4731.
50. W. Choi, F. Sanda, N. Kihara and T. Endo, *J. Polym. Sci. Part A: Polym. Chem.*, 1997, **35**, 3853-3856.
51. T. Endo, N. Nemoto and F. Sanda, *Macromol. Symp.*, 2003, **192**, 25-30.
52. N. Nemoto, K. Yoshii, H. Kameshima, F. Sanda and T. Endo, *J. Polym. Sci. Part A: Polym. Chem.*, 2003, **41**, 185-195.
53. F. Sanda, J. Kamatani and T. Endo, *Macromolecules*, 1999, **32**, 5715-5717.
54. S. J. Jeon, M.-y. Jung and J. Y. Do, *Reactive and Functional Polymers*, 2016, **100**, 37-43.
55. M. Benazza, R. Kanso and G. Demailly, *Carbohydr. Res.*, 2010, **345**, 346-351.
56. Y. Tsuda, S. Noguchi and H. Niino, *Chem. Pharm. Bull.*, 2001, **49**, 1210-1213.
57. M. Adiyaman, S. P. Khanapure, S. W. Hwang and J. Rokach, *Tetrahedron Lett.*, 1995, **36**, 7367-7370.
58. D. Trimnell, W. M. Doane, C. R. Russell and C. E. Rist, *Carbohyd. Res.*, 1971, **17**, 319-326.
59. D. Trimnell, W. M. Doane and C. R. Russell, *Carbohyd. Res.*, 1972, **22**, 351-359.
60. N. von Wolff, C. Villiers, P. Thuéry, G. Lefèvre, M. Ephritikhine and T. Cantat, *Eur. J. Org. Chem.*, 2017, **2017**, 676-686.
61. T. P. Gustafson, A. T. Lonnecker, G. S. Heo, S. Zhang, A. P. Dove and K. L. Wooley, *Biomacromolecules*, 2013, **14**, 3346-3353.

Chapter 6

Concluding Remarks

6. Concluding Remarks

The feasibility of the conversion of 1,3-diols to six-membered cyclic carbonates using CO_2 carbonylation agent under mild reaction conditions (room temperature and atmospheric pressure) has been demonstrated. The limiting kinetic barriers can be overcome with readily available reagents leading to a one-pot procedure for the coupling of CO_2 with diols, with yields comparable to alternative methods using toxic or expensive reagents. This is promising for the development of a catalytic system, whereby the combined computational and experimental approach is useful for guiding catalyst design. A consideration of the reaction pathway for the strategy with CO_2 and TsCl leaving group proved vital in the synthesis of challenging sugar-based cyclic carbonates.

Novel cyclic monomers have been prepared from CO_2 and mannose, thymidine, and 2-deoxy-D-ribose sugars. The need to use protecting group chemistry to avoid undesired side reactions during synthesis should be viewed as means of introducing functionality into polymer backbones. The balance between the ease of cyclic carbonate synthesis and the ROP potential needs always to be considered. The highly ring-strained nature of the *trans*-configured cyclic carbonates fused to the furanose rings in thymidine and 2-deoxy-D-ribofuranose sugars necessitated inversion of the natural sugar stereochemistry to form the *cis*-analogue. This was achievable with the use of CO_2 and expanded the scope of sugar-based monomers beyond those accessible with traditional reagents proceeding *via* a nucleophilic addition-elimination mechanism.

The scalability of the monomer synthetic route is another important consideration when designing new monomers. Aside from being relevant industrially, this is also important at a lab scale to ensure enough monomer can be prepared to determine the polymerisation kinetic and thermodynamic parameters as well as for full materials characterisation and for investigating potential applications. For example, preparing polymer thin films using a thermal press often requires 5-10 g of material. Compared to the thymidine and ribose-derived monomers, the mannose based cyclic carbonate, requiring fewer synthetic steps, could be prepared on the largest scale (~3 g). Scalability was mainly limited by the high dilution and thus size of the reaction vessel required for the cyclocarbonation step as well as the isolation of the product from the reaction mixture by column chromatography.

Ring-opening polymerisation of the sugar-based cyclic carbonates proceeded readily and in a controlled fashion under mild reaction conditions (≤ 25 °C) with a simple organocatalytic approach. The *trans*-configured cyclic carbonate fused to the pyranose ring in D-mannose achieved full conversion under these reaction conditions compared to the equilibrium limited polymerisations of the *cis*-fused furanose cored monomers. Cyclic and linear topologies were observed for all polycarbonates and with no evidence of decarboxylation. The impact of the anomeric centre configuration on the polymerisability was observed with D-ribose based monomers and hints at a subtle effect of the fused furanose ring conformation on the cyclic carbonate ring strain.

The combination of furanose or pyranose rings in the polycarbonate backbones and the substituents about the rings led to high glass transition temperatures (T_g = 58 to 156 °C). Incorporation of 2-deoxy-D-ribofuranose into the flexible chain of TMC imparted stiffness to the main chain and led to higher T_g values and enhanced thermal degradation. Preliminarily biocompatibility testing of the thymidine-derived materials is promising for future biomedical applications of polymers from CO_2 and sugars. Focus should reside on the functionalisation of the monomers already reported and the preparation of different linkage types rather than the use of other monosaccharide building blocks.

Chapter 7

Experimental

7. Experimental

7.1. Materials

Anhydrous chloroform (containing amylene stabilisers), acetonitrile (99.8%) and dichloromethane (containing amylene stabilisers) were purchased from Sigma Aldrich. All other dry solvents were obtained using an Innovative Technology Inc. PS-400-7 solvent purification system (SPS) and dried over 3 Å molecular sieves for at least 24 hours prior to use. Solvents used for metal complexations were also degassed prior to use. 1,1,1,3,3,3- hexafluoro-2-propanol (HFIP) was obtained from FluoroChem and 1,1,1,3,3,3- hexafluoro-2-propanol (HFIP-d_2) from Cambridge Isotope Laboratories Inc. (D, 98%) and used without further purification. N4.5 CP grade CO_2 was purchased from BOC and fitted to a dedicated Schenk line, where it passed through a polycarbonate drying column before being introduced to reactions using standard Schlenk line techniques. All metal complexations were carried out under an atmosphere of argon using a glovebox and Schlenk line techniques.

1,2-*O*-isopropylidene-α-D-xylofuranose (**1i**), thymidine, 1-*O*-methyl-α-D-mannose, 1-*O*-methyl-4,6-*O*-benzylidene-α-D-glucose, 2-deoxy-D-ribose and 1-*O*-methyl-2-deoxy-D-ribofuranoside (**8-Me**) were purchased from Carbosynth and used without further purification. Anhydrous (±)-1,3-butanediol was purchased from Sigma Aldrich and handled in a glovebox. Benzyl alcohol (Sigma Aldrich) was vacuum distilled over CaH_2 and 4- methylbenzyl alcohol (Acros Organics) recrystallised from dry diethyl ether before being stored in a glovebox. Triethylamine (Aldrich) was refluxed and distilled over CaH_2 prior to use. 1,5,7-Triazabicyclo[4.4.0]dec-5-ene (TBD) (Sigma Aldrich) was dried over CaH_2 in anhydrous THF immediately prior to use and handled in a glovebox. 1,8- Diazabicyclo[5.4.0]undec-7-ene (DBU) (Alfar Aesar) was stored in a glovebox and used without further purification for CO_2 insertion reactions. For ROP, it was purified by vacuum distillation and stored in a glovebox prior to use. Column chromatography (Sigma Aldrich) was performed on silica gel (200-400 mesh particle size, 60 Å pore size) and spots visualised by UV light and/or staining with $KMnO_4$ solution. TLC analysis was performed on aluminium backed plates pre-coated with silica (UV Alugram SIL G/UV_{245nm}). All other reagents were purchased from either Sigma Aldrich or Alfa Aesar and used without further purification.

7.2. Methods

Melting points (mp) were measured on a variable temperature Griffen melting point apparatus. **Polarimetry** measurements were made on an Optical Activity LTD AA-10 automatic polarimeter. $[\alpha]_D$ values are given in 10^{-1} deg cm^2 g^{-1}. **Infra-red spectra** were recorded as thin films on a Perkin-Elmer 1600 Fourier transform spectrometer. All **NMR spectra** were recorded on a Bruker 400 MHz instrument at 25 °C except for quantitative $^{13}C\{^1H\}$ NMR spectra, which were recorded on a Bruker 500 MHz instrument. All ^{13}C NMR spectra were proton decoupled. Chemical shifts (δ) are reported in ppm and *J*-coupling constants, quoted in Hertz. Multiplets were assigned as s = singlet, d = doublet, dd = doublet of doublets, t = triplet and sp = septet. NMR spectra were referenced to residual solvent peaks: ^1H NMR spectra (400 MHz): δ_H = 7.26 ($CDCl_3$), 1.94 (MeCN-d_3), 4.79 ppm (D_2O); 1.72 ppm (THF-d_8), 2.08 (tol-d_8), 7.16 (C_6D_6), 3.31 (CD_3OD), 2.50 (DMSO-d_6) and 4.86 (HFIP-d_2); $^{13}C\{^1H\}$ spectra (101 MHz): δ_C = 77.16 ($CDCl_3$), 118.26 ppm (MeCN-d_3), 25.31 (THF-d_8), 137.48 (tol-d_8), 128.06 (C_6D_6), 49.00 (CD_3OD), 39.52 DMSO-d_6 and 68.07 ppm (HFIP-d_2). NMR analysis of metal complexes was carried out in deuterated solvent dried over 3 Å molecular sieves in a glovebox for at least 48 hours prior to use and carried out in NMR tubes fitted with Young's taps. **Mass spectrometry** were recorded with a microToF electrospray time-of-flight (ESI-ToF) mass spectrometer (Bruker Daltonik) in methanol, acetonitrile or water. **CHN microanalysis** was performed by Mr Stephen Boyer of London Metropolitan University.

Polymer number-average molecular weights (M_n) and dispersities Đ (M_w/M_n) were estimated by **size exclusion chromatography (SEC)** with a differential refractive index (RI) detector. For mannose based polycarbonates (Chapter 3), the 1260 SEC MDS system from Agilent was used with GPC grade THF (1 mL min^{-1}) as the mobile phase and polymeric samples dissolved in THF at a concentration of 2 mg ml^{-1}. The PL HFIPgel 300x7.5 mm column and PL HFIPgel 50x7.5 mm guard column were maintained along with the detector at 35 °C and calibrated with a set of polystyrene standards. For thymidine-based polycarbonates (Chapter 4) and poly(TMC-*co*-ribose) copolycarbonates (Chapter 5), the 1260 SEC MDS system from Agilent with manual injection was used with HPLC grade $CHCl_3$ (1 mL min^{-1}) as the mobile phase and polymeric samples dissolved in $CHCl_3$ at a concentration of 2 mg mL^{-1}. The RI detector was maintained at 35 °C and the PL gel 5μm mixed-D 300x7.5 mm column and 5μm PLgel 50x7.5 mm guard column calibrated with a set of polystyrene standards. For

poly(**12α**), which was only soluble in HFIP (Chapter 5), a Polymer Laboratories PL-GPC 50 integrated system was used with 2 x PL HFIPgel columns (maintained at 40 °C) and calibrated to PMMA standards.

All glass transition temperatures (T_g) were measured by **differential scanning calorimetry (DSC)**. For mannose and thymidine- based polycarbonates (Chapters 3 and 4), a MicroSC multicell calorimeter from Setaram was used and the Calisto program for collecting and processing data. Both measurement and reference cells were 1 mL Hastelloy C cells and in a glovebox, between 5-10 mg of polymeric material was loaded into the measurement cell with the reference cell left empty. The experiment was performed under nitrogen gas and the sample heated from 20 to 200 °C at a rate of 1 K min^{-1} and then cooled at the same rate. A second heating and cooling cycle was carried out immediately following completion of the first. For ribose-based polymers and copolymers (Chapter 5), DSC traces were recorded on a TA Instruments DSC Q20. Samples (2-5 mg) were sealed in an aluminium pan and alongside an empty reference pan, rapidly cooled to –40 °C and then heated to 200 °C at a rate of 10 K min^{-1} before being cooled back to –40 °C at the same rate. A second heating and cooling cycle was carried out following completion of the first.

A Setsys Evolution TGA 16/18 from Setaram was used for all **thermogravimetric analysis (TGA)**; the Calisto program was employed to collect and process the data. The sample was loaded into a 170 µL alumina crucible and the analytical chamber purged with argon (200 mL min^{-1}) for 40 min prior to starting the analysis. The sample was then heated under an argon flow (20 mL min^{-1}) from 30 to 500 °C at a rate of 5 K min^{-1}. During the heating ramp, evolving gas was taken off from the analytical chamber to a mass spectrometer through a stainless-steel capillary by Pfeiffer Vacuum. The mass spectrometer was a Omnistar GSD 320 equipped with a quadrupole mass analyser and a SEM detector.

Matrix-assisted laser desorption ionisation-time of flight (MALDI-ToF) mass spectrometry was conducted using a Bruker Autoflex speed MALDI Mass Spectrometer equipped with a 2 kHz Smartbeam-II laser. A solution of trans-2-[3-(4-tert-butylphenyl)-2-methyl-2-propenylidene]malononitrile (DCTB) matrix in $CHCl_3$, THF or HFIP (10 mg mL^{-1}) was added to a $CHCl_3$, THF or HFIP solution of polymer (5 mg mL^{-1}) with sodium trifluoroacetate (0.1 mol L^{-1} in HFIP or THF) in a 25:5:1 ratio, and the samples centrifuged for 1 min. A micropipette was used to spot ~1-2 µL of the solution onto a polished steel

MALDI plate and the solvent allowed to evaporate in air. Positive ion MALDI spectra were obtained in reflector mode and laser intensity varied. The data was analysed using the Flex Analysis software, version 3.4 (build 76). The molecular weight distributions and percentage of cyclic and linear polymeric species, were obtained through analysis of the data in the Polytools software package 1.31.

All **single-crystal X-ray diffraction** analysis was carried out by Dr Gabriele Kociok-Köhn on a Nonius Kappa CCD diffractometer using Cu-K_α radiation (λ = 1.54184 Å) at 150 K. ***Powder diffraction patterns*** were recorded by Bethan Charles (Chapter 3), Dr Gabriele Kociok-Köhn (Chapter 4) or Mr Alan Carver (Chapter 5) on a Bruker Advance D8 diffractometer with Cu-K_α radiation (λ = 1.5406 Å) at 298 K. The sample was ground with a pestle and mortar before being transferred to a disk. Data was recorded from a 2θ of 4 to 60° with 0.02 steps s^{-1} and 0.5 s $step^{-1}$.

Contact Angles Measurements (Chapter 4) were made on a DataPhysics OCA_{50} micro instrument. 2 μL water droplets were dropped onto the polymer surface and the SCA20 software package used to measure both the right and left-hand contact angles. Polymer films were prepared by drop-casting 1 wt% polymer solutions in CH_2Cl_2 onto glass slides and allowing the solvent to evaporate before drying in a vacuum oven overnight at 40 °C. 10 measurements were recorded over 3 polymer films and compared to measurements taken on the glass slide as a control and films of the monomer prepared in the same manner.

Cell attachment studies (Chapter 4) were performed with the MG-63 bone cancer cell line. These were maintained in corning T75 cell culture flasks at 37 °C in FBS^+ growth medium (87 v/v% Dulbecco's Modified Eagle Medium, 10% fetal bovine serum (FBS), 1% penicillin streptomycin, 1% non-essential amino acids and 1% sodium pyruvate). Cells were passaged every 4 days by removing the growth medium and washing with phosphate-buffered saline (PBS) solution (10 ml) before treatment with trypsin (5 ml), to detach the cells from the culture flask. The trypsin was removed by centrifugation (1000 rpm, 15 minutes) in growth media (10 ml) and the cell sediment then re-suspended in fresh growth media (10 ml). Following staining of the cell suspension (100 μL) with trypan blue (100 μL), the number of live cells was counted with a Luna dual fluorescence cell counter immediately prior to attachment studies. Thin films were prepared by drop casting polymer solutions in CH_2Cl_2 (as for the contact angle measurements detailed above) of 0.25, 0.5, 0.75 and 1 wt% onto

glass slides. These were sterilised with a 70% EtOH aqueous solution and glued into the wells of a Corning Costar 24 cell culture plate with Norland Optical Adhesive 63. Setting of the glue and further sterilised under UV light was carried out in a Heoroff UV 500 crosslinker at 100 μJ cm^{-2} for 15 minutes. After washing the wells with PBS solution (0.5 ml), cells were seeded in growth media (0.5 ml) at a density of 10, 000 live cells cm^{-2}. 3 repeats were performed for each polymer wt% and compared to empty wells and glass controls. After 1 or 24 hour incubation periods at 37 °C, the media was removed and each well washed with PBS solution (2 × 0.5 ml). Attached cells were fixed with formalin solution (0.5 ml, 10% formaldehyde, 90% PBS). After 15 minutes, this was removed and the wells washed with PBS solution (2 × 0.5 ml) before staining with 4,6-diamidino-2-phenylindole (DAPI) solution (150 μL, 0.002% DAPI in PBS). The solution was removed after 15 minutes and any residual fluorescent staining agent removed by washing with PBS solution (2 × 0.5 ml). Care was taken to ensure minimum light exposure during the staining procedure. Cell images were recorded using a EVOS digital optical microscope under low light at 10x objective. 6 images were recorded at different locations for each well plate and images analysed using ImageJ software 1.7.0_55 (32-bit) to determine the cell count.

7.3. Chapter 2

7.3.1. General procedure for CO_2 insertion (Table 2.01)

Under an argon atmosphere, anhydrous (±)-1,3-butanediol (0.5 ml, 5.6 mmol, 1 equiv.) was transferred to an oven-dried Schlenk and dried solvent (1 to 4 ml) added. The argon atmosphere was then replaced with CO_2 using standard Schlenk line techniques by subjecting the stirring mixture to three cycles of vacuum followed by purging with CO_2 at atmospheric pressure. The solution was then left to saturate with CO_2. This was monitored *via* the bubbler attached to the CO_2 line and when no further uptake was observed (<1 h), neat DBU or TBD solution (1 to 3 equiv.) was added dropwise. All aliquots taken for NMR analysis were carried out under a stream of CO_2 gas. The reaction at 8 bars CO_2 pressure was carried out in a stainless-steel autoclave (Entry 16, Table 2.01).

7.3.2. Synthesis of cyclic carbonates 2a-2j (Table 2.02)

Following the CO_2 insertion procedure (above), for the diol (1 equiv., 1.7 mol L^{-1} in anhydrous chloroform or acetonitrile) with DBU reagent (1 equiv.), the reaction mixture was left to stir under a CO_2 atmosphere (1 atm pressure) for 2 hours at room temperature before triethylamine (1 equiv.) and TsCl (1 equiv., 0.5 mol L^{-1} in anhydrous chloroform or acetonitrile) were added. After stirring overnight, volatiles were removed under reduced pressure and the cyclic carbonate product isolated by column chromatography (1-5% acetone/$CHCl_3$ eluent).

For sugar-based diols **2i** and **2j** (1 equiv., **0.1 mol L^{-1}** in anhydrous chloroform or acetonitrile) and following the CO_2 insertion procedure above, with DBU reagent (1 equiv.), better yields were obtained on cooling the reaction mixture to 0 °C in an ice-water bath and allowing it to saturate with CO_2 (4 h). Triethylamine (1 equiv.) and TsCl (1 equiv., 0.5 mol L^{-1} in anhydrous chloroform or acetonitrile) were then added and the reaction mixture allowed to slowly warm to room temperature. After 24 hours, the solvent was removed under reduced pressure and the crude reaction mixture immediately subject to column chromatography (1-5% acetone/$CHCl_3$ eluent).

4-Methyl-[1,3]-dioxan-2-one (2a)[1]

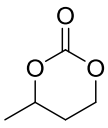

Isolated as a colourless oil (0.440 g, 68%); R_f 0.61 (1:1 acetone: $CHCl_3$); ^{1}H NMR (400 MHz, $CDCl_3$): δ_H (ppm) 4.68-4.44 (1H, m, CHMe), 4.46-4.21 (2H, m, OCH_2), 2.06-2.00 (1H, m , $OCH_2CH\underline{H}$), 1.78-1.88 (1H, m, $OCH_2C\underline{H}H$), 1.35 (3 H, d, *J* 6.3 Hz, CH_3); $^{13}C\{^1H\}$ NMR (101 MHz, $CDCl_3$): δ_C (ppm) 148.9 (C=O), 75.7 (CH), 66.9 (CH_2O), 28.4 (CH_2), 20.9 (CH_3), in accordance with the literature.[1] HR-MS (ESI): $[C_5H_8O_3 + Na]^+$ Theo. *m/z* 139.0371 found 139.0386; Found: C, 51.63; H, 7.04. $C_5H_8O_3$ requires C, 51.72; H 6.94%.

(R)-4-Methyl-[1,3]-dioxan-2-one (R-2a)

Isolated as a white crystalline solid (0.440 g, 68%); $[\alpha]_D^{25}$ +26 (*c* 1.0 in $CHCl_3$).

(S)-4-Methyl-[1,3]-dioxan-2-one (S-2a)

Isolated as a white crystalline solid (0.455 g, 70%); $[\alpha]_D^{25}$ -27 (*c* 1.0 in $CHCl_3$).

4R,6R-Dimethyl-[1,3]-dioxan-2-one (2b)[1,2]

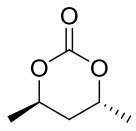

Isolated as a yellow oil (0.331 g, 53%); R_f 0.60 (1:1 acetone: $CHCl_3$); ^{1}H NMR (400 MHz, $CDCl_3$): δ_H (ppm) 4.74-4.66 (1H, m, CHMe), 1.93 (1H, t, *J* 5.6 Hz, CH_2), 1.43 (3H, d, *J* 6.5 Hz, CH_3); $^{13}C\{^1H\}$ NMR (101 MHz, $CDCl_3$): δ_C (ppm) 149.5 (C=O), 72.6 (CH), 34.0 (CH_2), 20.9 (CH_3), in accordance with the literature.[1, 2] HR-MS (ESI): $[C_6H_{10}O_3 + Na]^+$ Theo. *m/z* 153.0522 found 153.0556; Found: C, 55.49; H, 7.61. $C_6H_{10}O_3$ requires C, 55.37; H, 7.75%.

4-Phenyl-[1,3]-dioxan-2-one (2c)[5]

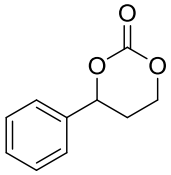

1-Phenylpropane-1,3-diol (**1c**) was synthesised in two steps from acetophenone and dimethyl carbonate following the literature procedures.[3, 4] The cyclic carbonate was isolated as a colourless oil, which solidified on standing (0.332 g, 55%); R_f 0.72 (1:1 acetone: $CHCl_3$); ^{1}H NMR (400 MHz, $CDCl_3$): δ_H (ppm) 7.48-7.32 (5H, m, Ph-H), 5.52 (1H, dd, *J* 9.8, 3.7 Hz, CHO), 4.61-4.40 (2H, m, CH_2O), 2.39-2.32 (1H, m, $OCH_2C\underline{H}H$), 2.30-2.20 (1H, m, $OCH_2CH\underline{H}$); $^{13}C\{^1H\}$ NMR (101 MHz, $CDCl_3$): δ_C (ppm) 148.8 (C=O), 137.9 (quaternary C), 129.1 (*m*-PhC), 129.0 (*o*-PhC), 125.7 (*p*-PhC), 80.2 (CH), 66.9 (CH_2O), 29.4 (CH_2), consistent with previous reports.[5] HR-MS (ESI): $[C_{10}H_{10}O_3 + Na]^+$ Theo. *m/z* 201.0528 found 201.0526; Found: C, 67.45; H, 5.74. $C_{10}H_{10}O_3$ requires C, 67.41; H, 5.66%.

5,5-Dimethyl-[1,3]-dioxolan-2-one (2d)[6]

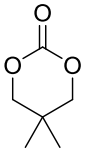

Isolated as a white powder (0.332 g, 53%); R_f 0.65 (1:1 acetone: $CHCl_3$); ^{1}H NMR (400 MHz, $CDCl_3$): δ_H (ppm) 4.04 (1H, s, CH_2), 1.09 (2H, s, CH_3); $^{13}C\{^1H\}$ NMR (101 MHz, $CDCl_3$): δ_C (ppm) 148.2 (C=O), 77.5 (quaternary C), 28.5 (CH_2), 21.1 (CH_3), in accordance with the literature.[6] HR-MS (ESI): $[C_6H_{10}O_3 + Na]^+$ Theo. *m/z* 131.0708 found. 131.0716; Found: C, 55.38; H, 7.67. $C_6H_{10}O_3$ requires C, 55.37; H, 7.75%.

5,5-Dimethoxy-[1,3]-dioxolan-2-one (2e)[6]

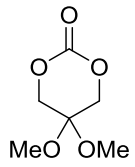

2,2-dimethoxy-propane-1,3-diol (**1e**) was prepared according to the literature procedure.[7] The cyclic carbonate was isolated as a white powder (0.291 g, 49%); R_f 0.63 (1:1 acetone: $CHCl_3$); ^{1}H NMR (400 MHz, $CDCl_3$): δ_H (ppm) 4.28 (2H, s, CH_2), 3.31 (3H, s, CH_3); $^{13}C\{^1H\}$ NMR (101 MHz, $CDCl_3$): δ_C (ppm) 147.9 (C=O), 92.2 (C), 69.9 (CH_2), 49.4 (OCH_3), in accordance with literature.[6] HR-MS (ESI): $[C_6H_{10}O_5 + Na]^+$ Theo. *m/z* 185.0425 found 185.0434; Found: C, 44.52; H, 6.35. $C_6H_{10}O_5$ requires C, 44.45; H, 6.22%.

9-Phenyl-2,4,8,10-tetraoxaspiro[5,5]undecanone (2f)[8]

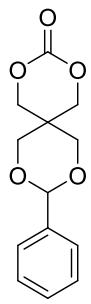

The benzylidene acetal-protected pentaerythritol diol (**1f**) was synthesised following the literature.[8] The cyclic carbonate was isolated as a white powder (0.257 g, 46%); R_f 0.62 (1:1 acetone: $CHCl_3$); ^{1}H NMR (400 MHz, $CDCl_3$): δ_H (ppm) 7.57-7.28 (5H, m, Ph-H), 5.50 (1H, s, CHPh), 4.70 (2H, s, CH_2 carbonate), 4.21 (2H, dd, *J* 10.6, 1.4 Hz, CH_2 acetal), 4.09 (2H, s, CH_2 carbonate), 3.88 (2H, dd, *J* 10.6, 1.4 Hz, CH_2 acetal); $^{13}C\{^1H\}$ NMR (101 MHz, $CDCl_3$): δ_C (ppm) 148.0 (C=O), 137.0 (ArC), 129.5 (ArCH), 128.5 (ArCH), 126.0 (ArCH), 102.4 (CH), 71.4 (CH_2), 70.4 (CH_2), 69.4 (2 × CH_2), in accordance with the literature.[8] HR-MS (ESI): $[C_{13}H_{14}O_5 + Na]^+$ Theo. *m/z* 273.0738 found 273.0727; Found: C, 62.23; H, 5.67. $C_{13}H_{14}O_5$ requires C, 62.39; H, 5.64%.

Benzyl 5-methyl-2-oxo-1,3-dioxane-5-carboxylate (2g)[10]

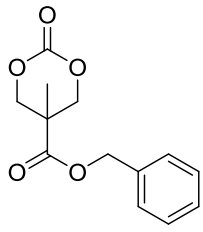

Benzyl protected 2,2-bis(hydroxymethyl)propionic acid (**1g**) was prepared according to the literature procedures.[6, 9] The cyclic carbonate was isolated as a colourless oil, which crystallised on standing (0.229 g, 41%); R_f 0.66 (1:1 acetone: $CHCl_3$); ^{1}H NMR (400 MHz, $CDCl_3$): δ_H (ppm) 7.49-7.22 (5H, m, Ar-H), 5.21 (2H, s, CH_2Ph), 4.70 (2H, d, *J* 10.9 Hz, CH_2), 4.20 (2H, d, *J* 10.9 Hz, CH_2), 1.32 (3H, s, CH_3); $^{13}C\{^1H\}$ NMR (101 MHz, $CDCl_3$): δ_C (ppm) 171.0 (C=O), 147.5 (C=O carbonate), 134.9 (ArC), 130.0 (ArC), 128.9 (ArC), 128.3 (ArC), 73.0 (2 × OCH_2), 68.0 (OCH_2Ph), 40.3 (quaternary C), 17.6 (CH_3), consistent with the

literature data.[10] HR-MS (ESI): $[C_{13}H_{14}O_5]^+$ Theo. *m/z* 251.0914 found 251.0938; Found: C, 62.25; H, 5.68. $C_{13}H_{14}O_5$ requires C, 62.39; H, 5.64%.

[1,3]-Dioxolan-2-one (2h)[11]

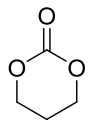

Trimethylene carbonate (TMC) was isolated as a white powder and recrystallised from dry diethyl ether to give colourless flakes (0.389 g, 68%); R_f 0.48 (1:1 acetone: $CHCl_3$); ^{1}H NMR (400 MHz, $CDCl_3$): δ_H (ppm) 4.41 (4H, t, *J* 5.7 Hz, CH_2O), 2.11 (2H, q, *J* 5.7 Hz, CH_2); $^{13}C\{^1H\}$ NMR (101 MHz, $CDCl_3$): δ_C (ppm) 148.6 (C=O), 68.0 (CH_2O), 21.7 (CH_2), in agreement with literature data.[11] HR-MS (ESI): $[C_4H_6O_3 + Na]^+$ Theo. *m/z* 125.0209 found 125.0208; Found: C, 47.09; H, 5.97. $C_4H_6O_3$ requires C, 47.06; H, 5.92%.

Cyclic 1,2-O-isopropylidene-3,5-O-carbonate-α-D-xylofuranose (2i)[12]

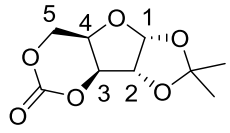

Isolated as a white powder (0.724 g, 67%); R_f 0.51 (1:1 acetone: $CHCl_3$); ^{1}H NMR (400 MHz, $CDCl_3$): δ_H (ppm) 6.00 (1H, d, *J* 3.7 Hz, H-1), 4.88 (1H, d, *J* 2.8 Hz, H-3), 4.74 (1H, d, *J* 3.7 Hz, H-2), 4.63-4.59 (1H, m, H-5), 4.56-4.52 (2H, m, H-4, H-5'), 1.50 (3H, s, $C(CH_3)_2$), 1.33 (3H, s, $C(CH_3)_2$); $^{13}C\{^1H\}$ NMR (101 MHz, $CDCl_3$): δ_C (ppm) 146.4 (C=O), 113.1 ($\underline{C}(CH_3)_2$), 105.3 (C-1), 83.9 (C-2), 82.5 (C-3), 69.2 (C-4), 66.8 (C-5), 26.8 ($C(\underline{C}H_3)_2$), 26.3 ($C(\underline{C}H_3)_2$), in agreement with the literature.[12] HR-MS (ESI): $[C_9H_{12}O_6 + Na]^+$ Theo. 239.0526 *m/z* found 239.0592; Found: C, 49.98; H, 5.66. $C_9H_{12}O_6$ requires C, 50.00; H, 5.60%.

Cyclic 1,2,3-O-methyl-4,6-O-carbonate-α-D-glucopyranoside (2j)[13]

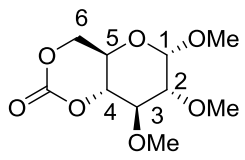

1,2,3-*O*-Methyl-α-D-glucopyranoside was prepared in 3 steps from commercial available 1-*O*-methyl-4,6-*O*-benzylidene-α-D-glucopyranoside following the literature procedure.[13] After 24 hours stirring at room temperature, the 4,6-bicyclic carbonate monomer was isolated by column chromatography with 1% acetone/$CHCl_3$ (0.347 g, 62%); R_f 0.71 (1:1 acetone: $CHCl_3$); ^{1}H NMR (400 MHz, $CDCl_3$): δ_H (ppm) 4.87 (1H, d, *J* 3.6 Hz, H-1), 4.47 (1H, dd, *J* 9.8, 5.8 Hz, H-6), 4.21 (1H, dd, *J* 9.8, 9.3 Hz, H-6'), 4.05 (2H, ddd, *J* 9.8, 9.3, 5.8 Hz, H-5), 4.00 (1H, dd, *J* 9.8, 9.3 Hz, H-4), 3.65 (1H, t, *J* 9.3 Hz, H-3), 3.64 (3H, s, OMe), 3.55 (3H, s, OMe), 3.48 (3H, s, OMe), 3.26 (1H, dd, *J* 9.3, 3.6 Hz, H-2); $^{13}C\{^1H\}$ NMR (101 MHz, $CDCl_3$): δ_C

(ppm) 147.4 (C=O), 98.9 (C-1), 81.0 (C-4), 79.8 (C-2), 79.4 (C-3), 69.7 (C-6), 61.3 (C-5), 59.9 (OMe), 59.7 (OMe), 56.2 (OMe), in accordance with the literature.[13] HR-MS (ESI): $[C_{10}H_{16}O_7 + Na]^+$ Theo. *m/z* 271.0794 found 271.0769; Found: C, 48.45; H, 6.59. $C_{10}H_{16}O_7$ requires C, 48.39; H, 6.50%.

7.3.3. Ligand Synthesis

2,6-Diisopropyl-N-((2Z,4E)-4-((pyridin-2-ylmethyl)imino)pent-2-en-2-yl)aniline (HL1)[15]

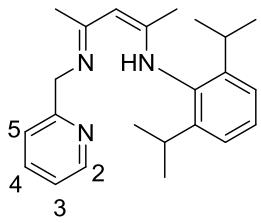

Following the literature procedure,[14] to a stirring solution of 2-(2,6-di-*iso*-propylphenylimido)-2-pentene-4-one[15] (10.1 g, 39 mmols, 1 equiv.) and DMAP (4.4 ml, 42.9 mmols, 1.1 equiv.) in toluene (50 ml), was added *p*-TSA (0.05 mol%) and the reaction heated to reflux. Water was removed as a toluene azeotrope using Dean-Stark apparatus and volatiles removed after 24 hours *in vacuo*. The resulting brown residue was dissolved in diethyl ether (30 ml), washed with saturated aqueous Na_2CO_3 (3 × 30 ml) and dried over $MgSO_4$. Removal of the solvent under reduced pressure and recrystallisation from hexane gave the β-diketiminato ligand **HL1** as large pale yellow crystals (8.66 g, 64%); ^{1}H NMR (400 MHz, $CDCl_3$): δ_H (ppm) 11.34 (1 H, br s, NH), 8.53 (1H, ddd, *J* 4.8, 1.7, 0.9 Hz, 2-Py-H), 7.64 (1H, td, *J* 7.7, 1.7 Hz, 4-Py-H), 7.31 (1H, d, *J* 7.8 Hz, 5-Py-H), 7.18-6.99 (4H, m, 3-Py-H, 3×Ar-H), 4.79 (1H, s, $CH_3C(N)C\underline{H}$), 4.60 (2H, s, NCH_2), 2.93 (2H, sp, *J* 6.9 Hz, $ArC\underline{H}(CH_3)_2$), 2.00 (3H, s, CH_3C), 1.69 (3H, s, CH_3C), 1.19 (6H, d, *J* 7.0 Hz, $ArCH(C\underline{H}_3)_2$), 1.10 (7H, d, *J* 6.8 Hz, $ArCH(C\underline{H}_3)_2$); $^{13}C\{^1H\}$ NMR (101 MHz, $CDCl_3$): δ_c (ppm) 166.5, 160.1, 155.6 (2 × imine-C and Py-C) 149.3, 146.6, 138.0, 136.9, 122.8, 122.8, 121.9, 120.4, (Ar-C and Py-C), 94.5 ($CH_3C(N)\underline{C}H$), 48.9 (NCH_2), 28.1 ($Ar\underline{C}H(CH_3)_2$), 23.8 ($ArCH(\underline{C}H_3)_2$), 22.9 ($ArCH(\underline{C}H_3)_2$), 21.7 ($\underline{C}H_3C$), 19.3 ($\underline{C}H_3C$); HR-MS (ESI): $[C_{23}H_{30}N_3]$ Theo. *m/z* 348.2845 found 348.2456; Found: C, 78.72; H, 8.74; N 12.11. $C_{23}H_{31}N_3$ requires C, 79.04; H, 8.94; N 12.02%.

N-(3,5-Di-tert-butyl-2-hydroxy)-N-(2-pyridylmethyl)-amine (HL2)[16]

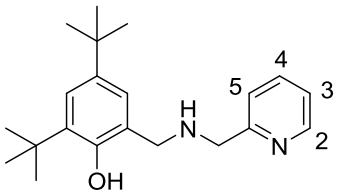

Following the literature procedure,[16] DMAP (0.52 ml, 5 mmol, 1 equiv.) was added to a solution of 3,5-di-*tert*-butyl-2-hydroxybenzaldehyde[17](1.17 g, 5 mmol, 1 equiv.) in MeOH (30 ml). After stirring at room temperature for 3 hours, $NaBH_4$ (0.19 g, 5 mmol, 1 equiv) was added slowly (over a period of 1 hour) and the reaction monitored by TLC. After 24 hours, a loss of the yellow colour of the Schiff base was notable and subsequent removal of volatiles *in vacuo* afforded a pale yellow solid. Following neutralisation in distilled water (30 ml) with glacial acetic acid, extraction into DCM (3 × 30 ml) and drying of the combined extracts over $MgSO_4$, removal of the solvent under reduced pressure afforded a sticky pale yellow residue. Washing with hexane at -78 °C gave a white powder (1.34 g, 82%); R_f 0.22 (6:3 Hexane: EtOAc); ^{1}H NMR (400 MHz, C_6D_6): δ_H (ppm) 8.36 (1H, dd, *J* 4.1, 1.7 Hz, 2-Py-H), 7.50 (1H, d, *J* 2.4 Hz, Ar-H), 6.97 (1H, td, *J* 7.7, 1.8 Hz, 4-Py-H), 6.85 (1H, d, *J* 2.4 Hz, Ar-H), 6.62-6.56 (2H, m, 3-Py-H, 5-Py-H), 3,63 (2H, s, CH_2), 3.50 (2H, s, CH_2), 1.72 (9H, s, *t*-Bu), 1.35 (9H, s, *t*-Bu); ^{13}C{^{1}H} NMR (400 MHz, C_6D_6): δ_C (ppm) 158.5, 155.6, 149.6, 140.6, 136.2, 136.1, 128.3, 128.1, 127.8, 123.8, 123.1, 122.6, 122.3, 122.0 (6 CH + 5 quaternary), 53.2 (CH_2), 53.2 (CH_2), 35.4 ($\underline{C}(CH_3)_3$), 34.4 ($\underline{C}(CH_3)_3$), 32.0 ($C(\underline{C}H_3)_3$), 30.1 ($C(\underline{C}H_3)_3$); HR-MS (ESI): $[C_{21}H_{30}N_2O + Na]^+$ Theo. 349.2256 m/z found 349.2273; Found: C, 77.72; H, 9.34; N 8.62. $C_{21}H_{30}N_2O$ requires C, 77.26; H, 9.26; N 8.58%.

2,4-Di-tert-butyl-6-[(pyridin-2-ylmethyl-imino)methyl]phenol (HL3)[18]

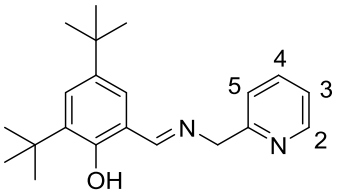

Following the literature procedure,[18] DMAP (2.12 ml, 21.3 mmol, 1 equiv.) was added to a stirred solution of 3,5-di-*tert*-butyl-2-hydroxybenzaldehyde (5.00 g, 21.3 mmol, 1 equiv.) in methanol (50 ml). The resulting yellow solution was refluxed overnight and monitored by TLC (Hexane: EtOAC). Removal of the volatiles *in vacuo* and recrystallisation from hexane afford intensely yellow crystals of the Schiff base **HL3** (4.97 g, 73%); R_f 0.35 (6:3 Hexane: EtOAc); ^{1}H NMR (400 MHz, C_6D_6): δ_H (ppm) 14.13 (1H, br s, OH), 8.43 (1H, dd, *J* 4.6, 1.4 Hz, 2-Py-H), 7.87 (1H, s, HC=N), 7.58 (1H, d, *J* 2.5 Hz, Ar-H), 7.02-7.00 (2H, m, 5-Py-H, 4-Py-H), 6.94 (1H, d, *J* 2.5 Hz, Ar-H), 6.61-6.58 (1H, m, 3-Py-H), 4.64 (2H, s, CH_2), 1.65 (9H, s, *t*-Bu), 1.33 (9H, s, *t*-Bu); ^{13}C{^{1}H} NMR (101 MHz,

C_6D_6): δ_C (ppm) 68.4 (CH=N), 158.9, 158.8, 149.7, 140.3, 137.1, 136.4, 127.2, 126.8, 122.1, 121.7, 118.7 (6 CH + 5 quaternary), 65.2 (CH_2), 35.4 ($\underline{C}(CH_3)_3$), 34.3 ($C(\underline{C}H_3)_3$), 31.8 ($C(\underline{C}H_3)_3$), 29.8. ($C(\underline{C}H_3)_3$); HR-MS (ESI): $[C_{21}H_{28}N_2O + Na]^+$ Theo. 347.2094 m/z found 347.2084; Found: C, 77.68; H, 8.63; N 8.54. $C_{21}H_{28}N_2O$ requires C, 77.74; H, 8.70; N 8.63%.

7.3.4. General procedure for diethyl zinc complexations

Under an atmosphere of argon, a 1 mol L^{-1} solution of diethylzinc in hexane (613 µL, 0.613 mmol, 1 equiv.) was added dropwise to a stirring solution of ligand (0.2g, 0.613 mmol, 1 equiv.) in hexane. Colour changes were noted immediately from pale yellow to purple for **HL1** and **HL2** or yellow to orange/red for **HL3**. After 24 hours of stirring at room temperature, the mixture was centrifuged for L2ZnEt and L3ZnEt, the supernatant decanted off and the resulting precipitate dried under reduced pressure. Following the literature procedure,[19] no centrifugation was required in the case of L1ZnEt, which was isolated upon removal of the solvent under reduced pressure.

L1ZnEt[19] was isolated as a white powder (0.236 g, 87%); ^{1}H NMR (400 MHz, $CDCl_3$): δ_H (ppm) 8.48 (1H, d, *J* 4.3 Hz, 2-Py-H), 7.66 (1H, td, *J* 7.7, 1.7 Hz, 4-Py-H), 7.22 (1H, d, *J* 7.8 Hz, 5-Py-H), 7.19 – 7.12 (4H, m, 3-Py-H, 3×Ar-H), 4.91 (2H, s, NCH_3), 4.76 (1H, s, $CH_3C(N)C\underline{H}$), 3.11 (2H, sp, *J* 6.9 Hz, $ArC\underline{H}(CH_3)_2$), 2.10 (3H, s, CH_3C), 1.69 (3H, s, CH_3C), 1.20 (6H, s, $ArCH(C\underline{H}_3)_2$), 1.18 (6H, s, $ArCH(C\underline{H}_3)_2$), 0.62 (3H, t, *J* 8.1 Hz, Zn-$CH_2C\underline{H}_3$), -0.22 (2H, q, *J* 8.1 Hz, Zn-$C\underline{H}_2CH_3$); $^{13}C\{^1H\}$ NMR (101 MHz, C_6D_6): δ_C (ppm) 166.4, 165.9, 159.7 (imine-C and Py-C), 148.8, 146.3, 142.2, 136.6, 125.4, 123.7, 122.0, 121.6 (Ar-C and Py-C), 95.3 ($CH_3\underline{C}(N)CH$), 54.9 ($N\underline{C}H_2$), 28.2 ($Ar\underline{C}H(CH_3)_2$), 24.7 ($ArCH(\underline{C}H_3)_2$), 24.0 ($ArCH(\underline{C}H_3)_2$), 23.8 ($\underline{C}H_3C$), 22.1 ($\underline{C}H_3C$), 13.3 (Zn-$CH_2\underline{C}H_3$), -0.72 (Zn-$\underline{C}H_2CH_3$) in agreement with the literature data.[19] No satisfactory elemental analysis could be obtained despite multiple attempts.

L2ZnEt was isolated as a white powder (0.206 g, 80 %); ^{1}H NMR (400 MHz, C_6D_6): δ_H (ppm) 7.87 (1H, d, *J* 5.0 Hz, 2-py-H), 7.39 (1H, d, *J* 2.7 Hz, Ar-H), 6.77 (1H, d, *J* 2.7 Hz, Ar-H), 6.64 (1H, td, *J* 7.7, 1.6 Hz, 4-Py-H), 6.24 (1H, dd, *J* 7.1, 5.5 Hz, 3-Py-H), 6.07 (1H, d, *J* 7.8 Hz, 5-Py-H), 3.56 (1H, d, *J* 10.8 Hz, CH_2), 3.13-3.02 (2H, m, CH_2), 2.90 (1H, d, *J* 16 Hz, CH_2), 1.83 (9H, s, *t*-Bu), 1.69 (3H, Zn-$CH_2C\underline{H}_3$), 1.40 (9H, s, *t*-Bu), 0.75-0.85 (2H, m, Zn-$C\underline{H}_2CH_3$); $^{13}C\{^1H\}$ NMR (101 MHz, C_6D_6): δ_C (ppm) 164.8, 156.0, 148.0, 138.0,

137.9, 134.2, 125.3, 123.9, 122.8, 122.6, 121.7 (6 CH + 5 quaternary) 54.2 (CH_2), 52.5 (CH_2), 35.7 ($\underline{C}(CH_3)_3$), 34.0 ($\underline{C}(CH_3)_3$), 32.4 ($C(\underline{C}H_3)_3$), 30.4 ($C(\underline{C}H_3)_3$), 14.1 (Zn-$CH_2\underline{C}H_3$), -2.1 (Zn-$\underline{C}H_2CH_3$). Despite multiple attempts, no satisfactory elemental analysis could be obtained.

L3ZnEt was isolated as a yellow powder (0.195 g, 76%); ^{1}H NMR (400 MHz, C_6D_6): δ_H (ppm) 8.50 (1H, d, *J* 4.8 Hz, 2-Py-H), 7.78 (1H, d, *J* 2.7 Hz, Ar-H), 7.53 (1H, s, HC=N), 6.98 (1H, d, *J* 2.6 Hz, Ar-H), 6.89 (1H, td, *J* 7.7, 1.7 Hz, 4-Py-H), 6.55 (1H, d, *J* 7.9 Hz, 5-Py-H), 6.48 – 6.36 (1H, dd, *J* 4.6, 1.1 Hz, 3-Py-H,), 4.31(2H, s, CH_2), 1.82 (9H, s, *t*-Bu), 1.48 (9H, s, *t*-Bu), 1.45 (3H, t, *J* 8.0 Hz, $CH_2C\underline{H}_3$), 0.05 (2H, q, *J* 8.0 Hz, $C\underline{H}_2CH_3$); $^{13}C\{^1H\}$ NMR (101 MHz, C_6D_6): δ_C (ppm) 171.2, 169.7, 157.6, 149.0, 142.1, 138.6, 134.7, 129.9, 129.8, 124.5, 123.8, 118.3 (6 Ar-C, 5 Py-C, C=N), 64.4 (CH_2), 36.1 ($\underline{C}(CH_3)_3$), 34.2 ($\underline{C}(CH_3)_3$), 31.9 ($C(\underline{C}H_3)_3$, 30.0 ($C(\underline{C}H_3)_3$, 13.5 (Zn-$CH_2\underline{C}H_3$), 1.7 (Zn-$\underline{C}H_2CH_3$). Despite multiple attempts, no satisfactory elemental analysis could be obtained.

7.4. Chapter 3

Cyclic 1-O-methyl-2,3-O-isopropylidene-4,6-O-carbonate-α-D-mannopyranoside (3)

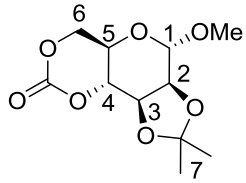

2,3-*O*-isopropylidene protection of commercially available 1-*O*-methyl-α-D-mannose was carried out following the literature procedure.[20] DBU (2.2 ml, 15 mmol, 1 equiv.) was added dropwise to a CO_2 saturated solution of protected mannose (3.5 g, 15.0 mmol, 1 equiv., 0.1 mol L^{-1} in anhydrous acetonitrile). After 2 hours, stirring at room temperature, the solution was cooled to 0 °C in an ice-water bath and allowed to further saturate with CO_2 before triethylamine (2.1 ml, 15 mmol, 1 equiv.) was added. A solution of TsCl (2.84 g, 15 mmol, 1 equiv. 0.5 mol L^{-1} in anhydrous acetonitrile), also saturated with CO_2 at 0 °C was then transferred dropwise *via* cannula to the solution of CO_2-inserted sugar. The reaction mixture was allowed to warm to room temperature and left for 24 hours before being concentrated under reduced pressure at room temperature. The crude reaction mixture was immediately subjected to column chromatography (1% acetone/$CHCl_3$) and the 4,6-cyclic carbonate product isolated as colourless needles following recrystallisation from dry diethyl ether (2.24 g, 57%), mp 128-129 °C (ether); R_f 0.77 (1:1 acetone: $CHCl_3$, $KMnO_4$ stain); FTIR (thin film)/cm^{-1} 1763 (C=O); ^{1}H NMR (400 MHz, $CDCl_3$): δ_H (ppm) 4.99 (1H,

d, *J* 0.4 Hz, H-1), 4.50 (1H, dd, *J* 10.1, 6.1 Hz, H-6), 4.29-4.20 (3H, m, H-6', H-3, H-2), 4.14 (1H, dd, *J* 10.3, 7.5 Hz, H-4), 3.97 (1H, dt, *J* 10.3, 6.1 Hz, H-5), 3.42 (3H, s, OMe), 1.54 (3H, s, 7-Me), 1.37 (3H, s, 7-Me); $^{13}C\{^{1}H\}$ NMR (101 MHz, $CDCl_3$): δ_C (ppm) 147.4 (C=O), 110.5 (C-7), 99.3 (C-1), 79.1 (C-4), 75.6 (C-2), 74.0 (C-3), 69.3 (C-6), 57.8 (C-5), 55.8 (OMe), 28.1 (7-Me), 26.2 (7-Me); HR-MS (ESI): $[C_{11}H_{16}O_7 + Na]^+$ Theo. *m/z* 283.0794 found 283.0772; Found: C, 50.72; H, 6.24. $C_{11}H_{16}O_7$ requires C, 50.77; H, 6.20%.

Typical Polymerisation Procedure

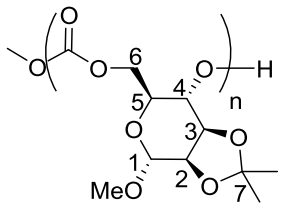

Under an argon atmosphere, TBD (10 μL, 1 mol L^{-1} solution in dry CH_2Cl_2) was added to a solution of monomer (260 mg, 1.00 mmol) and 4-methylbenzyl alcohol (10 μL, 1 mol L^{-1} solution in dry CH_2Cl_2) in anhydrous CH_2Cl_2 (1 ml). The mixture was stirred at room temperature and monomer conversion monitored by ^{1}H NMR spectroscopy of aliquots taken and quenched with benzoic acid. Following removal of the solvent under reduced pressure, the crude product was dissolved in the minimum amount of CH_2Cl_2 and precipitated from diethyl ether. The product was isolated by centrifugation (3000 rpm, 15 minutes) and precipitated once more from diethyl ether to afford a white solid (218 mg, 84%); FTIR (thin film)/cm^{-1} 1763 (C=O); ^{1}H NMR (400 MHz, $CDCl_3$): δ_H (ppm) 4.91-4.89 (1H, s, H-1), 4.73 (1H, br s, H-4), 4.33-4.22 (3H, m, H-6, H-6', H-3), 4.11-4.10 (1H, m, H-2), 3.88 (1H, br s, H-5), 3.36-3.37 (3H, s, OMe), 1.53 (3H, s, 7-Me), 1.32 (3H, s, 7-Me); $^{13}C\{^{1}H\}$ NMR (101 MHz, $CDCl_3$): δ_C (ppm) 154.5 (C=O), 110.1 (C-7), 98.0 (C-1), 75.8, 75.7 (C-2, C-3), 74.3 (C-4), 66.6 (C-6), 65.9 (C-5), 55.3 (OMe), 27.8 (7-Me), 26.4 (7-Me); M_n (SEC) 13 600 g mol^{-1}; Đ 1.17; T_g (DSC under Ar) 150 °C; TGA under Ar: 170-350 °C, 98% mass loss. For conversion *versus* time, M_n and Đ, aliquots were taken at set time intervals, quenched with benzoic acid and analysed by ^{1}H NMR spectroscopy ($CDCl_3$) and SEC.

Equimolar ring-opening experiments

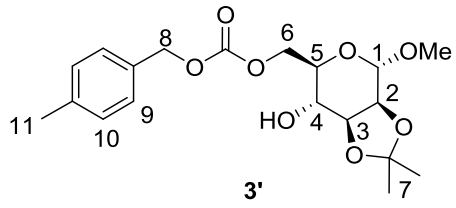

3'

To monomer **3** (40 mg, 0.15 mmol, 1 equiv.) in $CDCl_3$ (0.4 ml) was added 4-methyl benzyl alcohol (18 mg, 0.15 mmol, 1 equiv.) and a catalytic amount of TBD (3 μL, 1 mol L^{-1} solution in dry CH_2Cl_2, 2 mol%) and the reaction stirred overnight in the NMR tube. Full conversion to 4-methyl benzyl ring-opened monomer was determined by NMR spectroscopy with an 88% preference for 1-*O*-methyl-2,3-isopropylidene-6-*O*-(4-methylbenzyl)-carbonate-α-D-mannopyranoside (**3'**); ^{1}H NMR (400 MHz, $CDCl_3$): δ_H (ppm) 5.12 (2H, d, *J* 1.2 Hz, H-8), 4.88 (1H, s, H-1), 4.63 (1H, s, -OH), 4.41 (2H, m, *J* 4.8 Hz, H-6), 4.14 – 4.07 (2H, m, *J* 4.4, 2.4 Hz, H-2, H-3), 3.72 (1H, dt, *J* 9.5, 4.8 Hz, H-5), 3.57 (1H, ddd, *J* 9.5, 4.4, 2.4 Hz, H-4), 3.35 (3H, s, OMe), 2.34 (3H, s, H-11), 1.47 (3H, s, *i*-Pr), 1.33 (3H, s, *i*-Pr); ^{13}C{^{1}H} NMR (101 MHz, $CDCl_3$): δ_C (ppm) 155.7 (C=O), 109.8 (C-7), 98.5 (C-1), 78.2 (C-3), 75.6 (C-2), 69.9 (C-8), 68.9 (C-5), 68.4 (C-4), 67.1 (C-6), 55.2 (OMe), 28.0 (*i*-Pr), 26.1 (*i*-Pr), 21.3 (C-11); HR-MS (ESI): $[C_{19}H_{26}O_8 + Na]^+$ Theo. *m/z* 405.1520 found 405.1565.

Deprotection experiments

To polymer (17.6 mg, 9330 g mol^{-1}, Đ 1.15) in $CDCl_3$ (0.4 ml) was added 80:20 CF_3COOH: H_2O (1 μL) and the reaction stirred in the NMR tube at room temperature. Periodically, the reaction was monitored by NMR spectroscopy and SEC. After 24 hours, only 17% deprotection was observed so a further 1 μL of 80:20 CF_3COOH: H_2O was added. Following a further 24 hours stirring at room temperature, 70% removal of the ketal protecting group was observed alongside a $CDCl_3$, THF, HFIP and D_2O insoluble precipitate. No free monomer was detected.

***Preliminary investigation into the synthesis of 1-O-methyl-2,3-O-carbonate-4,6-O-carbonate-α-D-mannopyranoside: Isolation of 1-O-methyl-2,3-O-carbonate-α-D-mannopyranoside*[21]**

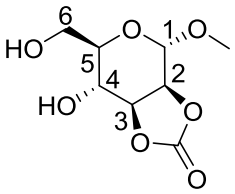

DBU (1.36 ml, 9.08 mmol, 2 equiv.) was added dropwise to a CO_2 saturated suspension of 1-*O*-methy-α-D-mannopyranoside (1.00 g, 4.54 mmol, 1 equiv., 0.1 mol L^{-1} in anhydrous acetonitrile). After 2 hours, stirring at room temperature, the solution was cooled to 0 °C in an ice-water bath and allowed to further saturate with CO_2 before triethylamine (1.27 ml, 9.08 mmol, 2 equiv.) was added. A solution of TsCl (1.73 g, 9.08 mmol, 2 equiv., 0.5 mol L^{-1} in anhydrous acetonitrile, also saturated with CO_2 at 0 °C, was then transferred dropwise *via* cannula to the solution of CO_2-inserted sugar. The reaction mixture was allowed to warm to room temperature and left for 24 hours before being concentrated under reduced pressure at room temperature. The crude reaction mixture was immediately subjected to column chromatography (1%-10% acetone/$CHCl_3$) and the 2,3-cyclic carbonate product isolated as a white powder (290 mg, 15%); R_f 0.52 (1:1 acetone: $CHCl_3$, $KMnO_4$ stain); FTIR (thin film)/cm^{-1} 1790 (C=O); ^{1}H NMR (400 MHz, CD_3CN): δ_H (ppm) 4.99 (1H, s, H-1), 4.67 (2H, m, H-2, H-3), 3.85 (1H, d, *J* 5.8 Hz, 4-OH), 3.77 (1H, ddd, *J* 12.0, 6.0, 2.9 Hz, H-4), 3.68 (2H, m, 6-H), 3.54 (1H, dddd, *J* 10.0, 5.3, 2.9, 0.5 Hz, H-5), 3.37 (3H, s, OMe), 2.87 (1H, br t, *J* 6.2 Hz, 6-OH); ^{13}C{^{1}H} NMR (101 MHz, CD_3CN): δ_C (ppm) 154.9 (C=O), 97.0 (C-1), 80.8 (C-4), 77.3 (C-2), 70.2 (C-1), 68.8 (C-6), 62.0 (C-5), 55.4 (-OMe); HR-MS (ESI): $[C_8H_{12}O_7 + Na]^+$ Theo. *m/z* 243.0481 found 283.0467; Found: C, 43.64; H, 5.49. $C_{11}H_{16}O_7$ requires C, 43.72; H, 5.54%.

7.5. Chapter 4

3'-tosyl-5'-TBDMS-thymidine (4)

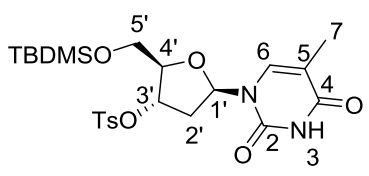

In a modified literature procedure,[22] under a stream of argon, *t*-$BuMe_2SiCl$ (TBDMSCl) (6.16 g, 40.9 mmol, 1.1 equiv.) was added, portion-wise, to a solution of thymidine (9.00 g, 37.2 mmol, 1 equiv.) and DMAP (0.454 g, 3.72 mmol, 0.1 equiv.) in anhydrous pyridine (45 ml). The reaction mixture was stirred at room temperature

and progress monitored by TLC (5'-TBDMS-thymidine; R_f 0.60 for 9:1 $CHCl_3$: EtOH). After 48 hours, TsCl (7.79 g, 40.9 mmol, 1.1 equiv.) was added and the reaction stirred for a further 48 hours at 25 °C, until TLC analysis showed consumption of the 5'-silyl thymidine. The reaction mixture was quenched by addition of methanol and the solvent removed *in vacuo*. The crude material was then extracted into $CHCl_3$, washed with H_2O and dried over $MgSO_4$. Recrystallisation from hot ethanol afforded a white crystalline solid (15.9 g, 84%); R_f 0.77 (9:1 $CHCl_3$: EtOH); ^{1}H NMR (400 MHz, $CDCl_3$): δ_H (ppm) 8.57 (1H, s, NH), 7.80 (2H, d, *J* 8.4 Hz, TsPh), 7.38 (3H, m, TsPh + 6-H), 6.30 (1H, dd, *J* 9.0, 5.4 Hz, H-1'), 5.06 (1H, d, *J* 6.3 Hz, H-3'), 4.26 (1H, q, *J* 2.0 Hz, H-4'), 3.85 (1H, dd, *J* 11.5, 2.0 Hz, H-5'), 3.73 (1H, dd, *J* 11.5, 2.0 Hz, H-5'), 2.46 (3H, s, TsMe), 2.41 (1H, ddd, *J* 14.1, 5.4, 1.1 Hz, H-2'), 2.02 (1H, ddd, *J* 14.1, 9.0, 6.3 Hz, H-2'), 1.89 (3H, d, *J* 1.2 Hz, Me-7), 0.90 (9H, s, *t*-BuSi), 0.09 (6H, d, *J* 0.5 Hz, Me_2Si); $^{13}C\{^1H\}$ NMR (101 MHz, $CDCl_3$): δ_C (ppm) 163.7 (C-4), 150.3 (C-2), 145.6 (C-6), 134.9, 133.5, 130.2, 128.0 (Ar-H), 111.4 (C-5), 85.1 (C-4'), 84.6 (C-1'), 80.8 (C-3'), 63.1 (C-5'), 38.6 (C-2'), 26.0 (SiC($\underline{C}H_3)_3$), 21.8 (TsMe), 18.4 (Si$\underline{C}(CH_3)_3$), 12.6 (C-7), -5.27 (Me_2Si), -5.44 (Me_2Si); HR-MS (ESI): $[C_{23}H_{34}N_2O_7SSi + Na]^+$ Theo. 533.1754 *m/z* found 533.1739; Found: C, 54.05; H, 6.79; N, 5.47. $C_{23}H_{34}N_2O_7SSi$ requires C, 54.10; H, 6.71; N, 5.49%.

3-N-Methyl-3'-tosyl-5'-TBDMS-thymidine (5)

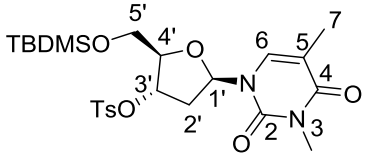

Following a procedure for the methylation of thymidine,[23] MeI (18.3 ml, 294 mmol, 10 equiv.) was added to a suspension of K_2CO_3 (20.3 g, 147 mmol, 5 equiv.) and 3'-tosyl-5'-TBDMS thymidine **4** (15 g, 29.4 mmol, 1 equiv.) in acetone (290 ml) and the reaction mixture stirred at room temperature.* After 24 hours, excess K_2CO_3 was removed by filtration and volatiles removed *in vacuo*. Recrystallisation from hot ether afforded large colourless blocks (14.5 g, 93%); R_f 0.68 (1:1 acetone: $CHCl_3$); ^{1}H NMR (400 MHz, $CDCl_3$): δ_H (ppm) 7.79 (2H, d, *J* 8.4 Hz, TsPh), 7.37 (3H, m, TsPh + H-6), 6.33 (1H, dd, *J* 8.9, 5.4 Hz, H-1'), 5.06 (1H, d, *J* 6.4 Hz, H-3'), 4.26 (1H, q, *J* 2.0 Hz, H-4'), 3.84 (1H, dd, *J* 11.5, 2.0 Hz, H-5'), 3.72 (1H, dd, *J* 11.5, 2.0 Hz, H-5'), 3.31 (3H, s, 3-Me), 2.46 (3H, s, TsMe), 2.43 (1H, dd, *J* 14.3, 8.9, 5.4 Hz, H-2'), 2.01 (1H, ddd, *J* 14.3,

* This procedure was also used to prepare 3-*N*-methyl thymidine from thymidine (4.8 g, 20 mmol, 1 equiv.) as white florets following recrystallisation from EtOAc (2.08 g, 41%) and 3-*N*-methyl-5'-tosyl-thymidine from 5'-tosyl-thymidine (1.00 g, 2.52 mmol, 1 equiv.) following recrystallisation from EtOH (0.669 g, 65%).

8.9, 6.4 Hz, H-2'), 1.90 (3H, d, *J* 1.2 Hz, 7-Me), 0.89 (9H, s, *t*-BuSi), 0.09 (6H, d, *J* 1.0 Hz, Me_2Si); $^{13}C\{^1H\}$ NMR (101 MHz, $CDCl_3$): δ_C (ppm) 163.6 (C-4), 151.1 (C-2), 145.6 (C-6), 133.5, 132.7, 130.2, 128.0 (TsPh), 110.4 (C-5), 85.4 (C-4'), 85.0 (C-1'), 80.8 (C-3'), 63.1 (C-5'), 38.7 (C-2'), 28.0 (3-Me), 26.0 ($SiC(\underline{C}H_3)_3$), 21.8 (TsMe), 18.4 ($Si\underline{C}(CH_3)_3$), 13.4 (7-Me), -5.3 (Me_2Si), -5.5 (Me_2Si); HR-MS (ESI): $[C_{24}H_{36}N_2O_7SSi + Na]^+$ Theo. 547.1910 *m/z* found 547.1908; Found: C, 54.99; H, 6.85; N, 5.44. $C_{24}H_{36}N_2O_7SSi$ requires C, 54.94; H, 6.90; N, 5.34%.

3-N-Methyl-3'-tosyl-thymidine (6)

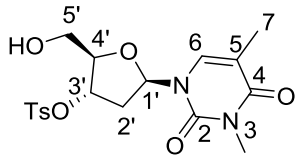

Following the general procedure outlined by Vaino and Szarek for silyl deprotection,[24] a 0.1 mol L^{-1} solution of 3-*N*-methyl-5'-TBDMS-3'-tosyl-thymidine **5** (12.6 g, 24 mmol, 1 equiv.) in methanol was treated with 1 wt% iodine and the reaction mixture heated to reflux for 2 hours (monitored by TLC with 1:1 acetone: $CHCl_3$ eluent). After cooling to room temperature, excess iodine was quenched with sodium thiosulfate until colourless. Volatiles were removed under reduced pressure and the residue extracted into EtOAc, washed with water and the organic layer dried over $MgSO_4$. Recrystallisation from hot EtOH afforded large colourless crystals suitable for single-crystal X-ray analysis (9.40 g, 95%); R_f 0.60 (1:1 acetone: $CHCl_3$); ^1H NMR (400 MHz, $CDCl_3$): δ_H (ppm) 7.82 – 7.75 (2H, m, Ar-H), 7.39 – 7.34 (2H, m, Ar-H), 7.32 (1H, d, *J* 1.2 Hz, H-6), 6.06 (1H, dd, *J* 8.4, 6.0 Hz, H-1'), 5.19 (1H, dt, *J* 6.4, 2.2 Hz, H-3'), 4.21 (1H, q, *J* 2.3 Hz, H-4'), 3.83 (1H, ddd, *J* 12.0, 3.3, 2.2 Hz, H-5'), 3.68 (1H, ddd, *J* 12.0, 6.9, 2.2 Hz, H-5'), 3.28 (3H, s, 3-Me), 3.07 (1H, dd, *J* 6.9, 3.3 Hz, 5'-OH), 2.49 (1H, ddd, *J* 14.3, 8.4, 6.4 Hz, H-2'), 2.44 (3H, s, TsMe), 2.35 (1H, ddd, *J* 14.3, 6.0, 2.1 Hz, H-2'), 1.89 (3H, d, *J* 1.2 Hz, 7-Me); $^{13}C\{^1H\}$ NMR (101 MHz, $CDCl_3$): δ_C (ppm) 163.6 (C-4), 151.1(C-2), 145.6 (C-6), 135.0, 133.3, 130.2, 127.9 (Ar-C), 110.5 (C-5), 88.3 (C-1'), 85.0 (C-4'), 80.8 (C-3'), 62.2 (C-5'), 37.5 (C-2'), 28.0 (3-Me), 21.8 (TsMe), 13.3 (7-Me); HR-MS (ESI): $[C_{18}H_{22}N_2O_7S + Na]^+$ Theo. 433.1045 *m/z* found 433.1047; Found: C, 52.71; H, 5.41; N, 6.90. $C_{18}H_{22}N_2O_7S$ requires C, 52.69; H, 5.40; N, 6.93%.

Cyclic 3-N-Methyl-3',5'-O-cis-carbonate-thymidine (7)

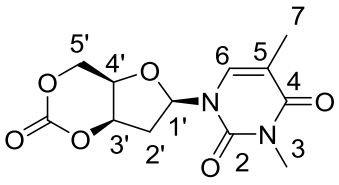

Under an inert atmosphere, 3-*N*-methyl-3'-tosyl-thymidine **6** (6.16 g, 15 mmol, 1 equiv.) was dissolved in anhydrous acetonitrile (150 ml, 0.1 mol L^{-1}). After three cycles of vacuum followed by CO_2, the solution was saturated with CO_2 at 0 °C in an ice-water bath. Under a stream of CO_2, DBU (2.2 ml, 15 mmol, 1 equiv.) was added dropwise and the solution allowed to warm to room temperature before being slowly heated to 40 °C. The reaction was monitored by NMR spectroscopy and after 48 hours, volatiles were removed under reduced pressure and the reaction mixture immediately subjected to column chromatography (9:1 $CHCl_3$: acetonitrile eluent). Recrystallisation from hot anhydrous toluene gave colourless needles suitable for single-crystal X-ray diffraction (2.20 g, 52%), mp 204-205 °C (toluene); R_f 0.35 (1:1 acetone: $CHCl_3$); FTIR (thin film)/ cm^{-1} 1749, 1702, 1673, 1637 (3 C=O, C=C); ^{1}H NMR (400 MHz, $CDCl_3$): δ_H 7.19 (1H, q, *J* 1.2 Hz, H-6), 6.37 (1H, dd, *J* 8.1, 4.3 Hz, H-1'), 5.15 (1H, ddd, *J* 5.6, 3.9, 1.3 Hz, H-3'), 4.69 (1H, dd, *J* 12.8, 1.8 Hz, H-5'), 4.60 (1H, dd, *J* 12.8, 2.4 Hz, H-5'), 4.35 (1H, ddd, *J* 3.9, 2.4, 1.8 Hz, H-4'), 3.34 (3H, s, 3-Me), 2.90 (1H, ddd, *J* 15.9, 8.1, 5.6 Hz, H-2'), 2.40 (1H, ddd, *J* 15.9, 4.3, 1.3 Hz, H-2'), 1.95 (3H, d, *J* 1.2 Hz, 7-Me); ^{13}C{^{1}H} NMR (101 MHz, $CDCl_3$): δ_C (ppm) 163.3 (C-4), 151.3 (C-2), 147.0 (C=O), 131.9 (C-6), 111.4 (C-5), 84.6 (C-1'), 79.5 (C-3'), 72.1 (C-4'), 66.9 (C-5'), 39.9 (C-2'), 28.0 (3-Me), 13.4 (7-Me); HR-MS (ESI): $[C_{12}H_{14}N_2O_6 + Na]^+$ Theo. 305.0736 *m/z* found 305.0749; Found: C, 51.09; H, 4.94; N, 9.94. $C_{12}H_{14}N_2O_6$ requires C, 51.07; H 5.00; N 9.93%.

Cyclic 3-N-Benzoyl- 3',5'-O-cis-carbonate-thymidine (7-Bz)

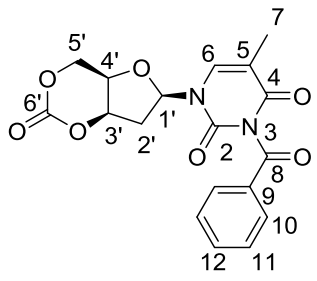

Following the procedure outlined above for the sequential one-pot silylation, tosylation of thymidine (6.0 g, 24.8 mmol, 1 equiv.), benzoyl chloride (4.3 ml, 27.2 mmol, 1.1 equiv.) was added dropwise and the reaction left to stir for a further 24 hours at room temperature. Quenching with methanol and removal of volatiles *in vacuo* gave the crude 3-*N*-benzoyl-3'-TBDMS-5'-tosyl thymidine as an oily residue. This was subjected to the same deprotection and cyclisation procedures as above. Column chromatography (10% acetone/$CHCl_3$ eluent) and precipitation from dry THF gave the product as white florets (3.0 g, 33%), mp 163-164 °C

(THF); R_f 0.72 (1:1 acetone: $CHCl_3$); FTIR (thin film)/cm^{-1} 1744, 1699, 1643, 1599 (C=O, C=C); ^1H NMR (400 MHz, CD_3CN): δ_H (ppm) 7.97 (2H, dd, *J* 8.5, 1.2 Hz, H-10), 7.74 (1 H, ddd, *J* 7.2, 4.2, 1.2 Hz, H-12), 7.57 (2H, ddd, *J* 8.5, 7.2, 1.2 Hz, H-11), 7.40 (1H, d, *J* 1.2 Hz, H-6), 6.21 (1H, dd, *J* 8.2, 3.6 Hz, H-1'), 5.18 (1H, ddd, *J* 5.6, 3.8, 3.6 Hz, H-3'), 4.64 (1H, dd, *J* 12.9, 2.2 Hz, H-5'), 4.59 (1H, dd, *J* 12.9, 1.7 Hz, H-5'), 4.39 (1H, ddd, *J* 3.8, 2.2, 1.7 Hz, H-4'), 2.88 (1H, ddd, *J* 15.9, 8.2, 5.6 Hz, H-2'), 2.44 (1H, dd, *J* 15.9, 3.6 Hz, H-2'), 1.88 (3H, d, *J* 1.2 Hz, 7-Me); $^{13}C\{^1H\}$ NMR (101 MHz, CD_3CN): δ_C (ppm) 170.6 (C-8), 163.8 (C-4), 150.6 (C-2), 148.3 (C-6'), 136.4, 136.4 (C-6, C-12), 132.6 (C-9), 131.3 (C-10), 130.4 (C-11), 112.0 (C-5), 85.6 (C-1'), 80.9 (C-3'), 73.4 (C-4'), 67.9 (C-5'), 40.0 (C-2'), 12.7 (C7-Me); HR-MS (ESI): $[C_{18}H_{16}N_2O_7 + Na]^+$ Theo. 395.0855 *m/z* found 395.0851; Found: C, 58.12; H, 4.41; N, 7.29. $C_{18}H_{16}N_2O_7$ requires C, 58.07; H 4.33; N 7.52%.

General Polymerisation Procedure

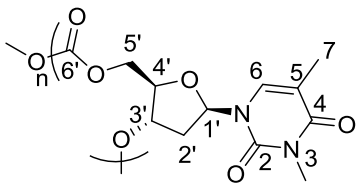

To monomer **7** (141 mg, 0.5 mmol, 100 equiv.) in anhydrous CH_2Cl_2 (0.2 ml, 2.5 mol L^{-1}) was added 4-MeBnOH (5 µL, 1 mol L^{-1} in CH_2Cl_2, 0.005 mmol, 1 equiv.) followed by TBD (5 µL, 1 mol L^{-1} in CH_2Cl_2, 0.005 mmol, 1 equiv.). The mixture was stirred and monitored by ^1H NMR spectroscopy of aliquots taken and quenched with benzoic acid. The polymerisation was quenched by addition of a solution of excess benzoic acid (~30 equiv.) in acetone and the solvent removed under reduced pressure. The crude solid was then dissolved in CH_2Cl_2, precipitated from acetone and washed several times with acetone to removed unreacted monomer. The polymer was isolated as a white powder (80 mg, 57%); FTIR (thin film)/ cm^{-1} 1752, 1698, 1668, 1633 (C=O, C=C); ^1H NMR (400 MHz, $CDCl_3$): δ_H (ppm) 7.34 (1H, s, H-6), 6.25 (1H, s, H-1'), 5.38 – 4.91 (1H, m, H-3'), 4.30 (3H, m, 2×H-5', H-4'), 3.28 (3H, s, 3-*N*-Me), 2.82 (1H, s, H-2'), 2.22 (1H, s, H-2'), 1.92 (3H, s, 7-Me); $^{13}C\{^1H\}$ NMR (101 MHz, $CDCl_3$): δ_C (ppm) 163.4 (C-4), 154.4, 153.6, 152.8 (C=O, polycarbonate), 151.1 (C-2), 133.0 (C-6), 110.1 (C-5), 84.7 (C-1'), 79.5 (C-4'), 76.5 (C-3'), 65.4 (C-5'), 39.2 (C-2'), 27.9 (3-Me), 13.5 (7-Me); M_n (SEC) 15.400 g mol^{-1}, Đ 1.28; T_g (DSC under Ar) 156 °C; TGA under Ar: 169- 302 °C, 91% mass loss. The polymer was insoluble in THF, EtOH, acetone, toluene, water and the PBS buffer solution used in the cell studies. It was highly soluble in chlorinated solvents namely $CHCl_3$, CH_2Cl_2 and HFIP.

L1ZnOEt (Figure 4.19A and Table 4.01, Entry 3) was prepared according to the procedure detailed by Williams *et al.*[25] and (BDI-1)ZnEt (Figure 4.19B and Table 4.01, Entry 4) according to Coates and co-workers.[26, 27]

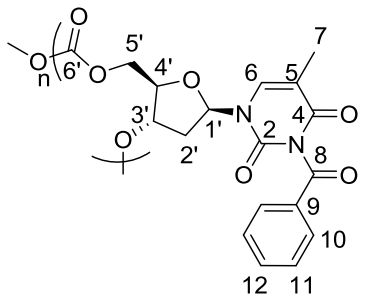

The same polymerisation procedure was followed for monomer **7-Bz**. The polymer was isolated as a white powder by precipitation from ether (74 mg, 68%); FTIR (thin film)/ cm^{-1} 1750, 1700, 1652, 1600 (C=O, C=C); ^{1}H NMR (400 MHz, $CDCl_3$): δ_H (ppm) 7.91 (2H, s, H-10), 7.64 (1H, s, H-11), 7.49 (2H, s, H-12), 7.33 (1H, s, H-6), 6.42 – 5.92 (1H, m, H-1'), 5.23 (1H, m, H-3'), 4.86 – 3.99 (3H, m, H-4', 2 × H-5'), 2.85 (1H, s, H-2'), 2.29 (1H, s, H-2'), 1.97 (3H, s, 7-Me); $^{13}C\{^{1}H\}$ NMR (101 MHz, $CDCl_3$): δ_C (ppm) 168.9 (C-8), 162.8 (C-4), 155.5, 154.5, 153.9 (C=O polycarbonate), 151.5 (C-2), 137.5 (C-12), 135.2 (C-6), 131.7 (C-9), 129.7 (C-10), 128.1 (C-11), 110.9 (C-5), 85.8 (C-1'), 81.6 (C-4'), 69.9 (C-3'), 65.9 (C-5'), 40.8 (C-2'), 12.8 (7-Me); M_n (SEC) 11.600 g mol^{-1}, Đ 1.33.

7.6. Chapter 5

1-O-Methyl-2-deoxy-α/β-D-ribofuranoside (8-Me)[28]

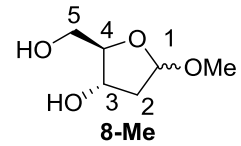

8-Me

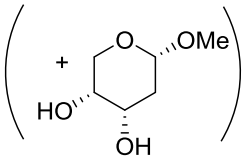

8'-Me

Following the literature procedure,[28] acetyl chloride (0.5 ml, 7 00 mmol, 0.4 equiv.) was added slowly to ice-cold methanol (50 ml) and the mixture stirred for 30 minutes at room temperature before being placed in the freezer at -18 °C. Once cooled, 2-deoxy-D-ribose (2.5 g, 18.6 mmol, 1 equiv.) was added in one portion and the solution left overnight in the freezer prior to neutralisation with solid sodium carbonate (0.5 g, 4.72 mmol, 0.25 equiv.). After warming to room temperature, the mixture was centrifuged (3000 rpm, 10 minutes) and the methanolic solution, containing the desired product, decanted off. Volatiles were removed under reduced pressure (at room temperature) and the crude methyl glycoside (yellow oil) further purified (to remove any residual salts) by dissolving in ethyl acetate (50 ml), centrifuging and decanting off the supernatant. The 1-*O*-methyl-2-deoxy-α/β-D-ribopyranose impurity (**8'-Me**) could be selectivity broken down with sodium (meta)periodate following a patented procedure.[29] To the oil dissolved in acetonitrile (20 ml), was added sodium (meta)periodate

(0.8 g, 3.73 mmol, 2 equiv.) and the resulting suspension stirred for several days. Addition of solid sodium bicarbonate (0.3 g, 3.73 mmol, 2 equiv.) and subsequent filtration of the reaction mixture afforded, upon concentration of the filtrate under reduced pressure **8-Me** (with 6% **8'-Me** impurity) as a viscous colourless oil (1.82 g, 66%, mixture of α and β-anomers); R_f 0.35 (9:1 CH_2Cl_2: MeOH); ^{1}H NMR (400 MHz, D_2O): δ_H (ppm) 5.21 (1H, dd, *J* 5.3, 2.7 Hz, H-1β), 5.16 (1H, dd, *J* 5.4, 1.1 Hz, H-1α), 4.34 (1H, ddd, *J* 10.8, 6.2, 2.0 Hz, H-3β), 4.25 (1H, ddd, *J* 7.4, 3.6, 2.5 Hz, H-3α), 4.07 (1H, ddd, *J* 7.0, 5.1, 3.7 Hz, H-4α), 3.97 (1H, dt, *J* 6.9, 4.3 Hz, H-3β), 3.72 (1H, dd, *J* 6.1, 4.2 Hz, H-5β), 3.69 (1H, dd, *J* 5.8, 4.3 Hz, H-5'β), 3.63 (1H, dd, *J* 12.8, 5.3 Hz, H-5'α), 3.57 (1H, dd, 12.8, 7.1 Hz, H-5'α), 3.37 (6H, s, OMe, α+β), 2.33 (1H, ddd, *J* 14.5, 7.3, 5.5 Hz, H-2'α), 2.22 (1H, ddd, *J* 13.9, 6.7, 2.7 Hz, H-2'β), 2.15 (1H, ddd, *J* 14.0, 11.0, 5.4 Hz, H-2β), 1.91 (1H, ddd, *J* 14.5, 2.4, 1.2 Hz, H-2α); ^{13}C{^{1}H} NMR (101 MHz, $CDCl_3$): δ_C (ppm) 103.6, 103.5 (C-1, α+β), 85.2, 84.8 (C-4, α+β), 70.4, 69.9 (C-3, α+β), 61.8, 60.8 (C-5, α+β), 53.4, 53.1 (OMe, α+β), 40.0, 39.4 (C-2, α+β); for the **8'-Me** impurity (single anomer); ^{1}H NMR (400 MHz, $CDCl_3$): δ_H (ppm) 4.66 (1H, dd (t), *J* 3.4, 2.3 Hz, H-1), 3.92 (1H, s, H-3), 3.70 – 3.54 (3H, m, 2 × H-5, H-4), 3.38 (3H, s, OMe), 2.61 (1 H, s), 2.08 (1H, ddd, *J* 14.5, 4.4, 2.3 Hz, H-2), 1.88 (1H, dt, *J* 14.5, 3.4 Hz, H-2'); ^{13}C{^{1}H} NMR (101 MHz, $CDCl_3$): δ_C (ppm) 98.3 (C-1), 67.3 (C-4), 66.5 (C-3), 59.6 (C-5), 55.5 (OMe), 34.9 (C-2); HR-MS (ESI): $[C_6H_{12}O_4 + Na]^+$ Theo. 171.0628 *m/z* found 171.0629; Found: C, 48.62; H, 8.14. $C_6H_{12}O_4$ requires C, 48.64; H 8.16%.

1-O-Benzyl-2-deoxy-α/β-D-ribofuranoside (8-Bn)[30]

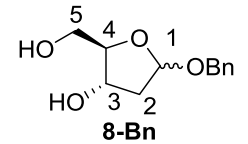

8-Bn

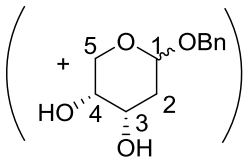

8'-Bn

In a modified literature procedure,[30] to a suspension of 2-deoxy-D-ribose (2.50 g, 18.6 mmol, 1 eq.) in benzyl alcohol (30 ml), was added 3 drops of conc. HCl. After 10 minutes, stirring at room temperature, pyridine (1 ml) was added and the reaction mixture subjected to column chromatography: 1:1 Hexane: EtOAc to remove the benzyl alcohol followed by 9:1 DCM: MeOH to eluent the desired **8-Bn** with 11% **8'-Bn** impurity as a colourless oil (2.79 g, 67%, mixture of α and β anomers); R_f 0.46 (9:1 CH_2Cl_2: MeOH); ^{1}H NMR (400 MHz, $CDCl_3$): δ_H (ppm) 7.42-7.28 (10H, m, Ph, α+β), 5.35 (1H, dd, *J* 5.7, 2.1 Hz, H-1β), 5.32 (1H, dd, *J* 4.1, 0.8 Hz, H-1α), 4.80 (1H, d, *J* 11.8 Hz, CH_2Ph- α), 4.76 (1H, d, *J* 11.8 Hz, CH_2Ph-β), 4.56 (1H, dd, *J* 4.3, 3.6, 2.6 Hz, H-3β).4.54 (1H, d, *J* 11.8 Hz, CH_2Ph-α), 4.53 (1H, d, *J* 11.8 Hz, CH_2Ph-β), 4.26-4.12 (2H, H-3α, H-4α), 4.08 (1H, dd, *J* 4.7, 3.7 Hz, H-4β), 3.75 (1H, dd,

J 11.8, 3.6, H-5α), 3.75 (1H, dd, *J* 11.7, 2.6, H-5β), 3.66 (1H, dd, *J* 11.7, 4.7, H-5'β), 3.63 (1H, dd, *J* 11.8, 4.7 Hz, H-5'α), 2.35 (1H, ddd, *J* 9.4, 6.7, 2.1 Hz, H-2β). 2.20-2.05 (2H, dd, *J* 5.8, 4.1 Hz, H-2α), 1.93 (1 H, dd, *J* 9.4, 3.0 Hz, H-2'β); $^{13}C\{^{1}H\}$ NMR (101 MHz, $CDCl_3$): δ_C (ppm) 128.8, 128.7, 128.7, 128.6, 128.2, 128.1, 128.1, 128.0 (Ph, α+β), 137.4, 137.6 (*i*-Ph, α+β), 103.7, 103.9 (C-1, α+β), 87.9, 87.9 (C-4, α+β), 72.5, 73.1 (C-3, α+β), 69.3, 70.2 (CH_2Ph, α+β), 63.4, 63.8 (C-5, α+β), 41.9, 42.9 (C-2, α+β); for the **8'-Bn** impurity (single anomer): ^{1}H NMR (400 MHz, $CDCl_3$): δ_H (ppm) 4.89 (1H, dd, *J* 3.4, 2.1 Hz, H-1), 4.76 (1H, d, *J* 11.8 Hz, CHHBn), 4.49 (1H, d, *J* 11.8 Hz, CHHBn), 3.97 (1H, br s, H-3), 3.73 – 3.58 (3H, m, H-4, 2 × H-5), 2.16 (1H, ddd, *J* 14.6, 4.2, 2.1 Hz, H-2), 1.93 (1H, dt, *J* 14.6, 3.5 Hz, H-2'); HR-MS (ESI): $[C_{12}H_{16}O_4 + Na]^+$ Theo. 247.0946 *m/z* found 247.0947; Found: C, 64.31; H, 7.23. $C_{12}H_{16}O_4$ requires C, 64.27; H 7.19%.

Attempted synthesis of cyclic-1-O-methyl-2-deoxy-3,5-O-trans-carbonate-α/β-D-ribofuranoside (9-Me): isolation of 1-O-methyl-2-deoxy-3,4-O-cis-carbonate-α/β-D-ribopyranoside (9'-Me)

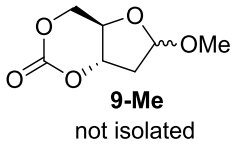

9-Me
not isolated

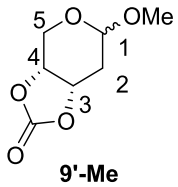

9'-Me

For example, the procedure outlined for the cyclocarbonation of 1-*O*-methyl-2,3-*O*-isoproplidene-α-D-mannopyranose to form cyclic carbonate **3** (Chapter 3) was followed with 1-*O*-methyl-2-deoxy-α/β-D-ribofuranoside **8-Me** (2.0 g, 13.5 mmol, 1 equiv.). Following column chromatography (5% acetone/$CHCl_3$), **9'-Me** was isolated as a colourless oil (0.259 g, 11%, mixture of α and β- anomers); R_f 0.63 (1:1 acetone: $CHCl_3$); for a sample highly enriched in the β-anomer: ^{1}H NMR (400 MHz, $CDCl_3$): δ_H (ppm) 5.00 – 4.93 (1H, m, H-3), 4.86 (1H, dd, *J* 6.3, 5.6 Hz, H-1), 4.71 (1H, dt, *J* 8.2, 1.5 Hz, H-4), 3.89 – 3.88 (2H, m, H-5), 3.39 (3H, s, OMe), 2.43 (1H, ddd, *J* 15.6, 5.6, 4.5 Hz, H-2), 1.83 (1H, ddd, *J* 15.6, 6.3, 3.7 Hz, H-2'); $^{13}C\{^{1}H\}$ NMR (101 MHz, $CDCl_3$): δ_C (ppm) 154.6, 154.5 (C=O, α +β), 96.8, 96.1 (C-1, α +β), 73.8, 73.7 (C-4, α +β), 71.7, 71.6 (C-3, α +β), 59.1, 59.0 (C-5, α +β), 55.7, 55.4 (OMe, α +β), 31.0, 29.6 (C-2, α +β). HR-MS (ESI) $[C_7H_{10}O_5 + Na]^+$ Theo. 197.0426 found 197.0435; Found: C, 48.64; H, 6.03. $C_7H_{10}O_5$ requires C, 48.45; H, 5.79%.

Cyclic 1-O-benzyl-2-deoxy-3,4-O-cis-carbonate-α/β-D-ribopyranoside (9'-Bn)

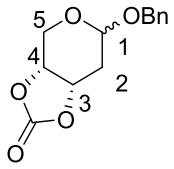

1-*O*-Benzyl-2-deoxy-α/β-D-ribopyranoside (**8'-Bn**) (2.0 g, 8.92 mmol, 1 equiv.) was synthesised according to the procedure outlined for 1-*O*-Benzyl-2-deoxy-α/β-D-ribofuranoside (**8-Bn**, above) but with an extended reaction time of 3 hours. The procedure for cyclocarbonation with CO_2, detailed for the synthesis of cyclic-*O*-methyl-2,3-*O*-isoproplidene-α-D-4,6-carbonate-mannopyranose (**3**) was then followed. The cyclic carbonate product (**9'-Bn**) was isolated by column chromatography (5% acetone/$CHCl_3$) as a colourless oil to white crystalline solid depending upon the ratio of α:β (1.61 g, 72 %). For the β-anomer: R_f 0.66 (1:1 acetone:$CHCl_3$); ^{1}H NMR (400 MHz, $CDCl_3$): δ_H (ppm) 7.39 – 7.28 (5H, m, Ph-H), 5.09 – 5.05 (1H, t, *J* 6.1 Hz, H-1), 5.01 – 4.95 (1H, m, H-3), 4.77 (1H, d, *J* 11.8 Hz, C<u>H</u>HBn), 4.72 (1H, ddd, *J* 8.2, 1.9, 1.0 Hz, H-4), 4.53 (1H, d, *J* 11.8 Hz, CH<u>H</u>Bn), 3.97 (1H, dd, *J* 13.8, 1.9 Hz, H-5), 3.89 (1H, *J* 13.8, 1.0 Hz, H-5'), 2.45 (1H, ddd, *J* 15.7, 5.6, 4.3 Hz, H-2), 1.91 (1H, ddd, *J* 15.7, 6.5, 3.7 Hz, H-2); ^{13}C{^{1}H} NMR (101 MHz, $CDCl_3$): δ_C (ppm) 154.5 (C=O), 137.3 (*i*-Ph), 128.7 (Ph), 128.1 (Ph), 94.2 (C-1), 73.7 (C-4), 71.6 (C-3), 69.6 (CH_2Bn), 59.2 (C-5), 29.6 (C-2). For the α- anomer: R_f 0.52 (1:1 acetone:$CHCl_3$); ^{1}H NMR (400 MHz, $CDCl_3$): δ_H (ppm) 7.39 – 7.32 (5H, m, Ph-H), 4.88-4.70 (4H, m, H-1, H-3, H-4, CH<u>H</u>Bn), 4.53 (1H, d, *J* 12.1 Hz, C<u>H</u>HBn), 4.10 (1H, dd, *J* 12.9, 6.0 Hz, H-5), 3.86 (1H, dd, *J* 12.9, 4.9 Hz, H-5'), 2.26 (1H, ddd, *J* 15.1, 5.7, 4.3 Hz, H-2), 2.15 (1H, ddd, *J* 15.1, 5.9, 5.0 Hz, H-2'); ^{13}C{^{1}H} NMR (101 MHz, $CDCl_3$): δ_C (ppm) 154.5 (C=O), 137.1 (*i*-Ph), 128.6 (Ph), 128.1 (Ph), 94.5 (C-1), 71.7 (C-4), 71.3 (C-3), 69.6 (CH_2Bn), 59.2 (C-5), 31.2 (C-2); HR-MS (ESI): $[C_{13}H_{14}O_5 + Na]^+$ Theo. 273.0733 found 273.0740. Found: C, 62.41; H, 5.63. $C_7H_{10}O_5$ requires C, 62.39; H, 5.64%.

1-O-Methyl-2-deoxy-3-tosyl-5-TBDMS-α/β-D-ribofuranoside (10)

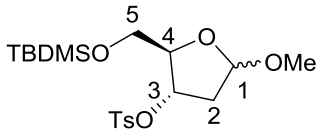

In a modified literature procedure,[22] conc. HCl (4 drops) was added to a stirring solution of 2-deoxy-D-ribose (5.00 g, 37.2 mmol, 1 equiv.) in methanol (60 ml). After 30 minutes, the reaction was quenched by addition of anhydrous pyridine (2 ml) and volatiles removed *in vacuo*. To the resulting oil and a catalytic amount of DMAP (0.488 g, 3.72 mmol, 0.1 equiv.), in anhydrous pyridine (40 ml), was added TBDMSCl (6.02 g, 40.0 mmol, 1.1 equiv.) portion wise. After 2 hours stirring at 25 °C, TsCl (7.64 g, 40.0 mmol, 1.1 equiv.) was added and the

reaction mixture stirred for a further 12 hours before being quenched with methanol (4 ml). Following the removal of volatiles under reduced pressure, the crude product was purified via a silica plug with CH_2Cl_2 eluent to afford a colourless oil (12.7 g, 82%, mixture of α- and β- anomers); R_f 0.75 (1:1 acetone:$CHCl_3$); ^{1}H NMR (400 MHz, $CDCl_3$): δ_H (ppm) 7.78 (4H, d, *J* 8.1 Hz, ArH, α+β), 7.33 (4H, d, *J* 8.1 Hz, ArH, α+β), 5.09 (1H, dd, *J* 5.4, 3.3 Hz, H-1α), 5.03-5.00 (2H, m, H-3α, H-1β), 4.95 (1H, ddd, *J* 7.6, 2.9, 1.8 Hz, H-3β), 4.21 (1H, dd, *J* 5.4, 2.6 Hz, H-4β), 4.10-4.06 (1H, m, H-4α), 3.63 (2H, dd, *J* 11.3, 2.8 Hz, H-5β), 3.55 (1H, dd, *J* 10.7, 5.2 Hz, H-5α), 3.47 (1H, dd, *J* 10.7, 6.8 Hz, H-5'α), 3.34 (3H, s, β-OMe), 3.30 (3H, s, α-OMe), 2.44 (6H, s, TsMe, α+β), 2.30 (1H, ddd, *J* 14.5, 5.4, 4.1 Hz, H-2α), 2.20-2.12 (2H, m, H-2', α+β), 2.04, (1H, d, *J* 14.4 Hz, H-2β), 0.84 (18H, s, *t*-BuSi, α+β), 0.00 (12H, s, Me_2Si, α+β); ^{13}C{^{1}H} NMR (101 MHz, $CDCl_3$): δ_C (ppm) 145.1, 145.0, 133.9, 133.7 (ArC, α+β), 130.1, 130.0, 128.0, 128.0 (ArCH, α+β), 105.3, 105.1 (C-1, α+β), 84.1, 83.8 (C-3, α+β), 81.7, 80.4 (C-4, α+β), 63.3, 62.6 (C-5, α+β), 55.6, 55.1 (OMe, α+β), 39.6, 39.3 (C-2, α+β), 25.9, 25.8 ($SiC(\underline{C}H_3)_3$, α+β), 21.8 (TsMe, α+β), 18.4, ($Si\underline{C}(CH_3)_3$, α+β), -5.3, -5.4, -5.4, -5.5 (Me_2Si, α+β); HR-MS (ESI): $[C_{19}H_{32}O_6SSi+ Na]^+$ Theo. 439.1581 *m/z* found 439.1593; Found: C, 54.82; H, 7.75. $C_{19}H_{32}O_6SSi$ requires C, 54.78; H, 7.74%.

1-O-Methyl-2-deoxy-3-tosyl-α/β-D-ribofuranoside (11)

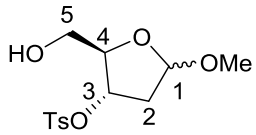

Following the general procedure reported by Vaino and Szarek for silyl deprotection,[24] iodine (3.0 g, 1 wt%) was added to a 0.1 mol L^{-1} solution of **10** (12.7 g, 28.8 mmol, 1 equiv.) in methanol (300 ml) and the reaction mixture heated to reflux for 4 hours. After cooling to room temperature, excess iodine was quenched with $Na_2S_2O_3$ until colourless and volatiles removed under reduced pressure. The resulting residue was extracted into EtOAc, washed with water and the organic layer dried over MgSO4 to afford the product as a colourless oil (7.19 g, 78%, mixture of α- and β- anomers); ^{1}H NMR (400 MHz, $CDCl_3$): δ_H (ppm) 7.78 (4H, d, *J* 8.3 Hz, ArH, α+β), 7.36 (4H, d, *J* 8.3 Hz, ArH, α+β), 5.12 (1H, dd, *J* 5.6, 2.6 Hz, H-1α), 5.08 (1H, ddd, *J* 6.8, 4.2, 2.7 Hz, H-3α), 5.03 (1H, dd, *J* 5.2, 1.0 Hz, H-1β), 4.91 (1H, ddd, *J* 8.4, 4.2, 2.4 Hz, H-3β), 4.31 (1H, dd, *J* 2.9, 2.7 Hz, H-4α), 4.21 (1H, dd, *J* 7.1, 3.1 Hz, H-4β), 3.76 (1H, ddd, *J* 12.2, 4.3, 2.9 Hz, H-5β), 3.63 (1H, ddd, *J* 12.4, 3.0, 2.9 Hz, H-5α), 3.49 (1H, ddd, *J* 12.4, 10.2, 2.9 Hz, H-5'α), 3.60 – 3.49 (1H, m, H-5'β), 3.37 (3H, s, α-OMe), 3.35 (3H, s, β-OMe), 2.73 (1H, dd, *J* 10.2, 3.0 Hz, 5-α-OH), 2.45 (6H, s, TsMe, α+β), 2.30 (1H, ddd, *J* 15.0, 5.6, 4.2 Hz, H-2α), 2.24 (1H, ddd, *J* 15.0, 7.1, 2.5 Hz, H-2'α), 2.03 (2H, ddd, *J* 14.7, 2.4, 1.1 Hz,

H-2β), 1.74 (1H, dd, *J* 8.5, 4.4 Hz, β5-OH); $^{13}C\{^{1}H\}$ NMR (101 MHz, $CDCl_3$): δ_C (ppm) 145.4, 145.2 (Ar, α+β), 133.3, 133.7 (Ar, α+β), 130.2, 130.1, 128.1, 128.0 (ArC, α+β), 105.4, 104.8 (C-1, α+β), 85.7, 82.7 (C-3, α+β), 81.3, 79.6 (C-4, α+β), 63.3, 61.7 (C-5, α+β), 55.8, 55.1 (OMe, α+β), 40.5, 39.7 (C-2, α+β), 21.8, 21.2 (TsMe, α+β); HR-MS (ESI): $[C_{13}H_{18}O_6S + Na]^+$ Theo. *m/z* 325.0721 found 325.0743; Found: C, 51.65; H, 6.07. $C_7H_{10}O_5$ requires C, 51.64; H, 6.00%.

Cyclic 1-O-methyl-2-deoxy-3,5-O-cis-carbonate-α/β-D-ribofuranose (12α, 12β)

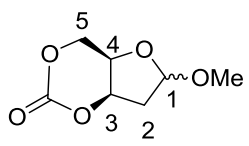

A solution of **11** (7.06 g, 23.4 mmol, 1 equiv.) in anhydrous acetonitrile (230 ml, 0.1 mol L^{-1}) was saturated with CO_2 at 0 °C in an ice-water bath. Under a stream of CO_2, DBU (3.5 ml, 23.4 mmol, 1 equiv.) was added dropwise and the solution allowed to warm to room temperature. After 48 hours, volatiles were removed under reduced pressure and the crude oil immediately subjected to flash column chromatography ($CHCl_3$, 1% then 5% acetone/$CHCl_3$ eluent). The α-rich fraction ($CHCl_3$ to 1% acetone/$CHCl_3$ eluent) was recrystallised from dry ether to afford pure **12α** as large colourless needles (1.55 g, 38%); mp 67-68 °C (ether); R_f 0.57 (1:1 acetone: $CHCl_3$); FTIR/cm^{-1} (thin film) 1744 (C=O); ^{1}H NMR (400 MHz, $CDCl_3$): δ_H (ppm) 5.22 (1H, dd, *J* 5.2, 2.6 Hz, H-1), 5.13 (1H, ddd, *J* 6.3, 4.9, 3.0 Hz, H-3), 4.48 (2H, qd, *J* 12.4, 2.1 Hz, H-5), 4.39 (1H, dt, *J* 4.9, 2.1 Hz, H-4), 3.37 (3H,s, OMe), 2.42 (1H, ddd, *J* 15.1, 5.2, 3.0 Hz, H-2), 2.36 (1H, ddd, *J* 15.1, 6.3, 2.6 Hz, H-2'); $^{13}C\{^{1}H\}$ NMR (101 MHz, $CDCl_3$): δ_C (ppm) 148.5 (C=O), 104.6 (C-1), 80.8 (C-3), 70.3 (C-4), 67.0 (C-5), 55.7 (OMe), 42.0 (C-2); HR-MS (ESI): $[C_7H_{11}O_5]^+$ Theo. 175.0606 *m/z* found 175.0609; Found: C, 48.28; H, 5.82. $C_7H_{10}O_5$ requires C, 48.45; H, 5.79%. The β-rich fraction (5% acetone/$CHCl_3$ eluent) was recrystallised from hot toluene to afford white needles of **12β** (1.71 g, 42%); mp 106-108 °C (toluene); R_f 0.47 (1:1 acetone:$CHCl_3$); FTIR (thin film)/ cm^{-1} 1741 (C=O); ^{1}H NMR (400 MHz, $CDCl_3$): δ_H (ppm) 5.15-5.04 (2H, m, H-1, H-3), 4.51 (1H, dt, *J* 5.7, 1.8 Hz, H-4), 4.37 (1H, dd, *J* 12.3, 1.8 Hz, H-5), 4.32 (1H, ddd, *J* 12.3, 1.8, 0.5 Hz, H-5'), 3.30 (3H, s, OMe), 2.39 (1H, d, *J* 14.6 Hz, H-2), 2.17 (1H, ddd, *J* 14.6, 5.6, 4.9, H-2'); $^{13}C\{^{1}H\}$ NMR (101 MHz, $CDCl_3$): δ_C (ppm) 149.0 (C=O), 104.3 (C-1), 80.7 (C-3), 73.6 (C-4), 66.8 (C-5), 54.7 (OMe), 41.2 (C-2); HR-MS (ESI): $[C_7H_{10}O_5 + Na]^+$ Theo. 197.042593 *m/z* found 197.0451; Found: C, 48.27; H, 5.89. $C_7H_{10}O_5$ requires C, 48.45; H, 5.79%.

General polymerization and copolymerisation procedure

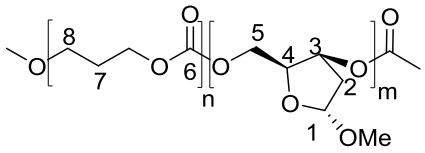

To **12α** (174 mg, 1 mmol) and TMC (102 mg, 1 mmol) in CH_2Cl_2 (0.34 ml, 5 mol L^{-1}) was added BnOH (40 μL, 0.04 mmol, 1 mol L^{-1} in CH_2Cl_2) followed by TBD (20 μL, 0.02 mmol, 1 mol L^{-1} in CH_2Cl_2) and the reaction stirred at room temperature. The polymerisation was quenched by addition of excess benzoic acid and poly(TMC-*co*-47mol%-**12α**) isolated as a white powder by precipitation from ether (210 mg, 76%); FTIR (thin film)/cm^{-1} 1741 (C=O); ^{1}H NMR (400 MHz, $CDCl_3$): δ_H (ppm) 5.39 – 5.23 (1H, m, H-3), 5.17 (1H, m, H-1), 4.36-4.31 (3H, m, H-4, H-5), 4.26 – 4.22 (4.5H, m, H-8), 3.37 (3H, s, OMe), 2.37 – 2.22 (2H, m, H-2), 2.05 (2.25H, q, *J* 6.2 Hz, H-7); ^{13}C{^{1}H} NMR (101 MHz, $CDCl_3$): δ_C (ppm) 155.1, 155, 154.9, 154.5, 154.4, 154.1 (C=O), 104.2 (C-1), 76.4 (C-3), 76.3 (C-4) 64.8 (C-5), 64.6 (C-8), 55.6 (OMe), 40.5 (C-2), 28.2 (C-7); M_n (SEC) 6380 g mol^{-1} (Đ 1.19).

1-O-Methyl-2,3-O-isopropylidene-4,6-O-thionecarbonate-α-D-mannopyranoside (13) and 1-O-methyl-2,3-O-isopropylidene-4O,6S-oxathiolanethione-α-D-mannopyranoside (14)

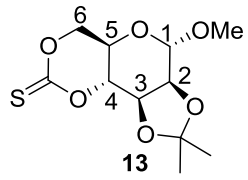

13

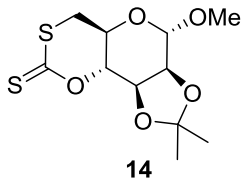

14

Addition of DBU (0.7 ml, 5.1 mmol, 1 equiv.) to a colourless solution of 1-*O*-methoxy-2,3-*O*-isopropylidene-α-D-mannopyranoside (2.0 g, 5.1 mmol, 1 equiv.) and CS_2 (0.3 ml, 5.1 mmol, 1 equiv.) in anhydrous acetonitrile (51 ml, 0.1 mol L^{-1}), resulted in an immediate colour change to yellow. After stirring at room temperature for 24 hours, NEt_3 (0.7 ml, 5.1 mmol, 1 equiv.) and a solution of TsCl (1.0 g, 5.1 mmol, 1 equiv., 0.5 mol L^{-1} in anhydrous acetonitrile) were added, and the reaction mixture stirred for a further 24 hours at room temperature. Volatiles were then removed under reduced pressure and the crude oil immediately subjected to column chromatography (1% acetone/$CHCl_3$). Recrystallisation from hexanes yielded orange/yellow crystals of **13** + **14** [0.516 g, 37% (**13**) + 0.224 g, 15% (**14**)]; R_f 0.72 (1:1 acetone: $CHCl_3$); FTIR (thin film)/ cm^{-1} 1467, 1415, 1389, 1382, 1389, 1200, 1078; ^{1}H NMR (400 MHz, $CDCl_3$) δ_H (ppm) 4.99 (1H, s, H-1, **13**), 4.97 (1H, s, H-1, **14**), 4.58 (1H, dd, *J* 9.8, 6.0 Hz, H-6, **13**), 4.40 (1H, t, *J* 6.0 Hz, H-6', **13**), 4.36 – 4.00 (8H, H-5, H-4, H-3, H-2, **13**+**14**), 3.43 (3H, s, OMe, **14**), 3.41 (3H, s, OMe, **13**), 3.20 (1H, t, *J* 10.7 Hz, H-6, **14**), 3.03 (1H, dd, *J* 11.1, 5.2 Hz, H-6', **14**), 1.53 (6H, s, Me, **13**+**14**), 1.36 (6H, s, Me, **13**+**14**); ^{13}C{^{1}H}

NMR (101 MHz, $CDCl_3$): δ_C (ppm) 206.0 (SC=S xanthate, **14**), 188.4 (OC=S, **13**), 110.6, 110.6 (C-1, **13**+**14**), 99.3 (C-4. **13**), 98.5 (C-4, **14**), 84.1 (C-2, **14**), 80.3 (C-2, **13**), 76.0 (C-2, **13**), 75.5 (C-2, **14**), 74.4 (C-3, **14**), 73.3 (C-3, **13**), 71.0 (C-6, **13**), 59.3 (C-5, **14**), 57.6 (C-5, **13**), 55.9 (OMe, **13**), 55.8 (OMe, **14**), 34.0 (C-6, **14**), 28.1, 28.1 (Me, **13**+**14**), 26.1 (Me, **13**); HR-MS (ESI) $[C_{11}H_{16}O_5S_2 + Na]^+$ Theo. 315.0337 *m/z* found 315.0302; $[C_{11}H_{16}O_6S_1 + Na]^+$ Theo. 299.0565 *m/z* found 299.0577.

1-O-Methyl-2-deoxy-3O,5S-oxathiolane-thione-ᴅ-ribofuranoside (15)

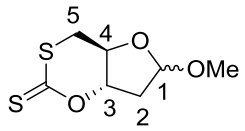

DBU (2.0 ml, 13.5 mmol, 1 equiv.) was added to a solution of 1-*O*-methoxy-2-deoxy-ᴅ-ribose, **8-Me** (2.0 g, 13.5 mmol, 1 equiv.) and CS_2 (0.8 ml, 13.5 mmol, 1 equiv.) in anhydrous acetonitrile (135 ml, 0.1 mol L^{-1}). After stirring at room temperature for 24 hours, NEt_3 (1.9 ml, 13.5 mmol, 1 equiv.) and TsCl (2.6 g, 13.5 mmol, 1 equiv., 5 mol L^{-1} in anhydrous acetonitrile), were added to the yellow reaction mixture, which turned an intense orange colour on stirring for a further 24 hours at room temperature. Volatiles were then removed under reduced pressure and the crude oil immediately subjected to column chromatography (1% acetone/$CHCl_3$). Several recrystallisations from hexanes yielded pale yellow crystals suitable for single-crystal X-ray diffraction (278 mg, 10%, mixture of α and β anomers); mp 90 °C (hexanes); R_f 0.69 (1:1 acetone: $CHCl_3$); FTIR (thin film)/ cm^{-1} 1440, 1377, 1272, 1249, 1185, 1032, 1104, 1015, 1005; ^{1}H NMR (400 MHz, $CDCl_3$): δ_H (ppm) 5.15 (1H, br d, *J* 5.3 Hz, H-1, β), 5.11 (1H, dd, *J* 5.8, 4.2 Hz, H-1, α), 4.67 (1H, ddd, *J* 10.9, 8.7, 7.1 Hz, H-3, β), 4.32 (1H, ddd, *J* 9.3, 8.8, 8.7 Hz, H-3, β), 4.20 (1H, ddd, *J* 9.8, 8.8, 6.3 Hz, H-4, α), 4.11 (1H, ddd, *J* 11.0, 8.7, 5.4 Hz, H-4 β), 3.40 (3H, s, OMe, α), 3.35 (3H, s, OMe, β), 3.25 (4H, m, H-5, α+β), 2.80 (1H, ddd, *J* 13.8, 8.7, 5.8 Hz, H-2, α), 2.45 (1H, dd, *J* 12.4, 7.1 Hz, H-2, β), 2.37 (1H, ddd, *J* 12.6, 10.9, 5.3 Hz, H-2', β), 2.17 (1H, ddd, *J* 13.6, 9.3, 4.2 Hz, H-2', α); ^{13}C{^{1}H} NMR (101 MHz, $CDCl_3$): δ_C (ppm) 208.1, 207.8 (SC=S, α+β), 104.3, 104.3 (C-1, α+β), 83.3 (C-3, α), 83.1 (C-3, β), 72.9 (C-4, β), 69.4 (C-4, α), 56.1 (OMe, α), 55.6 (OMe, β), 38.1 (C-5, β), 37.0 (C-5, α), 36.9 (C-2, α), 36.6 (C-2, β). Several attempts at HR-MS(ESI) in MeOH and MeCN, positive and negative mode did not detect the product; Found: C, 40.83; H, 4.74, $C_7H_{10}O_3S_2$ requires C, 40.76; H 4.89%.

7.7. References

1. B. Gabriele, R. Mancuso, G. Salerno, L. Veltri, M. Costa and A. Dibenedetto, *ChemSusChem*, 2011, **4**, 1778-1786.
2. K. Matsumoto, Y. Sato, M. Shimojo and M. Hatanaka, *Tetrahedron: Asymmetry*, 2000, **11**, 1965-1973.
3. P. Borowiecki, A. M. Wawro, P. Wińska, M. Wielechowska and M. Bretner, *Eur. J. Med. Chem.*, 2014, **84**, 364-374.
4. R. Balamurugan and S. Manojveer, *Chem. Commun.*, 2011, **47**, 11143-11145.
5. K. Chen, J. M. Richter and P. S. Baran, *J. Am. Chem. Soc.*, 2008, **130**, 7247-7249.
6. D. M. Pearson, N. R. Conley and R. M. Waymouth, *Adv. Synth. Catal.*, 2011, **353**, 3007-3013.
7. A. N. Zelikin, P. N. Zawaneh and D. Putnam, *Biomacromolecules*, 2006, **7**, 3239-3244.
8. R. P. Brannigan, A. Walder and A. P. Dove, *J. Polym. Sci. Part A: Polym. Chem.*, 2014, **52**, 2279-2286.
9. R. C. Pratt, F. Nederberg, R. M. Waymouth and J. L. Hedrick, *Chem. Commun.*, 2008, 114-116.
10. T. F. Al-Azemi, H. H. Dib, N. A. Al-Awadi and O. M. E. El-Dusouqui, *Tetrahedron*, 2008, **64**, 4126-4134.
11. J. Matsuo, K. Aoki, F. Sanda and T. Endo, *Macromolecules*, 1998, **31**, 4432-4438.
12. M. Dvorakova, M. Pribylova, R. Pohl, M. E. Migaud and T. Vanek, *Tetrahedron*, 2012, **68**, 6701-6711.
13. K. Mikami, A. T. Lonnecker, T. P. Gustafson, N. F. Zinnel, P. J. Pai, D. H. Russell and K. L. Wooley, *J. Am. Chem. Soc.*, 2013, **135**, 6826-6829.
14. X. Xu, Y. Chen, G. Zou and J. Sun, *Dalton Trans.*, 2010, **39**, 3952-3958.
15. X. He, Y. Yao, X. Luo, J. Zhang, Y. Liu, L. Zhang and Q. Wu, *Organometallics*, 2003, **22**, 4952-4957.
16. Y.-L. Wong, Y. Yan, E. S. H. Chan, Q. Yang, T. C. W. Mak and D. K. P. Ng, *J. Chem. Soc., Dalton Trans.*, 1998, 3057-3064.
17. L. F. Lindoy, G. V. Meehan and N. Svenstrup, *Synthesis*, 1998, **1998**, 1029-1032.
18. P. A. Cameron, V. C. Gibson, C. Redshaw, J. A. Segal, A. J. P. White and D. J. Williams, *J. Chem. Soc., Dalton Trans.*, 2002, 415-422.
19. Z. Dai, J. Zhang, Y. Gao, N. Tang, Y. Huang and J. Wu, *Cat. Sci. Technol.*, 2013, **3**, 3268-3277.
20. M. E. Evans and F. W. Parrish, *Carbohyd. Res.*, 1977, **54**, 105-114.
21. *Int. Pat.*, WO2016166682A1, 2016.
22. E. Larsen, T. Kofoed and E. B. Pedersen, *Synthesis*, 1995, **1995**, 1121-1125.
23. J. Adams, M. David and R. W. Giese, *Anal. Chem.*, 1986, **58**, 345-348.
24. A. R. Vaino and W. A. Szarek, *Chem. Commun.*, 1996, 2351-2352.
25. C. K. Williams, L. E. Breyfogle, S. K. Choi, W. Nam, V. G. Young, M. A. Hillmyer and W. B. Tolman, *J. Am. Chem. Soc.*, 2003, **125**, 11350-11359.
26. M. Cheng, A. B. Attygalle, E. B. Lobkovsky and G. W. Coates, *J. Am. Chem. Soc.*, 1999, **121**, 11583-11584.
27. B. M. Chamberlain, M. Cheng, D. R. Moore, T. M. Ovitt, E. B. Lobkovsky and G. W. Coates, *J. Am. Chem. Soc.*, 2001, **123**, 3229-3238.
28. O. R. Ludek and V. E. Marquez, *Tetrahedron*, 2009, **65**, 8461-8467.
29. *Int. Pat.*, WO2012/71508 A1, 2012
30. M. Quintiliani, J. Balzarini and C. McGuigan, *Tetrahedron*, 2013, **69**, 9111-9119.

Appendix

X-ray Diffraction Data and DFT Calculations

8. Appendix

8.1. Single-Crystal and Powder X-ray Diffraction Data

8.1.1. Chapter 2

L2ZnEt

Empirical formula	$C_{29}H_{40}N_2OZn$	
Formula weight	498.00	
Temperature	150(2) K	
Wavelength	0.71073 Å	
Crystal system	Tetragonal	
Space group	$I\,4_1/a$	
Unit cell dimensions	a = 17.4448(2) Å	α= 90°.
	b = 17.4448(2) Å	β= 90°.
	c = 35.9306(6) Å	γ= 90°.
Volume	10934.4(3) $Å^3$	
Z	16	
Density (calculated)	1.210 Mg/m^3	
Absorption coefficient	0.920 mm^{-1}	
F(000)	4256	
Crystal size	0.400 x 0.300 x 0.200 mm^3	
Theta range for data collection	3.864 to 27.083°.	
Index ranges	$-22 \le h \le 21$, $-22 \le k \le 22$, $-42 \le l \le 46$	
Reflections collected	90381	
Independent reflections	5979 [R(int) = 0.0840]	
Completeness to theta = 25.242°	99.2 %	
Absorption correction	Semi-empirical from equivalents	
Max. and min. transmission	0.839 and 0.702	
Refinement method	Full-matrix least-squares on F^2	
Data / restraints / parameters	5979 / 0 / 309	
Goodness-of-fit on F^2	1.130	
Final R indices [I>2sigma(I)]	R_1 = 0.0417, wR_2 = 0.0923	
R indices (all data)	R_1 = 0.0620, wR_2 = 0.1049	
Extinction coefficient	n/a	
Largest diff. peak and hole	0.459 and -0.518 $e.Å^{-3}$	

L3ZnEt

Empirical formula	$C_{58}H_{76}N_4O_2Zn_2$	
Formula weight	991.96	
Temperature	150(2) K	
Wavelength	0.71073 Å	
Crystal system	Monoclinic	
Space group	P 2_1/n	
Unit cell dimensions	a = 14.0693(2) Å	α= 90°.
	b = 13.0041(3) Å	β= 96.9222(13)°.
	c = 15.0466(3) Å	γ= 90°.
Volume	2732.84(9) $Å^3$	
Z	2	
Density (calculated)	1.205 Mg/m^3	
Absorption coefficient	0.920 mm^{-1}	
F(000)	1056	
Crystal size	0.500 x 0.250 x 0.200 mm^3	
Theta range for data collection	4.156 to 27.508°.	
Index ranges	$-18 \leq h \leq 18$, $-16 \leq k \leq 16$, $-19 \leq l \leq 19$	
Reflections collected	56556	
Independent reflections	6243 [R(int) = 0.0739]	
Completeness to theta = 25.242°	99.4 %	
Absorption correction	Semi-empirical from equivalents	
Max. and min. transmission	0.839 and 0.734	
Refinement method	Full-matrix least-squares on F^2	
Data / restraints / parameters	6243 / 0 / 314	
Goodness-of-fit on F^2	1.030	
Final R indices [I>2sigma(I)]	R_1 = 0.0363, wR_2 = 0.0853	
R indices (all data)	R_1 = 0.0596, wR_2 = 0.0954	
Extinction coefficient	n/a	
Largest diff. peak and hole	0.327 and -0.468 $e.Å^{-3}$	

(L3)$_2$Zn

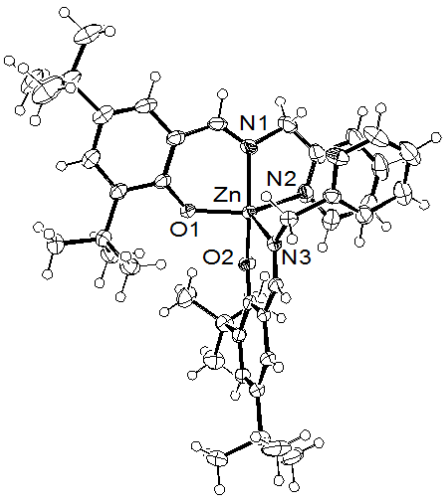

Empirical formula	$C_{42}H_{54}N_4O_2Zn$	
Formula weight	712.26	
Temperature	150(2) K	
Wavelength	0.71073 Å	
Crystal system	Triclinic	
Space group	$P\bar{1}$	
Unit cell dimensions	a = 11.9530(3) Å	α= 102.2444(10)°.
	b = 13.1518(3) Å	β= 101.3435(10)°.
	c = 13.7201(3) Å	γ= 104.2737(9)°.
Volume	1970.86(8) Å^3	
Z	2	
Density (calculated)	1.200 Mg/m^3	
Absorption coefficient	0.662 mm^{-1}	
F(000)	760	
Crystal size	0.600 x 0.400 x 0.250 mm^3	
Theta range for data collection	3.132 to 27.530°.	
Index ranges	$-15 \le h \le 14$, $-17 \le k \le 16$, $-17 \le l \le 17$	
Reflections collected	27452	
Independent reflections	8928 [R(int) = 0.0377]	
Completeness to theta = 25.242°	99.5 %	
Absorption correction	Semi-empirical from equivalents	
Max. and min. transmission	0.852 and 0.781	
Refinement method	Full-matrix least-squares on F^2	
Data / restraints / parameters	8928 / 0 / 454	
Goodness-of-fit on F^2	1.050	

Final R indices [I>2sigma(I)]	R_1 = 0.0374, wR_2 = 0.0866
R indices (all data)	R_1 = 0.0512, wR_2 = 0.0945
Extinction coefficient	n/a
Largest diff. peak and hole	0.413 and -0.452 e.Å^{-3}

8.1.2. Chapter 3

Cyclic 1-O-methyl-2,3-O-isopropylidene-4,6-O-carbonate-α-D-mannopyranose (3)

Empirical formula	$C_{11}H_{16}O_7$	
Formula weight	260.24	
Temperature	150.01(10) K	
Wavelength	1.54184 Å	
Crystal system	Orthorhombic	
Space group	$P2_12_12_1$	
Unit cell dimensions	a = 5.55420(10) Å	α= 90°.
	b = 14.2917(3) Å	β= 90°.
	c = 15.1105(3) Å	γ = 90°.
Volume	1199.46(4) Å^3	
Z	4	
Density (calculated)	1.441 Mg/m^3	
Absorption coefficient	1.043 mm^{-1}	
F(000)	552	
Crystal size	0.300 x 0.070 x 0.060 mm^3	
Theta range for data collection	4.258 to 73.162°.	
Index ranges	$-6 \leq h \leq 6$, $-17 \leq k \leq 15$, $-18 \leq l \leq 18$	
Reflections collected	23766	
Independent reflections	2384 [R(int) = 0.0362]	
Completeness to theta = 67.684°	99.9 %	
Absorption correction	Semi-empirical from equivalents	
Max. and min. transmission	1.00000 and 0.68008	
Refinement method	Full-matrix least-squares on F^2	
Data / restraints / parameters	2384 / 0 / 166	
Goodness-of-fit on F^2	1.046	
Final R indices [I>2sigma(I)]	R_1 = 0.0241, wR_2 = 0.0632	
R indices (all data)	R_1 = 0.0243, wR_2 = 0.0634	
Absolute structure parameter	0.06(5)	
Extinction coefficient	n/a	

Largest diff. peak and hole	0.169 and -0.192 e.Å^{-3}

Powder X-ray diffraction of poly(3)

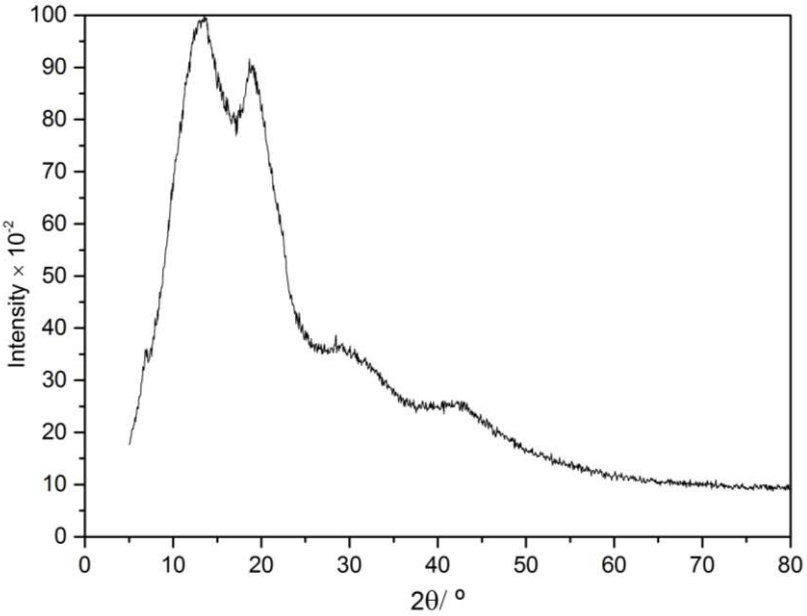

Figure A1. Powder X-ray Diffraction of mannose-derived polycarbonate ($M_{n,SEC}$ 7580 g mol^{-1}, Đ 1.13) showing no crystallinity.

8.1.3. Chapter 4

3-N-Methyl-3'-tosyl thymidine (6)

Empirical formula	$C_{18}H_{22}N_2O_7S$	
Formula weight	410.43	
Temperature	150(2) K	
Wavelength	1.54184 Å	
Crystal system	Monoclinic	
Space group	$P2_1$	
Unit cell dimensions	a = 6.44190(10) Å	α= 90°.
	b = 14.7348(2) Å	β= 106.3100(10)°.
	c = 10.71760(10) Å	γ= 90°.
Volume	976.37(2) Å^3	
Z	2	
Density (calculated)	1.396 Mg/m^3	
Absorption coefficient	1.859 mm^{-1}	
F(000)	432	

Crystal size	0.200 x 0.100 x 0.080 mm^3
Theta range for data collection	4.298 to 72.553°.
Index ranges	$-7 \leq h \leq 7$, $-18 \leq k \leq 17$, $-12 \leq l \leq 12$
Reflections collected	14552
Independent reflections	3741 [R(int) = 0.0372]
Completeness to theta = 67.684°	99.9 %
Absorption correction	Semi-empirical from equivalents
Max. and min. transmission	1.00000 and 0.52689
Refinement method	Full-matrix least-squares on F^2
Data / restraints / parameters	3741 / 1 / 260
Goodness-of-fit on F^2	1.045
Final R indices [I>2sigma(I)]	R_1 = 0.0286, wR_2 = 0.0736
R indices (all data)	R_1 = 0.0293, wR_2 = 0.0742
Absolute structure parameter	-0.003(8)
Extinction coefficient	n/a
Largest diff. peak and hole	0.135 and -0.342 e.$Å^{-3}$

Cyclic 3-*N*-methyl-3',5'-O-cis-carbonate-thymidine (7)

Empirical formula	$C_{12}H_{14}N_2O_6$	
Formula weight	282.25	
Temperature	150(2) K	
Wavelength	1.54184 Å	
Crystal system	Monoclinic	
Space group	$P2_1$	
Unit cell dimensions	a = 7.0627(2) Å	α= 90°.
	b = 9.6573(4) Å	β= 110.448(4)°.
	c = 10.0320(3) Å	γ= 90°.
Volume	641.13(4) $Å^3$	
Z	2	
Density (calculated)	1.462 Mg/m^3	
Absorption coefficient	1.016 mm^{-1}	
F(000)	296	
Crystal size	0.300 x 0.100 x 0.020 mm^3	
Theta range for data collection	6.572 to 72.400°.	
Index ranges	$-7 \leq h \leq 8$, $-11 \leq k \leq 9$, $-11 \leq l \leq 12$	
Reflections collected	5532	
Independent reflections	2172 [R(int) = 0.0267]	

Completeness to theta = 67.684°	99.6 %
Absorption correction	Semi-empirical from equivalents
Max. and min. transmission	1.00000 and 0.78559
Refinement method	Full-matrix least-squares on F^2
Data / restraints / parameters	2172 / 1 / 183
Goodness-of-fit on F^2	1.060
Final R indices [I>2sigma(I)]	R_1 = 0.0314, wR_2 = 0.0779
R indices (all data)	R_1 = 0.0330, wR_2 = 0.0792
Absolute structure parameter	0.01(11)
Extinction coefficient	n/a
Largest diff. peak and hole	0.139 and -0.175 e.$Å^{-3}$

Powder X-ray diffraction of poly(7)

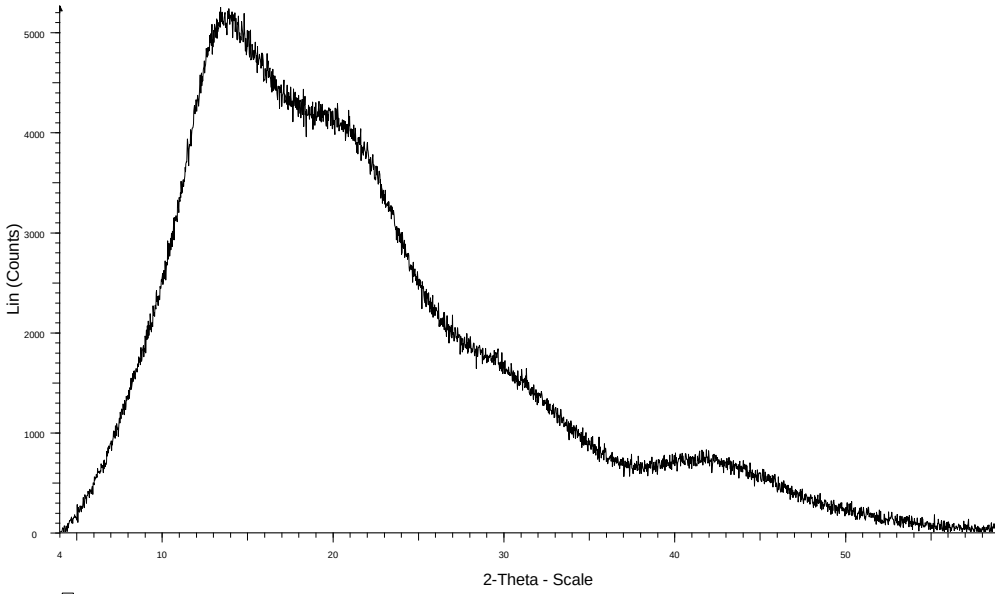

Figure A2. Powder X-ray diffraction of thymidine-derived polycarbonate ($M_{n,\,SEC}$ 15 400 g mol^{-1}, Đ 1.28, Table 4.01, Entry 6) showing amorphous character.

8.1.4. Chapter 5

Cyclic 1-O-benzyl-2-deoxy-3,4-O-cis-carbonate-α/β-D-ribopyranoside (9'-Bn)

Empirical formula	$C_{13}H_{14}O_5$
Formula weight	250.24
Temperature	150(2) K
Wavelength	1.54184 Å
Crystal system	Monoclinic

Space group	P 2_1	
Unit cell dimensions	a = 14.0052(2) Å	α= 90°.
	b = 6.18670(10) Å	β= 105.2291(12)°.
	c = 14.0375(2) Å	γ = 90°.
Volume	1173.58(3) $Å^3$	
Z	4	
Density (calculated)	1.416 Mg/m^3	
Absorption coefficient	0.920 mm^{-1}	
F(000)	528	
Crystal size	0.300 x 0.190 x 0.170 mm^3	
Theta range for data collection	5.195 to 71.984°.	
Index ranges	$-17 \leq h \leq 11$, $-7 \leq k \leq 7$, $-17 \leq l \leq 16$	
Reflections collected	10981	
Independent reflections	4429 [R(int) = 0.0215]	
Completeness to theta = 67.684°	99.9 %	
Absorption correction	Gaussian	
Max. and min. transmission	0.990 and 0.986	
Refinement method	Full-matrix least-squares on F^2	
Data / restraints / parameters	4429 / 1 / 325	
Goodness-of-fit on F^2	1.101	
Final R indices [I>2sigma(I)]	R_1 = 0.0286, wR_2 = 0.0708	
R indices (all data)	R_1 = 0.0288, wR_2 = 0.0711	
Absolute structure parameter	0.00(5)	
Extinction coefficient	n/a	
Largest diff. peak and hole	0.167 and -0.262 e.$Å^{-3}$	

Cyclic 1-O-methyl-2-deoxy-3,5-O-cis-carbonate-α-D-ribofuranose (12α)

Empirical formula	$C_7H_{10}O_5$	
Formula weight	174.15	
Temperature	150(2) K	
Wavelength	1.54184 Å	
Crystal system	Orthorhombic	
Space group	$P2_12_12_1$	
Unit cell dimensions	a = 5.85770(10) Å	α= 90°.
	b = 11.00620(10) Å	β= 90°.
	c = 11.88280(10) Å	γ= 90°.
Volume	766.096(16) $Å^3$	

Z	4
Density (calculated)	1.510 Mg/m^3
Absorption coefficient	1.126 mm^{-1}
F(000)	368
Crystal size	0.250 x 0.180 x 0.100 mm^3
Theta range for data collection	5.479 to 72.513°.
Index ranges	$-7 \leq h \leq 4$, $-13 \leq k \leq 13$, $-14 \leq l \leq 14$
Reflections collected	8745
Independent reflections	1517 [R(int) = 0.0229]
Completeness to theta = 67.684°	100.0 %
Absorption correction	Semi-empirical from equivalents
Max. and min. transmission	1.00000 and 0.68919
Refinement method	Full-matrix least-squares on F^2
Data / restraints / parameters	1517 / 0 / 110
Goodness-of-fit on F^2	1.108
Final R indices [I>2sigma(I)]	R_1 = 0.0238, wR_2 = 0.0590
R indices (all data)	R_1 = 0.0239, wR_2 = 0.0590
Absolute structure parameter	-0.04(6)
Extinction coefficient	n/a
Largest diff. peak and hole	0.128 and -0.173 e.$Å^{-3}$

Cyclic 1-O-methyl-2-deoxy-3,5-O-cis-carbonate-β-D-ribofuranose (12β)

Empirical formula	$C_7H_{10}O$	
Formula weight	174.15	
Temperature	150(2) K	
Wavelength	1.54184 Å	
Crystal system	Orthorhombic	
Space group	$P2_12_12_1$	
Unit cell dimensions	a = 7.56590(10) Å	α= 90°.
	b = 9.9805(2) Å	β= 90°.
	c = 10.2418(2) Å	γ= 90°.
Volume	773.37(2) $Å^3$	
Z	4	
Density (calculated)	1.496 Mg/m^3	
Absorption coefficient	1.115 mm^{-1}	
F(000)	368	
Crystal size	0.250 x 0.200 x 0.150 mm^3	

Theta range for data collection	6.192 to 72.264°.
Index ranges	$-9 \leq h \leq 8$, $-11 \leq k \leq 12$, $-12 \leq l \leq 12$
Reflections collected	4290
Independent reflections	1497 [R(int) = 0.0225]
Completeness to theta = 67.684°	99.8 %
Absorption correction	Semi-empirical from equivalents
Max. and min. transmission	1.00000 and 0.69375
Refinement method	Full-matrix least-squares on F^2
Data / restraints / parameters	1497 / 0 / 111
Goodness-of-fit on F^2	1.061
Final R indices [I>2sigma(I)]	$R_1 = 0.0241$, $wR_2 = 0.0616$
R indices (all data)	$R_1 = 0.0244$, $wR_2 = 0.0621$
Absolute structure parameter	-0.09(7)
Extinction coefficient	0.027(2)
Largest diff. peak and hole	0.163 and -0.150 e.Å^{-3}

1-O-Methyl-2,3-O-isopropylidene-4,6-O-thiocarbonyl-α-D-mannopyranoside (13) and 1-O-methyl-2,3-O-isopropylidene-4O,6S-dithiocarbonate-α-D-mannopyranoside (14)

Empirical formula	$C_{11}H_{16}O_{5.60}S_{1.40}$	
Formula weight	282.72	
Temperature	150.00(10) K	
Wavelength	0.71073 Å	
Crystal system	Monoclinic	
Space group	$P2_1$	
Unit cell dimensions	a = 5.3454(5) Å	α = 90°.
	b = 9.8811(8) Å	β = 101.098(8)°.
	c = 13.2873(10) Å	γ = 90°.
Volume	688.69(10) Å^3	
Z	2	
Density (calculated)	1.363 Mg/m^3	
Absorption coefficient	0.309 mm^{-1}	
F(000)	298	
Crystal size	0.600 x 0.400 x 0.240 mm^3	
Theta range for data collection	3.744 to 30.272°.	
Index ranges	$-7 \leq h \leq 6$, $-12 \leq k \leq 13$, $-18 \leq l \leq 18$	
Reflections collected	6125	
Independent reflections	3255 [R(int) = 0.0254]	

Completeness to theta = 25.242°	99.8 %
Absorption correction	Semi-empirical from equivalents
Max. and min. transmission	1.00000 and 0.97364
Refinement method	Full-matrix least-squares on F^2
Data / restraints / parameters	3255 / 7 / 184
Goodness-of-fit on F^2	1.041
Final R indices [I>2sigma(I)]	R_1 = 0.0427, wR_2 = 0.0956
R indices (all data)	R_1 = 0.0469, wR_2 = 0.0987
Absolute structure parameter	-0.04(5)
Extinction coefficient	n/a
Largest diff. peak and hole	0.286 and -0.266 e.Å^{-3}

1-O-Methyl-2-deoxy-3O,5S-dithiocarbonate-ᴅ-ribofuranoside (15)

Empirical formula	$C_7H_{10}O_3S_2$	
Formula weight	206.27	
Temperature	150.00(10) K	
Wavelength	1.54184 Å	
Crystal system	Orthorhombic	
Space group	$P2_12_12_1$	
Unit cell dimensions	a = 7.55350(10) Å	α= 90°.
	b = 12.29650(10) Å	β= 90°.
	c = 19.9749(2) Å	γ = 90°.
Volume	1855.30(3) Å^3	
Z	8	
Density (calculated)	1.477 Mg/m^3	
Absorption coefficient	4.954 mm^{-1}	
F(000)	864	
Crystal size	0.250 x 0.100 x 0.040 mm^3	
Theta range for data collection	4.222 to 73.152°.	
Index ranges	$-9 \leq h \leq 8$, $-15 \leq k \leq 14$, $-24 \leq l \leq 24$	
Reflections collected	17053	
Independent reflections	3697 [R(int) = 0.0346]	
Completeness to theta = 67.684°	100.0 %	
Absorption correction	Semi-empirical from equivalents	
Max. and min. transmission	1.00000 and 0.36298	
Refinement method	Full-matrix least-squares on F^2	
Data / restraints / parameters	3697 / 0 / 219	

Goodness-of-fit on F^2	1.073
Final R indices [I>2sigma(I)]	R_1 = 0.0244, wR_2 = 0.0630
R indices (all data)	R_1 = 0.0254, wR_2 = 0.0637
Absolute structure parameter	-0.014(9)
Extinction coefficient	n/a
Largest diff. peak and hole	0.213 and -0.263 e.Å^{-3}

Powder X-ray diffraction pattern of poly(12α)

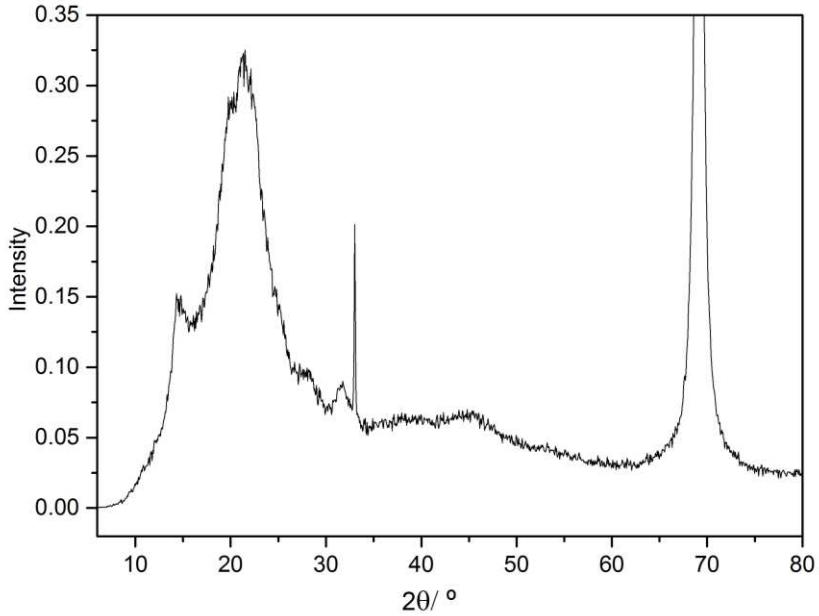

Figure A3. Powder X-ray diffraction pattern of poly (**12α**) ($M_{n,SEC}$ 25 600 g mol^{-1}, Đ 1.41) showing amorphous nature.

Powder X-ray diffraction pattern of poly(TMC-co-66mol%-12α)

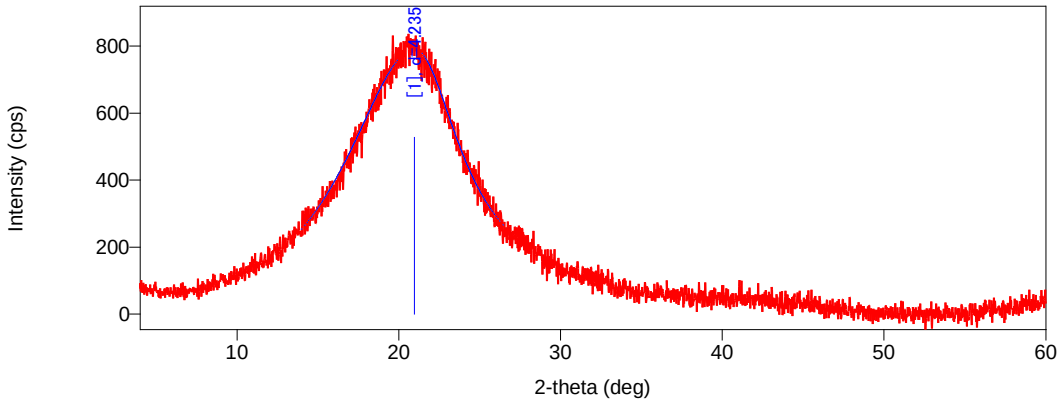

Figure A4. Powder diffraction of selected copolymer, poly(TMC-co-66mol%-**12α**) showing amorphous nature.

8.2. DFT Calculations

8.2.1. Chapter 2

Direct coupling of 1,3-butanediol and CO_2 in the absence of a catalyst (Figure 2.05)

Table A1. Computed Free Gibbs Energies at the rωb97xd/6-31++G(d,p)/cpcm=methanol/298 K level of theory for the direct coupling of (*R*)-1,3-butanediol and CO_2 in the absence of a catalyst.

Structure	G (Hartree)	ΔG (kcal mol^{-1})
CO_2	-188.53882	-
(*R*)-1,3-butanediol	-308.720022	-
H_2O	-76.413939	-
Cyclic carbonate (CC)	-420.840027	-
Diol (+CO_2)	-497.258842	**0.0 (reference)**
A	-497.250156	5.5
TS_{AB}	-497.183512	47.3
B	-497.241294	11.0
C	-497.245017	8.7
D	-497.237838	13.2
TS_{DE}	-497.157774	63.4
E	-497.244461	9.0
A'	-497.248766	6.3
$TS_{AB'}$	-497.180435	49.2
B'	-497.235759	14.5
C'	-497.244256	9.2
D'	-497.238097	13.0
$TS_{DE'}$	-497.15785	63.4
E'	-497.244973	8.7
CC (+H_2O)	-497.253966	3.1

DBU-aided CO_2 insertion and ring-closing (Figure 2.12)

Table A2. Computed Free Gibbs Energies at the rωb97xd/6-31+G(d)/cpcm=methanol/298 K level of theory for the coupling of (*R*)-1,3-butanediol with CO_2 in the presence of DBU.

Structure	G (Hartree)	ΔG (kcal mol^{-1})
DBU	-461.767329	-
CO_2	-188.538882	-
(*R*)-1,3-butanediol	-308.698783	-
H_2O	-76.403072	-
Cyclic carbonate (CC)	-420.829745	-
Diol (+DBU+CO_2)	-959.004994	**0.0 (reference)**
A	-958.99408	6.8
TS_{AB}	-958.983371	13.6
B	-959.014418	-5.9
TS_{BC}	-959.013594	-5.4
C	-959.018545	-8.5

D	-959.013651	-5.4
TS_{DE}	-958.946382	36.8
E	-958.970665	21.5
TS_{EF}	-958.961071	27.6
F	-958.98709	11.2
A'	-958.987274	11.1
$TS_{AB'}$	-958.974844	18.9
B'	-959.008702	-2.3
$TS_{BC'}$	-959.005974	-0.6
C'	-959.010334	-3.4
D'	-959.012944	-5.0
$TS_{DE'}$	-958.946125	36.9
E'	-958.969966	22.0
$TS_{EF'}$	-958.961087	27.6
F'	-958.990060	9.4
D S_N2	-959.009702	-3.0
TS_{DE} S_N2	-958.921093	52.6
E S_N2	-958.950345	34.3
$[DBU\text{-}CO_2]^{‡}$ (+ diol)	-958.988882	10.1
$DBU\text{-}CO_2$ (+ diol)	-959.001693	2.1
$[DBU\text{-}CO_2$ --primary OH$]^{‡}$	-958.932993	45.5
$[DBU\text{-}CO_2$ --secondary OH$]^{‡}$	-958.931713	46.0
Secondary OH-DBU adduct (+ CO_2)	-959.005540	-0.3
Primary OH-DBU adduct (+ CO_2)	-959.006135	-0.7
CC (+ H_2O+ DBU)	-959.000146	3.0

Full coordinates for all calculated structures are available *via* the corresponding Gaussian 09 output files, stored in the digital repositories: http://dx.doi.org/10.6084/m9.figshare.1333535

Tosylation and subsequent ring-closing steps (Figure 2.18)

Table A3. Computed Gibbs Free Energies at the rωb97xd/6-31+G(d)/cpcm=chloroform or methanol /298 K level of theory. All combinations of ion pairs were computed but only the lowest in energy are reported.

Structure	Chloroform		Methanol	
	G (Hartree)	ΔG (kcal mol^{-1})	G (Hartree)	ΔG (kcal mol^{-1})
NEt_3	-292.161443	-	-292.162060	-
TsCl	-1279.492029	-	-1279.494187	-
$HNEt_3Cl$	-752.986040	-	-752.993268	-
DBUHCl	-922.601085	-	-922.611038	-
NEt_3OTs	-1187.287611	-	-1187.294235	-
DBUHOTs	-1356.908931	-	-1356.918183	-
Cyclic carbonate (CC)	-959.009021	-	-959.018505	-
I (+ TsCl+ NEt_3)	-2530.662493	**0.0 (reference)**	-2530.674752	**0.0 (reference)**
II	-2530.641749	13.0	-2530.650790	15.0
[III]‡	-2530.615106	29.7	-2530.626196	30.5
IV (+ $HNEt_3Cl$)	-2530.680693	-11.4	-2530.701911	-17.0

V (+ $HNEt_3Cl$)	-2238.487149	-25.4	-2530.719056	-27.8
[VI]‡ (+ $HNEt_3Cl$)	-2238.538384	-3.1	-2530.686036	-7.1
VII (+ $HNEt_3Cl$)	-2530.715343	-33.2	-2530.737271	-39.2
(S)-**2a** + DBUHOTs + $HNEt_3Cl$	-2530.721027	**-36.7**	-2530.741196	-41.7
VIII	-2530.640391	13.9	-2530.652582	13.9
[IX]‡	-2530.624530	23.8	-2530.638360	22.8
X	-2530.663422	-0.6	-2530.676089	-0.8
XI (+ DBUHCl)	-2530.666091	-2.3	-2530.680599	-3.7
[XII]‡ (+ DBUHCl)	-2530.636103	16.6	-2530.653635	13.3
XIII (+ DBUHCl)	-2530.711971	-31.0	-2530.729637	-34.4
(R)-**2a** + NEt_3OTs + DBUHCl	-2530.714752	**-32.8**	-2530.735018	-37.8

Full coordinates for all calculated structures are available *via* the corresponding Gaussian 09 output files, stored in the digital repositories: http://dx.doi.org/10.6084/m9.figshare.1333544

Table A4. Computed Gibbs Free Energies at the rωb97xd/6-31+G(d)/cpcm=chloroform/298 K level of theory for ring closing of mono-tosylated di-carbonate species (Figure 2.19).

Structure	**G (Hartree)**	**ΔG (kcal mol^{-1})**
DBUHOTs	-1356.908931	-
Cyclic carbonate (CC)	-959.009021	-
CO_2	-188.53719	-
Primary tosylated carbonate and secondary $DBUH^+$ CO_3^-	-1966.215872	**0.0 (reference)**
Ring-closing Transition State	-1966.176867	24.5
CC + DBUHOTs + CO_2	-1966.260594	-28.1
CC + DBUHOTs + CO_2 (separately)	-1966.272177	-35.3

CO_2 insertion and ring-closing with L(1-3)ZnEt (Section 2.6)

Table A5. Computed Gibbs Free Energies at the rωb97xd/6-31+G(d)/cpcm=methanol/298 K level of theory for the targeted catalytic cycle (Figure 2.28) with L(1-3)ZnEt complexes.

Structure	**G (Hartree)**	**ΔG (kcal mol^{-1})**	**ΔΔG (kcal mol^{-1})**
(R)-1,3-butanediol (diol)	-308.698783	-	
Ethane	-79.750075	-	
CO_2	-188.538882	-	
Cyclic Carbonate (CC)	-420.829745	-	
H_2O	-76.403072	-	
L1ZnEt	-2916.429256	-	
L1ZnEt (+ 2 diol + CO_2)	-3722.365704	**0.0 (reference)**	
L1Zndiol primary (+ CO_2 + diol+ ethane)	-3722.397459	-19.9	

L1Zndiol secondary (+ CO_2 + diol+ ethane)	-3722.407605	-26.3	
L1ZnOC(O)OR primary (+ diol + ethane)	-3722.413141	-29.8	-9.8
L1ZnOC(O)OR secondary (+ diol + ethane)	-3722.413784	-30.2	-3.9
CC+ L1ZnOH (+ diol + ethane)	-3722.396152	-19.1	
CC + H_2O + L1Zndiol primary (+ ethane)	-3722.392611	-16.9	
CC+ H_2O + L1Zndiol secondary (+ ethane)	-3722.402757	-23.3	
L2ZnEt	-2860.149277	-	
L2ZnEt (+ 2diol + CO_2)	-3666.085719	**0.0 (reference)**	
L2Zndiol primary (+ diol + CO_2 + ethane)	-3666.124113	-24.1	
L2Zndiol secondary (+ diol+ CO_2 + ethane)	-3666.122501	-23.1	
CO_2 insertion TS into L2Zn-diol primary (+diol + ethane)	-3666.107853	-13.9	+9.2
CO2 insertion TS into L2Zn-diol secondary (+diol + ethane)	-3666.107870	-13.9	+10.2
L2ZnOC(O)OR primary (diol + ethane)	-3666.130832	-28.3	-4.2
L2ZnOC(O)OR secondary (diol + ethane)	-3666.130089	-27.8	-4.8
Primary ring-closing TS (+ diol + ethane)	-3666.049429	22.8	+50.6
Secondary ring-closing TS (+ diol + ethane)	-3666.049716	22.6	+50.9
CC + L2ZnOH (+ diol + ethane)	-3666.116862	-19.5	-
H_2O + L2Zndiol primary + CC (+ ethane)	-3666.119271	-21.1	-
H_2O + L2Zndiol secondary CC (+ ethane)	-3666.117659	-20.0	-
L3ZnEt	-2858.951337	-	
L3ZnEt (+ 2diol + CO_2)	-3664.887785	**0.0 (reference)**	
L3Zndiol primary (+ diol + CO_2 + ethane)	-3664.925745	-23.8	
L3Zndiol secondary (+ diol+ CO_2 + ethane)	-3664.925272	-23.5	
CO_2 insertion TS into L3Zn-diol primary (+diol + ethane)	-3664.906131	-11.5	+12.0
CO_2 insertion TS into L3Zn-diol secondary (+diol + ethane)	-3664.908782	-13.2	+10.6
L3ZnOC(O)OR primary (diol + ethane)	-3664.929958	-26.5	-2.6
L3ZnOC(O)OR secondary (diol + ethane)	-3664.932420	-28.0	-4.5
Primary ring-closing TS (+ diol + ethane)	-3664.855070	20.5	+48.5

Secondary ring-closing TS (+ diol + ethane)	-3664.855718	20.1	+46.6
CC + L3ZnOH (+ diol + ethane)	-3664.919028	-19.6	
H_2O + L3Zndiol primary + CC (+ ethane)	-3664.920897	-20.8	
H_2O + L3Zndiol secondary CC (+ ethane)	-3664.920424	-20.5	

8.2.2. Chapter 3

Initiation step in the ROP of 3 with TBD and 4-MeBnOH

Table A6. Computed Gibbs free energies at the rωb97xd/6-311+G(d,p)/6-31+g(d)/cpcm=dichloromethane/298 K level of theory for the ring-opening of **3** by 4-methylbenzyl alcohol promoted by TBD (initiation step, Figure 3.14).

	Structure	**G (Hartree)**	**ΔG (kcal mol^{-1})**
Starting Materials	TBD	–438.513199	-
	D-Mannose based monomer **3**	–954.701846	-
	4MeBnOH	–385.796245	-
	3+TBD+4MeBnOH	**–1779.011290**	**0.0 (reference)**
Attack *syn* to the isopropylidene ring of the monomer, yielding a *secondary* alcohol chain	**I_a**	–1779.006520	2.99321793
	$TS_{I\text{-}IIa}$	–1779.001811	5.948157811
	II_a	–1779.009453	1.152734033
	III_a	–1779.014208	–1.831071262
	$TS_{III\text{-}IVa}$	–1779.006571	2.961214971
	$IV_{a/d}$	–1779.029512	–11.434469
Attack *syn* to the isopropylidene ring of the monomer, yielding a *primary* alcohol chain	**I_b**	–1779.011747	–0.286771613
	$TS_{I\text{-}IIb}$	–1778.999971	7.102774371
	II_b	–1779.014334	–1.910137396
	III_b	–1779.013411	–1.330946589
	$TS_{III\text{-}IVb}$	–1778.99895	7.74346106
	$IV_{b/d}$	–1779.017319	–3.783251761
Attack *anti* to the isopropylidene ring of the monomer, yielding a *secondary* alcohol chain	**I_c**	–1779.0164	–3.20657099
	$TS_{I\text{-}IIc}$	–1778.998181	8.226015481
	II_c	–1779.007654	2.281622724
	III_c	–1779.009583	1.071157863
	$TS_{III\text{-}IVc}$	–1778.999836	7.187488086
	$IV_{c/a}$	–1779.029512	–11.434469
Attack *anti* to the isopropylidene ring of the monomer, yielding a *primary* alcohol chain	**I_d**	–1779.011747	–0.286771613
	$TS_{I\text{-}IId}$	–1778.999971	7.102774371
	II_d	–1779.014334	–1.910137396
	III_d	–1779.013411	–1.330946589
	$TS_{III\text{-}IVd}$	–1778.99895	7.74346106
	$IV_{d/b}$	–1779.017319	–3.783251761

Full coordinates for all the stationary points, together with the computed Gibbs free energy and vibrational frequency data, are available *via* the corresponding Gaussian 09 output files, stored in the digital repository: DOI: 10.6084/m9.figshare.3469466.

DFT modelling of the propagation step in the ROP of 3

Table A7. Computed Gibbs free energies at the rωb97xd/6-311+G(d,p)/6-31+g(d)/cpcm=dichloromethane/298 K level of theory for the ring-opening of **3** by 4-methyl benzyl alcohol promoted by TBD (propagation step from $\mathbf{IV_{a/c}}$, Figure 3.15).

	Structure	**G (Hartree)**	**ΔG (kcal mol^{-1})**
Starting Materials	TBD	–438.513199	-
	D-Mannose based monomer **3**	–954.701846	-
	4MeBnOH	–385.796245	-
	2 x 3+ TBD + 4MeBnOH	**–2733.713136**	**0.0 (reference)**
Attack *syn* to the isopropylidene ring of the monomer, yielding a *secondary* alcohol chain	$\mathbf{V_a}$	–2733.726885	–8.627621241
	$\mathbf{TS_{V\text{-}VIa}}$	–2733.711814	0.829566898
	$\mathbf{V_{Ia}}$	–2733.720479	–4.607798587
	$\mathbf{V_{IIa}}$	–2733.71965	–4.087593626
	$\mathbf{TS_{VII\text{-}VIIIa}}$	–2733.703396	6.11193766
	$\mathbf{V_{IIIa}}$	–2733.734161	–13.19337672
Attack *syn* to the isopropylidene ring of the monomer, yielding a *primary* alcohol chain	$\mathbf{V_b}$	–2733.730191	–10.70216599
	$\mathbf{TS_{V\text{-}VIb}}$	–2733.704064	5.692761648
	$\mathbf{V_{Ib}}$	–2733.721984	–5.552199632
	$\mathbf{V_{IIb}}$	–2733.718088	–3.107424568
	$\mathbf{TS_{VII\text{-}VIIIb}}$	–2733.709933	2.009911327
	$\mathbf{V_{IIIb}}$	–2733.720632	–4.703807464
Attack *anti* to the isopropylidene ring of the monomer, yielding a *secondary* alcohol chain	$\mathbf{V_c}$	–2733.722207	–5.692134139
	$\mathbf{TS_{V\text{-}VIc}}$	–2733.709569	2.238324603
	$\mathbf{VI_c}$	–2733.711567	0.984561621
	$\mathbf{V_{IIc}}$	–2733.723961	–6.792784925
	$\mathbf{TS_{VII\text{-}VIIIc}}$	–2733.717486	–2.72966415
	$\mathbf{V_{IIIc}}$	–2733.726337	–8.283746309
Attack *anti* to the isopropylidene ring of the monomer, yielding a *primary* alcohol chain	$\mathbf{V_d}$	–2733.725071	–7.489319915
	$\mathbf{TS_{V\text{-}VId}}$	–2733.706453	4.193642647
	$\mathbf{V_{Id}}$	–2733.712828	0.193272772
	$\mathbf{V_{IId}}$	–2733.712017	0.702182571
	$\mathbf{TS_{VII\text{-}VIId}}$	–2733.703686	5.92996005
	$\mathbf{V_{IIId}}$	–2733.734161	–13.19337672

Full coordinates for all the stationary points, together with the computed Gibbs free energy and vibrational frequency data, are available *via* the corresponding Gaussian 09 output files, stored in the digital repository: DOI 10.6084/m9.figshare.3469805.

Table A8. Computed Gibbs free energies at the rωb97xd/6-311+G(d,p)/6-31+g(d)/cpcm=dichloromethane/298 K level of theory for the ring-opening of **3** by 4-methylbenzyl alcohol promoted by TBD (propagation step from $\mathbf{IV_{b/d}}$, Figure 3.16).

	Structure	**G (Hartree)**	**ΔG (kcal mol^{-1})**
Starting Materials	TBD	–438.513199	-
	D-Mannose based monomer **3**	–954.701846	-
	4MeBnOH	–385.796245	-
	2 x 3+ TBD + 4MeBnOH	**–2733.713136**	**0.0 (reference)**
Attack *syn* to the isopropylidene ring of the monomer,	$\mathbf{V_a'}$	–2733.722605	–5.941882721
	$\mathbf{TS_{V\text{-}VIa}'}$	–2733.703797	5.860306551
	$\mathbf{V_{Ia}'}$	–2733.717882	–2.978157714

yielding a *secondary* alcohol chain	$\mathbf{V_{IIa'}}$	–2733.715928	–1.752005128
	$\mathbf{TS_{VII\text{-}VIIIa'}}$	–2733.707398	3.600646642
	$\mathbf{V_{IIIa'}}$	–2733.739755	–16.70366207
Attack *syn* to the isopropylidene ring of the monomer, yielding a *primary* alcohol chain	$\mathbf{V_{b'}}$	–2733.720621	–4.696904865
	$\mathbf{TS_{V\text{-}VIb'}}$	–2733.710538	1.630268382
	$\mathbf{VI_{b'}}$	–2733.723441	–6.466480245
	$\mathbf{V_{IIb'}}$	–2733.722473	–5.859051533
	$\mathbf{TS_{VII\text{-}VIIIb'}}$	–2733.702579	6.624612513
	$\mathbf{V_{IIIb'}}$	–2733.727337	–8.911255309
Attack *anti* to the isopropylidene ring of the monomer, yielding a *secondary* alcohol chain	$\mathbf{V_{c'}}$	–2733.723709	–6.634652657
	$\mathbf{TS_{V\text{-}VIc'}}$	–2733.709121	2.519448635
	$\mathbf{V_{Ic'}}$	–2733.714899	–1.106298367
	$\mathbf{V_{IIc'}}$	–2733.716931	–2.381396655
	$\mathbf{TS_{VII\text{-}VIIIc'}}$	–2733.710938	1.379264782
	$\mathbf{V_{IIIc'}}$	–2733.739755	–16.70366207
Attack *anti* to the isopropylidene ring of the monomer, yielding a *primary* alcohol chain	$\mathbf{V_{d'}}$	–2733.721851	–5.468740935
	$\mathbf{TS_{V\text{-}VId'}}$	–2733.707562	3.497735166
	$\mathbf{V_{Id'}}$	–2733.713984	–0.532127632
	$\mathbf{V_{IId'}}$	–2733.7097	2.156120924
	$\mathbf{TS_{VII\text{-}VIIId'}}$	–2733.703555	6.012163729
	$\mathbf{V_{IIId'}}$	–2733.727337	–8.911255309

Full coordinates for all the stationary points, together with the computed Gibbs free energy and vibrational frequency data, are available *via* the corresponding Gaussian 09 output files, stored in the digital repository: DOI: 10.6084/m9.figshare.3470105.

Table A9. Computed enthalpies at the rωb97xd or rM06-2X-D3/6-311+G(2d,p)/cpcm=dichloromethane/298 K level of theory for the isodesmic ring-opening of **3** and the glucose monomer (**2j**).

	Functional: rωb97xd		*Functional: rM06-2X-D3*	
Structure	**H (Hartree)**	**ΔΔH (kcal mol^{-1})**	**H (Hartree)**	**ΔΔH (kcal mol^{-1})**
Dimethyl carbonate (DMC)	–343.512806	-	–343.485841	-
D-Mannose based monomer **3**	–955.076703	-	–955.013129	-
D-Glucose based monomer **2j**	–916.946941	-	–916.884043	-
*DMC + **3***	*–1298.589509*	**0.0 (reference)**	*–1298.49897*	**0.0 (reference)**
D-Mannose based oligocarbonate	–1298.604623	–9.484171026	–1298.518514	–12.2640359
*DMC + **2j***	*–1260.459747*	**0.0 (reference)**	*–1260.369884*	**0.0 (reference)**
D-Glucose based oligocarbonate	–1260.475298	–9.758392459	–1260.389989	–12.61606845

Full coordinates for all the stationary points, together with the computed Gibbs free energy and vibrational frequency data, are available *via* the corresponding Gaussian 09 output files, stored in the digital repository: DOI: 10.6084/m9.figshare.3469283.

Table A10. Computed Gibbs free energies at the rωb97xd or rM06-2X-D3/6-311+G(2d,p)/cpcm=dichloromethane/298 K level of theory for the ring-opening of **3** and the glucose monomer (**2j**) with MeOH or *i*-PrOH.

	Functional: rωb97xd		*Functional: rM06-2X-D3*	
Structure	**G (Hartree)**	**ΔΔG (kcal mol^{-1})**	**G (Hartree)**	**ΔΔG (kcal mol^{-1})**
Methanol	–115.702205	-	–115.682959	-
i-Propanol	–194.286847	-	–194.250492	-
3	–955.137273	-	–955.074015	-
2j	–917.009385	-	–916.946786	
MeOH + **3**	–1070.839478	**0.0 (reference)**	–1070.756974	**0.0 (reference)**
Ring-opening to primary alcohol	–1070.833289	3.883653	–1070.75426	1.703059
Ring-opening to secondary alcohol	–1070.840881	–0.880395	–1070.759387	–1.514179
Preference for ring-opening by MeOH to give a secondary alcohol		*–4.764048*		*–3.217239*
i-PrOH + **3**	–1149.42412	0.0 (reference)	–1149.324507	0.0 (reference)
Ring-opening to primary alcohol	–1149.418671	3.419297	–1149.321669	1.780871
Ring-opening to secondary alcohol	–1149.424323	–0.127384	–1149.32634	–1.150224
Preference for ring-opening by i-PrOH to give a secondary alcohol		*–3.546681*		*–2.931095*
MeOH + **2j**	–1032.71159	**0.0 (reference)**	–1032.629745	**0.0 (reference)**
Ring-opening to primary alcohol	–1032.707165	2.776727325	–1032.628	1.095003
Ring-opening to secondary alcohol	–1032.711953	–0.227785767	–1032.634194	–2.791788
Preference for ring-opening by MeOH to give a secondary alcohol		*–3.004513092*		*–3.886791*
i-PrOH + **2j**	–1111.296232	**0.0 (reference)**	–1111.197278	**0.0 (reference)**
Ring-opening to primary alcohol	–1111.291211	3.150723	–1111.195695	0.993347
Ring-opening to secondary alcohol	–1111.296355	–0.077184	–1111.19992	–1.657879
Preference for ring-opening by i-PrOH to give a secondary alcohol		*–3.227906*		*–2.651226*

Full coordinates for all the stationary points, together with the computed free Gibbs energy and vibrational frequency data, are available *via* the corresponding Gaussian 09 output files, stored in the digital repository: DOI 10.6084/m9.figshare.346937.

8.2.3. Chapter 4

Ring-closing kinetics and thermodynamics (Figure 4.04 and Figure 4.09)

Table A11. Computed Gibbs free energies at the rωb97xd/6-31+G(d)/cpcm=acetonitrile/298 K level of theory for cyclic carbonate formation by intramolecular nucleophilic addition-elimination.

	Structure	**G /Hartrees**	**ΔG/ kcalmol^{-1}**
	Trans_ThyMe	-1026.099913	
	mannoseCC (**3**)	-954.883603	
	glucoseCC (**2j**)	-916.7632	
	$HNEt_3OTs$	-1187.29434	
Ring-closing by nuc. add. elim. of 3'-OH at 5'-tosylcarbonate	5tosylcarbonate	-2213.361183	0.0
	5tosylcarbonate_TS	-2213.339926	+13.3
	Trans_ThyMe + $HNEt_3OTs$	-2383.018394	-20.8
Ring-closing by nuc. add. elim. of 3'-OH at 5'-tosylcarbonate	3tosylcarbonate	-2213.359407	0.0
	3tosylcarbonate_TS	-2213.337688	+13.6
	Trans_ThyMe + $HNEt_3OTs$	-2213.394253	-21.9
Mannose (**3**): Ring-closing by nuc. add. elim. of 4'-OH at 6'-tosylcarbonate	MannCarbonate	-2142.136853	0.0
	MannCarbonate_TS	-2142.118305	+11.6
	MannoseCC+$HNEt_3OTs$	-2104.014351	-25.8
Glucose (**2j**): Ring-closing by nuc. add. elim. of 4'-OH at 6'-tosylcarbonate	GluCarbonate	-2103.992447	0.0
	GluCarbonate_TS	-1850.210171	+13.7
	GlucoseCC+$HNEt_3OTs$	-2104.05754	-27.1

Full coordinates for all the stationary points, together with the computed Gibbs free energy and vibrational frequency data, are available *via* the corresponding Gaussian 09 output files, stored in the digital repository: DOI: 10.6084/m9.figshare.4309559.

Table A12. Computed Gibbs free energies at the rωb97xd/6-31+G(d)/cpcm=acetonitrile/298 K level of theory for the formation of ***trans*-ThyMe** (hypothetical) and ***cis*-ThyMe** (**7**) by intramolecular S_N2-like ring-closing with 3'- or 5'-carbonate nucleophiles.

	Structure	**G /Hartrees**	**ΔG/ kcal mol^{-1}**
	Trans_ThyMe	-1026.099913	
	Cis_ThyMe (7)	-1026.11592	
	DBUHOTs	-1356.918481	
Intramolecular S_N2 ring-closing with 5'-carbonate nucleophile	5carbonate3tosyl	-2383.009237	0.0
	5carbonate3tosyl_TS	-2382.97299	+22.7
	Cis_ThyMe (7) + DBUHOTs	-2383.034401	-15.8
Intramolecular S_N2 ring-closing with 3'-carbonate nucleophile	5tosyl3carbonate	-2383.013888	0.0
	5tosyl3carbonate_TS	-2382.968715	+28.3
	trans_ThyMe + DBUHOTs	-2383.018394	-2.83

Full coordinates for all the stationary points, together with computed Gibbs free energy and vibrational frequency data, are available *via* the corresponding Gaussian 09 output files, stored in the digital repository: DOI: 10.6084/m9.figshare.4309616.

Ring Strain Calculations (Figures 4.05 to 4.07) and Initiation Step in the ROP of 7 with TBD and 4-MeBnOH (Figure 4.21)

Table A13. Computed Gibbs free energies at the rωb97xd/6-311++G(2d,p)/cpcm=dichloromethane/298 K level of theory for the isodesmic ring-opening with dimethyl carbonate (DMC) of ***trans*-ThyMe**, ***cis*-7**, ***cis*-7-Bz** and IPXTC (xyloseCC, **2i**). The values for the glucose and mannose monomers are in Table A9.

	Structure	**H /Hartrees**
Starting Materials	**Trans_ThyMe**	-1026.301977
	Cis_ThyMe (7)	-1026.317516
	Cis_7_Bz (7-Bz)	-1331.296124
	xyloseCC (**2i**)	-801.309791
	DMC	-343.512814
Products	DMC_Trans_ThyMe	-1369.838650
	DMC_Cis_ThyMe	-1369.838544
	Cis_7_Bz	-1674.818767
	DMC_xylose	-1144.832963

Full coordinates for all the stationary points, together with the computed Gibbs free energy and vibrational frequency data, are available *via* the corresponding Gaussian 09 output files, stored in the digital repository: DOI: 10.6084/m9.figshare.4309469.

Table A14. Computed Gibbs free energies at the rωb97xd/6-311++G(2d,p)/cpcm=dichloromethane/298 K level of theory for the ring-opening of ***trans*-ThyMe**, ***cis*-ThyMe (7)** and IPXTC (xyloseCC, **2i**) with MeOH or *i*-PrOH. The values for the glucose and mannose monomers are in Table A10.

	Structure	**G /Hartrees**	**ΔG/ kcal mol^{-1}**
Starting Materials	**Trans_ThyMe**	-1026.367241	-
	Cis_ThyMe (7)	-1026.381294	-
	xyloseCC (**2i**)	-801.362796	-
	MeOH	-115.702205	-
	i-PrOH	-194.286844	-
***Trans*-ThyMe (hypothetical)**	Trans_ThyMe + MeOH	-1142.069446	0.0
	MeOH_transThyMe_3	-1142.080069	-6.7
	MeOH_transThyMe_5	-1142.079064	-6.0
	Trans_ThyMe + *i*-PrOH	-1220.654085	0.0

	PrOH_transThyMe_3	-1220.66344	-5.9
	PrOH_transThyMe_5	-1220.66355	-5.9
***Cis*-ThyMe (7)**	cis_ThyMe + MeOH	-1142.083499	0.0
	MeOH_cisThyMe_3	-1142.07635	4.5
	MeOH_cisThyMe_5	-1142.083087	0.3
	cis_ThyMe + *i*-PrOH	-1220.668138	0.0
	PrOH_cisThyMe_3	-1220.659461	5.4
	PrOH_ cisThyMe_5	-1220.665093	1.9
IPXTC (**2i**)	xyloseCC+ MeOH	-917.065001	0.0
	MeOH_xylose_3	-917.057093	5.0
	MeOH_xylose_5	-917.061942	1.9
	xyloseCC+ *i*-PrOH	-995.64964	0.0
	PrOH_xylose_3	-995.64208	4.7
	PrOH_xylose_5	-995.646029	2.3

Table A15. Computed Gibbs free energies at the rωb97xd/6-311+G(d,p)/6-31+G(d)/cpcm=dichloromethane/298 K level of theory for the ring-opening of **7** with 4-methylbenzyl alcohol initiator and TBD catalyst.

	Structure	**G /Hartrees**	**ΔG/ kcal mol^{-1}**
Starting Materials	**7**	-1025.912381	
	TBD	-438.513199	
	4MeBnOH	-385.796245	
	Reference	**-1850.221825**	**0.0**
Ring-opening to free secondary OH (carbonate on primary)	I_a	-1850.222786	-0.6
	$TS_{I\text{-}IIa}$	-1850.210771	+6.9
	II_a	-1850.223471	-1.0
	III_a	-1850.231710	-6.2
	$TS_{III\text{-}IVa}$	-1850.217115	+3.0
	IV_a	-1850.230724	-5.6
Ring-opening to free primary OH (carbonate on secondary)	I_b	-1850.222285	-0.3
	$TS_{I\text{-}IIb}$	-1850.210171	+7.3
	II_b	-1850.223610	-1.1
	III_b	-1850.225922	-2.6
	$TS_{III\text{-}IVb}$	-1850.213885	+5.0
	IV_b	-1850.232327	-6.6

Full coordinates for all the stationary points, together with the computed Gibbs free energy and vibrational frequency data, are available *via* the corresponding Gaussian 09 output files, stored in the digital repository: DOI: 10.6084/m9.figshare.4309487.

Ring-opening of thymidine targets

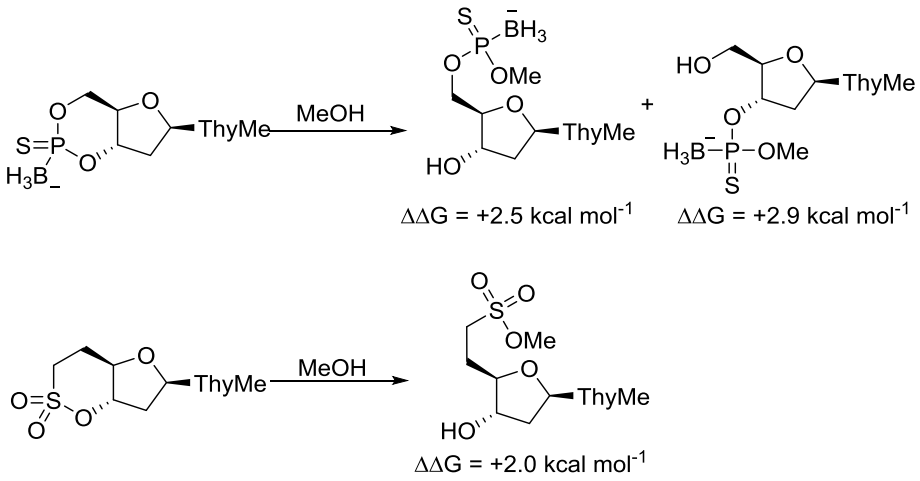

Scheme A1. Ring-opening thermodynamics (ΔΔG) with MeOH calculated at the rωb97xd/6-311+G(2d,p)/cpcm=dichloromethane/298 K level of theory for *trans*-3',5'-cyclic species of 3-*N*-methyl thymidine.

Table A16. Computed Gibbs free energies at the rωb97xd/6-311++G(2d,p)/cpcm=dichloromethane/298 K level of theory for the ring-opening of cyclic methyl thymidine derivatives **(Scheme A1)** with MeOH.

Structure	**G/Hartrees**	**ΔG/kcal mol^{-1}**
MeOH	-115.702205	-
ThyMeP	-1679.439102	-
ThyMeP + MeOH	-1795.141307	0.0 (reference)
MeOH ring-opening to expose 3'-OH	-1795.137373	2.5
MeOH ring-opening to expose 5'-OH	-1795.136662	2.9
ThyMeS	-1425.725095	-
ThyMeS + MeOH	-1541.4273	0.0 (reference)
MeOH ring-opening	-1541.424038	2.0

8.2.4. Chapter 5

Initiation step in the ROP of 12α, 12β and TMC with BnOH and TBD (Figure 5.09)

Table A17. Computed Gibbs free energies at the rωb97xd/6-311+G(d,p)/6-31+G(d)/cpcm=dichloromethane/298 K level of theory for the ring-opening of **12α**, **12β** and TMC by benzyl alcohol with TBD.

	Structure	**G (Hartree)**	**ΔG (kcal mol^{-1})**
	12α	-648.498978	-
	12β	-648.502445	
	TMC	-381.569395	
	TBD	–438.513199	-
	BnOH	-346.523501	-
	12α + **12β**+ TMC+ TBD+ BnOH	-2463.607518	**0 .0 (reference)**
Ring-opening of **12α** to yield a secondary alcohol	**I$_a^{\alpha}$** (+TMC+ **12β**)	-2463.606158	0.9
	TS$_{I\text{-}IIa}^{\alpha}$ (+ TMC+ **12**β)	-2463.591526	10.0
	II$_a^{\alpha}$ (+ TMC+ **12**β)	-2463.605260	1.4
	III$_a^{\alpha}$ (+T MC+ **12β**)	-2463.603273	2.7
	TS$_{III\text{-}IVa}^{\alpha}$ (+ TMC+ **12β**)	-2463.592375	9.5
	IV$_a^{\alpha}$(+ TMC+ **12β**)	-2463.609247	-1.1
Ring-opening of **12α** to yield a primary alcohol	**I$_b^{\alpha}$**	-2463.607652	-0.1
	TS$_{I\text{-}IIb}^{\alpha}$	-2463.593471	8.8
	II$_b^{\alpha}$	-2463.603172	2.7
	III$_b^{\alpha}$	-2463.602453	3.2
	TS$_{III\text{-}IVb}^{\alpha}$	-2463.588595	11.9
	IV$_b^{\alpha}$	-2463.610514	-1.9
Ring-opening of **12β** to yield a secondary alcohol	**I$_a^{\beta}$** (+ TMC + **12α**)	-2463.608178	-0.4
	TS$_{I\text{-}IIa}^{\beta}$ (+ TMC + **12α**)	-2463.588695	11.8
	II$_a^{\beta}$ (+ TMC + **12α**)	-2463.600032	4.7
	III$_a^{\beta}$ (+ TMC + **12α**)	-2463.599580	5.0
	TS$_{III\text{-}IVa}^{\beta}$ (+ TMC + **12α**)	-2463.586121	13.4
	IV$_a^{\beta}$ (+ TMC + **12α**)	-2463.605322	1.4
Ring-opening of **12β** to yield a primary alcohol	**I$_b^{\beta}$** (+ TMC + **12α**)	-2463.605912	1.0
	TS$_{I\text{-}IIb}^{\beta}$ (+ TMC + **12α**)	-2463.588325	12.0
	II$_b^{\beta}$ (+ TMC + **12α**)	-2463.599639	4.9
	III$_b^{\beta}$ (+ TMC + **12α**)	-2463.598167	5.9
	TS$_{III\text{-}IVb}^{\beta}$ (+ TMC + **12α**)	-2463.583984	14.8
	IV$_a^{\beta}$ (+ TMC + **12α**)	-2463.604258	2.0
Ring-opening of symmetrical **TMC**	**I^T** (+ **12α**+ **12β**)	-2463.604716	1.8
	TS$_{I\text{-}II}^T$ (+ **12α**+ **12β**)	-2463.587781	12.4
	II^T (+ **12α**+ **12β**)	-2463.600632	4.3
	III^T (+ **12α**+ **12β**)	-2463.597317	6.4
	TS$_{III\text{-}IV}^T$ (+ **12α**+ **12β**)	-2463.584977	14.1
	IV^T (+ **12α**+ **12β**)	-2463.608944	-0.9

Full coordinates for all the stationary points, together with computed Gibbs free energy and vibrational frequency data, are available *via* the corresponding Gaussian 09 output files, stored in the digital repository: DOI: 10.6084/m9.figshare.4644574.

Enthalpy of isodesmic ring-opening with dimethyl carbonate (DMC) (Figure 5.10A)

Table A18. Computed Gibbs free energies at the rωb97xd/6-311++G(2d,p)/cpcm=dichloromethane/298 K level of theory for the isodesmic ring-opening with dimethyl carbonate (DMC) of **12α**, **12β** and TMC.

Structure	***H (Hartree)***	***ΔΔH (kcal mol^{-1})***
Dimethyl carbonate (DMC)	-343.512814	-
12α	-648.698158	-
12β	-648.700746	-
TMC	-381.611588	-
9'-Bn	-879.655491	-
DMC + **12α**	-992.210972	0.0 (reference)
12α oligocarbonate	-992.221438	**-6.6**
DMC +**12β**	-992.213560	0.0 (reference)
12β oligocarbonate	-992.220930	**-4.6**
DMC +**TMC**	-725.124402	0.0 (reference)
TMC oligocarbonate	-725.134702	**-6.5**
DMC + **9'-Bn**	-1223.168305	0.0 (reference)
9'-Bn oligocarbonate	-1223.174014	**-3.6**

Full coordinates for all the stationary points, together with the computed Gibbs free energy and vibrational frequency data, are available *via* the corresponding Gaussian 09 output files, stored in the digital repository: DOI: 10.6084/m9.figshare.4644577.

Thermodynamics of ring-opening with MeOH/i-PrOH for 12α, 12β and TMC (Figure 5.10B)

Table A19. Computed Gibbs free energies at the rωb97xd/6-311+G(2d,p)/cpcm=dichloromethane/298 K level of theory for the ring-opening of **12α, 12β** and **TMC** with MeOH or *i*-PrOH.

	Structure	**G (Hartree)**	**ΔΔG (kcal mol^{-1})**
Starting Materials	Methanol	–115.702205	-
	i-PrOH	-194.286844	-
	12α	-648.746770	-
	12β	-648.747521	-
	TMC	-381.648642	-
12α Products	MeOH +**12α**	-764.448975	0.0 (reference)
	Ring-opening to 1° alcohol	-764.443008	3.7
	Ring-opening to 2° alcohol	-764.444442	2.8
	i-PrOH +**12α**	-843.033614	0.0 (reference)
	Ring-opening to 1° alcohol	-843.026393	4.5
	Ring-opening to 2° alcohol	-843.028605	3.1
12β Products	MeOH +**12β**	-764.449726	0.0 (reference)
	Ring-opening to 1° alcohol	-764.434326	9.7
	Ring-opening to 2° alcohol	-764.441263	5.3
	i-PrOH + **12β**	-843.034365	0.0 (reference)
	Ring-opening to 1° alcohol	-843.020818	8.5

	Ring-opening to 2° alcohol	-843.024458	6.2
TMC Products	MeOH +**TMC**	-497.350847	0.0 (reference)
	Symmetrical ring-opening	-497.347387	2.2
	i-PrOH + **TMC**	-575.935486	0.0 (reference)
	Symmetrical ring-opening	-575.929747	3.6

Full coordinates for all the stationary points, together with the computed Gibbs free energy and vibrational frequency data, are available *via* the corresponding Gaussian 09 output files, stored in the digital repository: DOI: 10.6084/m9.figshare.4644586.

CS_2 Ring-closing kinetics and thermodynamics (Figure 5.31)

Table A20. Computed Gibbs free energies at the rωb97xd/6-31+G(d)/cpcm=acetonitrile/298 K level of theory for formation of **15αβ** or **12αβ** *via* intramolecular S_N2-type displacement of a tosyl leaving group at the 5-position with a xanthate or carbonate nucleophile, respectively at the 3-position in 1-*O*-methy-2-deoxy-D-ribose (**8-Me**).

	Structure	**G /Hartrees**	**ΔG/ kcal mol^{-1}**
	15α	-1294.487635	-
	15β	-1294.486202	-
	Trans-**12α**	-648.559545	-
	Trans-**12β**	-648.554654	-
	DBUHOTs	-1356.918481	-
S_N2-type ring-closing to form **15α**	$3CS_2$_5Tosyl_8MeAlpha	-2651.381329	0.0 (reference)
	$3CS_2$_5Tosyl_8MeAlpha_TS	-2651.337428	27.5
	15α + DBUHOTs	-2651.403288	-13.8
	15α + DBUHOTs (separately)	-2651.406116	-15.6
S_N2-type ring-closing to form **15β**	$3CS_2$_5Tosyl_8MeBeta	-2651.377966	0.0 (reference)
	$3CS_2$_5Tosyl_8MeBeta_TS	-2651.336945	25.7
	15β + DBUHOTs	-2651.402083	-15.1
	15β + DBUHOTs (separately)	-2651.404683	-16.8
S_N2-type ring-closing to form *trans*-**12α**	$3CO_2$_5Tosyl_8MeAlpha	-2005.467505	0.0 (reference)
	$3CO_2$_5Tosyl_8MeAlpha_TS	-2005.426659	25.6
	Trans-**12α** + DBUHOTs	-2005.470487	-1.9
	Trans-**12α** + DBUHOTs (separately)	-2005.473135	-3.5
S_N2-type ring-closing to form *trans*-**12β**	$3CO_2$_5Tosyl_8MeBeta	-2005.467915	0.0 (reference)
	$3CO_2$_5Tosyl_8MeBeta_TS	-2005.425048	26.9
	Trans-**12β** + DBUHOTs	-2005.468976	-0.7
	Trans-**12β** + DBUHOTs (separately)	-2005.478026	-9.7

DBU facilitated CS_2 insertion (Figure 5.32)

Table A21. Computed Gibbs free energies at the rωb97xd/6-31+G(d)/cpcm=acetonitrile/298 K level of theory for DBU facilitated CS_2 insertion (*via* a trimolecular mechanism) at the 3- or 5-hydroxyl positions in 1-*O*-methy-2-deoxy-D-ribose (**8-Me**).

	Structure	**G /Hartrees**	**ΔG/ kcal mol^{-1}**
	8β-Me	-536.438652	-
	8α-Me	-536.444938	-
	DBU	-461.767363	-
	CS_2	-834.443404	-
DBU facilitated CS_2 insertion into the 3- or 5-OH of **8β-Me**	DBU + CS_2 + **8β-Me**	-1832.649419	0.0
	A	-1832.645222	2.6
	TS_{AB}	-1832.623138	16.5
	B	-1832.671944	-14.1
	A'	-1832.644876	2.9
	$TS_{AB'}$	-1832.621748	17.4
	B'	-1832.670410	-13.2
DBU facilitated CS_2 insertion into the 3- or 5-OH of **8α-Me**	DBU + CS_2 + **8α-Me**	-1832.655705	0.0
	A	-1832.643831	7.5
	TS_{AB}	-1832.620526	22.1
	B	-1832.66841	-8.0
	A'	-1832.642714	8.2
	$TS_{AB'}$	-1832.622704	20.7
	B'	-1832.665996	-6.5
DBU-CS_2 reaction	DBU + CS_2 (separately)	-1296.210767	0.0
	CS2 approaching DBU	-1296.202305	5.3
	[DBU----CS_2]‡	-1296.180181	19.2
	DBU-CS_2	-1296.213050	-1.4

Ring Strain Calculations (Figure 5.33)

Table A22. Computed Gibbs free energies at the rωb97xd/6-311+G(2d,p)/cpcm=dichloromethane/298 K level of theory for the ring-opening of **15α** and **15β** with MeOH or *i*-PrOH (Figure 5.33A).

	Structure	**G (Hartree)**	**ΔΔG (kcal mol^{-1})**
Starting Materials	Methanol	–115.702205	-
	i-PrOH	-194.286844	-
	15α	-1294.674500	-
	15β	-1294.673153	-
15α Products	MeOH +**15α**	-1410.376705	0.0 (reference)
	Ring-opening to 1°-SH	-1410.368366	5.2
	Ring-opening to 2°-OH	-1410.373119	2.3
	i-PrOH +**15α**		0.0 (reference)
	Ring-opening to 1°-SH	-1488.955678	3.6
	Ring-opening to 2°-OH	-1488.957579	2.4
15β Products	MeOH +**15β**		0.0 (reference)
	Ring-opening to 1°-SH	-1410.380403	-3.2

	Ring-opening to 2°-OH	-1410.376138	-0.5
	i-PrOH + **15β**		0.0 (reference)
	Ring-opening to 1° -SH	-1488.964811	-3.0
	Ring-opening to 2°-OH	-1488.959761	0.1

Table A23. Computed Gibbs free energies at the rωb97xd/6-311++G(2d,p)/cpcm=dichloromethane/298 K level of theory for the isodesmic ring-opening with dimethyl xanthate (DMX) of **15α** and **15β** (Figure 5.33B).

	Structure	**H /Hartrees**	**ΔH/ kcal mol^{-1}**
Starting Materials	**15α**	-1294.623607	-
	15β	-1294.622779	-
	DMX	-989.444393	-
15α Products	**15α** + DMX	-2284.0680	0.0 (reference)
	5_Trithiocarbonate	-2284.079455	-7.2
	dixanthate	-2284.083188	-9.5
15β Products	**15β** + DMX	-2284.067172	0.0 (reference)
	5_Trithiocarbonate	-2284.079121	-0.01
	dixanthate	-2284.082632	-0.02

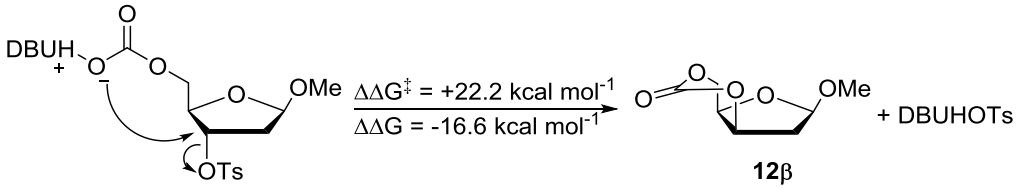

Scheme A2. Computed kinetics and thermodynamics at the rωb97xd/6-31+G(d)/cpcm=acetonitrile/298 K level of theory for ring-closing *via* an S_N2-type mechanism to form **12β**.

Table A24. Computed Gibbs free energies at the rωb97xd/6-31+G(d)/cpcm=acetonitrile/298 K level of theory for ring-closing *via* an S_N2 type mechanism by displacement the 3-tosyl with the 5-carbonate nucleophile to form **12β** (Scheme A2).

Structure	**G /Hartrees**	**ΔG/ kcal mol^{-1}**
12β	-648.575018	
3tosyl_5carbonate	-2005.467056	0.0 (reference)
3tosyl_5carbonateTS	-2005.431657	22.2
12β + DBUHOTs	-2005.482668	-9.8
12β + DBUHOTs (separately)	-2005.493499	-16.6